

**Jupiter Icy Moon Orbiter
High Capability Instrument Feasibility Study
Final Study Report**

4 February 2004

Prepared by

M. J. HART
NASA Programs
Civil & Commercial Division

Prepared for

NASA OFFICE OF SPACE SCIENCE
300 E Street SW
Washington, DC 20546

Contract No. FA8802-04-C-0001

Civil & Commercial Division

JUPITER ICY MOON ORBITER
HIGH CAPABILITY INSTRUMENT FEASIBILITY STUDY
FINAL STUDY REPORT

Prepared by

M. J. HART
NASA Programs
Civil & Commercial Division

4 February 2004

Civil & Commercial Division
THE AEROSPACE CORPORATION
El Segundo, CA 90245-4691

Prepared for

NASA OFFICE OF SPACE SCIENCE
300 E Street SW
Washington, DC 20546

Contract No. FA8802-04-C-0001

THIS PAGE INTENTIONALLY LEFT BLANK

JUPITER ICY MOON ORBITER
HIGH CAPABILITY INSTRUMENT FEASIBILITY STUDY
FINAL STUDY REPORT

Prepared

A handwritten signature in black ink that reads "Matthew J. Hart". The signature is written in a cursive style and is positioned above a horizontal line.

M. J. Hart
NASA Programs
Civil & Commercial Division

Approved

A handwritten signature in black ink that reads "John A. Maguire". The signature is written in a cursive style and is positioned above a horizontal line.

J. A. Maguire, Principal Director
NASA Programs
Civil & Commercial Division

THIS PAGE INTENTIONALLY LEFT BLANK

Table of Contents

1.0	Introduction	1
2.0	Study Objectives	3
3.0	Study Assumptions	5
4.0	Study Approach	9
5.0	Jupiter Icy Moon Orbiter Mission Overview.....	11
6.0	Summary Findings	15
7.0	Visible and Infrared Imaging Spectrometer.....	31
7.1	Science Utility	31
7.2	Design Drivers and Options Examined	32
7.3	Baseline Instrument Description	34
7.3.1	Radiometry	34
7.3.2	Optical Design	36
7.3.3	Processor.....	38
7.3.4	Structural Design	39
7.3.5	Thermal Design	40
7.3.6	Radiation.....	42
7.3.7	System Summary	44
7.4	Design Options	47
7.5	Key Technology Developments	52
7.6	Schedule Estimate	53
7.7	Legacy Instrument Description	53
8.0	Thermal Mapper	57
8.1	Science Measurements	57
8.2	Design Drivers and Options Examined	57
8.3	Baseline Instrument Description	59
8.3.1	Radiometry and Optical Design	60
8.3.2	Optical Design	64
8.3.3	Processor.....	66
8.3.4	Structural Design	67
8.3.5	Thermal Management System.....	69
8.3.6	Radiation.....	71
8.3.7	Summary Mass, Power, and Volume.....	73
8.4	Thermal Mapper Design Options	74
8.4.1	Design Excursions	74
8.4.2	100-1000 Micron Sensing	77
8.4.2.1	Optical Imaging.....	77
8.4.2.2	Composite Infrared Spectrometer (Cassini).....	78

8.4.2.3	Spectral and Photometric Imaging Receiver (Herschel)	78
8.4.2.4	Passive Radio Frequency Radiometry	79
8.4.2.5	Microwave Limb Sounder (EOS Aura)	79
8.5	Key Technology Developments	80
8.6	Schedule Estimate	81
8.7	Legacy Instrument Description	81
9.0	Laser Instruments	83
9.1	Measurement Objectives	83
9.2	Design Drivers and Options Examined	84
9.3	Baseline Instrument Description	85
9.4	Telescope Baselines	86
9.5	Design Options Description	88
9.6	Radiation Considerations	89
9.7	Mechanical and System Details	91
9.8	Key Technology Developments	94
9.9	Schedule Estimate	95
9.10	Legacy Instrument Description	95
10.0	Laser Reflection Spectrometer	99
10.1	Science Measurements	99
10.2	Design Drivers and Options Examined	99
10.3	Baseline Instrument Description	100
10.4	Mechanical realization of MSSRL	103
10.5	Radiation Design of MSSRL	106
10.6	Optical Design Options	107
10.7	Readiness of the Reflection Spectrometer	109
10.8	Schedule Estimate	109
10.9	Legacy Instrument Description	110
11.0	Interferometric Synthetic Aperture Radar	113
11.1	Science Measurements	113
11.2	Design Drivers and Options Examined	113
11.3	Baseline Instrument Description	115
11.4	Design Options Description	118
11.5	Key Technology Developments	122
11.6	Schedule Estimate	122
11.7	Legacy Instrument Description	123
12.0	Polarimetric SAR	127
12.1	Science Utility	127
12.2	Design Drivers and Options Examined	127
12.3	Baseline Instrument Description	128
12.4	Design Options Description	129
12.5	Key Technology Developments	132
12.6	Schedule Estimate	132

12.7	Legacy Instrument Description	133
12.8	SAR Data Rates	135
13.0	Subsurface Radar Sounder	139
13.1	Science Utility and Measurements.....	139
13.2	Design Drivers and Options Examined	139
13.3	Baseline Instrument Description	140
13.4	Design Options Description	143
13.4.1	Science During Spiral In/Spiral Out	143
13.5	Key Technology Developments	144
13.6	Schedule Estimate	144
13.7	Legacy Instrument Description	144
14.0	Radio Plasma Radar Sounder	147
14.1	Science Utility	147
14.2	Design Drivers and Options Examined	147
14.3	Baseline Instrument Description	148
14.4	Design Options Description	153
14.4.1	Observation of Jupiter.....	153
14.5	Key Technology Developments	153
14.6	Schedule Estimate	153
14.7	Legacy Instrument Description	154
15.0	Shared Instrument Resources	157
15.1	Scan Platform for Electro Optical Instruments	157
15.1.1	Instrument Interface to Scan Platform.....	158
15.1.2	Scan Platform	160
15.1.3	Platform Sensing	161
15.2	Pointing and Stability	162
15.3	Power Conversion, Processing, Distribution and Shielding	164
15.3.1	Current Technology	164
15.3.2	Silicon Carbide.....	165
15.3.3	Wire Insulation	166
15.3.4	Shielding for Power Electronics	167
15.3.5	Advanced Shielding for High Radiation Environments.....	168
15.4	On-Board Data Storage and Processing.....	171
15.4.1	Existing Data Storage Technology.....	172
15.4.2	Retrieval Time and Rate	172
15.4.3	Flight Certification/Availability	173
15.4.4	Limitations of Tape Recorder Mechanisms.....	173
15.4.5	Radiation and Shielding Issues.....	173
15.4.6	Potential Future Technologies	174
15.4.7	Longevity and Redundancy	175

15.5	Telecommunication Resources.....	175
15.5.1	RF Communication Using 3-meter or 5-meter Dish Antenna.....	178
15.5.2	Method 2: Laser Communication Option for JIMO.....	180
15.5.3	Method 3: RF Communication Using a Relay Satellite.....	183
15.6	Instrument Thermal Management.....	184
15.6.1	Visible and IR Imaging Spectrometer Thermal Management.....	185
15.6.2	Thermal Mapper Thermal Management.....	186
15.6.3	Radiator and Heat Pipe Thermal Management.....	189
16.0	Instrument Test.....	191
16.1	Facilities.....	193
16.2	Notional Test Plan.....	193
16.3	Design for Test.....	194
16.4	Potential EMC/EMI Test Issues.....	194
16.4.1	Systems Issues.....	194
16.4.2	Magnetometer Issues.....	195
16.4.3	Infrared Instrument Issues.....	195
16.4.4	RF Instrument Issues.....	195
	Appendix A. Tables and Figures.....	197
	Table of Figures.....	197
	Table of Tables.....	198
	Appendix B. Coverage Analyses.....	201
	Appendix C. Communication Linkage.....	221
	Appendix D. Relevant Radiation Environments.....	222
	Appendix E. Ion Plume Effects.....	231
	Appendix F. On Board Storage Technology Examples.....	235
	Appendix G. Legacy Approaches to 100 – 1000 Micron Remote Sensing.....	239
	Appendix H. Technology Readiness Levels Descriptions.....	249

1.0 Introduction

This report documents the findings of a study conducted by The Aerospace Corporation on the feasibility of High Capability Instruments to support the science goals of the Jupiter Icy Moon Orbiter Mission (JIMO). JIMO is the first mission of NASA's Prometheus Program, chartered with development and exploitation of space nuclear power for use in missions of planetary exploration. Proposed mission concepts utilize a space nuclear fission reactor, coupled to a power conversion system, to generate hundreds of kilowatts of electric power for electric-propulsion, telecom, and science instruments. The Prometheus paradigm results in tens of kilowatts of power being available for remote sensing instruments, and motivates new instrument concepts that can take advantage of the power and reap greater science return than currently available from space remote sensing instruments.

The term High Capability Instruments (HCI) refers to a class of instruments capable of taking advantage of large amounts of available power, and providing enhanced performance in terms of sensitivity, spatial and spectral resolution, duty cycle, and data rate. The instruments described in this report were selected for study based on meeting a high-priority subset of the overall preliminary science goals identified by the JIMO Science Definition Team. They were selected in order to establish a baseline for feasibility of a suite of science instruments that could potentially accomplish the ultimate, and yet to be fully defined, science goals of the mission. They are not, however, to be considered representative of the actual JIMO Payload Suite.

The candidate instruments included for study include a visible and infrared imaging spectrometer, a thermal mapper, a laser altimeter, a multi-spectral laser surface sampler, an interferometric synthetic aperture radar (InSAR), a polarimetric synthetic aperture radar (PSAR), a subsurface radar sounder, and a radio plasma sounder. In addition to a baseline design description for each instrument, a number of design options were explored and documented in order to identify the overall trade space drivers. Instrument support resources, such as data management, telecom, thermal management, pointing stability, and protection from the natural and induced radiation environment are also discussed. Driving technologies for each instrument type were identified, as well as an estimate of the development time for each instrument. Information on heritage or legacy instruments similar to those considered is also presented herein.

2.0 Study Objectives

In performance of the study The Aerospace Corporation study team was asked to address the following topics:

1. Instrument trade space to assist in optimization of instrument performance, resource needs, and physical parameters.
2. Instrument resource needs such as power, data rate, data storage, computational needs, and others.
3. Instrument physical parameters, such as mass, volume, and others.
4. Technologies that need to be developed for an instrument to reach JIMO flight readiness.
5. Schedule estimates for instrument development.
6. Instrument requirements such as pointing accuracy, duty cycles, fields of view, etc.
7. Datasets produced by the instrument (types, characteristics, size, and others as needed).
8. Effects of radiation and electromagnetic environment from Jupiter and the spacecraft on the design and performance of the instrument.
9. Critical instrument components requiring radiation hardening.

In addition to these items, it is noted where existing technology falls short of meeting the needs of the instruments.

Basic description of each instrument, including physical parameters, data rates and processing, along with discussion of the trade space options examined, technology development items, heritage instruments and development time are provided in Sections 7-14. Design issues common to all instruments such as thermal management, pointing stability, radiation shielding, environmental effects and the impacts on technology selection, data storage, and telecommunications are addressed in Section 15. Section 16 summarizes integration and test issues for the instruments. There are a number of appendices at the end of this report that address topics such as coverage analyses, radiation and thermal environments, Ion plume effects, and other topics.

3.0 Study Assumptions

The following section documents the major constraints and assumptions during this study.

The set of candidate instruments and top-level requirements for each were provided by the customer early in the study. These are shown in Table 3.0-1. The requirements centered on top-level performance parameters such as spatial, and spectral resolution, and sensitivity. Other necessary functional requirements were derived internally, without interaction with the JIMO Science Definition Team or the external science and instrument community at the request of the customer. When necessary, the study relied on prior experience with remote sensing instruments, limited planetary instrument experience, and publicly available data to derive additional needed information.

The assumed launch date of 2012 for the Jupiter Icy Moon Orbiter was derived from the concept schedule presented at the Lunar Planetary Institute's Forum on Concepts and Approaches for Jupiter Icy Moon Orbiter, June 12-14, 2003 [Ref 3.1]. Given this launch date, the latest technology readiness cut-off was selected as 2007, based on estimates of new technology development times discussed later in this report. A number of enabling technologies that are unlikely to be developed within this time frame are highlighted as well. The technology readiness cut off date is defined as the timeframe by which the technology needed to develop the set of baseline instruments would mature to Technology Readiness Level (TRL) 5.

Table 3.0-1 Top Level Instrument Requirements

Instrument	Requirements
Imaging Spectrometer	<100 m spatial resolution R = ~300 spectral resolution (higher spectral or spatial resolution would be even better) Visible (0.4-0.5 microns) and IR (1-5 microns) spectral range
Thermal Mapper	Spatial resolution of 100-300 meters Covers 5-1000 microns Low spectral resolution acceptable
Laser Spectrometer	Spectral resolution variable (some wavelengths more important than others) 5-10 micron spectral range
Laser Altimeter	10 m horizontal resolution 1 m vertical resolution
Radio Sounder	None
Radar Sounder	At depths from 2 to 30 km at 100 m vertical resolution At depths from 100 m to 2 km at 10 m vertical resolution
SAR / InSAR	10 m horizontal resolution

In addition to these top-level requirements, a set of top-level payload accommodation parameters were provided and are shown in Table 3.0-2. These parameters were used as guidelines in sizing each of the instruments. Because it is unlikely that all of the instruments described in this paper will be accommodated on the spacecraft, the accommodation parameters were not interpreted as strict constraints imposed on the overall instrument suite.

Table 3.0-2 Top Level Payload Accommodation Parameters

Accomodation Parameter	Value
Total Payload Mass	600 kg
Total Payload Power	45 kWe
Data Rate	> 10 Mb
Pointing	1.0 mrad kontrol, 0.1 mrad knowledge, .0035 mrad/sec stability
EMC/EMI	Isolation for Magnetic and ESD cleanliness
Data Volume	230 Gb/day, 50 Tb total

The following discussion identifies the baseline instruments and highlights their design rationale.

The imaging spectrometer covers the 1-5 micron band in 300 channels. It includes a 3-color visible imager that covers the band from 0.4-0.5 microns. The spatial resolution requirement is less than 100 m. The baseline instrument uses 100 m ground sample distance; design excursions at 50 and 20 m resolution were examined. The original requirement was for a spectral resolution of 300 m, resulting in 458 channels; however, this requires technology unavailable in the JIMO time period. Relaxation of this requirement to 300 spectral channels allows for the design of a feasible instrument, with minimal impact to the overall science. Changes needed to address a 458-channel instrument are addressed in Section 7.

The thermal mapper instrument has a maximum spatial resolution requirement of 300 m. This was chosen for the baseline instrument, and excursions to 200 and 100 m ground sample distance were examined. The baseline instrument covers the 5-100 micron range instead of 5-1000 micron range at a spectral resolution of 2. In the sub-millimeter wavelength regime (100-1000 micron wavelengths), there are a number of options for implementation ranging from Far IR photometers to microwave radiometers, many of which differ significantly from a mapper instrument in regards to measurement type. These options for the sub-millimeter regime are discussed along with the description of the baseline instrument.

The laser spectrometer is a new instrument, without a direct analogue to legacy instruments. For the purposes of assessing the feasibility of such an instrument, a limited number of discrete wavelengths in the 4-10 micron range were selected for detection. These correspond to a limited sampling of organic and inorganic

materials not necessarily representative of surface constituents present on the Icy Moons.

Laser altimetry is required to produce measurements with 1 m vertical resolution and 10 m horizontal resolution. The approach taken on the instrument herein provides for a more data intensive scanning approach, from which additional information such as local slopes can be inferred. This instrument augments the laser spectrometer data type by spatially locating the identified surface constituents, in addition to the primary mission of developing a high fidelity altimetry map.

The radar instruments included in the study include interferometric and polarimetric synthetic aperture radars (InSAR and PSAR), a radar sounder and radio sounder. The InSAR is assumed to operate at 35 GHz, although it is acknowledged that the surface dielectric properties are unknown. The InSAR and PSAR provide 10 m horizontal resolution.

The radar sounder is conceived to operate at multiple interleaved frequencies to return subsurface horizon data at 100 m vertical resolution at depths of 2-30 km, and 10 m vertical resolution at depths of 100 m to 2 km. The Radar Sounder consists of a high frequency and low frequency antenna, the low frequency dipole being shared with the radio sounder. No requirement was levied on the vertical resolution performance of the radio sounder and 3 km was assumed for this parameter.

The principle data taking period for the baseline instrument suite was assumed to nominally operate in a circular orbit at a nominal altitude of 100 km above the surface of each of the icy Galilean moons: Callisto, Ganymede, and Europa. This altitude is consistent with the altitude range discussed at the LPI JIMO Forum. There were concerns about orbit stability at Europa and a desire to understand the feasibility of operating the instruments during the approach and departure spiral periods. This led to the selection of two additional altitudes for study: 400 km was assumed as an alternative low altitude science orbit altitude that may prove to be stable at Europa, and 10,000 km was picked as a representative altitude at the start of the spiral-in period. The performance of each baseline instrument was evaluated at 10,000 km in order to assess its utility in a dramatically different altitude regime.

The instrument coverage swath width and corresponding fields of view are sized to provide two-fold global coverage at each moon, assuming a minimum time in the science orbit of 60 days. It is assumed that Earth would be in view of the spacecraft 60% of each orbit. The icy moons were treated as black bodies at 80-100 degrees Kelvin, and the effects of Jupiter's thermal fluence on the icy moons were assumed to be negligible.

Instrument mass and power estimates are based on grass-roots roll-ups at the subsystem and component level. In areas where actual data was lacking, the component masses were scaled from heritage instruments using mass, power or volume as appropriate, or first principles. In some cases, such as for shielding, mass was calculated based on material density and volume.

The study assumed instrument payload architecture shares thermal, data storage, data processing, and telecommunication resources. The resource needs of each of the instruments in these areas (in terms of mass, power, memory or data rate) are book-kept individually for each instrument. A compromise was made between minimizing shielding mass, cable run length, and volume required in determining the location of instrument power, command, and processing electronics. Central processing and power electronics that could conceivably be shared among instruments were located in a central shielded vault inside the spacecraft bus. Small, shielded vaults containing instrument-unique command and processing electronics were located nearer to their instrument. Thermal radiator resources were assumed to be co-located in the form of a parasitic radiator mounted to the side of the spacecraft bus. All dimensional questions, including cabling lengths and heat pipe run lengths were determined to first order using the JIMO concept vehicle dimensions as outlined in [Ref 3.2]. It is assumed that electronic parts are designed to 100krad total dose, as is commonly available today for space applications, and that shielding is required to limit the total dose seen by electronic parts.

References

[Ref 3.1] “Jupiter Icy Moon Orbiter – Mission Characteristics Overview to the Forum on Concept and Approaches for Jupiter Icy Moon Orbiter,” John Cassani, The Jet Propulsion Laboratory, June 12-13, 2003.

[Ref 3.2] “Jovian Icy Moon Tour Mission Review”, Ashley G. Davies, et. al., The Jet Propulsion Laboratory, November 19, 2002.

4.0 Study Approach

The study flow is illustrated in Figure 4.0-1. Study drivers include the environment at the icy moons, the top-level requirements as defined by the customer, and the major assumptions discussed in Section 3. The icy moons drive the instrument design in primarily two ways: geometry and environment. Ganymede is the largest moon, resulting in the highest ground track rate for a fixed 100 km altitude science orbit. For the passive electro-optical (EO) instruments, which include the Visible Imager and IR Imaging Spectrometer, and the thermal mapper, this sets an upper limit on the allowable integration time, which sets the instrument sensitivity threshold.

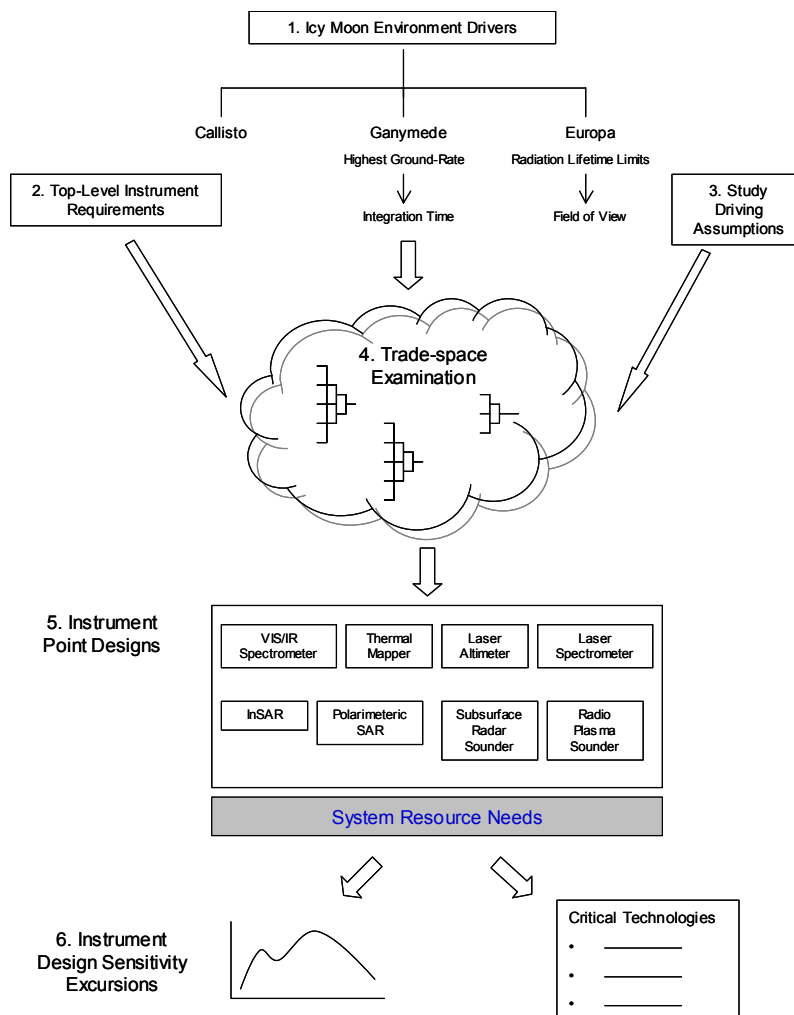


Figure 4.0-1: Study approach.

Europa orbits Jupiter in a high radiation environment, which constrains the duration of the science orbit, based on the radiation-compensated life of critical electronics on-board the spacecraft. This sets a lower limit on the coverage

swath width needed to achieve two-fold global coverage, which drives the instrument duty cycle, focal length, and aperture of the systems. The active radar instruments are less sensitive to these constraints. Integration time is not an issue and swath width can be controlled to meet the coverage constraints. The primary driving performance requirements on the instruments include spatial resolution for the EO and radar instruments, and spectral resolution for the EO instruments.

Referring back to Figure 4.0-1, the driving requirements, environments, and assumptions were used in brainstorming a set of feasible strawman instrument concepts to be explored during the study. These concepts were matured to baseline instrument point designs. System resource needs such as thermal management, telecom, data processing and storage, shielding, and pointing control were sized for the baseline instrument suite. Trade space excursions were conducted in order to assess the sensitivity of the design trade space to major system drivers such as resolution, and operating altitude. Critical technologies that need to be developed to enable these instruments are identified.

Also included is a discussion of the impacts of the natural and induced environments and issues surrounding integration and test of the instruments.

5.0 Jupiter Icy Moon Orbiter Mission Overview

The Jupiter Icy Moon Orbiter, the first mission under NASA's Prometheus Program, is an ambitious project to develop a safe, reliable, affordable space system that combines nuclear fission generated electricity, electric propulsion systems and science instruments. The Jupiter Icy Moon Orbiter mission objective is to produce unprecedented scientific data on the structure, composition and evolution of Jupiter's three icy Galilean moons, Callisto, Ganymede and Europa, as well as study the Jupiter environment. The current strawman calls for launch on a Delta IV Heavy Launch Vehicle in the 2011-2012 time frame. Missions must be capable of being implemented within 6 years of approval to proceed. The program assumes a substantial investment in order to develop and utilize Nuclear Electric Propulsion (NEP) technologies within that time frame.

A typical mission profile for JIMO consists of a single launch from a Delta IV Heavy. After a 6-year cruise to Jupiter, the spacecraft will enter into orbit around Callisto, conduct remote sensing scientific investigations for 6 to 9 months, and then depart for similar encounter missions at Ganymede and then at Europa.

The encounter phase at each of the moons begins at the point where the JIMO spacecraft is captured by the local gravity field of the moon. Simplistically, the Nuclear Electric Propulsion (NEP) subsystem on the JIMO spacecraft is used to "pump down" the trajectory into a very high, roughly circular orbit. The NEP subsystem continuous thrust is used to gradually reduce altitude, in a roughly circular spiral, down to a low altitude science mission orbit. The spacecraft then spends several months conducting science investigations in one or more low altitude orbits of different variety. It then departs the moon in a similar fashion, by using the NEP subsystem to raise the altitude to escape the moon's gravity and begin the cruise to the next encounter. This entire process takes approximately 6 months in the current concept.

The Europa encounter is unique to the mission design because of the high radiation fluence, which results in limited spacecraft life once in the vicinity of Europa. It is estimated that the time which the spacecraft may remain in the science orbit at Europa may be 30–50 percent less than at Ganymede and Callisto, because of the radiation-induced lifetime problem. The start of the Europa encounter is similar to the encounter at Callisto and Ganymede, with a period of spiraling-in to a low altitude science orbit. Gravitational perturbations from Jupiter may also affect the stability of the low altitude science orbit at Europa. This may require either increased station-keeping maneuvers, a higher altitude science orbit, or a reduced orbit inclination range. Finally, because of planetary protection requirements, the mission must be designed so the vehicle does not impact Europa after the end of the encounter. Solutions to this include

boosting the spacecraft to a higher altitude orbit where it will remain indefinitely, departing from Europa entirely, and impacting the spacecraft onto Io or Jupiter.

A picture of a notional spacecraft is given in Figure 5.0-1.

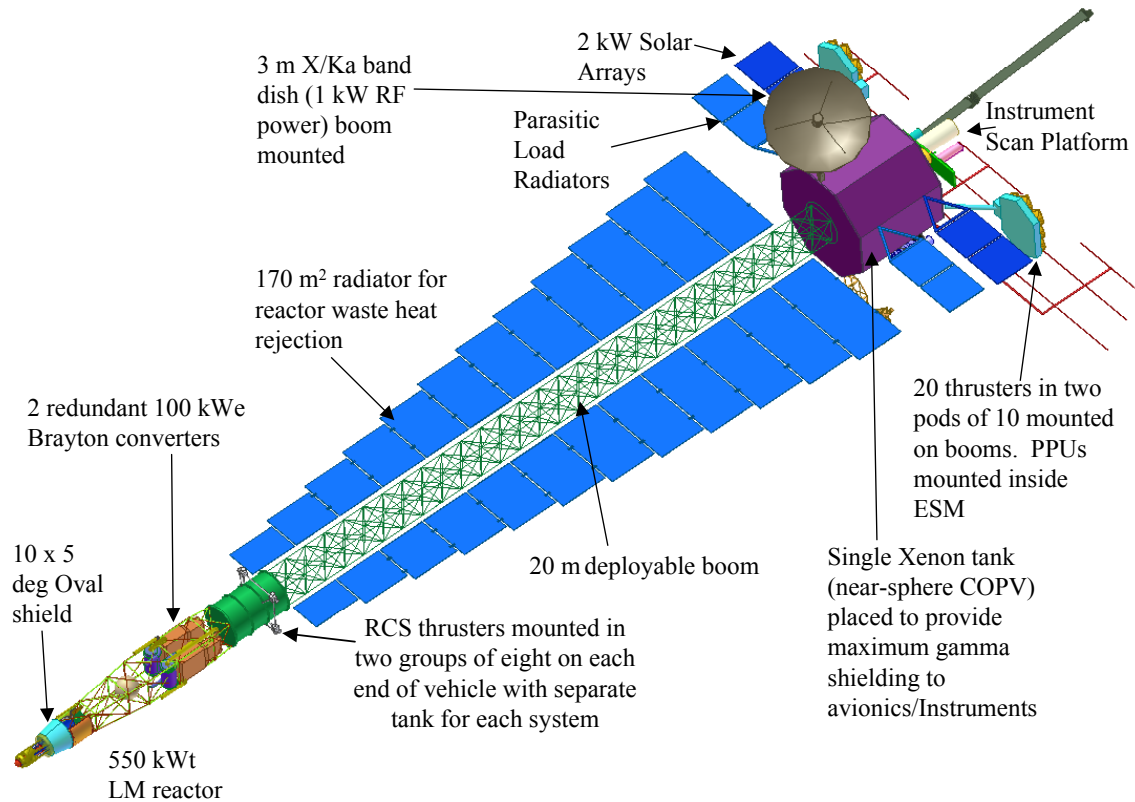


Figure 5.0-1: Pre decisional JIMO spacecraft concept (Reprinted courtesy of NASA).

The spacecraft consists of a deployable boom with the nuclear reactor and power conversion system at one end, and the spacecraft bus, electric propulsion thruster clusters and instrument platform at the other. Radiators to reject waste heat from the reactor are affixed along the central boom. Parasitic load radiators to reject heat from the electrical power system and instruments are located on the spacecraft bus. The reactor is located behind an oval shield which acts as a barrier to high energy neutrons from the reactor, providing a cone shaped volume envelope surrounding the spacecraft forward of the shield structure. Instruments will be mounted on the forward or nadir facing side of the bus or on a scan platform. In this concept, the scan platform will also be mounted on the forward side of the bus, pointing in the same direction as the electric propulsion thruster pods.

It is important to note that this is a strawman concept only, and does not necessarily reflect current flight system planning.

[Ref 5.1] “Jupiter Icy Moon Orbiter Industry Kick-off,” Karla Clark, The Jet Propulsion Laboratory, April 22, 2003.

6.0 Summary Findings

Table 6.0-1 lists the primary accommodation parameters for the set of baseline instruments. The mass, power and data rate numbers listed in the table represent the total required, which accounts for the need for multiple instruments, as in the cases of the spectrometer and thermal mapper. The total mass and power numbers also account for that fraction of the mass and power attributable to thermal control and data handling provided by the spacecraft.

Tables 6.0-2-6.0-9 summarize the design and performance parameters for each of the baseline instruments. The mass and power numbers in these tables reflect the instrument only and not spacecraft provided resources, and are therefore somewhat lower. These tables also summarize the required technology developments and development times. Table 6.0-10 summarizes the technology development items that enable the instrument set selected for this study.

Visible Imager/IR Imaging Spectrometer

Table 6.0-2 summarizes the visible imager/IR imaging spectrometer. The spectrometer consists of two identical instruments, each with a 14.8-degree field of view. This instrument is a push-broom imager that performs reflection spectroscopy and is only effective on the dayside of the body. In order to achieve two-fold coverage in 60 days, two instruments are needed to create an effective 30-degree swath. The visible imager senses 3 bands in the 0.4-0.5 micron range. The spectrometer senses 300 spectral bands in the 1-5 micron range. The total combined data rate is 42 Mbps (2 x 21 Mbps). Power requirements are very modest at 5 W average, and pointing is achievable with existing technology. These instruments are mounted to a scan platform, which can be used for pointing and to provide dynamic isolation from the spacecraft bus.

For the spectrometer, 300 spectral channels are achievable with existing technology and the instrument development time is a relatively short 46 months. In order to accommodate the higher spectral resolutions that are desired, the optical design could be simplified; a dispersive prism at the focus of the instrument could be replaced with a high density grating linear variable filter. To achieve a spectral resolution of 300 would require roughly 485 channels. Linear variable filters that could meet this need do not yet exist and are an area of technology investment and development. It is estimated that this technology would take on the order of 84 months to develop, assuming a funded development program.

Focal plane development and testing will be required to assure that suitable detectors are available for this mission. The high data rate associated with the

large number of spectral channels is also a technology concern. The baseline instrument set generates approximately 4 times the anticipated available bandwidth in the JIMO time frame.

Thermal Mapper Instrument

Table 6.0-3 summarizes the thermal mapper instrument. The instrument is also configured for push-broom imaging from an altitude of 100 km. The sensor has a 5.5 deg cross-track field of view, which means that 3 sensors are needed to form the 15 deg swath width needed to achieve two-fold global coverage in 30 days. The optics for this instrument are also quite small, with a 2.45 cm aperture and 4.2 cm focal length. The imager consists of two detector arrays: a HgCdTe array similar to that used by the IR spectrometer for wavelengths shorter than 12.5 microns; and a microbolometer array for the longer wavelengths out to 100 microns. Instrument integration time of 167 msec is based on 1 pixel smear and the highest ground speed at Ganymede. A spectral resolution of 2 (center wavelength/bandwidth) with some overlap between bands results in 12 spectral bands across the desired spectral range of 8 to 100 microns. Mass and power are also modest. This instrument uses an integrated cryocooler to maintain temperature of the focal plane and cool the optics to 60 K. For the three shortest wavelengths, 62.5-micron pixels are summed 2 by 2 in order to achieve acceptable signal to noise. For the nine longer wavelengths, time delay integration across multiple rows of the microbolometer array is required to achieve acceptable signal to noise. The data rate for a single instrument is 72.8 kbps.

The instrument can probably be developed using existing technology. Cryocooler development or testing may be required, however. The point of reference for the cryocooler is the TRW advanced Mini Pulse Tube cryocooler. This unit was developed in 1995 and has no flight heritage. Development time is estimated at 53 months based on analogy to THEMIS (2001 Mars Odyssey) and TES (Mars Global Surveyor).

Laser Altimeter

Table 6.0-4 summarizes the laser altimeter. The instrument illuminates the surface with a 50 m spot beam that scans across a 15-degree swath. The system strives to achieve about 2000 collected 1-micron photons per emitted laser pulse. The resulting 800 signal electrons are based on performance of the linear mode Perkin Elmer 1-micron Si avalanche photo-diode. The 15-degree FOV requirement for the 100 km altitude case poses a considerable design constraint on the laser pulse rate and energy per pulse to achieve the contiguous 50-meter diameter sample spots on the surface.

The system is bistatic in design, similar to MOLA and ICESat. To achieve the high coverage rate, a scanning prism is used to deflect the laser beam to a spot

on the icy moon's surface. Pointing knowledge is derived purely from diagnostics on the transmit beam. Because the receive telescope has a large FOV (15 deg and 5 deg for the 100 and 400 km cases, respectively), it is assumed that the measured spot will fall somewhere on a large detector array. The detector array does not provide any enhanced resolution since any 50 m diameter ground spot will be well within a single pixel. The array, therefore, only accommodates the optical constraints of the telescope design. This design results in a linear array about 1 mm by 10 mm at the detection plane where each of ten pixels would be equivalent to current flight hardened analog detectors.

The most challenging aspect of the laser altimeter was choosing the most optimum telescope and optical path to minimize full system mass and maximize science return. The off-axis telescope design accommodates the large 15-degree FOV but scales in mass quickly with aperture size. Consequently this forces a trade on laser power squared vs. aperture size for the telescope, in order to constrain mass growth.

The laser altimeter requires technology development in the areas of radiation compensated Nd:YAG laser, coordinated transmit and receive scanning, and active thermal control at higher altitudes to meet its design requirements. A radiation compensated Nd:YAG laser is currently at TRL 4 and would have to progress to TRL 5 before Phase B initiation. A recent study identified that the average time to progress from TRL 4 to TRL 5 is 1.5 years. Coordinated transmit and receive scanning capability is currently stated at TRL 3 which means it would take, on average, 2.9 years to develop the technology required to mature it to TRL 5. Detectors and processing algorithms must be developed and validated for the environment, also. Overall development time for the instrument is 53 months once these technologies reach TRL 5 based on analogy to MOLA and GLAS.

Multi-Spectral Selective Reflection Lidar (MSSRL)

Table 6.0-5 summarizes the multi-spectral selective reflection lidar (MSSRL), a laser reflection spectrometer. The general concept for the instrument is to transmit a number of discrete wavelengths, half of which will be on resonance for the above species and half that are off-resonance. A separate narrow line width laser emits each wavelength of interest. As in the case of the laser altimeter, all the wavelengths will be painted simultaneously on the moon's surface transverse to the ground track. A single but separate telescope, which is bore-sighted to the full FOV, will collect the reflected intensities. All of the transmitted wavelengths will be superposed into a single scanning footprint so that the sampling strategy will copy nearly identically that of the laser altimeter.

The instrument was conceived based on capabilities that are available in the industry but as such do not exist. As in the case of the laser altimeter, the MSSRL should undergo a 1-2 year architecture study and trade space

examination. Preliminary tests should be conducted on materials of interest to clarify the true signal levels and show their consistency with the detection concept. A validation of the concept could be completed in 1-2 years using COTS technologies. The packaging of the laser bars and integrated micro-lenses are near TRL 5. A TRL 6 version of the transmitter could be ready 3 years after definition of the desired wavelengths. A detector concept would need to be defined early and built and tested, and one would also need to demonstrate optical compatibility with the dispersion specification of the receive prism. The detector and integration with a prism could be demonstrated in 2-3 years at TRL 6. The estimate for the instrument development time once the needed technologies reach TRL 6 is no less than 62 months, based on analogy to ALIAS, once technology development is complete.

Interferometric SAR

Table 6.0-6 summarizes the interferometric SAR. The InSAR is composed of two electronically steered antenna (ESA) pairs separated by a 5 m boom. Each antenna pair contains a receive-only (passive) antenna and a radar (active) antenna, for a total of four antennas. The transmit power is evenly split between each transmit/receive antenna pair. Each antenna beam will point between 20 and 45 degrees off nadir. The boom length (antenna separation) is 5 m.

The InSAR was designed to map two 30 km swaths; one is to the left and one is to the right of the ground track (nadir). The purpose of mapping two swaths on either side of the ground track is to mitigate the fact that the spacecraft altitude will not be known with sufficient accuracy to provide accurate absolute height. These swaths will provide global coverage of Europa twice in 30 days. The maximum usable swaths for the present design well exceed the required 30 km swath widths. The InSAR has the tightest pointing control and knowledge requirements of any of the instruments in the suite. The InSAR requires 1.7 and 6.6 kW power at 100 and 400 km, respectively. The raw data rate is above 2 Tbps, but it can be reduced to about 56 Mbps through processing before downlink.

Needed technology development centers on high-power, space-qualified Ka band transmitters, new processing algorithms for use on board the spacecraft, and a system to isolate the antennas from bus dynamics (vibration) that could reduce contrast. Transmitter technology is currently estimated at TRL 3-4, requiring approximately 3 years of development time, predominantly in the area of reducing mass and volume. On-board data processing algorithm development is also at the same level of maturity, although it is difficult to estimate the time required for new algorithm development. Vibration isolation is more mature, but existing approaches must be validated for this application. Instrument development time, once technology is mature, is greater than 76 months.

Polarimetric SAR

Table 6.0-7 summarizes the polarimetric SAR. This instrument uses a cylindrical reflector antenna, which will point between 20 and 45 degrees off nadir. The instrument requires 200 W average power at 100 km, and operates at a frequency of 3 GHz. Processed data rate is 36.737 Mbps. Pointing requirements are not overly stringent.

Further development of low mass/low volume/radiation tolerant radar electronics is desirable, but not necessary. The relatively high data rate for this instrument requires development of advanced data processing techniques, as with the InSAR.

Radar Sounder

Table 6.0-8 summarizes the radar sounder. The subsurface radar sounder utilizes two antennas: one is for higher frequency (above 10 MHz) operation and a second is for lower frequency (10 MHz and below) operation. The low frequency antenna is a 73.2 m dipole (optimized to 2 MHz). It will be employed by the radio sounder as well. The high frequency antenna is a 10 m Yagi antenna with three Yagi radiators of 3 m (optimized to 50 MHz). Both antennas will be oriented in the cross-track direction pointing directly nadir.

Both antennas are fed by a single transmitter, which transmits a maximum peak power of 1 kW at 100 km and 16 kW at 400 km. The transmitter operates with a 27% duty factor for 0.63 kW of average power at 100 km and 8.7 kW of average power at 400 km.

The radar sounder is designed to operate in a band spanning 3 MHz – 50 MHz (100 m – 6 m). There is a minimum of 5 frequencies available throughout this band for near simultaneous (interleaved) operation.

Space qualified transmitters in the bands and powers levels of the subsurface sounder have not been flown and will require development. Current technology is estimated at TRL 4, requiring 3 years to mature to TRL 5. Instrument development time is 39 months, once technology development is complete.

Radio Sounder

Table 6.0-9 summarizes the radio sounder. The radio sounder requires no new technology development. The device uses a 72 m dipole antenna and operates between 400 kHz and 2 MHz. The instrument generates 5.18 Mbps, raw and operates on 85 W power.

The antenna design for the JIMO application is a key issue. Because the ionospheres of the icy moons are believed to be more tenuous than the Earth's ionosphere, coverage at the higher frequencies used in the earlier designs is not required. This leads to a lower frequency instrument than previously designed and a longer dipole antenna.

Development time for this instrument is estimated at 34 months, and there are no technology developments identified for this instrument.

Key Technology Developments

Table 6.0-10 summarizes all the key technology developments that enable the instruments. As seen from the table, most of the enabling technologies have development times within 36 months, assuming a focused, funded development effort. A number of standouts include light-weight shielding, rad hard electronics and technology necessary to achieve spectral resolution of 300. Shielding is the largest system driver in terms of mass. The average shielding mass fraction is about 50% across the instruments, with the EO instruments being higher, and the radar instruments being lower. Light-weight shielding or, alternatively, 100 Mrad hard electronics, provide the most leverage, but are questionable within the JIMO development time frame. For the purposes of addressing feasibility of these instruments, conventional shielding was employed.

In some cases, instrument development times exceeded the time between the start of JIMO development (anticipated to be 2007) and the proposed 2012 launch date. Specific technologies, such as light weight shielding, high density linear variable filters, and rad hard electronics, may not be achievable within the JIMO development timeframe. Instruments development times exceeding the anticipated JIMO development time include the laser spectrometer, which is an entirely new instrument, the InSAR, and the polarimetric SAR. While functional InSARs and polarimetric SARs have flown on the shuttle, the pathway to transition of that application to the Jupiter environment is complex and drives the length of the instrument development effort. The length of the visible / IR imaging spectrometer development time is driven by the high spectral resolution of 300, and the consequent need for linear variable filter technology development. Reducing the capability of the spectrometer to 300 spectral channels allows development within the JIMO timeframe.

Table 6.0-1: Baseline Instrument Summary – 100 km Altitude

Instrument	No. Units	Power		Mass		Data Rate			Data Handling		Thermal Control		
		Total Average (W)	Total Peak (W)	Total (kg)	% Shielding Mass	Total Raw (Mbps)	Total Processed (Mbps)	Duty Cycle	Storage Estimate (Gb)	Spacecraft Electronics Mass (kg)	Average Thermal Dissipation (W)	Spacecraft Radiator Area (m ²)	Spacecraft Radiator Mass (kg)
Vis/IR Imaging Spectrometer	2	10	13	147	88%	42	42	50%	77	0.5	5	0.4	4
Thermal Mapper	3	151	152	107	58%	0.2	0.2	100%	1	0.8	76	24 kg cryocooler mass book-kept w/instrument total	
Laser Altimeter	1	1428	1428	76	13%	1	1	100%	4	1	1357	5	31
Laser Reflection Spectrometer	1	704	704	49	20%	1	1	100%	4	0.7	690	20 kg cryocooler mass book-kept w/ instrument total	
Interferometric SAR	1	1683	7923	337	36%	2332	56	100%	8563	8	337	1	8
Polarimetric SAR	1	204	1424	131	32%	150	37	100%	550	3	41	0.2	1
Subsurface Radar Sounder	1	2734	13454	131	37%	5	5	100%	19	3	547	2	12
Radio Plasma Sounder	1	87	172	81	60%	0.1	0.1	100%	0.5	1	17	0.1	1
Total	1	7001	25269	1060		2531	142		9218	19		9	57

Table 6.0-2: Baseline Vis/IR Imaging Spectrometer Performance Summary

Baseline Vis / IR Imaging Spectrometer Performance	Design Description	Rationale
Field of View	14.8 deg	Dayside Global Coverage in 30 days
Imaging Method	Push broom	Simple design
Optical Speed	2.7	Diffraction limited
Focal Length	27 mm	100 m GSD at 100 km
Aperture Size	10 mm	Maximize SNR at the diffraction limit
Cross Track Pixels	260	100 m ground sample distance (GSD)
Pixel Size	27 microns	1 pixel per GSD
Integration Time	52 msec	1 pixel smear at Ganymede
Spectral Channels	300	300 spectral channel baseline is achievable with current technology. Spectral resolution of 300, or 458 channels, requires technology development
Number of Sensors	2	Dayside imaging only, coarse estimate of two needed for two-fold global day side coverage
Sensor Mass	71 kg	100 km altitude
Sensor Power	5 W	100 km altitude
Sensor Data Rate	21 Mbps	300 In-scan channels, 14 Bits per channel
Pointing Stability	1.31 mrad/sec	Lowest ground speed at Europa
Technology Development	None for baseline, high density linear variable filters are needed for spectral resolution of 300.	
Estimated Technology Development Time	84 months	High density linear variable filters may require up to 7 years to develop for spectral resolution of 300.
Estimated Instrument Development Time	46 months	Analogy to MRO/CRISM, Cassini/VIMS

Table 6.0-3: Baseline Thermal Mapper Performance Summary

Baseline Thermal Mapper Performance	Design Description	Rationale
Field of View	5.5 deg	Two-fold global coverage in 30 days
Imaging Method	Push broom	Simplified design
Optical Speed	1.7	Diffraction limited
Focal Length	41.7 mm	300 m GSD at 100 km
Aperture Size	24.5 mm	Maximize SNR
Cross-track Pixels	29 & 32	Based on band
Pixel Size	62.5 & 125 microns	Based on band
Integration Time	167 msec	1 pixel smear at Ganymede
Spectral Channels	12	Center frequency limit for spectral resolution of 2
Number of Sensors	3	Two-fold global coverage in 30 days
Sensor Mass	36 kg	100 km altitude
Sensor Power	50 W	100 km altitude
Sensor Data Rate	72.8 kbps	12 channels, 10 bit system
Pointing Stability	1.31 mrad/sec	Slowest ground speed at Europa
Technology Development	None	
Estimated Technology Development Time	None	
Estimated Instrument Development Time	53 months	Analogy to MO/THEMIS and MGS/TES

Table 6.0-4: Baseline Laser Altimeter Performance Summary

Baseline Laser Altimeter Performance	Design Description	Rationale
Receive Telescope FOV	15	Two-fold global coverage in 30 days
Detection	Static Nadir Pointing Receive Telescope	Accommodates scanning beam
Receive Telescope Optical Speed	2.67	
Focal Length	40 cm	300 m GSD at 100 km
Aperture Size	15 cm	Maximize SNR
Detector	Avalanche Photo Diode	2000 1 micron photons per pulse
Design	Bistatic	MOLA / GLAS
Scanning Approach	Multifaceted rotating prism	Beam Scan Rate
Laser	End-pumped slab design	High power, short pulse width, high pulse rates
Number of Sensors	1	Two-fold global coverage in 30 days
Sensor Mass	44 kg	100 km altitude
Sensor Power	1.4 kW	100 km altitude
Sensor Data Rate	1 Mbps	Estimate to obtain required measurement
Pointing Stability	0.183 mrad/sec	Slowest ground speed at Europa
Technology Development	Cooling, receive telescope, scanning prism, rad hard detectors	
Estimated Technology Development Time	36 months	Higher performance, rad hard detectors
Estimated Instrument Development Time	53 months	Analogy to MOLA, GLAS

Table 6.0-5: Baseline Laser Reflection Spectrometer Performance Summary

Baseline Laser Spectrometer Performance	Design Description	Rationale
Receive Telescope FOV	15	Two-fold global coverage in 30 days
Detection	Static Nadir Pointing Receive Telescope	Accommodates scanning beam
Receive Telescope Optical Speed	2.67	
Focal Length	40 cm	300 m GSD at 100 km
Aperture Size	15 cm	Maximize SNR
Detector	Dispersive Prism and HgCdTe Array	2000 1 micron photons per pulse
Design	Similar to Differential Absorption Lidar (DIAL)	
Scanning Approach	Multifaceted rotating prism	Bean Scan Rate
Laser	Diode laser stack with individually mounted lenses	Enables incoherent superposition of many laser diodes in the far field.
Number of Sensors	1	Two-fold global coverage in 30 days
Sensor Mass	49 kg	100 km altitude
Sensor Power	0.7 kW	100 km altitude
Sensor Data Rate	1 Mbps	Estimate to obtain required measurement
Pointing Stability	1.31 mrad/sec	Slowest ground speed at Europa
Technology Development	New development, transmit/receive coordination, receive dispersive prism	Components exist, instrument needs to be properly architected
Estimated Technology Development Time	36 months	Transmit/receive coordination
Estimated Instrument Development Time	>62 months	Analogy to ALIAS

Table 6.0-6: Baseline Interferometric SAR Performance Summary

Baseline Interferometric SAR Performance	Design Description	Rationale
Antenna	2 ESA	Interferometry
Duty Factor	0.2	Coverage, Pulse width
Frequency	35 GHz	JIMO Forum
Bandwidth	58 MHz	
Minimum PRF	2.776	
Swath Width	60 km	Typical Grazing Angles
Number of Sensors	1	Two-fold global coverage in 30 days
Sensor Mass	322 kg	100 km altitude
Sensor Average Power	1.7 kW	100 km altitude
Sensor Data Rate	55.9 Mbps	4 Bit BAQ
Pointing Stability	7.1 mrad/sec	Slowest ground speed at Europa
Technology Development	High power, space qualified Ka band transmitters, antenna jitter isolation, on-board data processing	
Estimated Technology Development Time	36 months	High power, space qualified Ka band transmitters
Estimated Instrument Development Time	> 76 months	Analogy to ERS-1, ERS-2, SRTM, ASAR

Table 6.0-7: Baseline Polarimetric SAR Performance Summary

Baseline Polarimetric SAR Performance	Design Description	Rationale
Antenna	Cylindrical Reflector	Polarimetry
Duty Factor	0.1	Coverage, Pulse width
Frequency	3 GHz	JIMO Forum
Bandwidth	52.8 MHz	
Minimum PRF	0.893 kHz	
Swath Width	60 km	Typical Grazing Angles
Number of Sensors	1	Two-fold global coverage in 30 days
Sensor Mass	127 kg	100 km altitude
Sensor Average Power	200 W	100 km altitude
Sensor Data Rate	36.737 Mbps	4 Bit BAQ
Pointing Stability	2 mrad/sec	Slowest ground speed at Europa
Technology Development	High power, space qualified transmitters, on-board data processing	
Estimated Technology Development Time	36 months	High power, space qualified transmitters,
Estimated Instrument Development Time	> 81 months	Analogy to Envisat-ASAR, SIR-C

Table 6.0-8: Baseline Radar Sounder Performance Summary

Baseline Radar Sounder Performance	Design Description	Rationale
Antenna	10 m Yagi & 73 m Dipole	Yagi: > 10 MHz, Dipole < = 10 MHz
Duty Factor	0.27	Coverage, Pulse width
Frequency	3, 5 10, 30, 40, 50 MHz	Multiple interleaved frequencies, uncertainty in subsurface properties
Pulse Length	300 microseconds	
PRF	150 Hz	
Number of Sensors	1	Two-fold global coverage in 30 days
Sensor Mass	117 kg	100 km altitude
Sensor Average Power	2.7 kW	100 km altitude
Sensor Data Rate	5.18 Mbps	
Sensor Pointing Stability	None	Very large beamwidth
Technology Development	High power, space qualified transmitters	
Estimated Technology Development Time	36 months	High power, space qualified transmitters
Estimated Instrument Development Time	39 Months	Analogy to MARSIS, SHARAD

Table 6.0-9: Baseline Radio Sounder Performance Summary

Baseline Radio Sounder Performance	Design Description	Rationale
Antenna	72 m Dipole	Yagi: > 10 MHz, Dipole < = 10 MHz
Duty Factor	0.27	Coverage, Pulse width
Frequency	400 kHz - 2 MHz Sweep	Uncertainties in Jovian moon ionospheres
Pulse Length	300 microseconds	
PRF	150 Hz	
Number of Sensors	1	Two-fold global coverage in 30 days
Sensor Mass	79 kg	100 km altitude
Sensor Average Power	85 W	100 km altitude
Sensor Data Rate	0.13 Mbps	
Pointing Stability	Coarse	Very large beamwidth
Technology Development	None	
Estimated Technology Development Time	None	
Estimated Instrument Development Time	34 months	Analogy to Alouette 1, Alouette 2, ISIS 1, ISIS B

Table 6.0-10: Key Technology Developments

Technology Development	Time to TRL 5 (Months)	Instrument Enabled								Instrument Subsystem Enabled								Comments		
		VIS/IR Spectrometer	Thermal Mapper	Laser Altimeter	Laser Spectrometer	InSAR	Polarimetric SAR	Radar Sounder	Radio Sounder	Instrument Processing Electronics	Instrument Power Electronics	Instrument FPAs, Detectors, Emitters	Instrument C&DH	Instrument Thermal Control	Instrument ADCS	Instrument Structure	Instrument Data Rate		Instrument Shielding	
Light Weight Radiation Shielding	UNK	x	x	x	x	x	x	x	x									x	Possible 2007 time frame	
High Performance Rad Hard Electronics	UNK	x	x	x	x	x	x	x	x		x		x		x			x	x	SiC a candidate in 2007 time frame
Lightweight Active Cooling	36	x	x	x									x							
High Density Linear Variable Filter	84	x																		Necessary to achieve spectral resolution of 300.
Rad Compensated Nd:YAG Lasers	24				x															
Receive Telescope Design	24			x	x															
Beam Transmit and Receive Coordination	24			x	x															
Rad Hard Detector Arrays	24	x	x	x	x					x										
Scanning Prisms	36			x	x															
Dispersive Prisms	36				x															
Space Qualified High Power Ka Band Transmitters	36					x	x	x		x	x								x	
Space Qualified Processors 1 GFLOP	36					x	x	x		x									x	
Rad Hard Dielectric Structures	UNK	x	x	x	x													x		Likely in 2007 time frame
Antenna Jitter Isolation	36					x	x												x	
Data processing algorithms	36	x		x		x	x	x												x
Diode Laser Bars With Integrated Microlenses	24			x																

7.0 Visible and Infrared Imaging Spectrometer

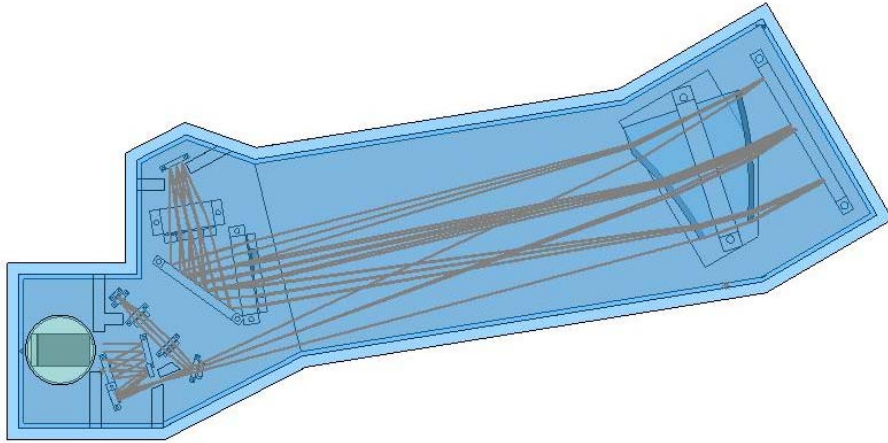


Figure 7.0-1: Visible and IR imaging spectrometer.

7.1 Science Utility

Near IR observations will detect various chemical species of the icy satellites. The IR Spectrometer will support observations in the wavelength range of 1 to 5 microns with a spectral resolution of 300 and a spatial resolution of 100 meters/pixel or better. It will support spatial coverage of 90% or greater with repeated coverage to look for changes.

The Visible Imager will make observations in the wavelength range of 0.4 to 0.5 microns with spectral resolution of 40 and spatial resolution of 100 meters/pixel or better. It will support spatial coverage of 90% to search for short-lived species and repeated coverage to look for changes.

7.2 Design Drivers and Options Examined

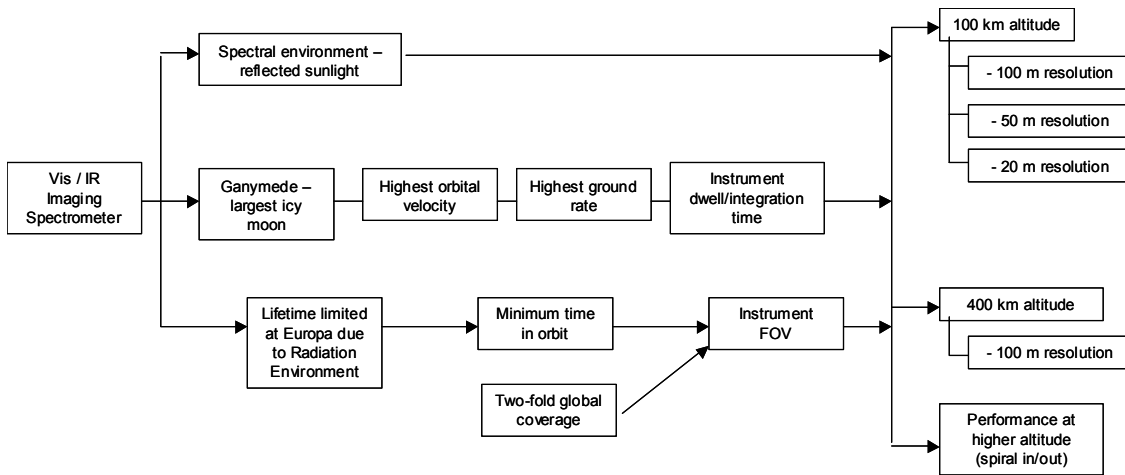


Figure 7.2-1: Visible and infrared imaging spectrometer trade space.

The design drivers for the spectrometer instrument and trade space options examined are shown in Figure 7.2.1. There were 5 main design drivers for the spectrometer; 1) Europa's radiation environment, 2) ground speeds over Ganymede, 3) the lowest albedo of Callisto (0.19), 4) 100m GSD or resolution, and 5) the breakdown of the IR band into 300 spectral bands.

The high radiation environment of Europa had a large design impact on the instrument field of view and the mass. Due to a time in orbit on the order of 30 days, the required field of view is 14.8 degrees. The 14.8-degree field of view was achieved with a non-reimaging fore optics and a spectrometer reimaging the slit. Shielding, with a very high mass, was used to encase the instrument for protection against electrons trapped in the Jovian environment. An aperture cover was utilized to protect the instrument when the sensor was non-operational. The cover is currently designed to have some, although reduced, performance in the event of a cover removal mechanism failure.

The other four drivers affect the signal-to-noise-ratio (SNR). Factors limiting SNR were ground speed, spectral bandwidth, ground footprint, and f-number. The ground speed is based on a nadir viewing push-broom sensor. For the largest moon, Ganymede, the orbital velocity, and ground rate are at their peak, and the dwell time is at the minimum. To reduce ground speed and improve SNR, backscanning could be designed in; however, this adds a high degree of technical complexity and risk, as well as reduces coverage per orbit and introduces a more complex data acquisition scenario requiring more detailed command planning.

The baseline spectrometer spectral breakdown is 300 channels for the 1-5 microns IR band, and 3 channels for the 0.4-0.5 micron visible band. Spectral bandwidth is still a variable to be traded with some room for improvement if the number of bands were to be reduced. The SNRs in the 4-5 micron bands are quite low, and data may be difficult to extract. These bands could be combined in a single band with higher SNR, eliminated altogether if the data for this spectral region were determined to be a low priority.

Ground Sample Distance (GSD) drove altitude, focal length and pixel size. The 100-meter GSD requirement coupled with the 100-kilometer altitude, and 27-micron pixel size established the 27 mm focal length. The SNR requirements drove aperture diameter to its maximum limit based on the f-number lower limit of 2.7 for this instrument. The baseline design is at the f-number lower limit with no room for improvement other than technological gains. This study included trades for sensors with 50 and 20-meter resolution (100km altitude), and one design excursion for 100 meter resolution from a 400 kilometer altitude.

A sensor meeting these performance goals has been designed and evaluated. In addition, performance of the baseline sensor and the 400-kilometer sensor version were evaluated at various “spiral in” positions. Performance was evaluated for the sensors at 100, 1000, 5000, and 10000-kilometer altitudes.

7.3 Baseline Instrument Description

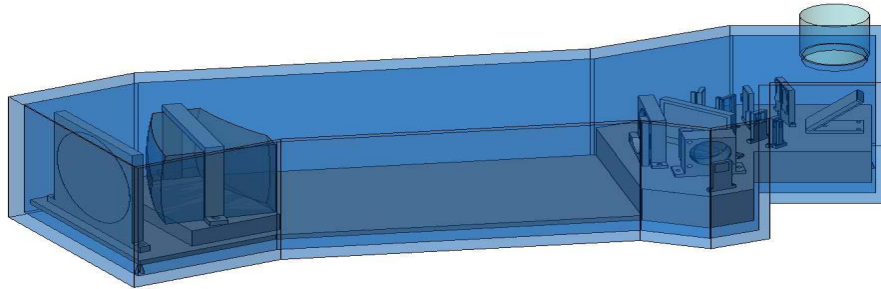


Figure 7.3-1: Infrared imaging spectrometer.

7.3.1 Radiometry

This instrument is configured for push-broom imaging from an altitude of 100 km. The maximum ground speed at this altitude is 1800 m/sec at Ganymede. Integration time is one sample per dwell (1 pixel of smear) at the maximum ground speed.

The imager swath width is 14.8 degrees, in order to support the goal of a global map of Europa. It has a GIFOV of 100 m on the target surface. Note that since the imager detects reflected light from the Sun; it can only be used on the Sun side of the orbit, and its use is limited to about half of each orbit. The 14.8-degree swath width supports a global map of Europa within 30 days.

A three-color visible imager has three bands across the 0.4 to 0.5 micron wavelength range. The imaging spectrometer is to cover the spectral band from 1 to 5 microns with 300 spectral bands across that range. This amounts to an average spectral sampling interval of 13 nm/pixel. For the maximum illumination configuration, the solar constant at Earth was scaled by the square of the ratio of the distances of the Earth and Jupiter from the Sun. The Sun was assumed to have a spectral distribution equivalent to a 6000 K black body. The Icy Moons were assumed to have a minimum expected albedo of 0.2, which is the case for Callisto. Assuming the moons are Lambertian scatterers, the spectral radiances of the target range from 203 micro-Watts/cm²-sr-micron at the 1-micron wavelength to 1.22 micro-Watts/cm²-sr-micron at 5 microns. The moons have been calculated to have negligible self-emissions at wavelengths up to 5 microns.

The imager has a single optical system using an all-reflecting four-mirror telescope operating at a maximum optical speed of F/2.7. A prism-based spectrometer is placed at the focus of the telescope. Hybrid silicon PIN diode arrays are used for the three channel visible imager (rather than CCD's) for their radiation resistance. The visible imager has a set of 3 linear arrays with the same effective pixel size as the IR spectrometer and placed adjacent to the entrance slit of the IR spectrometer at the focus of the telescope. The focal length of the telescope is determined to be 27 mm, and the diameter of the telescope entrance pupil is 10 mm. The number of cross-track pixels needed to cover the 14.8-degree swath is 258. This is calculated by dividing 14.8 degrees by the angular pixel size of 1 milliradian (0.0573 dg). An even number of 260 pixels is used in the design. The integration time for 1 pixel of smear is about 52.55 msec at the fastest expected ground speed (at Ganymede). This is calculated by dividing the 100-meter GIFOV by the ground speed of 1800 m/sec.

The detector material selected for the instrument is HgCdTe made of 5-micron cutoff material. Using this material, it is relatively easy to build arrays of high quality with good operability in the focal plane, and to tune the cutoff wavelength. Using a detector array with 27 micron pixels should allow most of the energy from a single point on the target into one pixel, and therefore give good ensquared energy performance for an optical system near the diffraction limit. The optical Q for this concept is calculated as 0.5.

A minimum spectrometer detector array size of 260 cross-track pixels by 300 spectral is needed to meet the resolution requirement at 100 km. The visible imager uses a set of 3 linear arrays with 260 pixels in the cross-track direction and 1 pixel in the in-track direction. The HgCdTe focal plane is cooled to 105 °K or below to keep dark current to acceptable levels.

The raw data rate from one spectrometer is 20.8 Mbits/sec. This assumes a 14-bit system and a 56 msec integration time. The three-band visible imager would add another 0.2 Mbits/sec, and the total data rate for one imager would be 21.0 Mbits/sec.

The total dose on the focal planes will be kept below 150 krad via shielding. Radiation issues are discussed in more detail in a separate section.

The spectral radiances of the dimmest target range from 203 micro-Watts/cm²-sr-micron at the 1-micron wavelength to 1.22 micro-Watts/cm²-sr-micron at 5 microns. The number of signal electrons for the minimum radiance in this band (5 micron wavelength) would be 7014 assuming a 13 nm bandwidth for the channel, a system transmittance of 0.5, and a quantum efficiency of 0.8. The ideal SNR (if it were photon noise limited) would be 84:1. This design has less SNR when other noise sources and reduced illumination levels at less-than-optimum portions of the swath or orbit are taken into consideration. Work is in progress to explore modifications to the design that would improve the SNR for the IR spectrometer. A summary description of the baseline can be found in

Table 7.4.1 under case 1. A graph of the SNR vs. waveband can be found in Figure 7.4.1.

The SNR for the visible channel is expected to be on the order of 1150:1 for each of the 3 bands within .4 to .5 microns. This is based on similar detector input parameters to the IR band but with inband reflected solar radiance adjusted for a larger bandwidth of approximately 33 nm for each of the 3 bands in a region of the blackbody curve for the lower wavelengths.

7.3.2 Optical Design

The optical design of the spectrometer consists of a four-mirror off-axis non-reimaging telescope with a 10 mm aperture located on the tertiary mirror as the fore optics with a prism based spectrometer in the aft. The mirrors are constructed of beryllium to reduce radiation effects. The slit is reimaged using calcium fluoride transmissive elements. The system f-number is 2.7, and the focal length is 27mm. The FOV is 14.9 degrees to cover the swath width of 260 km from a 100km altitude. The 1 to 5 micron band is dispersed over 300 pixels in the inscan direction with the dispersive calcium fluoride prism, for simultaneous viewing in all the spectral channels. Figure 7.3.2.1, below, shows the optical layout of the imaging spectrometer. The dispersion is depicted in Figure 7.3.2-1.

The visible channel is split off just after the intermediate image with a dichroic beamsplitter. The three visible channels are generated with 3 strip filters at the focal plane. Each filter covers one row or strip of 27-micron pixels. Figure 7.3.2-2a and b are CodeV optical raytrace diagrams, YZ and XZ profiles respectively. Not shown in the raytraces is a flat fold mirror added to the front end of the optical train for better orientation of the bench onto of the payload platform of spacecraft.

The aperture cover incorporates a 4.5 cm thick window. It is used to shield against nuclear radiation, primarily, trapped electrons encountered in the Jovian environment during periods where data are not collected. The aperture will be opened for data collection. The choice of calcium fluoride will allow some signal throughput if the aperture removal mechanism fails. An aperture cover made of 45 mm of calcium fluoride serves primarily as protection against the severe radiation environment when the sensor is non-operational. This material was chosen as a safety precaution. If the aperture removal mechanism fails, the instrument will still be able to partially operate. Throughput is reduced by roughly 21% for 1 to 5 microns. The SNR for 1 to 5 microns will be reduced by 11%. The cover will suffer radiation damage as specified in the radiation Section 7.3.6, but would allow degraded throughput with reduced SNR should the removal mechanism fail.

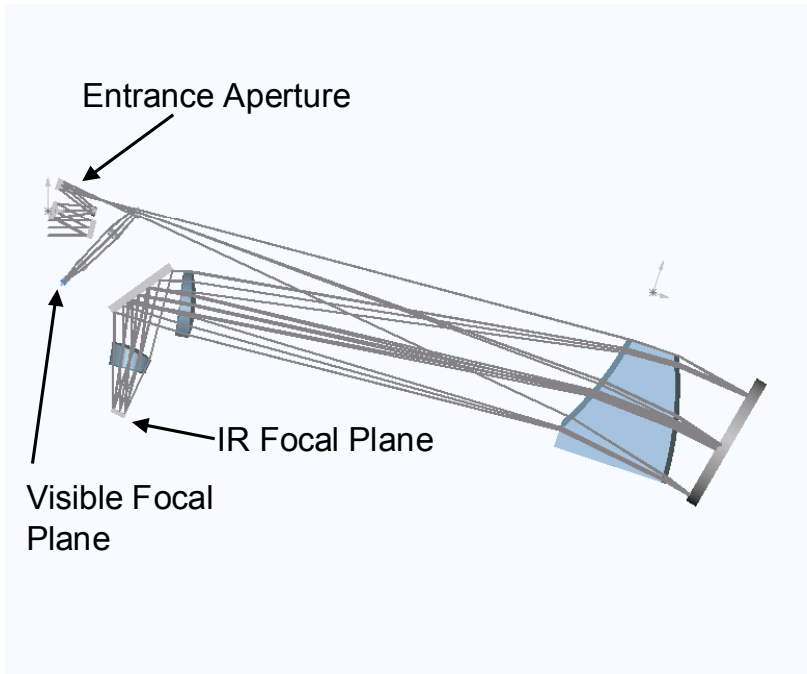


Figure 7.3.2-1: Imaging spectrometer view of optical configuration in dispersive plane with visible channel.

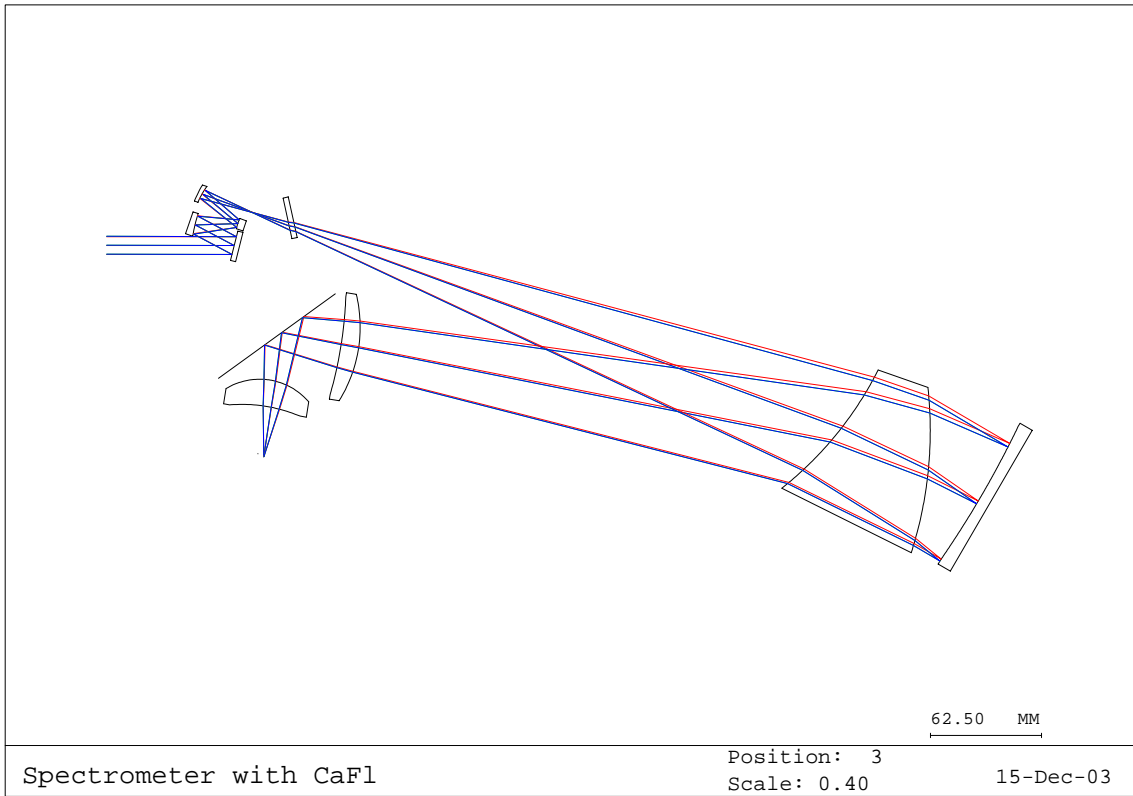


Figure 7.3.2-2: Raytrace (YZ profile) of shared front-end optics with only IR backend, and only one wavelength visible.

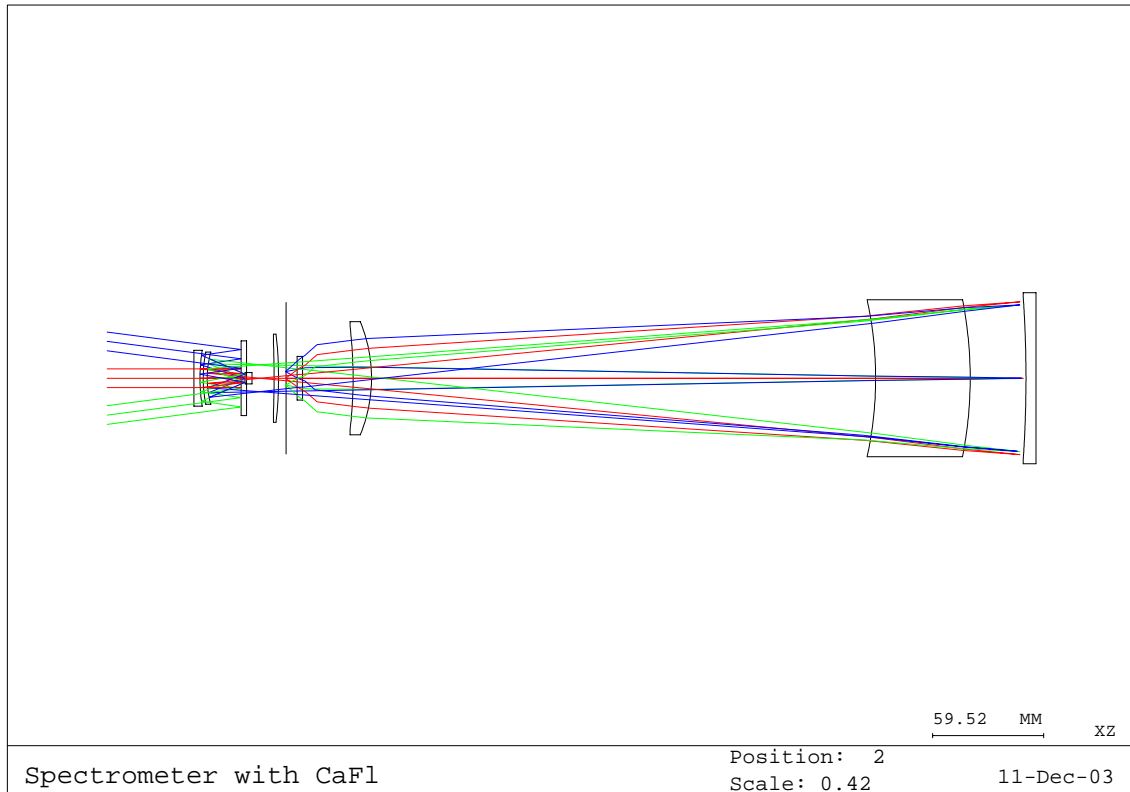


Figure 7.3.2-3: Raytrace (XZ profile) of shared front-end optics with only IR backend and only one wavelength.

7.3.3 Processor

The processors for the spectrometer were chosen based on the data rate requirements seen in Table 7.3.3-1 below.

The key circuits for the spectrometer are AD9245 A/D (14 bit) converter and Xilinx Vertex-II Pro FPGA processing chip for digital signal processing and will be located approximately 6 inches from the focal plane.

One 14.8-degree spectrometer has a maximum sample rate of 21 Mpixels per second. The focal plane power of 100 mW is required. The analog processor has a power requirement of 800 mW and a volume of 600 cubic centimeters, and a mass of mass 1.2 kg.

The combined digital processor for spectrometer and mapper has a power requirement of 5.5 W, and a volume of 300 cu cm, and a mass of 0.6 kg.

The baseline spectrometer design consists of redundant analog and digital processors for increased reliability. Totals for power and volume are summarized in the table below. Mass and volume would double to account for the redundant

processors. It is assumed only one processor type would be functioning at any given time, hence the power does not double.

Table 7.3.3-1: Data Rate Considerations

Parameter (Units)	Vis	IR	Total
Cross scan pixels	260	260	260
Inscan pixels	3	300	303
Bits per pixel	14	14	14
Integration time (s)	0.05255	0.05255	0.05255
Data rate (Mbps)	0.2	20.8	21.0

Table 7.3.3-2: Processor Mass, Power and Volume

Parameters Units	Mass (kg)	Power (W)	Volume (cu cm)
Focal Plane	*	0.1	*
Analog Signal Processors	1.2	0.8	600
Digital Signal Processors	0.6	5.5	300
Total	1.8	6.4	900
Total with Redundant	3.6	6.4	1800

*Logged with optics and structure.

7.3.4 Structural Design

The spectrometer is an optical instrument consisting of seven mirrors and six lenses and one beamsplitter. The assembly is enveloped by a 0.3” thick Tungsten housing, which provides radiation shielding. While this housing is a stout structural component and could support the various lenses and mirrors, mounting the optics directly to this outer shell has the potential to induce unwanted deformations onto the optics from thermal imbalances. Therefore, to minimize the optical distortions from thermal gradients and to provide a common reference surface for all the optical elements, an optical bench is provided.

The spectrometer bench is assumed to be a zero-coefficient of thermal expansion (CTE) and zero-coefficient of moisture expansion (CME) tailored honeycomb composite plate with 0.15-inch Graphite Epoxy facesheets and 0.5-inch thick 5/32-5056-0.001 3.8 pcf Aluminum honeycomb core. This bench design was created to ensure a first mode natural frequency of greater than 100 Hz – which will provide a stiffness measure known to be conservative for most optical designs. Also, several stand-off structures are necessary to mount to the optical bench at their necessary elevations. It is assumed that these components are thin-shelled structures manufactured of zero-CTE/CME Graphite Epoxy composites.

The mounting schemes for the standoffs and the optical components are intended to impart no stresses (and thus no ancillary distortions) across interfaces. The Beryllium mirrors are kinematically attached to embedded inserts

on the optical benches or to the composite stand-offs. The bench is kinematically mounted to the Tungsten block via three sets of Invar bi-pods. This study assumes all attachment mechanisms to be Invar flexures.

Either because of their shape or because of extreme sensitivity to local material mismatches, several of the Beryllium mirrors and the Calcium Fluoride lenses on the spectrometer cannot directly attach to the embedded inserts on the optical bench. These components require a separate support housing. Depending upon function and size of these components, different types of mounting schemes are used for this purpose, as shown in Figure 7.3.4.1. Lenses are attached to their bench mounts via a Titanium strap or clamp that wraps around the outer perimeter of the lens. Smaller Beryllium mirrors are sandwiched between two Titanium blocks, which are then kinematically mounted to the bench via embedded inserts. Larger Beryllium mirrors are attached to a separate Beryllium block at three tabs and then kinematically mounted to the bench. It is important to note that the detailed analyses necessary to determine the most appropriate mounting scheme was not performed for this study, but the assumed mounts are common options and good representations of the final design.

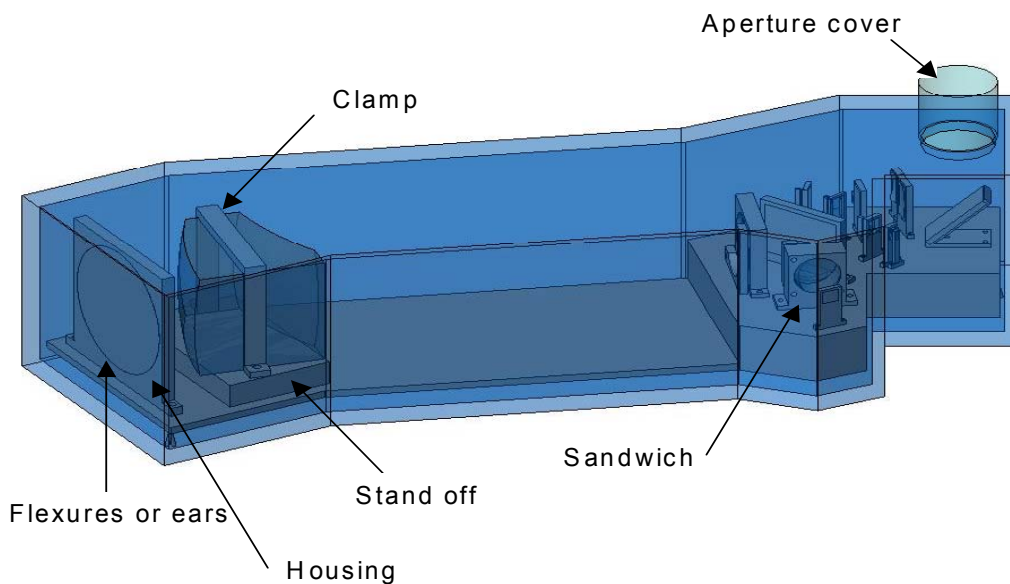


Figure 7.3.4-1: Baseline spectrometer with structural components.

7.3.5 Thermal Design

The imaging spectrometer is an individual unit dissipating roughly 100 mW at the focal plane array (FPA). The temperature requirement at the FPA is 105 K. Because of the relatively high temperature of the device and the relatively low

expected cooling requirements, a standard cryoradiator has been selected for the cooling objectives.

The cryoradiator will remove heat directly from the housing of the spectrometer, and will most likely be interfaced to the housing with a single conventional heat pipe or small radiator. A small heater will be used with each of the focal planes to maintain tight temperature control. Due to the sensitivity of the cryoradiator to environmental heat loads, a carefully designed solar/planet shield will need to be fitted to the cryoradiator to ensure its cold-temperature operation.

Assuming no environmental loading (perfect shielding), the cryoradiator area was calculated to be 0.080 m^2 . The corresponding radiator mass (including heat pipe and shielding) is between 1 and 2 kg. The parasitic heat loads are expected to be low, on the order of approximately 200 mW, based on a relatively simple radiation calculation using the dimensions of the spectrometer housing. The parasitic loads are expected to be minimal because the environmental temperature will likely be very close to the instrument target temperature of 105 K. Because the spectrometer housing has a fairly large footprint on the optical bench, however, conduction heat transfer from the bench could be significant in the presence of an appreciable bench-to-housing or bench-to-optics temperature gradient. High thermal resistance filler materials may be used to minimize bench-to-instrument heat transfer, and hence keep radiator size and weight to a minimum.

A uniform coating of high emissivity material or paint on the inside of the spectrometer housing enclosure should be used to help distribute interior heat effectively, achieving thermal uniformity for the optical components. A high thermal conductivity housing material will also help to create a thermally uniform environment within the enclosure. The outer surface of the housing will probably be shielded with multi-layer insulation to prevent environmental heat gains/losses by radiation.

An alternative possibility to the cryoradiator solution is to incorporate a pulse tube cryocooler. The main disadvantage is that at temperatures in the range of 100 K, most pulse tube models are optimally designed to remove on the order of several Watts of heat—an order of magnitude greater than the heat removal required for the spectrometer. Since the actual FPA dissipation is small and parasitic heat loads are anticipated to be low as well, the cryocooler will be operating in a regime of very low efficiency.

From heritage data, at a cold tip temperature of 100 K, for 300 mW of total cooling (the sum of the cooling requirement for the instrument plus assumed parasitic losses), the total specific power was extrapolated to be between 35 and 45 W/W and the total specific mass was estimated to be between 12 and 15 kg/W. These estimates yielded a total mass (thermo-mechanical unit plus

control electronics) of 3-5 kg and a total input power (to both the thermo-mechanical unit and control electronics) of 11-14 W.

The imaging spectrometer system also includes a digital signal processor (DSP) and analog signal processor (ASP). The DSP dissipates 5.5 W of heat, and the ASP dissipates 800 mW of heat. The operating temperature range of both processors is between 230K and approximately 300 K. A simple spreadsheet thermal analysis was used to determine whether insulation/heaters are required for the processor units. A mean environmental temperature of 100 K was assumed, and the temperature drop from the processor units to the optical bench below was assumed to be 15 K. Somewhat conservative values were assumed for surface emissivities, contact thermal resistances, and insulation thermal conductivity.

It was concluded that the DSP should be able to operate within its desired temperature range without any insulation, achieving a steady-state temperature of near 300 K assuming a steady 5.5 W dissipation. Still, heaters may be required for initial turn on. The ASP, however, will need to be insulated heavily (several inches of blanketing required) to ensure that it remains at its minimum specified temperature of 230 K. Positioning the ASP unit close to the DSP should also aid in keeping the ASP warm.

7.3.6 Radiation

The aperture cover, refractive lenses, and prism are vulnerable to permanent and transient radiation effects. All of the transparent optical elements can suffer darkening when exposed to high ionizing doses. For the imaging spectrometer, the only optical dielectric used is calcium fluoride, which can experience darkening due to color center formation. The effect is most pronounced at the short wavelength end of the spectrum. Calcium fluoride can also experience subsurface charging resulting from the buildup of charged particles that are stopped by the material. The aperture cover, being directly exposed to the external environment, is most vulnerable to these effects. Surface charging of the aperture cover could make this material undesirable since conductive coatings that might be used to mitigate surface charging would degrade performance in the infrared. (See Figure 7.3.4.1 for view of aperture cover)

Calcium fluoride will scintillate when exposed to ionizing particles; however, the process is not efficient unless the calcium fluoride material is doped. Cerenkov emission is limited by the refractive index of calcium fluoride, 1.47, and its effect, if any, will be limited to the short wavelength portion of the optical spectrum.

Both the visible and infrared focal planes are vulnerable to nuclear and ionizing radiation. Permanent damage in the detector readout circuitry or detector material can be severe in the mission environment. Readout circuit technology is expected to be available to meet mission radiation performance requirements.

The detector materials, both silicon and HgCdTe, are vulnerable to the displacement damage caused by high-energy electrons, protons and neutrons, all of which are components of the JIMO environment. The primary manifestations of displacement damage are loss of responsivity and increased dark current. Mitigation of these effects is difficult, but techniques are available that hold promise for meeting mission requirements. Focal plane detector development and testing will be required to assure that suitable focal planes will be available for this mission.

Special effort will be required to provide for a proper focal plane array shielding design. Ultimately, compound-shielding techniques will probably be required where 2 or more layers of alternating materials comprise a laminate that is optimized for shielding against a targeted radiation environment, in this case electrons.

Proposed designs will require detailed radiation transport analyses to assure that direct or indirect leakage paths do not exist that would spoil the performance of the shield. A sector analysis approach to estimating shielding performance will likely produce misleading results because the intense electron environment expected during data collection will access the focal plane array through the folded optical path. The radiation shielding analysis that is performed on each electro optical instrument will have to account for transport through indirect paths such as folded reflective optics.

Spurious transient focal plane responses will be induced by environmental electrons and secondary photons that could severely degrade the quality of data collected in both the visible and infrared focal plane arrays. Data from JPL indicate the total dose expected inside 2 inches of aluminum shielding after the 172 day mission exposure to the Jovian trapped electron environment is about 10^5 rad (Si), or an average of 6.7×10^{-3} rad (Si)/sec. In silicon, this corresponds to the generation of about 0.4 electrons/ $\mu\text{m}^3/\text{s}$ or about 307 electrons/pixel/integration time for a pixel that is $27 \times 27 \times 20 \mu\text{m}^3$, typical of the what would be expected for the imaging spectrometer visible focal plane array. Because of its smaller band gap, a HgCdTe focal plane array that is 15 μm thick and that has a long wavelength cutoff of 5.5 μm would experience an average of 640 electrons/pixel/integration time for the integration time of 26 ms. The expected average amplitude of radiation-induced transient responses will be larger when only affected pixels are considered because of the particulate nature of the energy deposition.

The noise floor that might be expected for these detectors is on the order of 70 electrons, so radiation transient mitigation techniques are desired. Perhaps the most direct method that can be considered is spatial and temporal over sampling, both of which are accompanied by weight and power penalties. Circumvention in the unit cell can be considered as an alternative; however, readout technology development would be required in order to implement this method. A more

detailed analysis of radiation transients is not warranted until after radiation transport issues have been explored in greater detail. Radiation transport analyses are highly dependent on the geometry, material selection and configuration of the instrument and electronics, and generally cannot be performed until a design at the box and layout level exists.

The prism material will emit Cerenkov radiation in the intense Jovial electron environment, but the relatively low refractive index of CaF at short wavelengths ($n < 1.47 @ 400 \text{ nm}$) implies that the effect will not be extreme. Data collected at the short wavelength end of the visible spectrum could be affected however. Doped CaF is an efficient scintillator, but high purity CaF is not, so scintillation of the prism should not present a problem. In general, spurious light emission from the prism can be minimized by minimizing the total volume of material comprising the prism.

For this prototype design, radiation shielding made up of 7.3 mm thick tungsten will be placed around and throughout the sensor to reduce electrons from entering and to dampen effects of radiation entering through the aperture. An aperture cover is used to reduce radiation when the sensor is not operational. The aperture removal mechanism is shielded as well to reduce damage to it.

7.3.7 System Summary

Each of the 2 sensors is approximately 74 kg in mass, and fits within a box 15.5cm wide by 56.8cm long and 19 cm high.

Table 7.3.7-1: Spectrometer System Summary

Spectrometer System Summary		
Parameter	Units	Result
Mass	kg	73.4
Power (peak)	W	6.3
Duty cycle	%	80
Power (average)	W	5.0
Maximum Dimensions	cm	15.5 x 56.8 x 19
Datarate	Mbps	21.00
Wavelength ranges	microns	.4-.5 and 1-5
FOV	degrees	14.9
Resolution	mrad	1.0

Densities were applied to the parts in the Computer Aided Design (CAD) model in order to approximate the mass. The following table shows a breakdown of each part and its mass. Power from appropriate components is summarized in Table 7.3.7-1 as well. As seen in Table 7.3.7-2, the required radiation shielding dominates the spectrometer mass totaling to about 90% of the total mass.

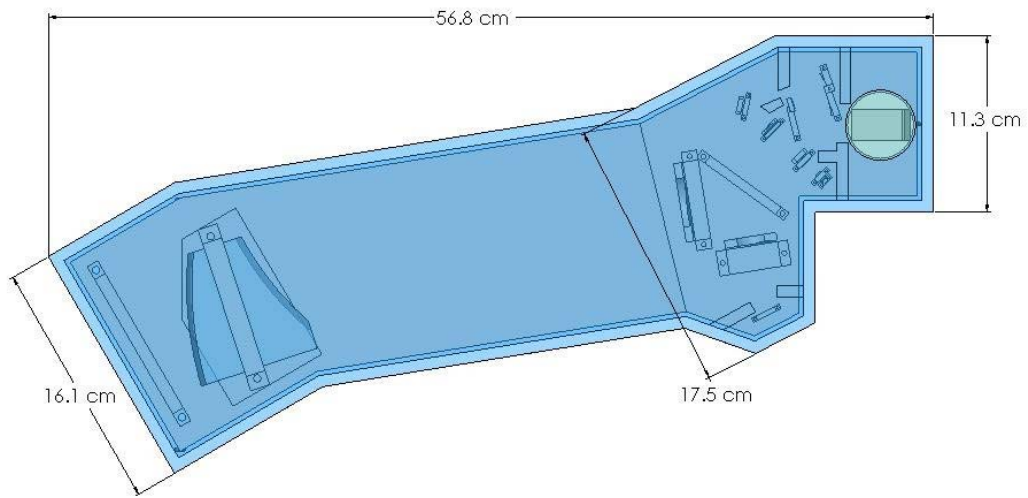


Figure 7.3.7-1: Spectrometer external dimensions – top view.

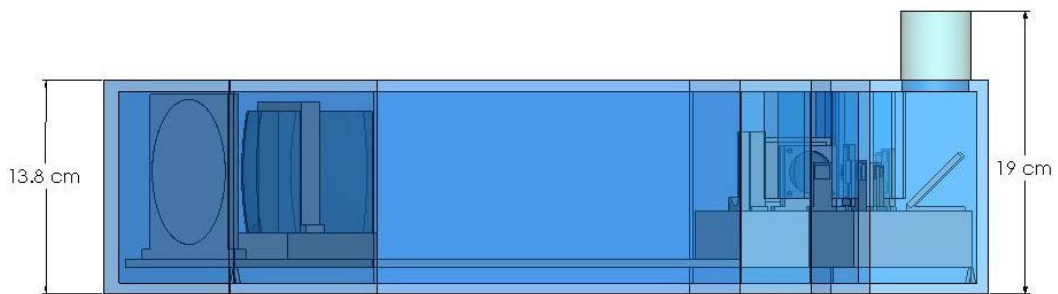


Figure 7.3.7-2: Spectrometer external dimensions – side view.

Table 7.3.7-2: Spectrometer Mass and Power Summary and Breakdown

Spectrometer Summary				73.4kg	6.3W
Mass Breakdown					
		#	Mass (ea.)	Mass (tot.)	Power (ea.)
			grams	grams	W
Total				73447.8	6.3
Optics				1,369.4	
<i>Shared</i>					
	Pointing Mirror	1	6.4985	6.5	
	Primary Mirror	1	2.9228	2.9	
	Tertiary Mirror	1	0.1807	0.2	
	Secondary Mirror	1	2.3713	2.4	
	Quaternary Mirror	1	1.2454	1.2	
	Beamsplitter	1	1.5598	1.6	
<i>Visible</i>					
	Vis Len 1	1	2.3836	2.4	
	Vis Len 2	1	1.2285	1.2	
	Vis Len 3	1	0.4014	0.4	
	Vis FPA	1	0.0759	0.1	
<i>IR</i>					
	Prism	1	1175.3409	1,175.3	
	IR Mirror 1	1	86.8366	86.8	
	IR Lens 1	1	42.8815	42.9	
	IR Mirror 2	1	20.3997	20.4	
	IR Lens 2	1	24.5497	24.5	
	IR FPA	1	0.5273	0.5	
Shielding				64,532.9	
	External (box)	1	47460.1826	47460.1826	
	Internal	1	2373.0091	2373.0091	
	Electronics	1	14699.67	14,699.7	
Structure				3,945.5	
	Optical Bench	1	2039.5555	2,039.6	
	Bipod Mount	3	0.7102	2.1	
<i>Clamps</i>					
	Pointing Mirror	1	6.7395	6.7	
	Primary and Tertiary Mirrors	1	1.7969	1.8	
	Secondary Mirror	1	2.4685	2.5	
	Quaternary Mirror	1	1.8934	1.9	
	Beamsplitter	1	2.9982	3.0	
<i>Visible Clamps</i>					
	Vis Len 1	1	2.2417	2.2	
	Vis Len 2	1	3.4386	3.4	
	Vis Len 3	1	1.9771	2.0	
	Vis FPA	1	0.4376	0.4	
<i>IR Clamps</i>					
	Prism	1	45.9462	45.9	
	IR Mirror 1	1	55.451	55.5	
	IR Lens 1	1	42.6156	42.6	
	IR Mirror 2	1	8.8546	8.9	
	IR FPA	1	1.9478	1.9	
	IR Lens 2	1	48.1713	48.2	
<i>Aperture</i>					
	Aperture Cover	1	224.6067	224.6	
	Aperture Cover Mechanism Structure	1	152.26	152.3	
	Aperture Cover Motor	1	1300	1,300.0	
	Optical Mounts		* included in optics mass		
Electronics				3,600.0	
	Analog Processor	2	1200	2,400.0	0.8
	Digital Processor	2	600	1,200.0	5.5
Thermal				2,000.0	
	Radiators shared	1	2000	2,000.0	

7.4 Design Options

Several cases were examined to assess changes required to the payload for higher resolution on the ground. The cases compare the nominal 100 km case with 100 meter GSD to two new cases at 100 km altitude with 50 and 20 meter GSDs respectively. Also examined was a 400 km altitude case with 100 m GSD. The cases are shown in Table 7.4.1 below.

Case 1 is the nominal 100 km operating altitude case with 100 m ground sample distance. Case 2 maintains the same operating altitude, but reduces the ground sample distance to 50 m. Case 3 reduces the ground sample distance further to 20 m. Case 4 increases the operating altitude to 400 km while maintaining 100 m ground sample distance. Cases 1 and 4 were selected in order to assess design sensitivity at alternative science orbit altitudes. Cases 2 and 3 were chosen to illustrate the effects of going to higher ground sample distance at the nominal 100 km operating altitude.

As seen from Table 7.4.1, when comparing Cases 2 and 3 with Case 1, the aperture diameter and the focal length scale inversely with the GSD, and the f-number remains the same. The raw analog data rate scales generally as the inverse square of the GSD due to maintained swath angle and reduced integration time. The number of cross scan pixels goes up inversely with the GSD, and the integration time drops with a one-to-one ratio with the GSD.

Table 7.4-1: Sensor Trades for Sensors Tailored to GSDs and Altitudes

Case	#	1	2	3	4
GSD	(m)	100.00	50.00	20.00	100.00
Slant range (nadir)/altitude	(km)	100.00	100.00	100.00	400.00
Aperture Diameter	(cm)	1.00	2.00	5.00	4.00
Effective Focal Length	(cm)	2.70	5.40	13.50	10.80
Mass	(kg)	73	299	2059	1276
Power	(W)	6.30	12.60	31.50	6.30
f/#		2.70	2.70	2.70	2.70
FOV	(degrees)	14.90	14.90	14.90	3.73
Ground Swath - angle	(km)	25.86	25.86	25.86	26.00
Ground Swath - pixel count	(km)	26.00	26.00	26.00	26.00
Slit Scan Rate	(km/sec)	1903	1903	1903	1806
Fore Optics Temp	(K)	210.00	210.00	210.00	210.00
AFT Optics Temp	(K)	170.00	170.00	170.00	170.00
FPA size (spatial)	(n)	260	520	1300	260
FPA size (spectral)	(m)	300	300	300	300
FPA pixel size	(microns)	27.00	27.00	27.00	27.00
FPA material		HgCdTe	HgCdTe	HgCdTe	HgCdTe
FPA cut-off wavelength	(microns)	5.50	5.50	5.50	5.50
FPA temperature	(K)	105.00	105.00	105.00	105.00
FPA Frame Rate	(Hz)	19.03	38.06	95.15	18.06
FPA Integration Time	(msec)	52.55	26.27	10.51	55.37
Raw Analog Rate	(Mpix/sec)	1.48	5.94	37.11	1.41
Digital Encoding	(bits/pixel)	14.00	14.00	14.00	14.00
Raw Digital Rate	(Mbits/sec)	20.78	83.12	519.52	19.72

In Case 4, the f-number is maintained, requiring the focal length and aperture to go up by a factor of 4. This is one to one scaling with the altitude variation. The only other minor modification is an adjustment to the integration time due to the altitude change. In Case 4, the sensor performs much like Case 1 but is 4 times larger in most linear dimensions and 17 times more massive.

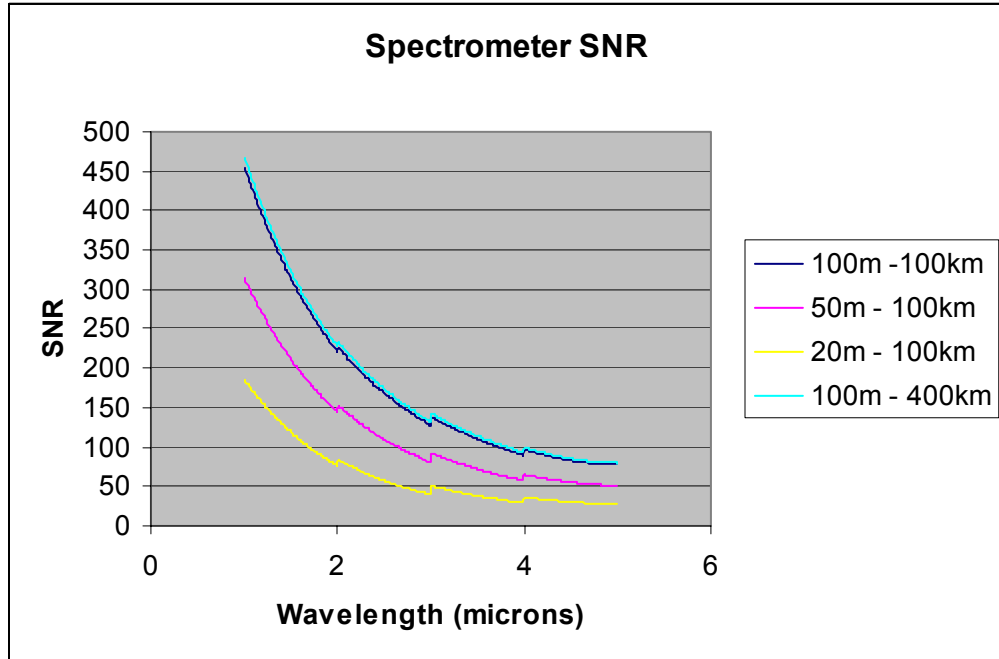


Figure 7.4-1: Sensor trades for sensors tailored to gsds and altitudes.

For the “spiral in” cases the sensor performance was evaluated for a fixed sensor design, with the assumption that the sensor would be operational as the spacecraft descends its final orbit altitude. Tables and graphs were generated for spiral in performance for Cases 1 and 4 described above. In Case 1, the sensor has 1 centimeter aperture and 100 km nominal operating altitude. In Case 4, the a sensor has a 4 cm aperature and operates at a nominal altitude of 400 km. Table 7.4-2 shows the trade with altitude when the ground sample distance is held constant. Table 7.4-3 illustrates how the performance of the Case 1 and Case 4 nominal point designs varies as altitude is increased. Figure 7.3-2 graphs the ground sample distance as a function of altitude for these two point designs. Figure 7.4-3 shows the scaling of the signal-to-noise ratio during as a function of increasing altitude. SNR increases due to the increasing coverage area. This is the scale factor applied across the spectral band and can be used together with Figure 7.4-1 to esitimate SNR at any given wave length.

Table 7.4-2: Design Sensitivity GSD=100 m, Altitude = 100, 400 km

Sensor Case		1	4
Altitude	(km)	100	400
Ground Sample Distance	(m)	100	100
Aperture Diameter	(cm)	1.00	4.00
Effective Focal Length	(cm)	2.70	10.80
Mass	(kg)	73	1276
Power	(W)	6	6
f/#		2.70	250.00
FOV	(degrees)	14.90	14.90
Fore Optics Temp	(K)	210.00	210.00
AFT Optics Temp	(K)	170.00	170.00
FPA size (spatial)	(n)	260	1040
FPA size (spectral)	(m)	300	300
FPA pixel size	(microns)	27.00	27.00
FPA material		HgCdTe	HgCdTe
FPA cut-off wavelenth	(microns)	5.50	5.50
FPA temperature	(K)	105.00	105.00
FPA Frame Rate	(Hz)	19.03	18.08
FPA Integration Time	(msec)	52.55	55.30
Spectrometer Raw Analog Rate	(Mpix/sec)	1.48	5.64
Digital Encoding	(bits/pixel)	14.00	14.00
Spectrometer Raw Digital Rate	(Mbits/sec)	20.78	78.99

Table 7.4-3: Performance Sensitivity of 100 and 400 km Point Designs Operating at Higher Altitudes

Sensor Case	#	1	1	1	1	4	4	4	4
Altitude	(km)	100	1000	5000	10000	400	1000	5000	10000
Ground Sample Distance	(m)	100	1000	5000	10000	100	1000	5000	10000
Slit Scan Rate	(km/sec)	1903	1650	1138	885	1903	1650	1138	885
Slit Oversampling Factor		1.00	11.53	83.61	215.02	0.95	2.74	19.86	51.08
SNR enhancement factor		1.00	3.40	9.14	14.66	0.97	1.66	4.46	7.15
Slit Dwell Time	(msec)	52.55	606.06	4393.67	11299.44	52.55	151.52	1098.42	2824.86
Ground Swath	(km)	25.86	258.60	1293.01	2586.03	103.44	258.60	1293.01	2586.03

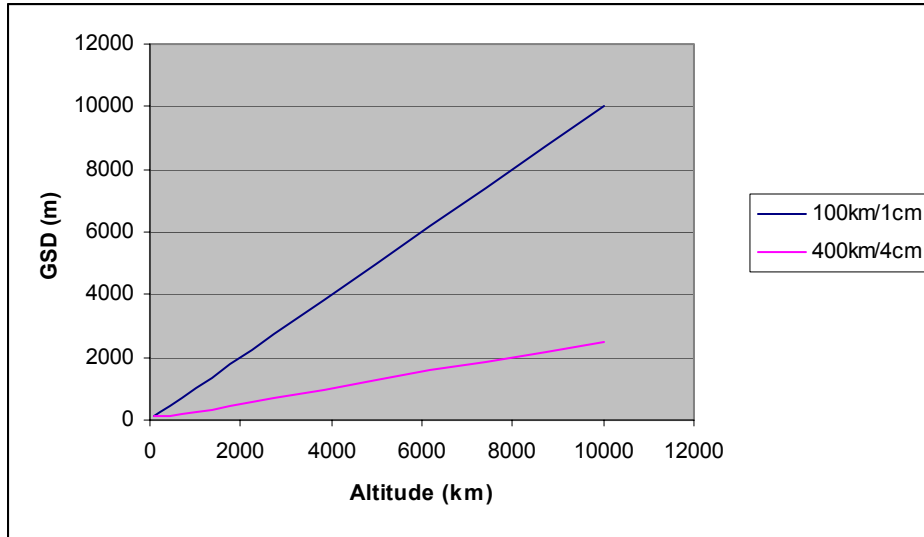


Figure 7.4-2: GSD vs. altitude for “spiral in”.

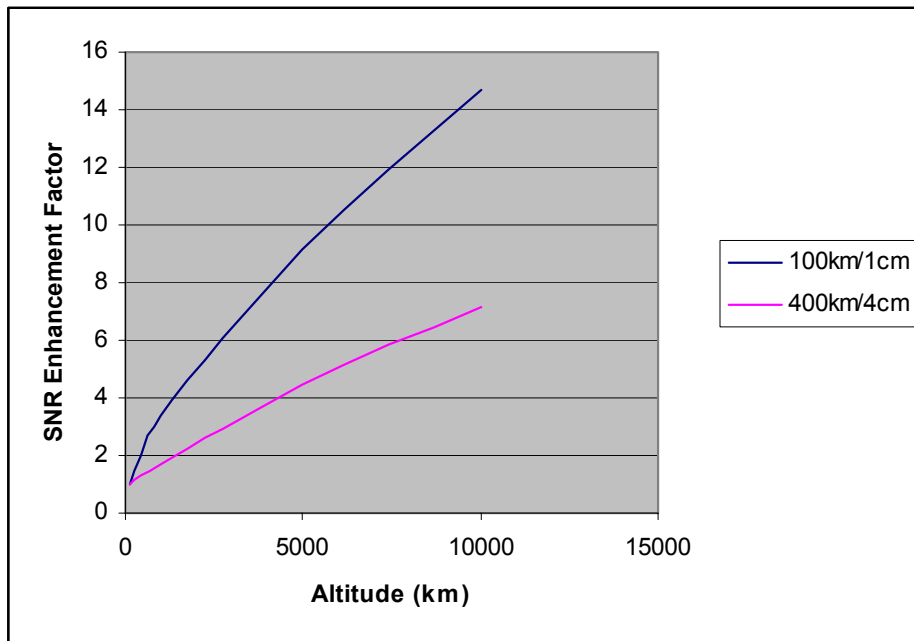


Figure 7.4-3: SNR scale factor vs. altitude for “spiral in”.

As indicated in Section 8.3.3 the digital processor for the mapper does not require much data throughput, hence the spectrometer digital processor could be shared with the thermal mapper. They have been identified individually to keep each instrument as a unit in itself.

We reviewed the option of the two spectrometers for better coverage. This impacts the design in several ways. Two imagers (with a total swath width of 29.6 degrees) are needed to support double coverage of a global map of Europa

within 15 or 30 days. If a second spectrometer were to be employed to double the field of view for double coverage over a 30 day period, the mass, power, volume and data rate would of course double. Coverage plots can be found in Appendix B, Coverage Analyses.

7.5 Key Technology Developments

The current baseline sensor as described above requires no technological developments to build. However, the baseline design is at the f-number lower limit with no room for improvement other than technological gains. Additionally, focal plane detector development and testing will be required to assure that suitable focal planes will be available for this mission.

In order to achieve higher spectral resolutions in a relatively simple design, a spectrometer is required that uses filters with discreet bands rather than a dispersive element such as a prism. The spectrometer optics could be simplified with well-designed filters since the prism would no longer be required. The optical design could resemble the thermal mapper, but could have a slightly larger field of view since the aperture would be smaller and the f-number is slightly larger.

A spectral resolution ($\lambda/\Delta\lambda$) of 300 equates to 485 bands. An individual sensor, configured as described above, could cover a 5.5 by 5.5 degree field of view. The field of regard required would be 14.8 degrees cross-track by 25.5 degrees in-track. With new technology and the current system design requirements, an array of 3x5 reimaging sensors (15 total) would be needed to cover the FOV and spectral resolution.

Although the linear variable filter technology is under development and has made strides, it is not capable of the 485 bands in the small space that is required by this FPA design. Our design space calls for pixel of 27 microns, 485 bands over 13 mm spatially. Current state-of-the-art capability for linear variable filters is 1-2.5 microns or 2.5 to 5 microns over a 12.5 mm length filter for 256 pixels or channels. This is about twice the size spatially, or half the fidelity desired. Linear variable filters currently cannot achieve the needed fidelity. It is estimated with funding and directed effort this type of performance for discreet wavebands could be achieved in roughly 7 years.

For this particular application the payload masses for the spectrometer is small relative to the entire spacecraft. However if the mass were to become a main driver, consideration of technological advancement in the light weighting of radiation shielding would be appropriate since the majority of the payload mass is its radiation shielding. The absence of shielding would require the development of new technology extreme rad hard electronics and devices.

7.6 Schedule Estimate

The development schedule for each instrument depends upon the time required for technology development and the time required to build the final instrument. The schedule for technology development includes the time required to mature a specific technology from its current technology readiness level (TRL) to a TRL of 5. The schedule for building the instrument includes the time required to design, fabricate, assemble and test the instrument in its final operational form.

As stated in Section 7.5, the visible and infrared imaging spectrometer requires no specific technology development effort to be undertaken to meet the baseline design. Extending the performance from 300 spectral channels to 485 requires the use of high density linear variable filters with an estimated development time of 84 months. Approaches to light weight shielding would benefit the instrument through an overall reduction in mass.

The schedule for developing the visible and infrared imaging spectrometer is based upon analogies to the development schedules of comparative legacy instruments as described in Section 7.7. The two legacy instruments represent two extremes for the development of this type of planetary electro-optical instrument. The visible and infrared map spectrometer (VIMS) built for Cassini was completed in 61 months while the Compact Reconnaissance Imaging Spectrometer for Mars (CRISM), being built for the Mars Reconnaissance Orbiter (MRO), is scheduled to be completed in 32 months. While five years is a rather long duration for the development of this type of instrument, fewer than three years is considered a very aggressive schedule. A recent study of cost and schedule for a variety of different optical, planetary instruments built in the 1990s identified that the average development time of 41.7 months [2]. The estimated development time for the visible and infrared imaging spectrometer, using the average of VIMS and CRISM development actual and planned durations, is 46.5 months. Although this duration is slightly greater than the average in [2], it should be a representative estimate for the baseline planning of the development time of the visible and infrared imaging spectrometer for the JIMO mission, once any technology developments are complete.

7.7 Legacy Instrument Description

The baseline design is a spectrometer with 3 visible bands between .4-.5 microns for color context imaging, with 300 spectral channels from 1-5 microns with a spatial resolution of 100 meters. Although a spectrometer with these exact characteristics has not flown before, there have been many similar instruments.

Two examples of space-based spectrometers are the Compact Reconnaissance Imaging Spectrometer for Mars (CRISM) planned for flight on the Mars Reconnaissance Orbiter (MRO) and the Visible and Infrared Mapping

Spectrometer (VIMS) that flew on the Cassini spacecraft. The characteristics of these instruments are summarized in Table 7.7.1 and the instruments are shown in Figures 7.7.1 and 7.7.2. CRISM consists of 3 subassemblies, a gimbaled Optical Sensor Unit (OSU), a Data Processing Unit (DPU), and the Gimbal Motor Electronics (GME). The entire OSU is gimbaled to allow off-track pointing and to remove groundtrack speed for long integration times. The IR focal plane is cooled with redundant cryogenic coolers. VIMS consists of two completely separate channels. The visible channel produces multispectral images spanning the spectral range 0.3-1.05 micrometers over 96 spectral bands. The infrared channel consists of a Cassegrain telescope, a conventionally ruled spectrometer grating, and a 256-element linear array focal plane assembly cooled to its required operating temperature by a passive radiator. It is configured as a “whiskbroom” scanning imager, using a two-axis scanning mirror.

The proposed JIMO instrument uses off-the shelf technologies for the majority of elements. Cryocoolers are an option for the thermal system. Although cryocoolers have been flown on the NASA EOS AIRS and HIRDLS instruments, some development will likely be required for a cryocooler tailored to the JIMO requirements. The visible channel hybrid silicon PIN diode array technology has flown on the Lewis and Hyperion instruments.

Table 7.7-1: JIMO Spectrometer Compared with Heritage Instruments

INSTRUMENT	Proposed Instrument	MRO/CRISM	Cassini/VIMS
Mass (kg)	73.4	22.8	40.1
Power (W)	6.4 peak	60 average	21.8 average
Data Rate (Mbps)	21 peak	10 peak	0.182 peak
Wavelength Range (microns)	IR: 1.0-5.0, Vis: 0.4-0.5	IR: 1.05-4.05, Vis: 0.4-1.05	IR: 0.86-5.1 Vis: 0.35-1.0
FOV (deg)	14.8	2.06	1.83
Resolution (mrad)	3.0	0.06	0.5

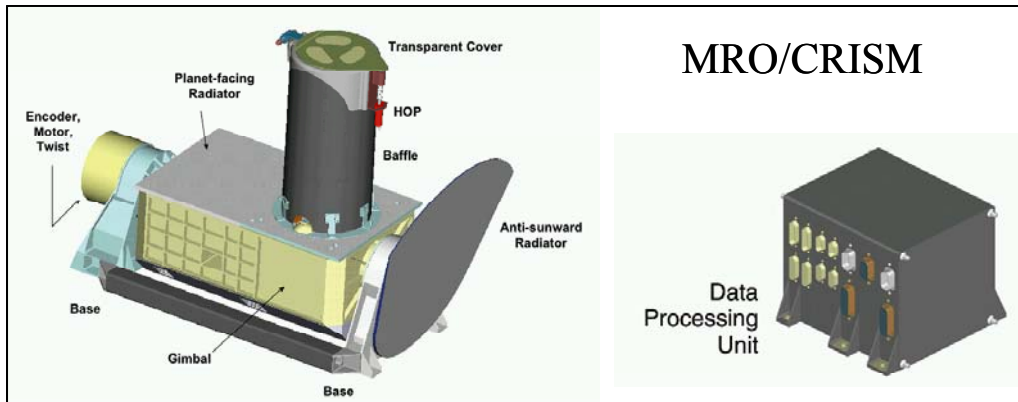


Figure 7.7-1: MRO/CRISM instrument (Reprinted courtesy of NASA).

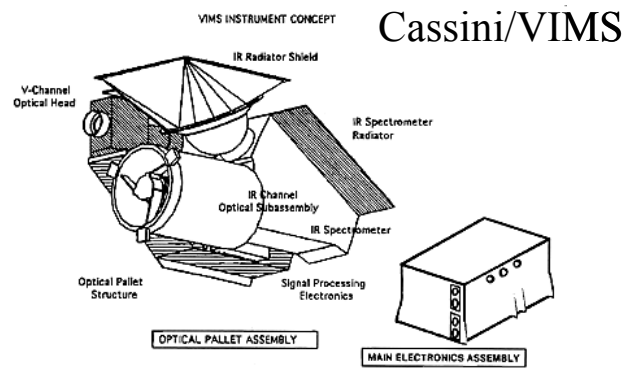


Figure 7.7-2: Cassini/VIMS instrument (Reprinted courtesy of NASA).

8.0 Thermal Mapper

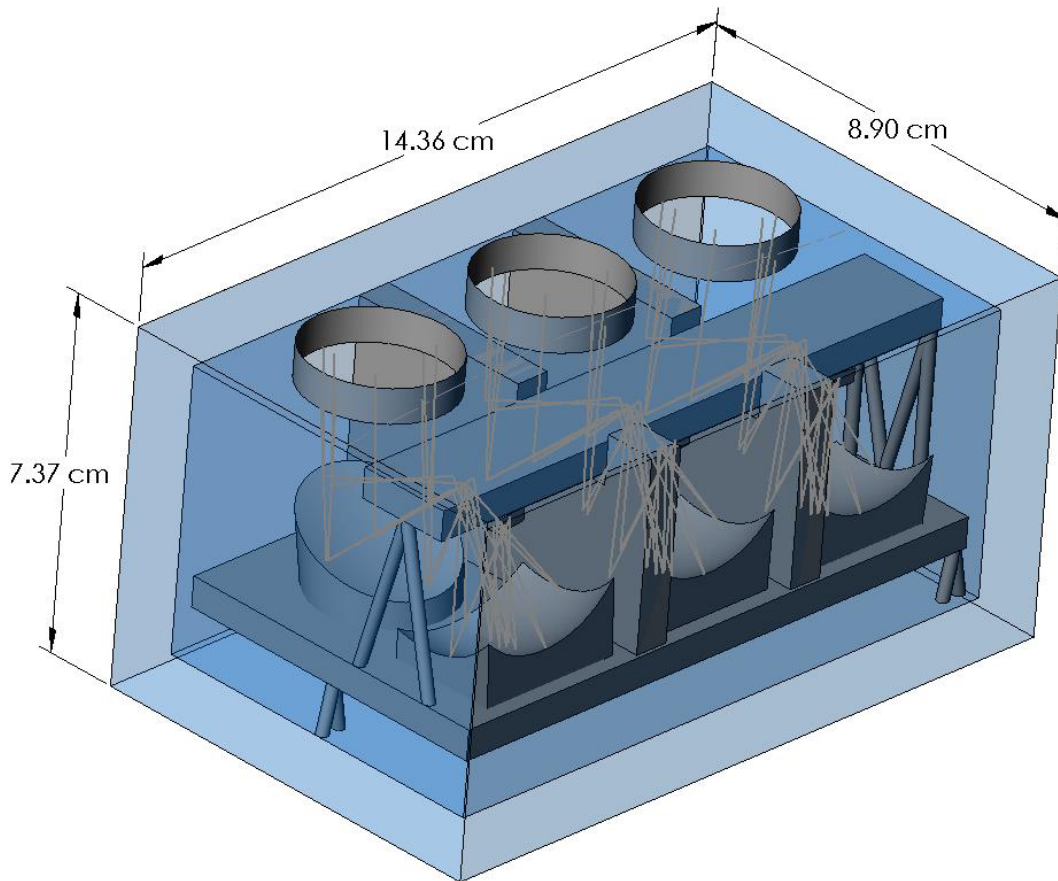


Figure 8.0-1: Thermal mapper.

8.1 Science Measurements

The thermal mapper will make observations in the wavelength range of 8 to 100 μm with a spectral resolution of 2 and spatial resolution of 300 meters/pixel or better. It will support spatial coverage of 90% and repeat observation at several times of day. It will be used for observations at night and at high latitudes to support polar coverage and investigations of volatile cold traps.

8.2 Design Drivers and Options Examined

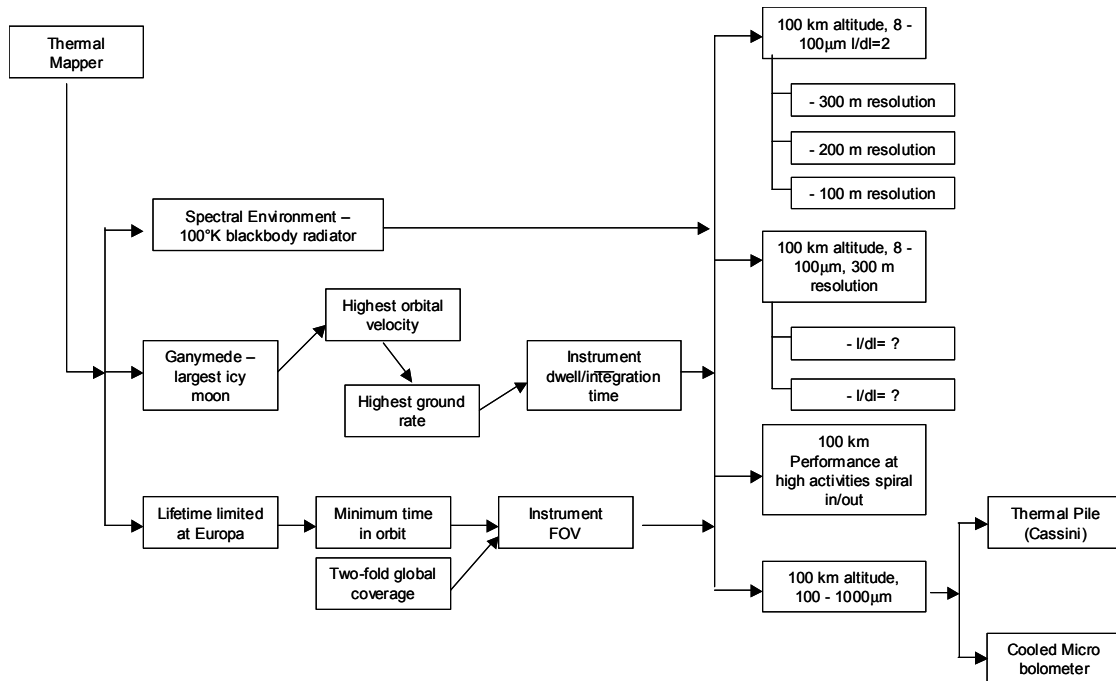


Figure 8.2-1: Thermal mapper trade space.

The design drivers and trade space examined for the thermal mapper are shown in Figure 8.2-1. There were six main drivers for the thermal mapper: 1) Europa's radiation environment, 2) 12 IR bands with the full spectrum being 6 to 100 microns, 3) sensor speeds over Ganymede, 3) the lowest temperatures (100K), 4) emissivity (0.36) of Europa, and 6) 300m ground sample distance.

The high radiation environment of Europa had a large design impact on the instrument field of view and the mass. Due to a shortened time in orbit on the order of 15 or 30 days, the required field of view is 14.8 degrees.

The full spectrum of 6 to 100 microns combined with a high radiation environment implied a reflective, reimaging, unobscured system. The 14.8-degree field of view was achieved with 3 three-mirror off-axis reimaging telescopes.

Shielding, with a very high mass, was used to encase the instrument for protection against electrons trapped in the Jovian environment. An aperture cover was utilized to protect the instrument when the sensor is non-operational. The cover is currently designed to have some, although reduced, performance in the event of a cover removal mechanism failure. The aperture cover is shown in context in Figure 8.3.3.2.

The 12 IR bands between 6 and 100 microns are achieved with strip filters over the FPA, with a delay for each band over a given ground position. This drove the in-scan FOV to the maximum limit for this optical design type.

Factors limiting SNR were ground speed, ground footprint, temperature, emissivity, and f-number of the instrument. The ground speed is based on a nadir viewing push-broom sensor. For the largest moon, Ganymede, the orbital velocity and ground rate are at their peak, and the dwell time is at the minimum. Backscanning is an option, which could be investigated in future studies to reduce ground speed and improve SNR. It was not considered in this study due to the high degree of complexity and risk, as well as reduced coverage per orbit and increased complexity in collection planning and commanding.

To improve SNR, sub-bandwidths could be broadened. The design is at the FOV limit for this design form. To improve SNR with TDI, some bands could be eliminated for focal plane space. Another option for future studies is to investigate other optical design forms with wider fields of view.

GSD drove altitude, focal length and pixel size. The 300-meter GSD requirement together with the 100-kilometer altitude and 125-micron pixel size drove a 41.7 mm focal length. The SNR requirements drove aperture diameter to its maximum limit based on the f-number lower limit of 1.6. The baseline design is at the f-number lower limit with no room for improvement other than technological gains. This study included trades for sensors with 200 and 100-meter resolution from a 100km altitude.

A sensor meeting these stringent requirements has been designed and evaluated. In addition, performance of the baseline sensor was evaluated at various “spiral in” positions. Performance was evaluated for the sensors at 100, 500, 1000, 5000, and 10000-kilometer altitudes.

8.3 Baseline Instrument Description

The thermal mapper instrument is configured for push-broom imaging from an altitude of 100 km. The required swath width of 14.8 degrees to support the goal of a global map of Europa within 15 days is achieved with three 5.5-degree FOV sensors with slightly overlapping FOVs. Each imager has a GIFOV of 300 m on the target surface. Note that since the imager detects IR radiation emitted from the moons, it can be used on both the sun side and the dark side of the orbit (100% duty cycle). Light from the Sun (direct or reflected from Jupiter) and light emitted by Jupiter are both assumed to be negligible in the wavelength ranges detected by the thermal imager.

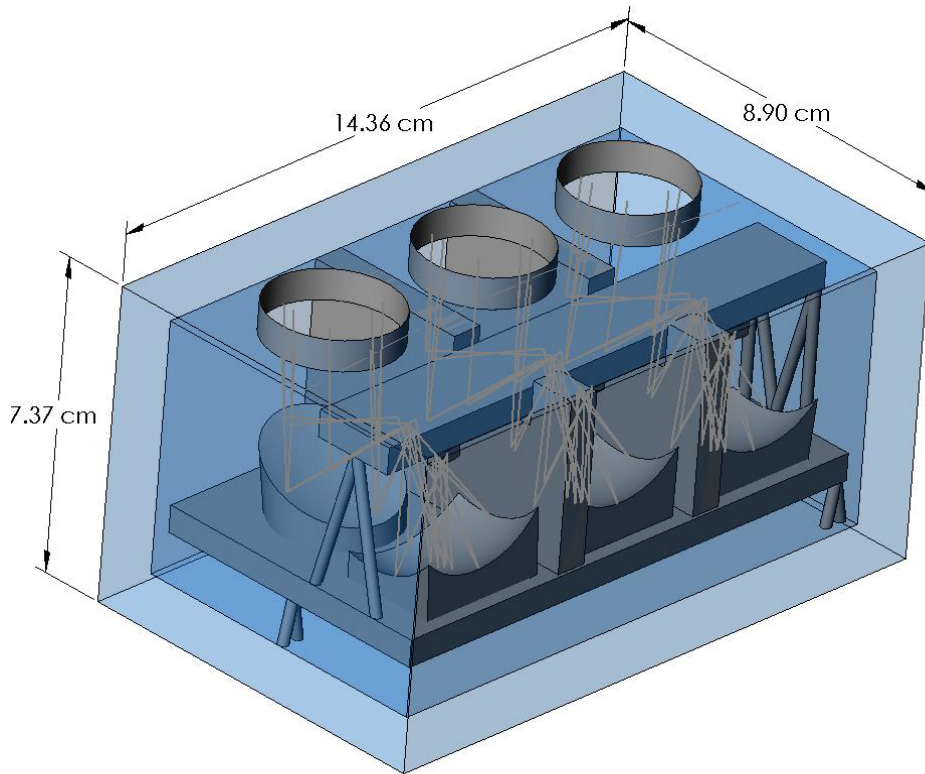


Figure 8.3-1: Thermal mapper instrument design.

8.3.1 Radiometry and Optical Design

A spectral resolution of 2 (center wavelength/bandwidth) is desired, which results in 12 spectral bands across the desired spectral range of 6 to 100 microns as shown in Tables 8.3-1 and 8.3-2.

The maximum ground speed at the 100 km altitude is 1800 m/sec at Ganymede. It is assumed that the integration time will be one sample per dwell (1 pixel of smear) at the maximum ground speed. The SNR varies for each channel shown in Tables 8.3-1 and 8.3-2. The baseline design does not use TDI. A tabular summary of the baseline parameters can be found in Table 8.4-1, Case 1.

The target radiance was estimated assuming an ideal black body radiator at 100K. The flux available in the wavelength bands below the 30 micron peak in the target black body curve drops off rapidly with decreasing wavelength because the spectral radiance of the target drops off exponentially for decreasing wavelength below the peak, and the bandwidths of the shortest wavelength channels are relatively small for a spectral resolution of 2 condition. Since an emissivity of 1.0 was assumed in the SNR calculations, a scale factor must be applied for the SNR to account for each moon's emissivity. The lowest emissivity

of the three moons is 0.36. The impact on the SNR would be the square root of this or 0.60. The SNRs would be reduced by 40% across all of the bands.

The lowest value for target radiance occurs in the 8-micron band (the shortest wave length band). Estimated high and low target radiance values are:

- Low of $2.70 \text{ E}12$ photons/cm²-s-sr for the band centered at 8 microns
- Band is 8 microns ± 2 microns (4 micron total bandwidth)
- Corresponds to roughly 0.017 micro-Watts/cm²-sr-micron
- High of $1.42 \text{ E}16$ photons/cm²-s-sr for the band centered at 59.5 microns
- Band is 59.5 microns ± 15 microns (30 micron total bandwidth)
- Corresponds to roughly 1.577 micro-Watts/cm²-sr-micron

Design drivers drove the f-number to F/1.7, and telescope field of view is limited to 5.0 degrees, so 3 individual thermal imagers are needed to cover the full 14.8-degree swath. The optical system for each imager consists of a three-mirror anastigmatic telescope with strip filters over the focal plane that defines the spectral bandpasses. Different wavelength data will be collected at slightly different times, as the detector array is push-broomed over the target.

The design incorporates a dual focal plane approach. It includes a microbolometer array of 125-micron pixels for the longest 9 wavelength bands (12.5 to 100 microns). It also includes a HgCdTe array of 62.5 micron pixels—summed 2x2 and operated at 60 °K—for the 3 shortest wavelength bands. The effective pixel size for the HgCdTe would be 125 microns due to the summing.

To achieve a SNR > 100:1 across all bands, TDI stages would be needed for 6 out of 9 of the longest wavelength bands. For the baseline no TDI is used and the SNR table is shown below.

The focal length of the telescope is determined to be 41.7 mm, for a telescope entrance pupil diameter 24.5 mm.

The angular GIFOV is 3 mrad or 0.172 degrees for 125-micron pixels. The number of cross-track pixels needed to cover a 5.0-degree swath is 29. In the interest of using round numbers and providing some overlap in the fields of the three individual imagers, the strawman design includes 32 cross-track pixels. This gives a telescope field of view of 32 times 0.172 degrees or 5.5 degrees.

The integration time for 1 pixel of smear is 167 msec at the fastest expected ground speed (at Ganymede). This is calculated by dividing the 300-meter GIFOV by the ground speed of 1800 m/sec.

The baseline uses a HgCdTe array of 62.5 micron pixels summed 2 by 2 for the shortest 3 wavelength bands is to use. Summing 2 by 2 increases the effective pixel size to 125 microns but requires twice as many pixels for cross-track coverage. The number of cross-track pixels needed to cover a 5-degree swath is 58. The strawman design includes 64 cross-track pixels to provide a small amount of overlap between the fields of the three individual imagers. This gives a telescope field of view of 5.5 degrees.

The complete HgCdTe array includes 64 cross-track by 12 in-track 62.5-micron pixels. The 12 in-track rows allow for 2 unused rows after each set of 2 used rows. The pattern would be 2 rows used, 2 rows unused, 2 rows used, etc.

A microbolometer array was chosen for the detector for the 9 longest wavelength channels, assuming a D^* value of 1×10^9 cm-Hz^{1/2}/watt for this detector type. Microbolometer arrays can be operated near room temperature and are responsive out to 100 microns. A pixel size of 125 microns was chosen in order to give an optical Q close to 1 near the middle of the wavelength band. This is a generally sound practice for imaging systems.

$$Q = (50 \text{ micron wavelength})(F \text{ number of } 1.7)/(125 \text{ micron pixel}) = 0.7$$

For the 9 longest wavelength bands, 32 pixels in the cross-track direction give a 5.5-degree swath. The pattern would be 1 row used, 1 row unused, 1 row used, etc. The HgCdTe focal plane will be cooled 60 °K to keep dark current to acceptable levels. The amount of electrical power needed for the set of 3 thermal imagers plus off-chip electronics would be about 35mW; they would generate about 7mW of heat due to dissipation and parasitic loads.

The design has a 10-bit system with a 167 msec integration time, and a data rate from one imager is 72.8 kbps. The total data rate from the set of 3 imagers is 218.4 kbps or 0.22Mbps.

The total dose on the focal planes will be kept below 150 krad via tungsten shielding around and throughout the sensor. Radiation issues are discussed in more detail in a separate section below.

Table 8.3-1 summarizes the radiometric performance for the three shortest wavelength bands.

Table 8.3-1: HgCdTe Channel Description and Performance

Channel Center Wavelength (μm)	Channel Bandwidth (μm)	Channel Radiance (ph/cm ² /s/sr)	FPA Flux as Function of Optics Diameter (ph/cm ² /s)	Noise Equivalent Irradiance of Detector (ph/cm ² /s)	2x2 Summed SNR for 2.45 cm Aperture
8	+/- 2	2.7007 X 10 ¹²	(9.773 X 10 ¹⁰)D _o ²	1.116 X 10 ¹⁰	74:1
10	+/- 2.5	3.1758 X 10 ¹³	(1.149 X 10 ¹²)D _o ²	1.395 X 10 ¹⁰	700:1
12.5	+/- 3.125	2.1111 X 10 ¹⁴	(7.639 X 10 ¹²)D _o ²	1.744 X 10 ¹⁰	3724:1

Table 8.3-2 summarizes the radiometric performance for the 9 longest wavelength bands.

Table 8.3-2: Microbolometer Channel Description and Performance

Channel Center Wavelength (μm)	Channel Bandwidth (μm)	Channel Radiance (ph/cm ² /s/sr)	FPA Flux as Function of Optics Diameter (ph/cm ² /s)	Noise Equivalent Irradiance of Detector (ph/cm ² /s)	Single row SNR for 2.45 cm Aperture	# TDI	Multi-row SNR for 2.45 cm Aperture
15.6	+/- 3.9	8.7922 X 10 ¹⁴	(3.181 X 10 ¹³)D _o ²	1.088 X 10 ¹³	18:1	32	102:1
19.5	+/- 4.9	2.5644 X 10 ¹⁵	(9.279 X 10 ¹³)D _o ²	1.360 X 10 ¹³	41:1	6	100:1
24.4	+/- 6.1	5.528 X 10 ¹⁵	(2.000 X 10 ¹⁴)D _o ²	1.702 X 10 ¹³	71:1	2	100:1
30.5	+/- 7.6	9.047 X 10 ¹⁵	(3.274 X 10 ¹⁴)D _o ²	2.128 X 10 ¹³	92:1	1	92:1
38.1	+/- 9.5	1.2217 X 10 ¹⁶	(4.421 X 10 ¹⁴)D _o ²	2.658 X 10 ¹³	100:1	1	100:1
47.6	+/- 11.9	1.401 X 10 ¹⁶	(5.070 X 10 ¹⁴)D _o ²	3.320 X 10 ¹³	92:1	1	92:1
59.5	+/- 15	1.417 X 10 ¹⁶	(5.127 X 10 ¹⁴)D _o ²	4.150 X 10 ¹³	74:1	2	105:1
74.4	+/- 18.6	1.2707 X 10 ¹⁶	(4.598 X 10 ¹⁴)D _o ²	5.190 X 10 ¹³	53:1	4	106:1
93	+/- 23	1.0489 X 10 ¹⁶	(3.795 X 10 ¹⁴)D _o ²	6.487 X 10 ¹³	35:1	8	99:1

With no TDI the SNR in some bands is below 100. These SNR values could be improved by other means such as alteration of the baseline to include broader bands, or back-scanning. These trades were not investigated due to the time limits and complexity. These are viable options for future trade studies.

8.3.2 Optical Design

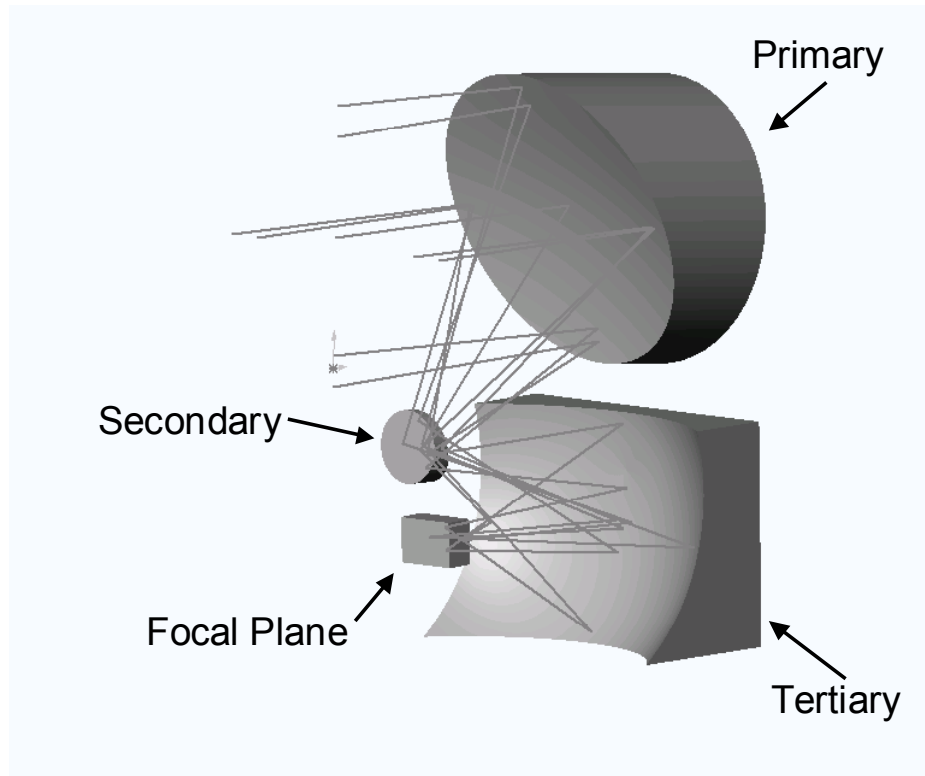


Figure 8.3.2-1: Thermal mapper single optical configuration.

The optical design was driven by focal plane requirements. It utilizes a 24.5 mm aperture with a 41.7 mm focal length and $f/1.7$. The required field of view is 5.5 degrees crosstrack by 3.9 degrees intrack. The bandwidth is 6 to 100 microns and there are 12 spectral bands. A relayed design is preferred to reduce straylight. A mirrored design has the advantage of more uniform throughput for the broad bandpass of the sensor. All this led us to a three mirror off axis design. This design is at the limit of the FOV and f-number. Polished beryllium mirrors are used to minimize radiation damage. The three mappers will be placed side by side on one common optical bench to maintain alignment. Figures 8.3.2-2 and 8.3.2-3 show the two planes of the optical layout.

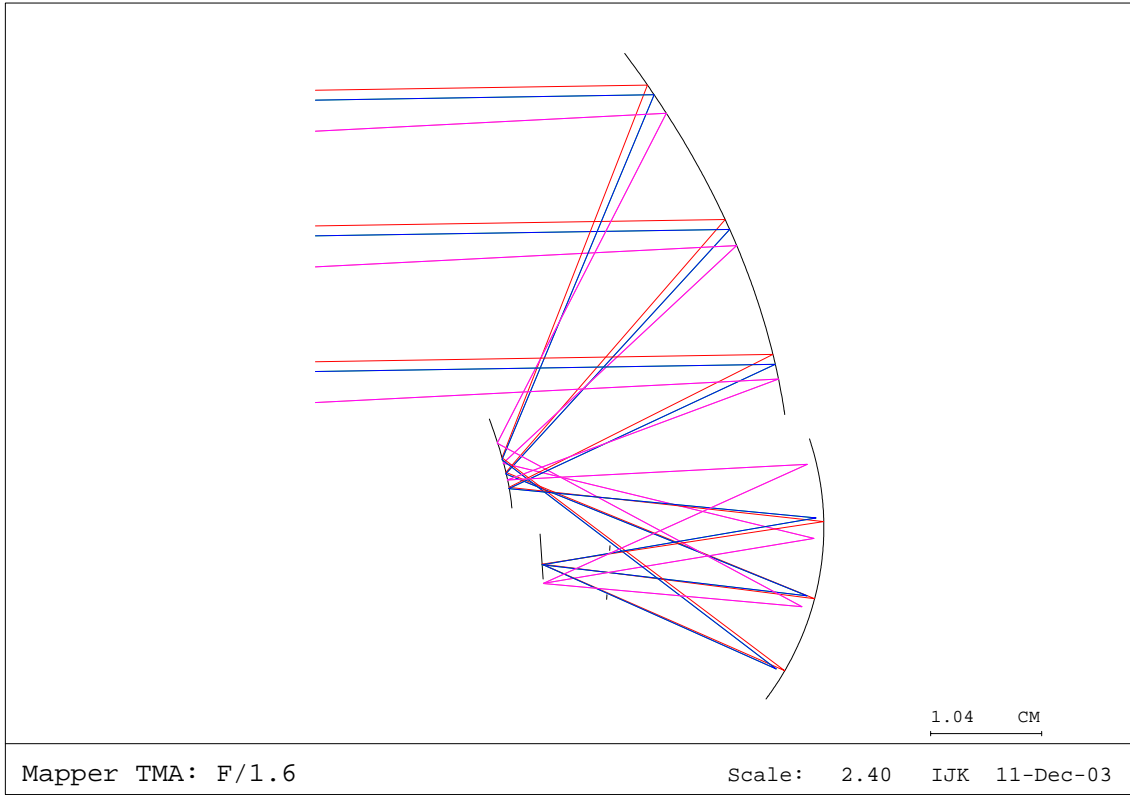


Figure 8.3.2-2: Thermal mapper optical YZ profile.

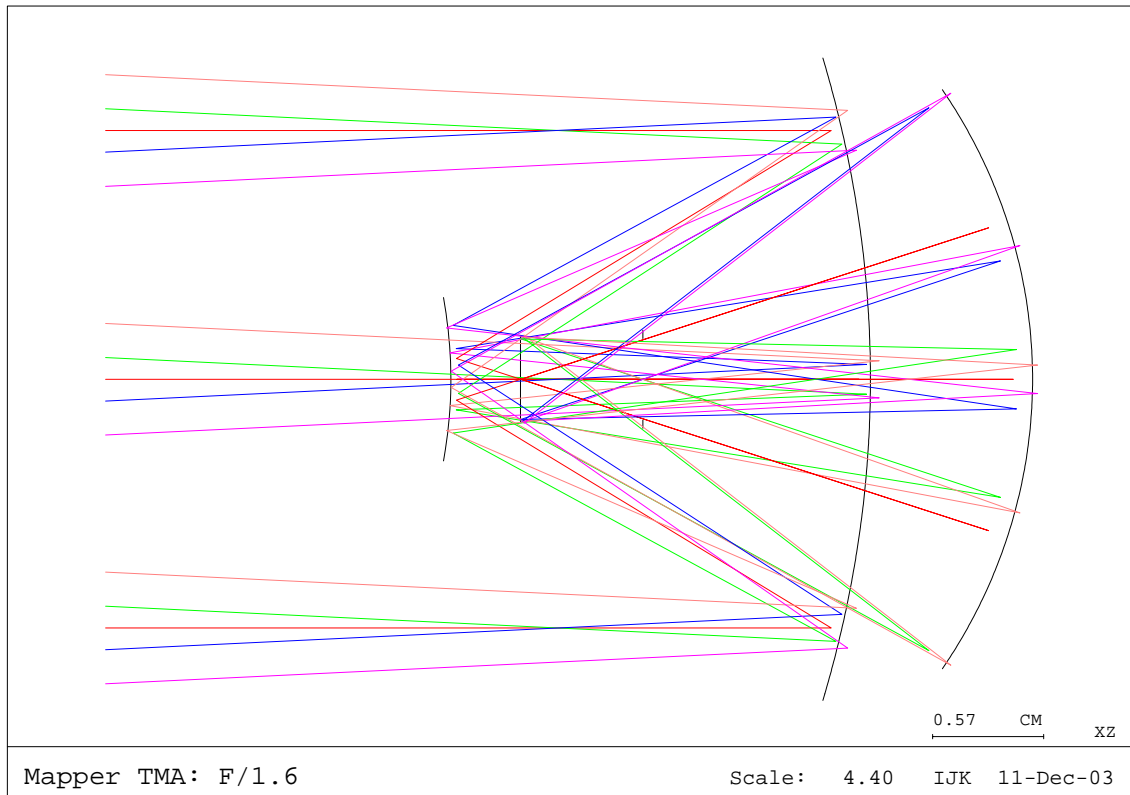


Figure 8.3.2-3: Thermal mapper optical XZ profile.

An aperture cover made of 35 mm of cesium iodide serves primarily as a protection against the radiation environment. This material was chosen as a safety precaution. If the aperture removal mechanism fails, the instrument will still be able to partially operate. Throughput is reduced by roughly 50% for 6 to 50 microns, but is reduced by about 90% beyond 50 microns so most of the data in this spectral region would be lost. The SNR for 6 to 50 microns would be reduced by 30%.

8.3.3 Processor

The three optical configurations share a single compartment and well as single analog and digital processors. The analog processor will be located within 300 mm of each focal plane. The digital processor will be located 6 inches from the focal planes. The key circuits are an A/D (10 bit) converter AD7933, for thermal mapper and a Xilinx Vertex-II Pro FPGA processing chip for digital signal processing. The maximum sample rate is 230 kpixels per second per sensor. This yields an overall datarate of 6.8Mbps. The required focal plane power is less than 2.33 mW summing to 7mW total for dissipation at FPA. The analog processor power required is 35 mW. The volume is 400 cubic cm, with a mass of 0.8 kg.

The digital processor for the mapper has a power requirement of 400mW, with a volume of 100 cubic cm, and a mass of 0.2 kg.

Table 8.3.3-1: Data Rates

Parameter (Units)	IR/Total
cross scan pixels	32
inscan pixels	12
bits per pixel	10
integration time (s)	0.167
Datarate per Unit (kbps)	23.0
Number of Units	3
Total Datarate (kbps)	69.0

Table 8.3.3-2: Processor Mass, Power and Volume

Parameters	Mass (kg)	Power (W)	Volume (cu cm)
Focal Plane	*	0.007	*
Analog Signal Processors	0.8	0.035	400
Digital Signal Processors	0.2	0.400	100
Total	1	0.442	500
Total with Redundant	2	0.442	1000

*Logged with optics and structure.

8.3.4 Structural Design

The thermal mapper is a set of three matching optical assemblies, all sharing the same structural support system. These assemblies are also enveloped by a 0.3”-thick tungsten housing for radiation shielding. As in the case for the spectrometer, an optical bench is provided to mount the disturbance sensitive components. A secondary bench is also necessary for the thermal mapper to mount the secondary mirror and focal plane.

The same first mode requirements used on the spectrometer were used to size the benches for the thermal mapper. Both the primary and secondary benches are assumed to be a zero-CTE/CME tailored honeycomb composite plate with 0.05-inch Graphite Epoxy facesheets and an 0.25-inch thick 5/32-5056-0.001 3.8 pcf Aluminum honeycomb core.

The mounting schemes for the benches and the optical components are intended to impart no stresses or distortion across interfaces. The secondary bench is kinematically mounted to the primary bench via Invar stand-offs—two flexured struts and one bipod. The primary bench is kinematically mounted to the tungsten block via three sets of Invar bi-pods. The beryllium structure is kinematically attached to embedded inserts on the optical benches. As for the spectrometer, this study assumes the attachment mechanisms to be Invar flexures.

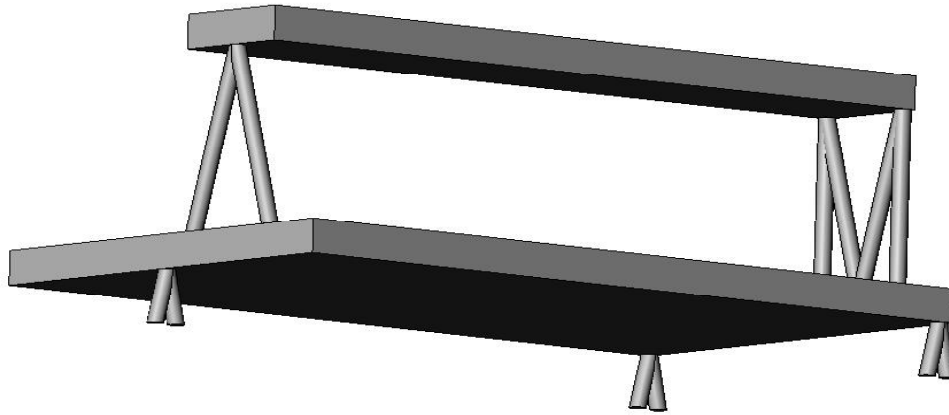


Figure 8.3.4-1: Thermal mapper optical bench and stand-offs.

The aperture mechanism shown in Figure 8.3.4-2 is a representation of the structure that may be required to move the aperture cover between imager uses. The motor, assumed to be a rotational actuator Moog type 2, was selected because of its known reliability and robustness for this type of environment.

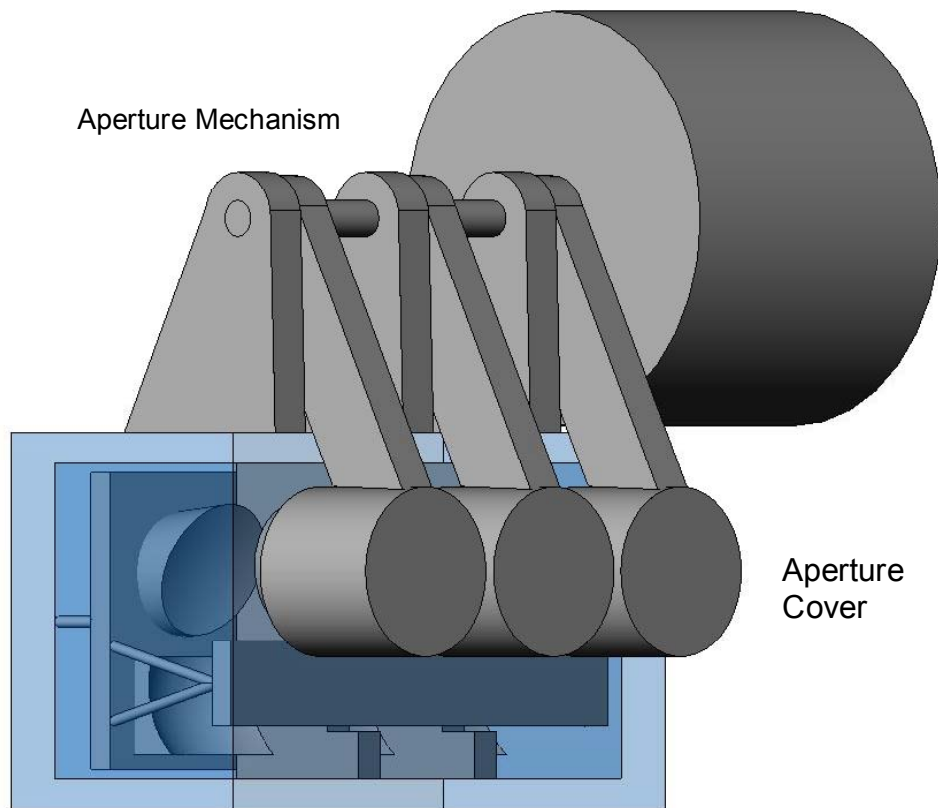


Figure 8.3.4-2: Possible aperture mechanism configuration.

8.3.5 Thermal Management System

The heat dissipation from each of the FPAs is 2.34 mW. The total dissipation from the three FPAs is 7.02 mW. The temperature requirement of the FPA is 60 K. Because of the very low power dissipation and small dimensions involved, it was concluded that the most efficient thermal management technique would be to cool the housing enclosing the optical components, which are in turn secured to an optical bench.

A single mini pulse tube cryocooler has been selected for the cooling objectives. The cryocooler will remove heat directly from the housing. The size and performance specifications for the cryocooler have been determined based on an evaluation of heritage instruments.

It is assumed that the optical components (mirrors and FPAs) will be fixed to the optical bench, which will be maintained at a (yet unknown) temperature.

Assuming that this temperature is greater than 60 K, which is a reasonable assumption, the cryocooler will need to remove the 7 mW generated at the FPAs, in addition to heat loads from the optical bench to the components and housing. Because the housing is cooled directly, the housing temperature must be maintained below 60 K to ensure a 60 K mean temperature on the optical components. Depending on the temperature of the optical bench and the interface design between the optical components and the bench, conduction heat transfer could contribute significantly to the overall heat load to the optical instruments.

The housing itself should be shielded from the environment using multi-layer insulation, with very low IR absorptivity/emissivity to prevent radiation heating from surrounding surfaces. On the inside of the enclosure, a uniform coating of low emissivity material would help distribute the heat effectively, achieving thermal uniformity for the optical components.

In regards to the cryocooler, a reasonable point of reference is the TRW Advanced Mini Pulse Tube cryocooler, Model PTC-001A-065-I. This unit was delivered in 1995, and has no flight heritage. However, it is capable of removing roughly 200 mW of heat while maintaining a cold tip temperature of 60 K (with heat rejection at 300 K). The total power input at this condition is 49 W. The thermo-mechanical unit weight is 2.25 kg, and the electronics weight is approximately 6 kg (8.25 kg total). It is expected that technology developments since this design should drive down both the power input and the weight for state-of-the-art models, which may be at TRL-7 levels by the JIMO technology freeze date of 2007.

A large quantity of heritage data shows that the total specific mass (total mass of thermo-mechanical unit and cooling electronics divided by cooling capacity) becomes increasingly large as the cooling requirement diminishes. For cooling on the order of 500 mW, this ratio is on the order of 15-20 kg/W. If the cooling requirement in the present case is very conservatively assumed to be 500 mW—or 70 times the nominal power dissipation at the three FPAs—a total mass of 7-10 kg is anticipated. If the parasitic heat loads are less, and the cooling requirement is only on the order of 100 mW (14 times the nominal dissipation), then the total specific mass is expected to be larger—probably on the order of 40-50. In that case, the total expected mass is approximately 4-5 kg. The total savings in mass for one-fifth the cooling capacity appears marginal. An option is to expend less effort into reducing parasitic losses to the housing and optical components and use a larger capacity cryocooler.

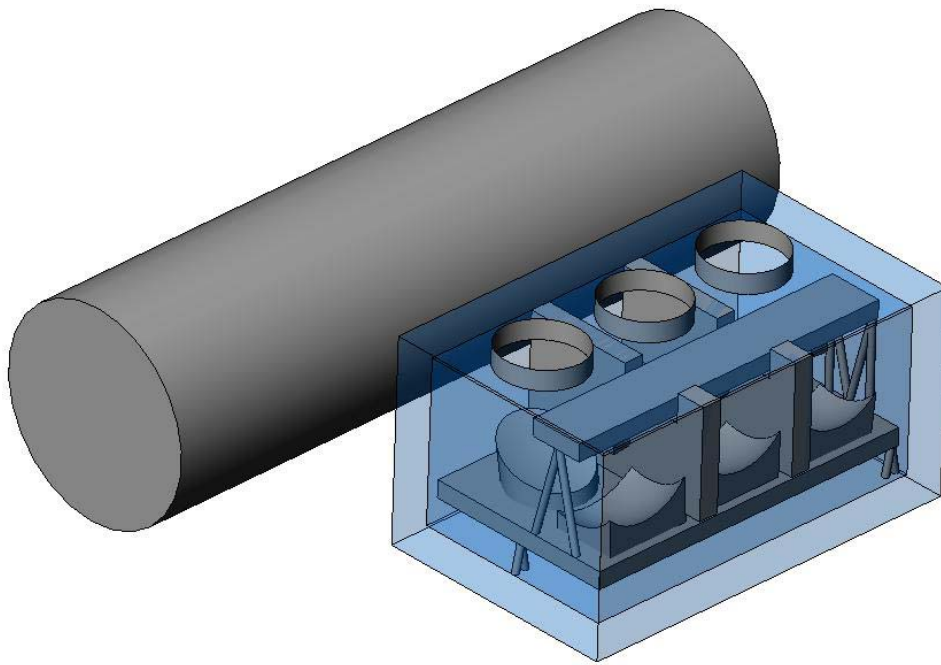


Figure 8.3.3-3: Cryo cooler volume comparison to thermal mapper.

8.3.6 Radiation

The cesium iodide aperture cover is vulnerable to permanent and transient radiation effects. All of the transparent optical elements can suffer darkening when exposed to high ionizing doses. The only optical dielectric used is cesium iodide, which can experience darkening due to color center formation. The effect is most pronounced at the short wavelength end of the spectrum. It can also experience subsurface charging resulting from the buildup of charged particles that are stopped by the material. The aperture cover, being directly exposed to the external environment, is most vulnerable to these effects. Surface charging of the aperture cover could make this material undesirable since conductive coatings that might be used to mitigate surface charging would degrade performance in the infrared.

The HgCdTe infrared focal planes are vulnerable to nuclear and ionizing radiation. Permanent damage in the detector readout circuitry or detector

material can be severe in the mission environment. Readout circuit technology is expected to be available to meet mission radiation performance requirements. The HgCdTe detector material is vulnerable to the displacement damage caused by high-energy electrons, protons and neutrons, all of which are components of the JIMO environment. The primary manifestations of displacement damage are loss of responsivity and increased dark current. Mitigation of these effects is difficult, but techniques are available that hold promise for meeting mission requirements. Microbolometer arrays are thought to be significantly less sensitive to radiation than the HgCdTe arrays, but there may be issues associated with damage to the dielectric support structure. Focal plane detector development and testing will be required to assure that suitable focal planes dielectric support structures will be available for this mission.

Spurious transient focal plane responses will be induced by environmental electrons that could severely degrade the quality of data collected in both the HgCdTe infrared focal plane arrays. Special effort will be required to provide for a proper focal plane array shielding design. Ultimately, compound-shielding techniques will probably be required, and proposed designs will require detailed radiation transport analyses to assure that direct or indirect leakage paths do not exist that would spoil the performance of the shield.

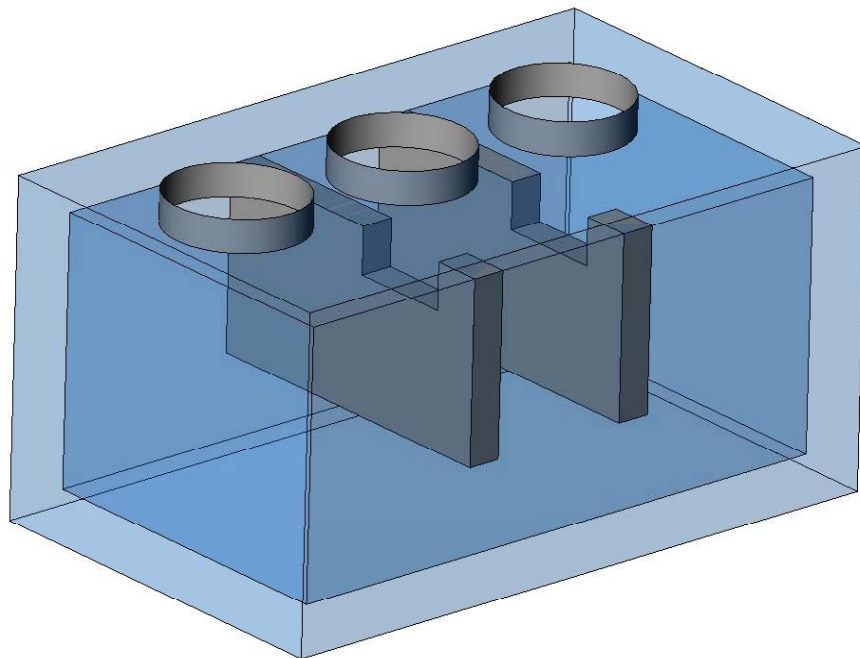


Figure 8.3.5-1: Thermal mapper radiation shielding.

For this prototype design, radiation shielding made up of 7.3 mm thick tungsten will be placed around and throughout the sensor to reduce electrons from entering and to decrease effects of radiation entering through the aperture. An aperture cover is used to reduce radiation when the sensor is not operational. The aperture removal mechanism is shielded as well to reduce damage to it.

8.3.7 Summary Mass, Power, and Volume

The system summary for the thermal mapper is given in Table 8.3.6-1. A more detailed breakdown of the mass and power is given in Table 8.3.7-2.

Table 8.3.6-1: Thermal Mapper Instrument System Summary

Mapper System Summary		
Parameter	Units	Result
Mass	kg	35.4
Power (peak)	W	50.4
Duty cycle	%	80
Power (average)	W	40.3
Volume	cm ³	942 (7.37x14.36x8.9)
Datarate	Mbps	0.069
Wavelength range	microns	6-100
FOV	degrees	14.9 (3 sensors 5.5° with some overlap)
Resolution	mrad	1.0

A Computer Aided Design (CAD) model was created for each of the major parts of the thermal mapper. The mass of the thermal mapper was approximated by applying densities to the CAD model parts. Table 8.3.6-2 shows a breakdown of the mass and power estimates for the appropriate components. Again, as with the spectrometer the shielding dominates, making up 60% of the overall sensor mass.

Table 8.3.6-2: Thermal Mapper Mass and Power Breakdown

Thermal Mapper Summary			35.4kg	50.4W	
Component	#	Mass (ea.)	Mass (tot.)	Power (ea.)	
		grams	grams	W	
Total			33378.9	50.435	
Optics			79.2		
	Primary Mirror	3	17.5	52.5	
	Secondary Mirror	3	0.2	0.6	
	Tertiary Mirror	3	8.5	25.5	
	Focal Plane Array	3	0.2	0.6	
Shielding			20,655.5		
	External (box)	1	7231.7	7,231.7	
	Internal	2	388.7	777.4	
	Electronics	1	12646.41	12,646.4	
Structure			2,622.3		
	Optical Bench	1	200	200.0	
	Secondary Optical Bench	1	60	60.0	
	Struts between benches	1	8.2	8.2	
	Struts between bench and shielding	3	0.71	2.1	
	Aperture Cover	3	198.4	595.2	
	Aperture Cover Mechanism Structure	3	152.26	456.8	
	Aperture Cover Motor	1	1300	1,300.0	
	Mirror Mounts				
Electronics			2,000.0		
	Analog Processor	2	800	1,600.0	0.035
	Digital Processor	2	200	400.0	0.4
Thermal			8,021.9		
	Cryo Cooler	1	8000	8,000.0	49
	ASP Heater	2	11.0	21.9	1

8.4 Thermal Mapper Design Options

8.4.1 Design Excursions

Several excursions from the baseline were examined. The nominal case assumed a 100-kilometer altitude with 300m resolution. Four additional cases were examined with 200 and 100-meter resolution with 1-pixel time delay integration (TDI) and 200 and 100 meter resolution with variable TDI. Table 8.4-1 shows the necessary modifications to the design and the performance associated with the new design. Case 1 is the baseline, Cases 4 and 5 are the

same as Cases 2 and 3 respectively except TDI is used to maintain (or exceed) nominal SNRs for each band. Each case below had an altitude of 100 kilometers and 125 micron pitch.

Table 8.4-1: Results of Thermal Mapper Trades at 100km Altitude and 125 Micron Pitch at Various GSD and Time Delay Integration Options

Case	#	1	2	3	4	5				
GSD	m	300	200	100	200	100				
Aperture	cm	2.45	3.68	7.36	3.68	7.43				
Focal length	cm	4.17	6.25	12.51	6.25	12.63				
Mass	kg	35.30	80.00	333.90	80.00	333.90				
Power	W	50.40	112.70	298.70	114.90	311.60				
Fno	#	1.70	1.70	1.70	1.70	1.70				
IFOV	mrad	3.00	2.00	1.00	2.00	1.00				
FOV X	dg	5.50	5.50	5.50	5.50	5.50				
FOV Y	dg	3.94	2.63	1.31	3.78	2.89				
Data rate	Mbps	0.22	0.50	1.98	0.50	2.02				
Integration Time	s	0.17	0.11	0.06	0.11	0.06				
Pixels X	#	32	48	96	48	97				
Pixels Y	#	23	23	23	33	51				
Det. area	cm ²	0.12	0.17	0.35	0.25	0.78				
Pix pitch HgCdTe	um	64.5	64.5	64.5	64.5	64.5				
Pix pitch MB	um	125.0	125.0	125.0	125.0	125.0				
FPA Temp	K	< 60	< 60	< 60	< 60	< 60				
Altitude	km	100	100	100	100	100				
Mid-band (um)	nTDI	SNR	nTDI	SNR	nTDI	SNR	nTDI	SNR	nTDI	SNR
8	1	74	1	61	1	43	2	86	2	60
10	1	700	1	572	1	404	1	572	1	402
12.5	1	3724	1	3041	1	2150	1	3041	1	2139
15.6	1	18	1	14	1	10	2	20	4	20
19.5	1	41	1	33	1	24	2	47	4	47
24.2	1	71	1	58	1	41	2	82	4	82
30.5	1	93	1	76	1	53	2	107	4	106
38.1	1	100	1	82	1	58	2	115	4	115
47.6	1	92	1	75	1	53	2	106	4	105
59.5	1	74	1	61	1	43	2	86	4	85
74.4	1	53	1	43	1	31	2	62	4	61
93	1	35	1	29	1	20	2	41	4	40

The aperture diameters scale inversely and linearly with the GSD to account for area loss. The integration time scales linearly with the GSD. Since we are in the photoelectron noise limited range of the detector, the readout noise is low and, for Cases 2 and 3, the SNR scales with the square root of the scale factor for the integration time.

Cases 4 and 5 are similar to Cases 2 and 3 respectively in that the apertures and GSDs correspond. Time delay integration was added to several channels to bump up the SNR to or slightly above the SNR of the nominal case. The required field of view in the along track plane was limited to the nominal Y-FOV.

TDI cases were explored to achieve SNRs above 100 for each band. The results are given in Table 8.4-2 below. Unfortunately the sensor inscan or FOV Y becomes too large for this optical design type, so these were ruled out as options but are shown to illustrate what is needed in terms of TDI to achieve an SNR of 100. An option to reduce the FOV and have more TDI per channel is to eliminate some of spectral bands.

Table 8.4-2: Thermal Mapper Excursions with Increased TDI for Uniform SNRs at or Above 100

Case	#	1	6	7		
GSD	m	300	200	100		
Aperture	cm	2.45	3.677	7.428		
Focal length	cm	4.17	6.251	12.627		
Mass	kg	35.30	124.500	348.200		
Power	W	50.40	80.000	333.900		
Fno	#	1.70	1.700	1.700		
IFOV	mrad	3.00	2.00	1.00		
FOV X	dg	5.50	5.500	5.500		
FOV Y	dg	3.94	11.858	10.980		
Data rate	Mbps	0.22	0.495	2.020		
Integration Time	s	0.17	0.111	0.055		
Pixels X	#	32	48.2	97.3		
Pixels Y	#	23	105.0	196.0		
Det. area	cm ²	0.12	0.790	2.979		
Pix pitch HgCdTe	um	64.5	64.5	64.5		
Pix pitch MB	um	125.0	125.0	125.0		
FPA Temp	K	< 60	< 60	< 60		
Altitude	km	100	100	100		
Mid-band (um)	nTDI	SNR	nTDI	SNR	nTDI	SNR
8	1	74	3	105	6	105
10	1	700	1	572	1	402
12.5	1	3724	1	3041	1	2139
15.6	1	18	50	101	100	101
19.5	1	41	9	100	18	100
24.2	1	71	3	101	6	100
30.5	1	93	2	107	4	106
38.1	1	100	2	115	3	100
47.6	1	92	2	106	4	105
59.5	1	74	3	105	6	105
74.4	1	53	6	107	11	102
93	1	35	12	99	25	101

A caveat for use of TDI with a push-broom sensor with filtered channels is that the pointing and alignment must be more precise. The inscan travel vector would ideally be less than one-quarter pixel variation over the time delay. More TDI implies a higher precision in this regard.

Another excursion from the baseline was to evaluate performance of the baseline sensor as it spirals into the moon. Table 8.4-3 shows the performance of the thermal mapper at several altitudes during spiral in.

Table 8.4-3: Baseline Sensor Performance

Altitude (km)	GFP (km)	Ground Track Speed (m/s)	Dwell Time for 1 speed (sec)	Expected SNR (combined)
100	0.3	1833	0.164	100:1
500	1.5	1493	1.005	247:1
1000	3	1196	2.508	391:1
5000	15	392	38.26	1528:1
10000	30	184	163	3153:1

8.4.2 100-1000 Micron Sensing

The original requirements for the thermal imager included coverage in the 100 to 1000 micron range. This section briefly discusses a few options for augmenting the strawman thermal mapper with an instrument capable of imaging at wavelengths from 100 to 1000 microns. A more detailed discussion including references is provided in Appendix G.

Both passive optical and passive radio frequency (RF) instruments could potentially be used for imaging in this interval. There are instruments being developed/flown for astronomy, solar system exploration, and earth science that might provide heritage for JIMO.

The technology most appropriate for observing in the 100–1000-micron range depends upon specific science objectives. This interval would depend on the specific science objectives. Candidate technologies are briefly described below. A more detailed discussion including references is provided in Appendix G.

8.4.2.1 Optical Imaging

One option would be to use an optical imager with a spectral resolution of 2 similar to the strawman thermal mapper. Two types of optical detectors used for the far infrared are bolometers and thermopiles. Cassini is carrying an instrument that uses thermopiles and Herschel (formerly FIRST) will carry an instrument that uses bolometers. The sections below list some of the parameters for these two instruments and consider the relevance of each instrument to JIMO. These are just two examples and are not intended to represent the full range of instruments that use bolometers and/or thermopiles.

8.4.2.2 Composite Infrared Spectrometer (Cassini)

The Composite Infrared Spectrometer (CIRS) consists of a 0.5-meter F/6 Cassegrain beryllium telescope, a reference interferometer to provide scan mechanism control and timing for data sampling, and two science Fourier transform spectrometers (FTS). One FTS covers mid-infrared and the other covers far-infrared. The Far-infrared interferometer (FIR) is a polarizing Michelson interferometer measuring from 17 to 1000 microns using two thermopile detectors. Each thermopile detector includes a concentrator and has a 4.3-mrad (0.25-degree) diameter circular FOV. CIRS could provide a single 436-meter pixel from 100-km altitude if back-scanning were used. The exposure time can range from 2 to 50 seconds. The operating temperature of the telescope and the FIR focal plane is 170 K. The instrument (including both spectrometers) has a mass of 39.24 kg and requires 26.4 Watts of power.

Note that there is a substantial amount of current research and development effort focused on linear and 2-D thermopile arrays for imaging. A linear array could potentially be used to achieve a wide FOV in the cross-track direction to support a push-broom approach for global mapping.

8.4.2.3 Spectral and Photometric Imaging Receiver (Herschel)

The Spectral and Photometric Imaging Receiver (SPIRE) will be one of three instruments on ESA's Herschel Space Observatory. SPIRE includes a 3-band imaging photometer that will simultaneously observe at 250, 350, and 500 microns with a spectral resolution around 3. Its FOV will be 4 by 8 arcmin (0.067 by 0.133 degree). SPIRE also includes an imaging Fourier transform spectrometer (FTS) that will observe the range of wavelengths from 200 to 670 microns. Its FOV will be greater than 2 arcmin (0.033 degrees). The instrument is sensitivity limited by thermal emission from the telescope, which is cooled to 80 K. Detector arrays will be cooled to 0.3 K using superfluid Helium (^3He).

SPIRE will have five arrays of feedhorn-coupled bolometers. These will have a "spider web" design. Each consists of a web-like mesh of silicon nitride, which absorbs light and conducts the energy to the tiny thermistor that sits at the center of the web. The thermistor is made of neutron transmutation doped (NTD) germanium. It takes about 100 photons in the far-infrared/submillimeter range to heat it up enough to generate an electrical signal. The bolometer's web-like structure reduces the bolometer's heat capacity and gives SPIRE a relatively high mapping speed.

SPIRE is clearly designed for astronomical investigations of distant objects that emit very little light. However, SPIRE does use a type of micro-bolometer in supercooled detector arrays that are sensitive out to 670 microns. It is conceivable that this type of micro-bolometer array could be of use for JIMO without cooling it to 0.3 K.

8.4.2.4 Passive Radio Frequency Radiometry

Another alternative would be to use passive radio frequency (RF) radiometry in the sub-millimeter range. A wavelength of 100 microns corresponds to a frequency of 3 THz, and 1000 microns corresponds to 300 GHz. One instrument used to study atmospheric gases at Earth is discussed below. The technology demonstrated in this instrument includes passive radiometers at 640 GHz and 2.5 THz that could provide some heritage for JIMO. The wavelengths corresponding to 640 GHz and 2.5 THz are 469 and 120 microns, respectively.

8.4.2.5 Microwave Limb Sounder (EOS Aura)

The microwave limb sounder (MLS) instrument to be flown on the EOS Aura spacecraft will have a capability for sub-millimeter radiometry. The EOS MLS instrument has radiometers in five spectral regions at 118, 190, 240, and 640 GHz, and at 2.5 THz. Advanced planar-technology mixers are used in all the radiometers. A sub-harmonically pumped mixer is used at 640 GHz, and a fundamental mixer is used at 2.5 THz. The local oscillator at 640 GHz is solid state, and the local oscillator at 2.5 THz uses a CO₂-pumped methanol (CH₃OH) gas laser. All radiometers operate at ambient temperature.

Atmospheric signals for the 640 GHz radiometer are collected by a three-reflector antenna system that vertically scans the limb. The antenna design has a primary reflector dimension of 1.6 meter projected in the vertical direction at the limb tangent point. A switching mirror following the GHz antenna system provides radiometric calibration by switching to views of calibration targets or to space.

The atmospheric and calibration signals for the 2.5 THz radiometer are obtained via a dedicated telescope and scanning mirror whose operation is synchronized with that of the GHz antenna and the GHz switching mirror. The 2.5 THz primary mirror dimension in the "limb vertical" direction is ~25 cm.

The instrument individual measurement integration time is 1/6 second. The FOV beam widths (defined as the full width between half-power points) at 640 GHz and 2.5 THz are each less than 0.06 degrees. EOS MLS has a mass of 440 kg, power of 530 Watts, data rate of 100 kb/sec, and 5-year on-orbit design lifetime.

While MLS is implemented as a limb sounder, an alternative implementation for similar hardware could include cross-track scanning or use of a conical scan. To achieve practical scanning rates, an MLS type instrument might require a larger footprint than imagers operating at shorter wavelengths.

8.4.2.6 Summary

The science goals for imaging in the wavelength range of 100 to 1000 microns need further definition to determine which type of technology is most appropriate. There are a few candidate technologies that could be of some use for the JIMO mission. For each, the most difficult requirement to meet would be global mapping of the icy moons within limited time frames. (The most difficult

challenge would be global mapping of Europa within 15 days.) The difficulty stems from the relatively low target radiances in this wavelength range and the relatively high ground speed for the baseline 100 km altitude orbits. Given that new phenomenology is being investigated, however, a larger footprint might be acceptable.

Optical imaging could potentially be done using thermopiles or micro-bolometers as detectors. Two instruments were considered as examples that provide some insight into current applications of these types of detectors. One was the CIRS instrument on Cassini and the other was the SPIRE instrument on Herschel.

Another alternative using more mature technology would be to use passive RF radiometry in the sub-millimeter range. The EOS MLS instrument was considered as an example of this technology that provides some insight into current applications for earth science. The EOS MLS instrument has radiometers at 118, 190, 240, and 640 GHz, and at 2.5 THz. The 640 GHz and 2.5 THz radiometers might be of use for JIMO investigations in the sub-millimeter range (120 and 469 microns).

A system like EOS MLS for JIMO could be used with a conical scan or it could be pointed to nadir and scanned cross-track. This raises questions regarding the expected thermal emissions and the appropriate science measurements. Questions regarding the appropriate footprint and desired coverage would have to be addressed.

There are also questions that would need to be addressed regarding potential difficulties operating in and surviving the high radiation environment.

Overall, imaging in the wavelength range from 100 to 1000 microns has practical difficulties, but there are technologies that appear promising depending on the science goals and acceptable tradeoffs.

8.5 Key Technology Developments

While there are no major technology developments required for this instrument, the baseline design is at the f-number lower limit with no room for improvement other than technological gains. Specific areas meriting further investigation to determine the degree to which technology development is needed include rad-hard focal plane dielectric structures and approaches to compound shielding. Focal plane detector development and testing will be required to assure that suitable focal planes will be available for this mission. It is also likely that some development will likely be required for a cryocooler tailored to the JIMO requirements.

8.6 Schedule Estimate

As stated in Section 8.5, the thermal mapper requires no specific technology development effort to be undertaken to meet its design requirements. All technologies required by the instrument are at a TRL of 5 or higher.

The schedule for developing the thermal mapper is based upon analogies to the development schedules of comparative legacy instruments as described in Section 8.7. The Thermal Emission Imaging System (THEMIS) built for the 2001 Mars Odyssey mission was completed in 40 months while the Thermal Emission Spectrometer (TES) built for Mars Global Surveyor (MGS) was built in only 19 months. The TES built for MGS, however, was a rebuild of the instrument using spare parts from the original TES instrument built for Mars Observer (MO). The original TES for MO required 67 months to build. Using the average of the Odyssey/THEMIS and MO/TES development durations, the estimated time to develop the thermal mapper is 53.5 months. Although this duration greater than the average in [2], it should be a representative estimate for the baseline planning of the development time of the thermal mapper for the JIMO mission, once any needed technology development is complete.

8.7 Legacy Instrument Description

Previous planetary IR instruments include the Thermal Emission Imaging System (THEMIS) that flew on the 2001 Mars Odyssey mission and the Thermal Emission Spectrometer (TES) that flew on both Mars Observer and Mars Global Surveyor. The characteristics of these instruments are listed in Table 8.8.1 and the instruments are shown in Figures 8.8.1 and 8.8.2. THEMIS consists of a thermal infrared imaging spectrometer with an all-reflective, three-mirror f/1.7 anastigmatic telescope and a 320 x 240 micro-bolometer array stabilized by a thermal electric cooler with 9 filters mounted directly over the focal plane, and a visible imager with a 1024 x 1024 silicon array with 5 stripe filters mounted directly on the detector. TES consists of three measurement channels: a spectrometer, a bolometer or radiance channel, and a reflectance or albedo channel. The detectors are three sets of 2x3 pyroelectric arrays and provide 3 km spatial resolution to all 3 channels. TES has a pointing mirror which allows views of deep space, nadir, and aft and forward limbs.

The proposed JIMO instrument uses off-the shelf technologies for the majority of elements. The microbolometer array technology was flight-proven on THEMIS. The thermal system relies on cryocoolers and cryocoolers have flown on the NASA EOS AIRS and HIRDLS instruments. However, the particular model chosen for this design (the TRW Advanced Mini Pulse Tube cryocooler, Model PTC-001A-065-I) does not have flight heritage. Some development will likely be required for a cryocooler tailored to the JIMO requirements.

Table 8.7-1: JIMO Thermal Mapper Compared to Heritage Instruments

INSTRUMENT	Proposed Instrument	Odyssey/THEMIS	MGS/TES
Mass (kg)	36.2	12.8	14.6
Power (W)	49.4 peak	14 average	15.6 average
Data Rate (Mbps)	0.069 peak	1.0 peak	0.5 average
Wavelength Range (microns)	IR: 6-100	IR: 6.6-15.0, Vis: 0.42-0.87	Spec: 6.25-50 Rad: 4.5-100 Refl: 0.3-2.7
Number of Bands	12	IR-9, Vis-5	Spec-143
FOV (deg)	5.5 each for 3 identical sensors	IR-4.6x3.5, Vis-2.9	1.4 x 0.95
Resolution (mrad)	3.0	IR-0.25, Vis-0.045	7.9

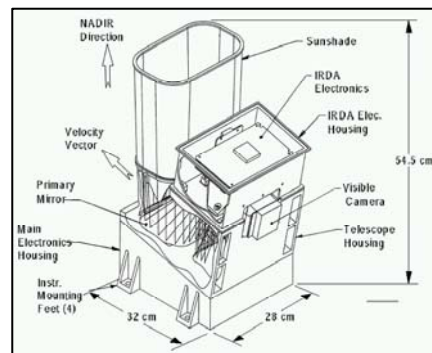


Figure 8.7-1: Mars Odyssey THEMIS instrument (Reprinted courtesy of NASA).



Figure 8.7-2: Mars Global Surveyor TES instrument (Reprinted courtesy of NASA).

9.0 Laser Instruments

9.1 Measurement Objectives

The laser altimeter will take measurements used to construct a topographic map of the surfaces of the icy satellites at better than 10 meters/pixel spatial scale and better than or equal to 1-meter vertical accuracy. Global coverage is supported. Repeat observations will support detection of changes arising from internal processes.

The laser altimeter will support targeted topographic mapping of craters on the icy satellites and surrounding terrains at better than 10-meter pixel spatial scale and better than or equal to 1-meter relative vertical accuracy. This includes the site of a potential lander. Topography at 10-meter horizontal and 1-meter vertical resolution will be obtained for the same locations profiled for thermal, compositional, and structural horizons.

The laser altimeter supports time dependent altimetry in combination with gravity. It supports determination of the surface motion that correlates with the eccentricity tidal potential to 1-meter accuracy. Performing this from orbit requires equivalent radial orbit determination accuracy. It also requires determining k_2 and h_2 to an accuracy of 0.005 at all the satellites. In terms of percentage uncertainty in the result, this is a higher measurement requirement at Europa than at the other icy moons.

By seeking to achieve full planetary coverage twice on Europa within 30 days, the laser altimeter will require considerably more capability than has been developed for any previous mission. In addition, the goal of increasing the 3-D resolution, facing the radiation environment and taking advantage of the effectively limitless bus power will suggest interesting challenges for the development of the instrument. Because the orbit will be designed for full coverage it was natural to explore related sampling strategies for both the altimeter and spectrometer. In effect the altimeter will establish a high spatial frequency map of the surface and the spectrometer will rely on the range information of the altimeter and provide effectively an order of magnitude less spatial resolution of the surface content. For the purposes of this study, the instruments are treated as separate entities on the nadir panel, but they will both be bounded by the same sampling constraints.

9.2 Design Drivers and Options Examined

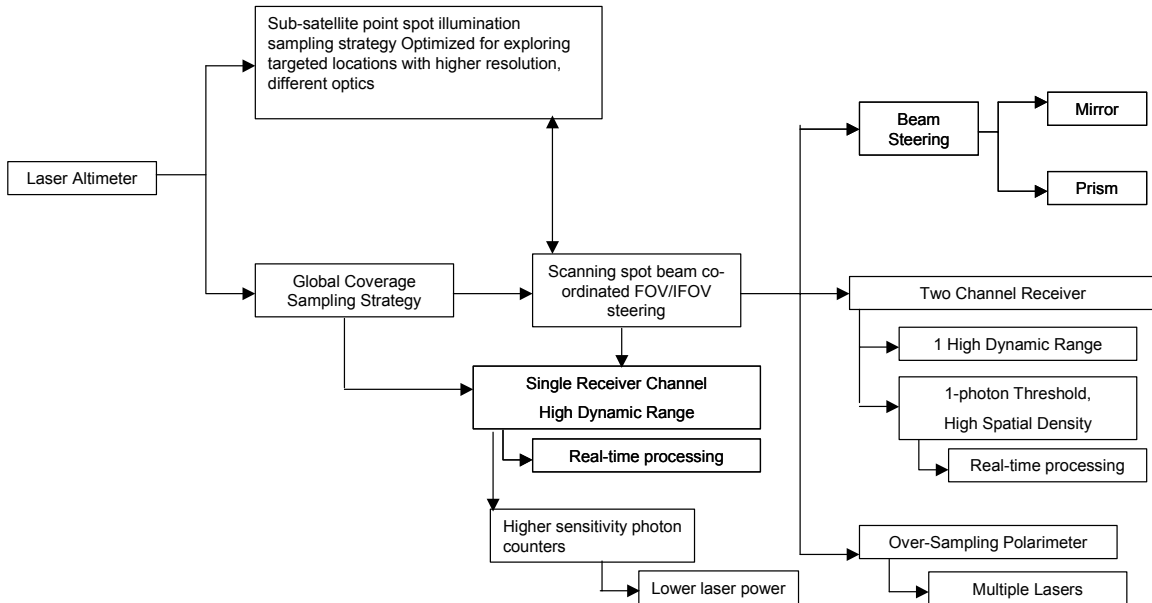


Figure 9.2-1: Laser altimeter trade space.

The laser altimeter trade space is presented in Figure 9.2-1. The laser altimeter requirements are driven by the goal of full planet coverage and the radiation dosage limits encountered near Europa. The data set should exceed surface topography with lateral resolution of 10 meters and height resolution of 1 meter. The Aerospace strawman laser altimeter design is derivative in signal levels and sampling strategies from the MOLA and ICESat missions, which meet or exceed the above goals. Our approach has been to baseline performance on the JIMO mission using sensitivities validated by the above systems, but consider alternatives that enhance system performance and increase science output beyond the JIMO baseline. The goal of achieving full planetary coverage in such a short period is a significant enhancement over all previous missions. Our approach places tangentially contiguous 50 m diameter laser illumination spots on the surface of Europa or the other moons as shown later in Figure 9.3-1. As the ground track moves across the surface, a rotating prism or other beam scanner will move the laser beam transverse to the ground track to cover the required FOV at the appropriate angular speed. A prism currently appears to be the lowest risk mechanism for translating the laser across the surface within the FOV of the receive telescope. The angular rates shown in Table 1 below have been demonstrated for rotating prisms while scanning mirrors would have considerable overshoot thus requiring additional control of the laser power or accepting large fractions of laser illuminations beyond the FOV boundary to accommodate the mirror turn around.

Alternatively, full coverage could be abandoned and the beam could be articulated with a smaller ground footprint and higher number density of samples

to resolve structural details at much less than 10 meters laterally. In such cases, high-speed steering mirrors would be required for both the transmit and receive apertures. Terrestrial aircraft topography measurements have employed highly over-sampled analysis to reveal high-resolution details of topography. A large portion of the FOV would be sacrificed and not measured to accommodate the dwells and multiple pulses needed to sample particular areas commensurate with the ground track speed. Another alternative would be to have a second smaller unit dedicated to such campaigns while the principle system completed the global mapping.

9.3 Baseline Instrument Description

This mission's primary challenge has been the design of the optical system. In each of these applications, laser radiation is emitted to some prescribed footprint size and painted on the surface of the Jovian moon (see Figure 9.3-1) transverse to the ground track. The laser instruments are both bistatic, similar to MOLA and ICESat.

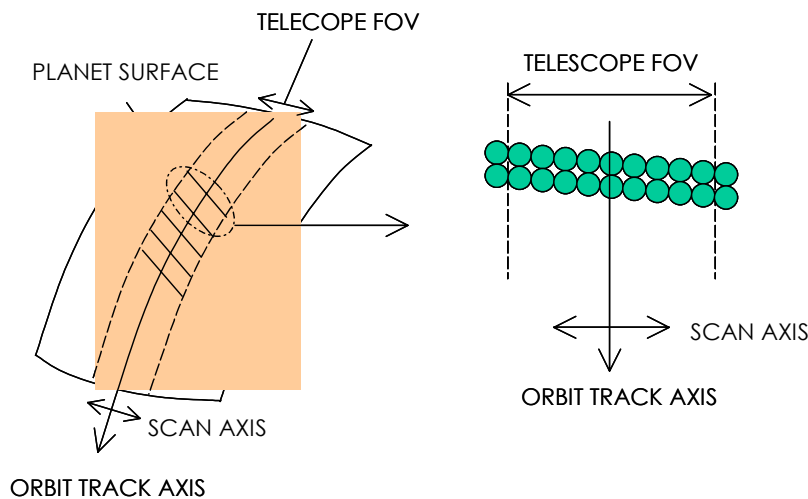


Figure 9.3-1: Planet coverage method: orbit track is wider than a single altimeter or spectrometer pixel by scanning.

Scattered light in each application is collected by a separate but larger aperture telescope whose FOV and boresight are aligned with the transmitted laser beam. As described elsewhere in this section and Section 10, the requirements to achieve full coverage at altitudes of 100 and 400 km resulted in FOVs of 15 and 5 degrees, respectively. The complexity of the telescopes to meet the specified field-of-views (FOVs) was traded against scanning approaches. The combined ground track rates and swath widths imply that unacceptable cross track rates will be encountered if one chooses a small FOV telescope and mounts it on a gimbal or attempts to use a scanning flat mirror. Static nadir pointed telescopes capable of collecting the full extent of a scanning transmitted laser beam have

been designed for these instruments as the baseline approach. The underlying design requirements were (1) meet the FOV, (2) make the detector plane flat and let it reside within the spacecraft, to meet radiation-shielding requirements and finally (3) minimize mass. Because both instruments were subject to similar constraints for the receiving telescope, the telescope designs are described in this section. Optical path alternatives will be explored separately for each instrument.

9.4 Telescope Baselines

Two static nadir-pointing telescopes were designed for the two FOV cases 5 and 15 degrees. It can be assumed that the design scales with aperture size and therefore only the optical surface relationships are presented here.

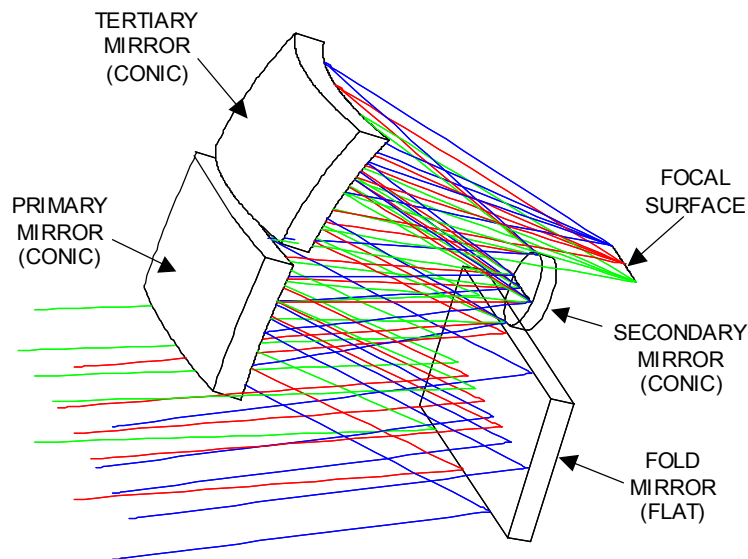


Figure 9.4-1: Three mirror unobscured anastigmat with a 15-degree field-of-view, FOV limits are indicated by different colored rays.

The 15-degree FOV for the 100 km altitude was accommodated by an unobscured three-mirror anastigmat with a fold flat. The design uses a $f/2.67$ so for a 15 cm aperture is has a focal length of 40 cm. The field of view is linear. Because the initial design placed the detector plane well outside the spacecraft, the additional flat was inserted to flip the telescope. Both the optical layout/path and CAD work-up of the off-axis is depicted in Figures 9.4-1 and 9.4-2.

The 5-degree FOV was accommodated an on axis design which we varied for 2 aperture versions. A 25 cm aperture version had an $f/2.67$ with a linear field of view. It is an unobscured three-mirror anastigmat with a fold flat. A 50 cm version has an $f/1.1$ design with approximately a 50% diametric obscuration, which is equivalent to a 25% areal obscuration. Once again because the detector would lie away from the spacecraft, an additional flat was added to place

the detector within a cutout on the axis of the primary. A 70% transmission was assumed end-to-end. Figure 9.4-2 depicts both the optical layout/path and CAD work-up of this telescope design.

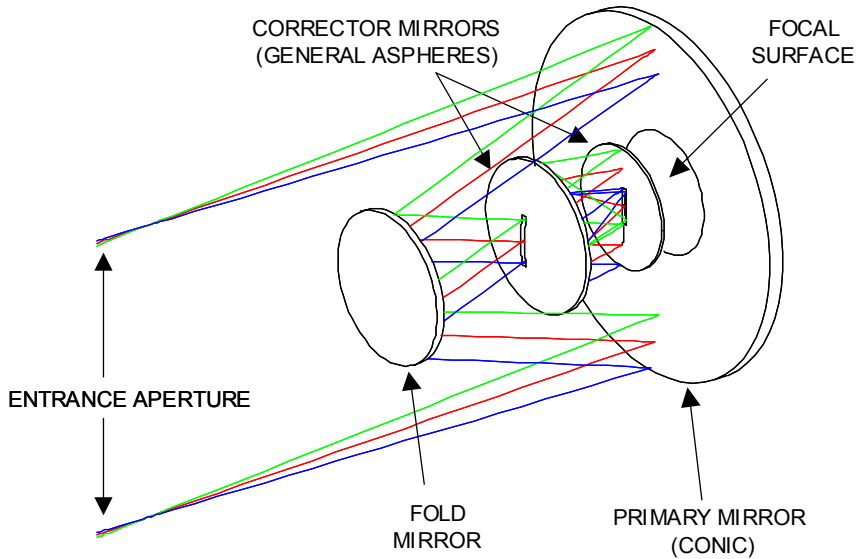


Figure 9.4-2: On axis telescope system with a 5-degree linear field-of-view.

The system scaling assumes albedos measured on Earth ice (50%) and strives to achieve about 2000 collected 1-micron photons per emitted laser pulse. The resulting 800 signal electrons are based on performance of the linear mode Perkin Elmer 1-micron Si avalanche photo-diode. By applying a standard link analysis and making some preliminary decisions about telescope diameter we derive pulse energies and pulse rates for a JIMO altimeter point design. The 15-degree FOV requirement for the 100 km altitude case poses a considerable design constraint on the laser pulse rate and energy per pulse to achieve the contiguous 50-meter diameter sample spots on the surface. A summary of the designs for both FOVs is listed in Table 9.4-1.

Table 9.4-1: Point Designs for the Laser Altimeter at 400 and 100 km Altitudes on Europa

Alt (km)	Ground Track (m/s)	Swath (km)	FOV (deg)	Tele D. (cm)	Pulse Rate (kHz)	E (mj) per Pulse	Trans. Power (W)	Bus Power (kW)	Total Mass Goal (kgs)	Scan Rate (Rad/s)
400	1017	34.9	5	25	15	25	400	8	<80	1.8
100	1305	25.7	15	15	15	4	60	1.2	<30	6.8

The system is bistatic as were MOLA and ICESat (Figure 9.5-1). To achieve the high coverage rate, the scanning prism will deflect the laser beam to a spot on the surface so any pointing knowledge is derived purely from diagnostics on the transmit beam. Some of the laser light could be diverted into an off-nadir star-tracker as has been validated in GLAS to calibrate any laser transmit path beam wander. Because the receive telescope has a large field-of-view (15 deg and 5 deg for the 100 and 400 km cases respectively), it is assumed that the measured spot will fall somewhere on the large detector array. The detector array does not provide any enhanced resolution since any 50 m diameter ground spot will be well within a single pixel. The array therefore only accommodates the optical constraints of the telescope design. This design results in a linear array about 1 mm by 10 mm at the detection plain where each of the ten pixels would be equivalent to the current flight hardened analog detectors.

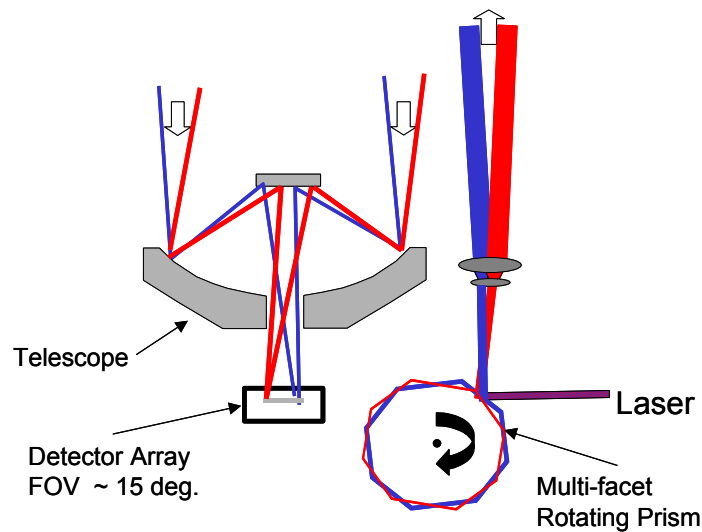


Figure 9.4-3: Bistatic baseline schematic of laser altimeter.

9.5 Design Options Description

As stated in the design assumptions, flight proven assumptions were used to derive pulse rates etc. The Perkin-Elmer 1-micron linear detector has an approximate NEI of 10, thus the signal strategy for MOLA and ICESat was to have a high SNR (~100) receive signal that could be cross correlated with the outgoing pulse shape. In this manner, similar to sub-pixel interpolation in passive systems one can achieve considerably enhanced resolution within the 50-meter diameter of the ground spot. One should achieve the 10-meter lateral resolution or better. The height resolution is determined both by the laser pulse-width, the detector speed, and the SNR. If limited only by the pulse-width, then once again high SNR can help to sub-pixel determine the height as a function of time as long as the detector is fast enough (> 1 GHz). In addition, crossover data collection will help to sub-pixel the height measurement by cutting back bias errors. MOLA had a 10 ns laser pulse-width and after full data set reduction, relative heights

were achieved to approximately 16 cm relative resolution. GLAS appears to have improved on that by a factor of three using a laser pulse approximately half the width (~ 5ns).

There is considerable development in alternative detectors and sampling strategies. New solid-state III-V detectors show promise for getting to NEIs of 1. Hybrid devices, which integrate semiconductor photo cathodes and photomultiplier-like gain regions show similar promise of high linear gain without excess readout noise. This additional performance could be used to reduce laser power/mass or increase sampling rate and thus increase lateral resolution.

Non-linear detectors (Geiger-mode) have also been demonstrated for obtaining high resolution NEI 1 detection of surfaces. In most cases these have been applied to low SNR regimes and high pulse sampling because these devices latch after a photoelectron is generated whether due to signal, dark current or radiation. If one is over-sampling, then false events can be de-correlated by their inconsistency with the overall data set. The JIMO data campaign is likely to be very well suited to this type of detector because one does not expect to encounter multiple scattering events in range like one observes on Earth from aerosols or foliage. Still the radiation and normal dark current pose a considerable noise issue, and one would therefore like over-sampling or lateral correlation to resolve noise ambiguities. In order to apply this highly sensitive and high resolution detection strategy on JIMO, we would be required to design a variable IFOV on our large FOV telescope or alternatively pursue a scanned narrow FOV telescope with such a detector array on axis. While the telescope would be simpler, the gimbals or scan mirrors would be complex and massive to accommodate the required transverse rates. These more complex designs will be discussed in the appendix to this section.

The laser for the altimeter is based on slab designs recently demonstrated by Northrop Grumman Space Technologies. Their new end-pumped slab has been demonstrated at powers ranging from hundreds of Watts to over 1 kW, pulsewidths from 0.75 ns to 10 ns and pulse rates from 5 kHz to 37 kHz. The masses of the device are conservative based on current TRL 4-5 maturity and do have margin for additional mass reduction. The masses for the two point designs are in the full system mass Table 9.4-1.

9.6 Radiation Considerations

In the case of the laser the principal elements of concern are the laser crystal and pump laser diodes. Extensive development and testing have been performed on both elements in a variety of configurations. To date no impact in performance or permanent damage has been observed from a laser diode that is based on a III-V material system. Testing has been done up to 2 Mrads and while the quoted total dose rate is higher at Europa, it is unlikely that the higher rates will trigger an effect over and above what has not been observed at the

lower dose rates. Likewise, the laser material has been tested up to 1.5 Mrads. The laser materials do respond to radiation and especially the material base-lined for this instrument. However, irrespective of the total dose rate, the laser reaches a saturation limit in damage based on defect density limits for the crystal system. Depending on the laser design it is possible that reasonable performance can still be extracted at or above the saturating radiation damage level. Adding a chemical agent to the material, which effectively hardens the laser, can minimize the saturating level of damage. The hardening agent will slightly modify the laser from optimum performance in efficiency, but it will still perform well within the design constraints of this mission.

The final area of concern for the altimeter is the detector. Radiation effects were measured on both the Silicon based APD flown on MOLA and a commercial InGaAs APD. Neither of the components suffered total dose permanent damage that was detectable, however the Si device which was enhanced for 1 micron response by increasing the thickness showed detectable effects from the radiation doses. The radiation events look effectively like photon responses at the detector output. Through data correlation and processing algorithms much of the radiation noise could be eliminated. Data obtained from the InGaAs indicated complete immunity from the radiation. It was suggested that the small active regions where carriers are generated have too small of a cross section (extinction) for any of the high-energy events. Each device is different and any postulated device would need to be tested to resolve all concerns posed by radiation.

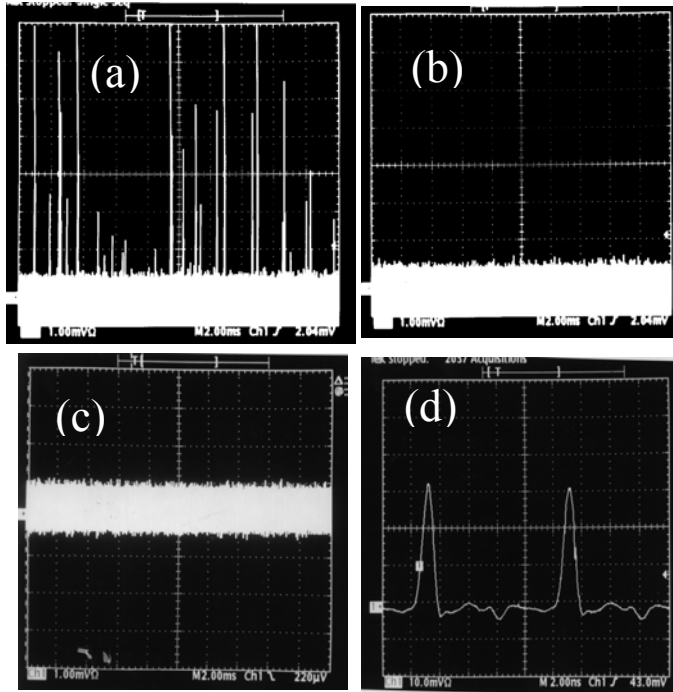


Figure 9.6-1:5. Co^{60} γ -ray test results for Si and InGaAs APDs. (a) Dark response of EG&G Si-APD at 25 krad/month; (b) Dark response of EG&G Si-APD with no radiation; (c) Dark response InGaAs APD at 250 krad/month, 10x higher dose rate than (a); (d) Photon response of InGaAs APD to low level laser light, after receiving 100 krad γ -rays. Note: voltage scale 10x lower than Figure 5(a)-5(c). Scans (a), (b) and, (c) are 20 ms full scale, scan (d) is 100 ns full scale. Zero is offset for (c) and (d) compared to (a) and (b).

9.7 Mechanical and System Details

As discussed above the most challenging aspect of the laser altimeter was choosing the most optimum telescope and optical path to minimize full system mass and maximize science return. The off-axis telescope design accommodates the large 15-degree FOV but scales in mass quickly with aperture size. Consequently we were forced to trade the laser power squared vs. aperture size for the telescope, as shown in Figure 9.7-1 and Figure 9.7-2.

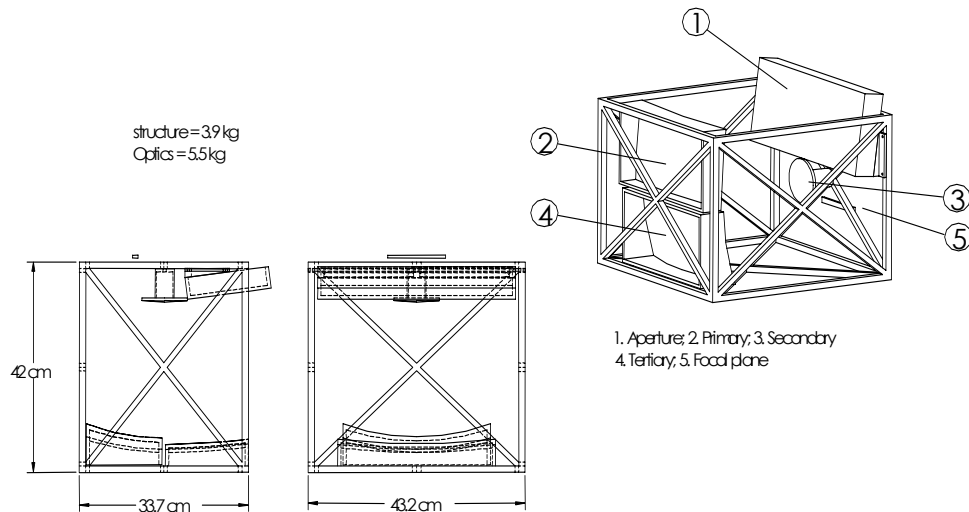


Figure 9.7-1: 15cm un-obscured anastigmat off-axis telescope with 15 degree linear FOV. The 15-degree linear FOV is aligned parallel to the long axis of the entrance aperture.

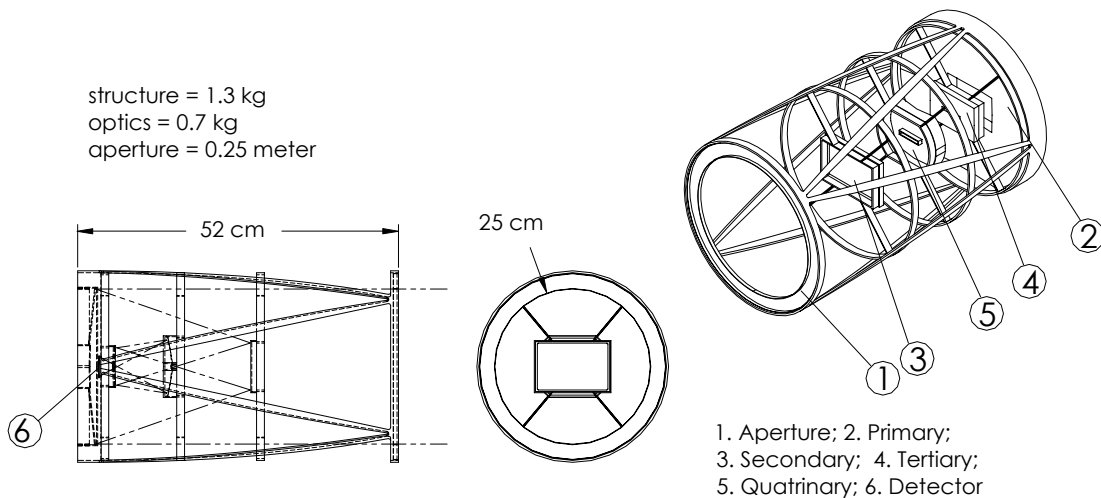


Figure 9.7-2: Mechanical realization of the 25 cm on-axis telescope with 5 degree FOV. Blackened Mylar would cover the exterior tube skeleton to keep out stray light.

We depict a first cut lightweight mechanical realization of the off-axis astigmat and the on-axis. The 15 cm aperture results in a total mass of 9.4 kg for just the telescope assembly. While an additional reduction in aperture would have helped reduce the mass to nearly one-fourth its weight, the laser power would have increased considerably and resulted in higher overall system mass.

The scanning mechanism for the transmit beam is a multi-faceted mirror. To accommodate a 15-degree FOV, each facet must cover at least a 7.5-degree rotation angle. For the 15 degree FOV requirement, the optimal number of facets for the scan mirror is 48. For the 5 degree FOV case, the optimal number of facets is 144. These values also minimize the spin rate of the mirror, the result of which is to minimize the laser pulse repetition rate. To prevent the laser beam from reflecting back into the laser cavity, the minimum number of facets any rotating mirror must have is three. Further, to prevent the laser beam from missing the mirror entirely, the maximum number of mirror facets is seven. With these fewer number of facets, to maintain a constant revisit rate, both the mirror spin rate and the laser pulse rate must be increased significantly from that required for the 48 facet case.

Table 9.7-1 lists the optimal requirements for the scanner to achieve the 100 km, 15 degree FOV and the 400 km, 5 degree FOV cases. The mass includes the mirror, motor, and electronics required to operate the system. The mirror size is assumed to be 5 cm in diameter (based on a beam diameter of about 1 mm for the 400 km case) with a mass of less than 0.5 kg. The motor is assumed to be a direct drive, DC torque motor. This type of motor minimizes weight, size, power, and response time while maximizing rate and position accuracies. The power to maintain a constant scan rate (33 rpm for the 15 degree FOV case) is much less than 1 watt, however, 1 watt is allocated to provide a reasonable startup time. The driving requirements are due to the 100 km, 15 degree FOV case. These values will scale up with mirror size. Mirror size can be estimated as:

$$\text{Mirror Radius} = R = 2 \cdot D / \sin(\gamma)$$

Where: D = Laser Beam Width on Mirror

γ = FOV Angle

Table 9.7-1: Motor Requirements

Alt (Km)	FOV (Deg)	Revisit Rate (Sec)	Laser Footprint (Meters)	Pulse Rate (KHz)	# of Facets	Scan Rate (rad/s)	Mass (kg)	Peak Power (kw)
100	14.9	0.038	50	13.526	48	3.4	4.5	.001
400	5.05	0.049	50	14.245	142	0.9	4.5	.001

**Table 9.7-2: Summary of Contributing Masses and Powers
for the Laser Altimeter**

Orbit Altitude	100 km	400 km
Laser System	30 kg	80 kg
Telescope System	9.4 kg	2 kg
Prism and other Optics	4.5 kg	4.5 kg
Electronics (w/shielding)	10 kg	10 kg
Total Mass	43.9 kg	96.5 kg
Laser Power (prime)	1.2 kW	8 kW
Detector, Electronics and Beam Control	200 W	200 W
Total Power	1.4 KW	8.2 kW

Shown in Table 9.7-2 is a summary of the estimated masses. The most accurate mass estimate is for the telescope. The laser is at TRL 4 and the mass is based on a breadboard. It is estimated as a high mass and should come down with optimization. Similar situations exist with the prism assembly and the electronics.

9.8 Key Technology Developments

The laser altimeters as specified in the baseline have a very strong head start toward realization. The lasers of interest have been demonstrated in the laboratory at breadboard levels. Other government programs are investigating space qualification of laser sources at the requisite power levels. The current highest risk is cooling and two approaches are being developed. One would entail development of a liquid cooling loop for the laser and the alternative would require heat pipes with a removal interface of 50 watts/cm². Based on other funded programs and current state of laser knowledge it appears that the required laser is at TRL 4 and moving quickly to TRL 5 while the cooling capability has been demonstrated on another instrument at related, but not exactly similar levels. This risk could be reduced if NASA performed complementary development of a laser and cooling capability.

The mission concept is new and while it depends on technologies that have been demonstrated in related applications, they have not been proven for this application. That would include the telescope, scanning prism plus transmit

telescope, and appropriate detector array. It is important to define the detailed altimeter architecture early to identify any other technologies that can be applied but require additional development. This area is under heavy investigation and a variety of approaches could be conceived to achieve both basic and extended science goals. Detectors and processing algorithms must be developed and validated for the environment and thus comprise the most important area of readiness for the laser altimeter. Existing technologies must be subjected to environments and tested real-time with decorrelation algorithms designed to remove background or radiation induced false hits. Detectors with higher performance and resistance to radiation are currently at TRL 4.

9.9 Schedule Estimate

As stated in Section 9.9, the laser altimeter requires technology development in the laser, cooling system and higher performance, radiation-resistant detectors. Since lasers similar to the required capability are currently approaching TRL 5 and the cooling system is maturing quickly as well, they could both achieve a TRL 6 within two years. Detectors with higher performance and resistance to radiation might be developed within the next three years. Devices at TRL 6 could be demonstrated in two to three years but require cooperative investment with other agencies. It is unlikely that other agencies will pursue the radiation problem as vigorously as NASA needs and therefore NASA will need to design its own focused effort.

The schedule for developing the laser altimeter is based upon analogies to the development schedules of comparative legacy instruments as described in Section 9.7. The Geoscience Laser Altimeter System (GLAS) built for the Ice, Cloud, and Land Elevation Satellite (ICESat) mission was completed, after a series of developmental delays, in 62 months while the second version of the Mars Orbiter Laser Altimeter (MOLA2) built for Mars Global Surveyor (MGS) was completed in only 19 months. The MOLA instrument built for MGS, however, was a rebuild of the original MOLA instrument built for Mars Observer (MO). The original MOLA instrument required 34 months to build. The average development time of the ICESat/GLAS and MO/MOLA instruments is 48 months. Given the instrument development difficulties that occurred with GLAS, resulting in a 21-month delivery delay and an 18-month launch delay, and other laser instruments such as the Multi-Beam Laser Altimeter (MBLA) planned for the Vegetation Canopy Lidar (VCL) mission, which was subsequently cancelled due to development difficulties with the MBLA, it is recommended to use the development time of the ICESat/GLAS instrument of 62 months as the baseline schedule for the JIMO laser altimeter.

9.10 Legacy Instrument Description

The design concept for the JIMO laser altimeter is derived from the Mars Orbiter Laser Altimeter (MOLA) that flew on both the Mars Observer and Mars Global

Surveyor, and the Geoscience Laser Altimeter System that flew on the ICESat satellite. Both systems use a diode pumped, Q-switched Nd:YAG laser transmitter. The MOLA receiver is 50 cm diameter while GLAS is 1 m diameter. The primary difference between the JIMO instrument and the heritage instruments is the radiation environment which will require the development of rad hard Nd:YAG laser technology. In addition, a more complex beam scanner on transmit and an IFOV scanner will be required on the receiver to accommodate the high coverage rates at Europa.

Table 9.10-1: Proposed Laser Altimeter vs. Legacy Instruments

INSTRUMENT	Proposed	MGS/MOLA2	ICESAT/GLAS
Mass (kg)	56.2	28	300
Power (W)	900 Peak	34.2 Peak	350 Peak
Data Rate (Mbps)	0.482 Peak	0.064 Peak	0.52 Peak
Wavelength [microns]		1.064	1.064 and 0.532
Power per pulse [mJ]	4 mJ, 15 kHz	40-45mJ, 10Hz, 10 ns/pulse	75mJ, 35mJ, 40 Hz, 4 ns/pulse
Vertical Resolution (m)	50 cm	2 m local (relative) and 30 m global	15 cm real-time, post-processed to <5 cm

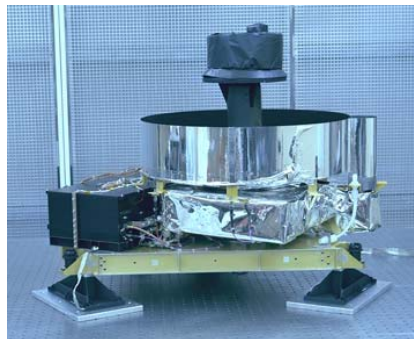


Figure 9.10-1: MGS/MOLA2 (Reprinted courtesy of NASA).



Figure 9.10-2: ICESat/GLAS (Reprinted courtesy of NASA).

10.0 Laser Reflection Spectrometer

10.1 Science Measurements

The laser reflection spectrometer will make mid-IR observations in the wavelength range of 4-10 microns with spatial resolution of approximately 200 meters/pixels, and with greater than 90% spatial coverage. It will remotely sense organics (via mid-IR spectroscopy) in surface layers for all icy moons.

10.2 Design Drivers and Options Examined

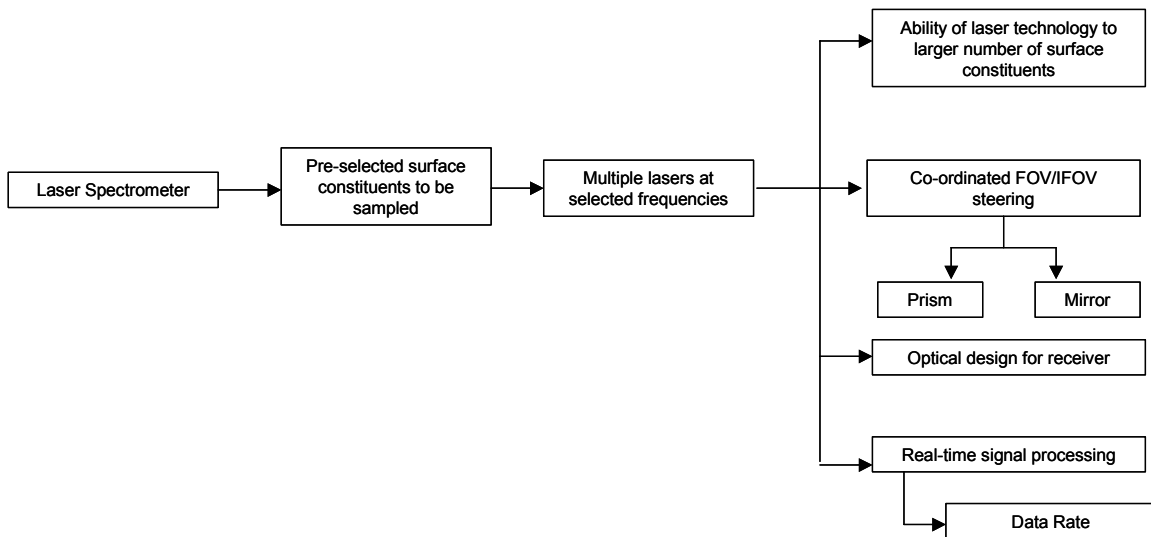


Figure 10.2-1: Laser absorption spectrometer trade space.

The trade examined for the laser absorption is shown in Figure 10.2-1. The need has arisen for an active laser spectrometer for JIMO. Because the Jupiter icy moons have extremely low surface temperatures and reflect little sunlight, passive thermal IR emissions and visible reflections are in many cases too weak to derive useful high-resolution spectral information. It has been proposed to use a laser-based instrument to actively interrogate the various key species that might be contained at or near the surface of each moon using lines resonant with specific molecular species of great interest. In the presence of the species of interest, an “on-resonance” wavelength signal will be significantly enhanced due to selective reflection, a well-known laboratory method for characterization of crystals in the IR-FIR spectral region¹. We call this new type of remote sensing surface chemical analyzer the Multi-Spectral Selective Reflection Lidar (MSSRL). The list of potential life relevant species is large so we scope the requirements and demonstrate the general capability of this instrument, using five specific molecules of known interest, although other molecules might be added or substituted based upon specific science drivers. We have selected NH₃ (ammonia), CH₄ (methane), CO₂ (carbon dioxide), CO (carbon monoxide), and CH₃OH (methanol). Isolated absorption lines were identified for each species

with a neighboring (spectrally close $< 10 \text{ cm}^{-1}$) off resonance line that did not overlap with absorptions in any of the other species in the interrogation set. Thus the general concept for the instrument is to transmit 10 wavelengths, five of which will be on resonance for the above species and five that are off-resonance. A separate narrow line width laser emits each wavelength of interest. The laser pairs are modulated 180° out of phase with respect to each other. After a roundtrip to the moon's surface and back through the receive telescope both wavelengths are incident upon the same spectrally resolved photo-detector. Each wavelength will be reflected equally and produce a dc photo response in the absence of the species of interest. In the presence of the species of interest, a portion of the "on" wavelength radiation will be enhanced due to the resonant reflection effect resulting in an imbalance in the reflected light. The differential reflection produces an ac component in the photo response that serves to indicate the presence of the compound.

As in the case of the laser altimeter all MSSRL wavelengths will be painted simultaneously on the moon's surface transverse to the ground track. A single but separate telescope will collect the reflected intensities, which is bore-sighted to the full FOV. All of the transmitted wavelengths will be superposed into a single scanning footprint so that the sampling strategy will copy nearly identically that indicated in Figure 9.3-1. This instrument will allow direct correlation between surface content and ice topography and should prove a powerful tool for understanding the chemical content in the ice and the processes that create that ice on these moons. As previously noted other wavelengths than the five selected here could be handled by extending the general approach.

10.3 Baseline Instrument Description

Because of the surface reflection enhancement effect, the technique used for MSSRL is distinct from traditional differential absorption Lidar (DIAL) where the absorption produces a reduction in intensity. In hardware design, however, MSSRL is similar to DIAL. The MSSRL limiting technology is effectively the transmitted laser power to the surface of the moon. Consequently a balance has been struck between sample size, aperture and laser power, trying to keep laser power below ten watts for any given wavelength. The reflection effect is limited to the first few hundred microns of the surface material; therefore unlike traditional DIAL, this technique applied to JIMO will not require range resolution. The laser altimeter will establish the surface profile and MSSRL will determine surface content for the established topography. As a result, the MSSRL will continuously illuminate to allow full sample integration and thus permit use of low peak power (continuous wave) laser diodes to excite the surface species. In addition, a larger sample size (200 meter diameter ground spot size) was chosen to further lower the power requirements. This choice also relaxes the scan requirements because fewer footprints/second will be required to cover the same FOV compared to that of the laser altimeter.

Table 10.3-1: Sample Selections for Laser Lines for Five Species of MSSRL

Species	On λ (cm⁻¹)	Off λ
NH ₃	1070	1060
CO	2139	2149
CO ₂	2345	2335
CH ₃ OH	1029	1039
CH ₄	1301	1291

(Note: 3000-3600 cm⁻¹ and 1550-1750 cm⁻¹ were avoided because of potential water ice interference.)

Listed in Table 10.3-1 are the 10 wavelengths chosen to allow detection of the 5 species selected. Assuming a sample size of 200 meters produced an integration period of ~1 ms per detection spot. Using a similar link analysis as applied above for the altimeter we were able to derive the required laser powers and telescope sizes to achieve at least 1000 signal electrons per species. The assumptions applied were a detector quantum efficiency of 0.2 and a surface reflectivity of 10%. It can be assumed that all the transmit radiation wavelengths hit a single ground spot despite their wide spectral diversity. This novel transmitter concept will be described below.

Table 10.3-2: Point Design Calculation of MSSRL for the Two Cases (100 km & 400 km)

Alt (km)	Ground Track (m/s)	Swath (km)	FOV (deg)	Tele D. (cm)	Trans. Power 10 μ m (W)	Trans. Power 2.5 μ m (W)	Bus Power 10 λ 's (kW)	Scan Rate (Rad/s)
400	1017	34.9	5	50 On-axis	1.5	6.0	0.5	0.56
100	1305	25.7	15	25 Off-axis	0.5	1.0	0.35	1.7

(Note: Only the powers for the lowest and highest wavelengths are tabulated, but the bus power includes all ten transmitters using the same link calculation.)

Once again the two telescope types described in the introduction were applied to the 100 km 15 degree FOV case and the 400 km 5 degree FOV case. In Table 5, we display the results of the link calculation using the assumptions listed earlier and the goal of trading laser peak power and aperture weight. There are two significant differences between this general system design and that of the laser altimeter. The optical path of the telescope must be re-collimated so that all the light can be passed through a dispersive prism made out of BaF₂, CaF₂, or NaCl. Secondly, a Germanium or well-developed HgCdTe detector is assumed in linear mode vs. the low NEP detectors or photon counting detector used in the altimeter. The detectors will be designed to map in correlation to the chosen wavelengths and the dispersion properties of the prism. It is likely that only 5 detectors (or detector arrays –5 by 128) would be required.

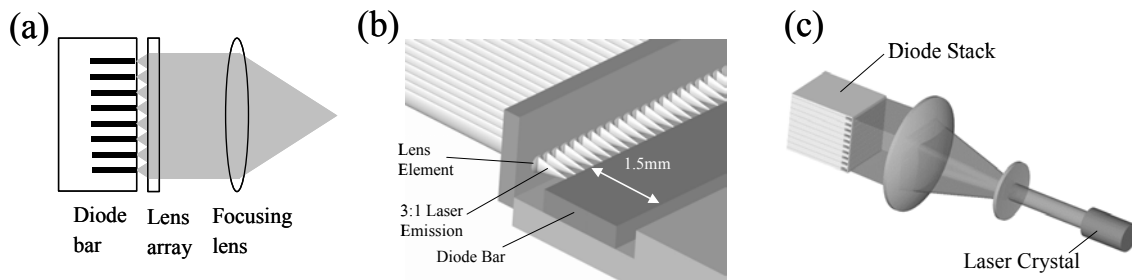


Figure 10.3-1: NASA ESTO diode stacking technology developed for solid-state laser pumping. (a) Schematic of elements (b) CAD depiction (c) elements stacked for diode pump module to excite a laser crystal.

The transmitter is a novel design and allows the potential to minimize peak laser power per emitter. Under NASA-ESTO funding The Aerospace Corporation has developed a diode laser stack that has lens arrays individually mounted to each laser diode element. The general concept of the NASA ESTO work is to use high performance GaP microlenses in conjunction with arrays of single mode laser emitters to enable an incoherent superposition of many laser diodes in the far field. The building block concept is depicted in Figure 10.3-1. The diode laser technology that would be applied here is the quantum cascade laser that has been proven to emit over the entire wavelength region of interest. Thus each wavelength bar would contain 20-100 emitters per cm laser bar. Each of those emitters would be a Bragg grating single mode device designed to operate within a particular temperature window. The interfacing lens array would have custom GaP micro-lenses with curvatures appropriate to the particular wavelength so that after the final collimation optic this device's ground footprint would match that of the other diode bars. This design allows for systematic compensation of all the wavelengths so they match up in divergence once they are in the far field. Each element in the stack is individually addressable and therefore could be oscillated in phase or out of phase with its partner wavelength. This design allows one to spread the required peak power among many emitters so in the case of the 6 W transmitter, no single diode element would need to be greater

than 60 mW if 100 emitters are laid out on the chip. Quantum cascade lasers up to 1 watt have been demonstrated, leaving considerable design margin consistent with their current maturity. The overall dimensions of the stack are small, less than 64 cm³. A CAD simulation of the stack is shown in Figure 10.3-2. The device will run on low voltage DC and therefore require a simple compact power supply. One potential complicating issue will be that the entire stack will need to run cryo-cooled probably near 100 K. This could necessitate a substantial cryocooler to accommodate the conservative several 100 watts required to power these devices. There is considerable directly relevant research being carried out and this would be a critical area of investment that could decrease mass.

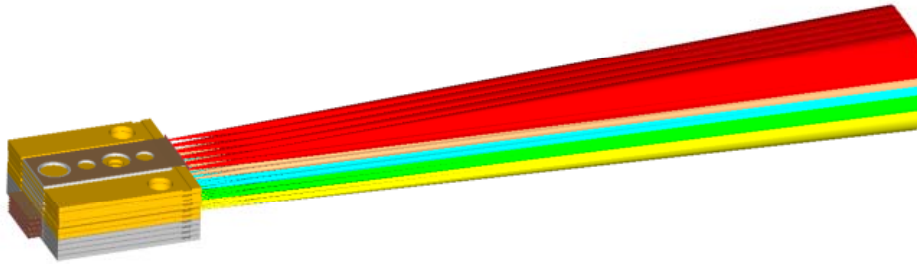


Figure 10.3-2: Multicolor stack of ten diode bars; two bars each at wavelengths 2.5, 3.5, 4.5, 5.5, 6.5 and 10 microns.

10.4 Mechanical realization of MSSRL

As described earlier minimizing total laser power requires increasing telescope diameter to maintain a conservative link budget. Our biggest uncertainty in the mass and power resides with the laser transmitter. Depending on the maturity of the quantum cascade laser and the ability to achieve certain powers as a particular temperature a significant swing could occur in power and mass required to achieve the point design listed in Table 10.3-2. Additional systems engineering is required to establish a baseline given current state-of-the-art for quantum cascade laser capability.

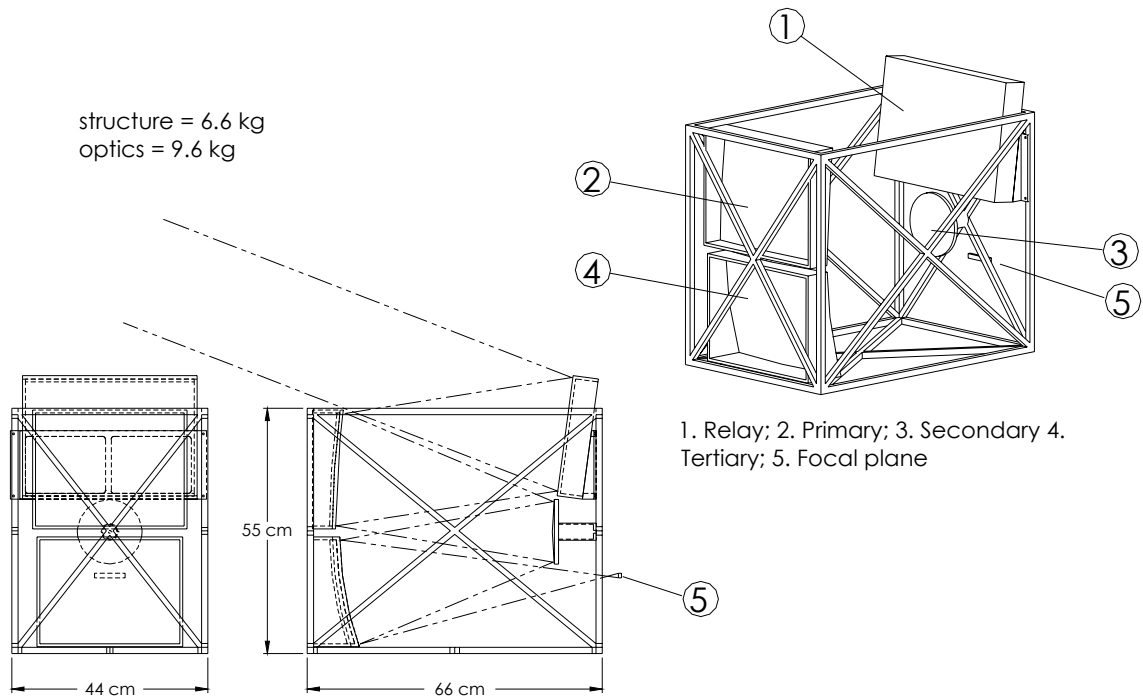


Figure 10.4-1: 25cm unobscured anastigmat spectrometer receiver telescope with 15 FOV.

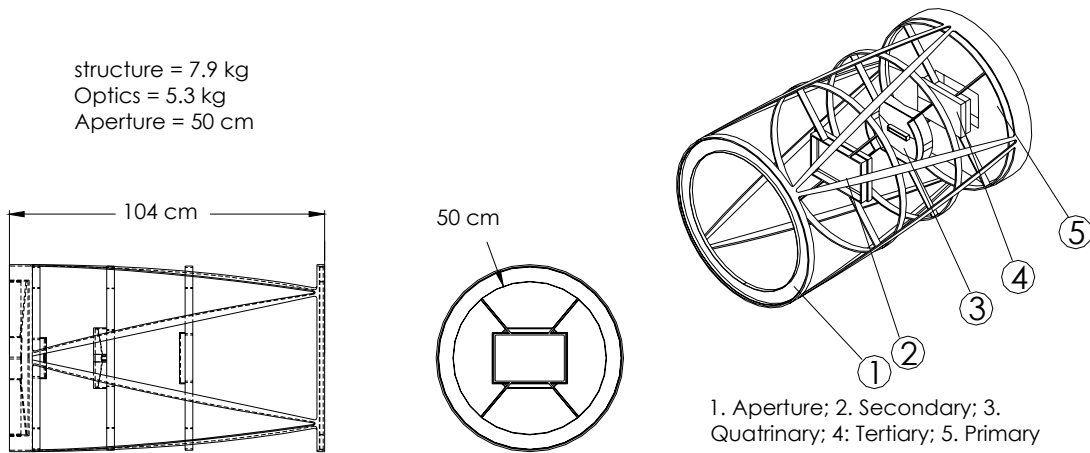


Figure 10.4-2: 50 cm telescope on-axis telescope for 5 deg FOV and 400 km data case. Blackened Mylar would cover the exterior tube skeleton to keep out stray light.

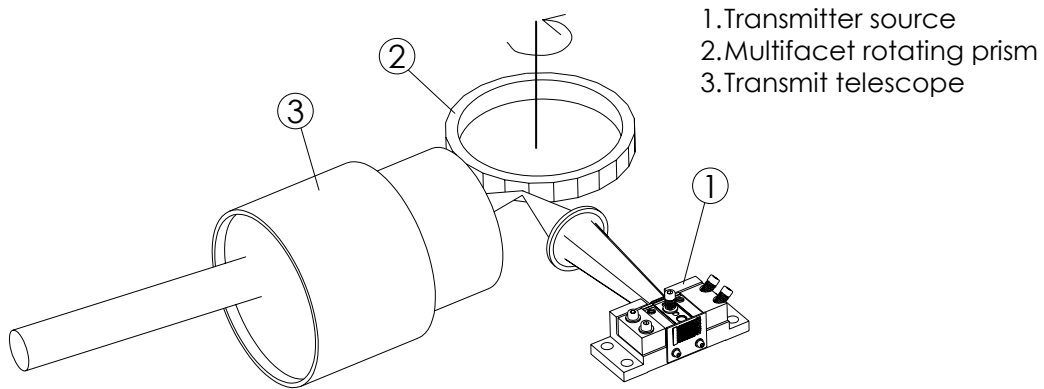


Figure 10.4-3: Spectrometer transmitter detail. Scanner is a rotating multifacet mirror with N sides. Each prism facet sweeps the transmitter beam 5-15 degrees across the track depending on altitude.

We have developed a mechanically compact transmitter package by choosing to incoherently superpose the multiple laser stripes from 10 laser bars, which comprise the required 10 wavelengths. As depicted in Figure 10.4-3, the collimated stack can be focused onto the facet of the rotating prism used to scan the beam thus minimizing the total mass. The final transmission exit aperture would be between 1-2 inches in diameter and depends on our choices for the scanning prism face size and the micro-lens diameters for the final system wavelengths.

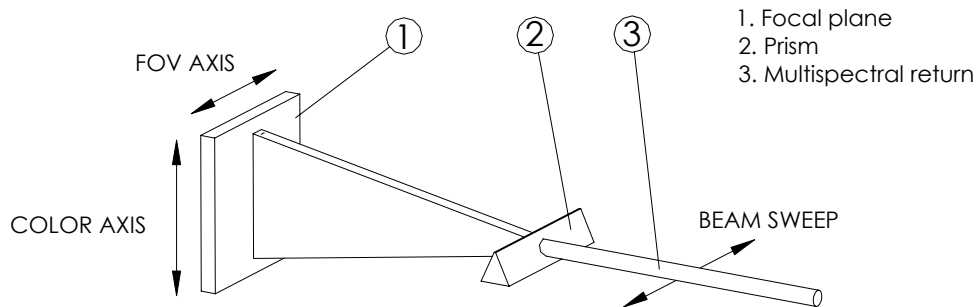


Figure 10.4-4: Spectrometer receiver focal plane detail.

The receiver for the MSSRL is optically more complex than the altimeter because of the requirement to split out the various wavelengths. In Figure 10.4-4 we show what occurs with a collimated beam at the detection plane of each of the telescopes. We cannot specify the final prism material without a clear choice of wavelengths. For the wavelengths chosen, NaCl, Germanium or Zinc Selenide

would be required in the configuration depicted. None of these materials have much dispersion especially to separate the closely space wavelengths. If modulating the transmitter cannot accommodate these closely space wavelengths then one might need to explore a grating concept. There are a number of choices of detector arrays already developed that appear to have the sensitivity required and the geometric definition of the pixels properties. If the specifics do not exist, the technology is well within the capabilities of the industry. Furthermore there is some flexibility in the detector due to the slow speeds; they can probably be built in large formats to simplify the dispersive prism and telescope optical design. The data processing and system control should be very straight forward because the speed of the detector is six orders of magnitude slower than in the case of the altimeter. Simple compact electronics should apply. Because of the slower scan rates we may be able to avoid using a rotating prism and employ a fast steering mirror. This would also allow dwelling on each targeted ground spot for the ~ 1 ms integration time. The telescope designs have been adjusted for the parameter shown in Table 10.3-2 and their detail specifications are shown in Figures 10.4-1 and 10.4-2.

10.5 Radiation Design of MSSRL

In many respects the MSSRL is similar to the laser altimeter but with respect to radiation may be more resistant. The laser source is based purely on diode laser devices in primarily III-V compounds and from the historical data presented earlier has never shown any deleterious response to radiation. Because the quantum cascade lasers are somewhat out of the mainstream for laser devices, there is some slight chance that antimonide or some other elements could pose a problem. This must be double checked to insure reliability. The electronics for the system are quite slow and thus can be run in fault tolerant configurations to insure radiation resistance without unique radiation designs. The only area of uncertainty is the detector. HgCdTe has been tested extensively for SBIRS and STSS on the defense side. While these detectors have proven radiation resistant, it is not clear that they would work as well for the MSSRL application (near photon counting). The instrument will be very responsive to increases in dark current that is another byproduct of radiation damage. The radiation impact on Germanium devices is not known, and it is recommended that these and others be investigated during the design phase.

Table 10.5-1: Summary of Contributing Masses and Powers for the MSSRL

	100 km	400km
Laser plus Cryocooler	20 kg	30 kg
Telescope System	16.2 kg	13.2 kg
Prism and other optics	2 kg	2 kg
Electronics (w/shielding)	10 kg	10 kg
Total Mass	48.2 kg	55 kg
Laser and Cooler Power (Prime)	0.5 kW	0.75 kW
Detector, Electronics & Beam Con.	200 W	200 W
Total Power	0.7 kW	0.95 kW

10.6 Optical Design Options

Because of the optical complexity of achieving full coverage with the right granularity of the data in a short time, alternate optical designs were considered. In the current configuration no attempt to scan the IFOV of the receiver in conjunction with the scan of the transmitter prism was attempted. If such a design could be realized then one could take advantage of higher resolution detectors for each ground sample. Some sample approaches are depicted below for how one would treat the light as it hits the detection plane. The most prudent approach would be to spit the light between a single detector element similar to ICESat and an array allowing both signals to be collected. The unpixelized collection could help resolve detector dropouts in the multi-element array by providing the high SNR signal profile in time.

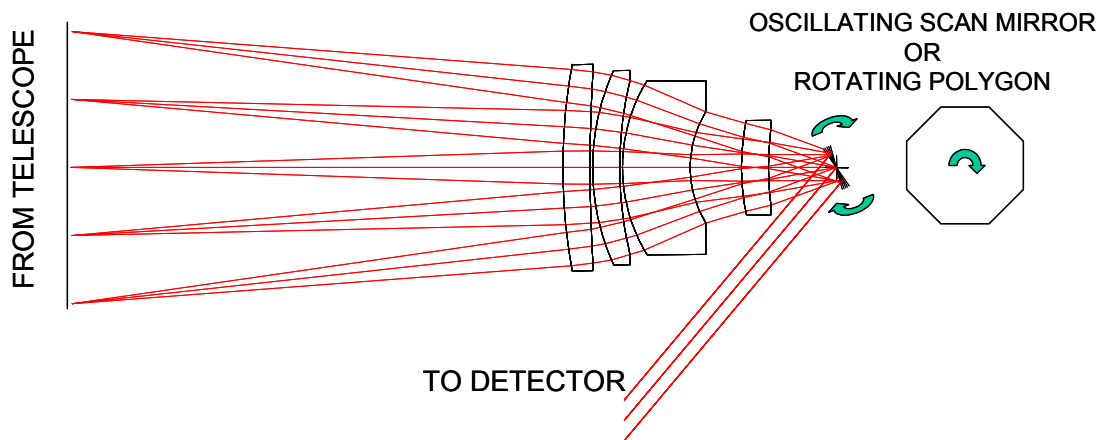


Figure 10.6-1: This design implements an f-theta lens combination. On the left is the detector plane indicating different incident points based on what IFOV we are sampling. The turning prism or polygon must be synchronized with the transmit rotating prism. It may be possible to achieve both functions with the single rotating prism.

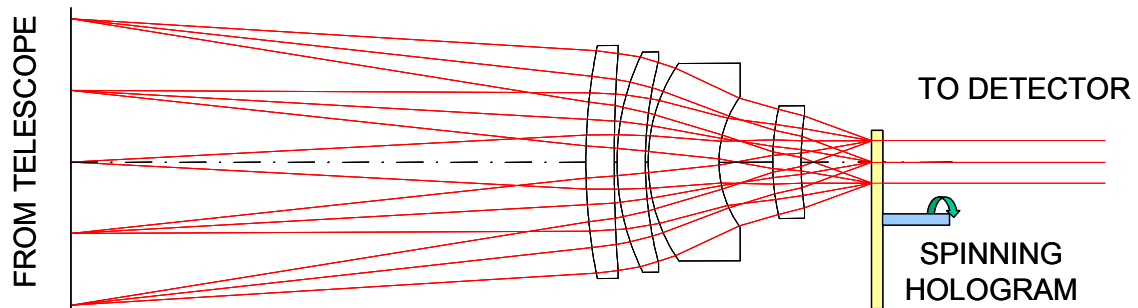


Figure 10.6-2: As in Figure 10.6-3, an f-theta lens is applied however a spinning hologram is used at the focus to re-collimate the light irrespective of the incident IFOV. The spinning grating will compensate for each incident IFOV allowing a common single detector axis.

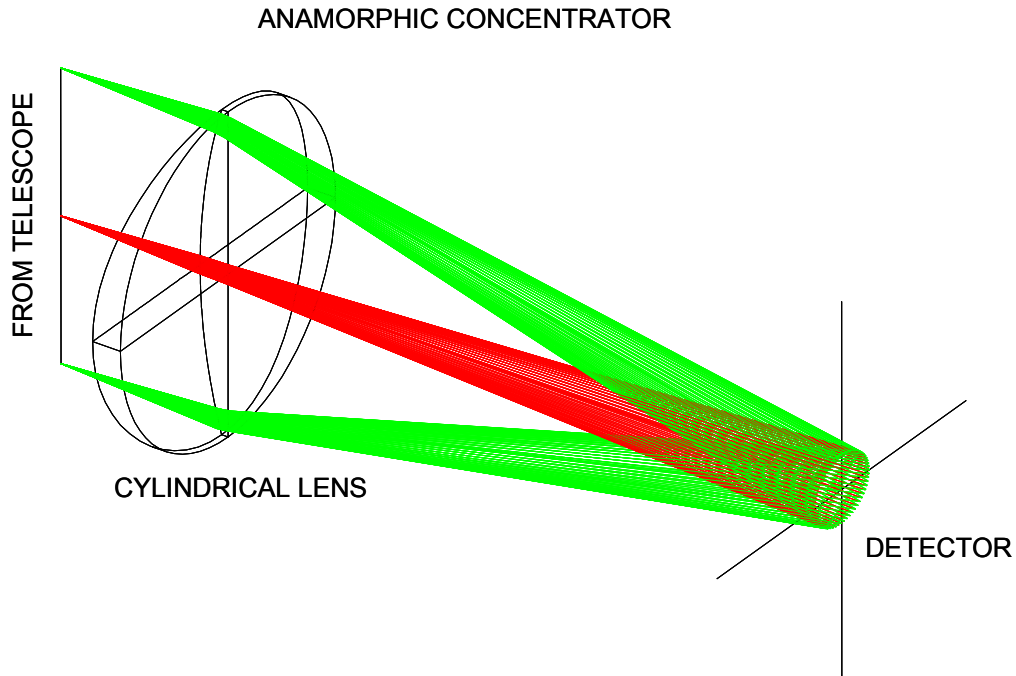


Figure 10.6-3: An anamorphic concentrator would also allow a single detection point.

10.7 Readiness of the Reflection Spectrometer

The MSSRL was conceived based on capabilities that exist in the industry, but as such, does not exist. As in the case of the laser altimeter, the MSSRL should undergo a 1-2 year architecture and trade space study. Preliminary tests should be conducted on materials of interest to clarify the true signal levels and show their consistency with the detection concept. A validation of the concept could be completed in 1-2 years using COTS technologies. The transmitter is based on many quantum cascade lasers grown on a single diode bar. The current quantum cascade laser technology must still be demonstrated in bar format similar to the transformation that has been demonstrated with a variety of other laser elements. Furthermore one would need to develop a detailed system design based on the wavelengths of interest to be determined by the science community. The packaging of the laser bars and integrated micro-lenses are near TRL 5 currently based on the NASA ESTO research effort. The detector and integration with a prism is currently at TRL 4.

10.8 Schedule Estimate

As stated in Section 10.7, the laser spectrometer requires technology development for the transmitter and the detector integration with the receive prism. If wavelengths were defined in the next 6 months, a TRL 6 version of the transmitter could be ready in 3 years. Additionally, the detector concept would need to be defined early and built and tested to demonstrate compliance with the

environment. One would also need to demonstrate optical compatibility with the dispersion specification of the receive prism. The detector and integration with a prism could be demonstrated in 2-3 years at TRL 6.

The laser spectrometer is a new instrument and requires development in many areas from up-front system architecting, materials and component testing and validation, to packaging and overall system validation. The schedule for developing the laser spectrometer is difficult to estimate because no space-based instrument of this nature has ever been developed before. The development schedule for the analogous system, the Aircraft Laser Infrared Absorption Spectrometer (ALIAS) is an aircraft-based instrument, is not representative. Given that this is a developmental laser instrument, it is recommended to set a baseline schedule no shorter than the baseline laser altimeter schedule. Based on the recommendations stated in Section 9.6 for the laser altimeter, the recommended baseline development schedule for the laser spectrometer should be set no less than 62 months.

10.9 Legacy Instrument Description

Nothing like the proposed Multi-Spectral Laser Spectrometer has flown in space to date. The Aircraft Laser Infrared Absorption Spectrometer (ALIAS) instrument is a high resolution four-channel scanning Tunable Diode Laser (TDL) and Quantum-Cascade (QC) laser spectrometer (3.4 to 8 μm) that makes direct, simultaneous measurements (e.g., HCl, NO₂, CH₄, N₂O, CO, and water isotopes, including vertical profiles of the tracers) in the stratosphere and troposphere at sub-parts-per-billion sensitivities; however, these are in-situ measurements at the aircraft. The proposed JIMO instrument would be a remote sensing instrument like the Differential Absorption Lidar systems developed by NASA LaRC. The powers are considerably lower because the integration periods are long and the range is short. Specific technologies that will require further development for a space-based instrument include Quantum cascade lasers at the appropriate wavelengths, scanning optics and Barium Fluoride prisms for the receive channel.

Table 10.9-1: Proposed MSLS vs. Legacy Instruments

	Proposed Instrument	ER-2/ALIAS-I
Mass (kg)	48.2	72
Power (W)	400	UNK
Data Rate (Mbps)		UNK
Wavelength Range (microns)	5 - 8	3.4 - 8

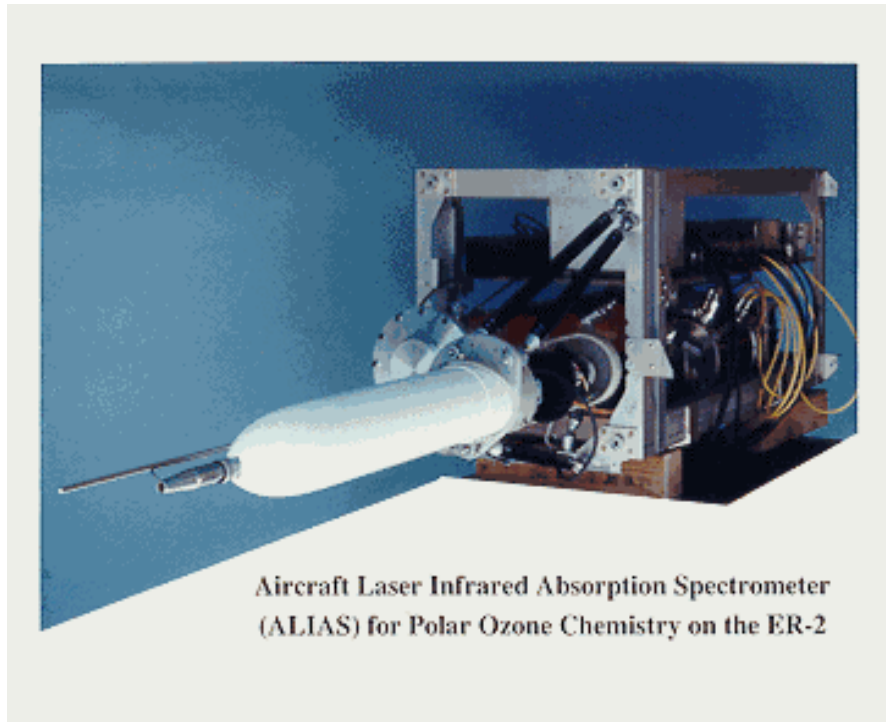


Figure 10.9-1: ALIAS instrument (Reprinted courtesy of NASA).

11.0 Interferometric Synthetic Aperture Radar

11.1 Science Measurements

The Interferometric SAR is designed to map the surface of each moon at very high resolution both horizontally (10m) and vertically (1 m). The end products produced by the InSAR instrument are digital elevation (topographic) maps as well as high quality 10-look SAR imagery utilizing 10 overlapping images. This imagery will be taken at a wavelength an order of magnitude different from that of the proposed polarimetric SAR and will therefore provide independent and complementary information about the surface.

11.2 Design Drivers and Options Examined

The general design flow for the InSAR design is shown in Figure 11.2-1. InSAR surface mapping in three dimensions requires frequencies where the ground penetration is to be small relative to the required vertical resolution. Once the frequency is appropriately selected, the pulse repetition frequency and antenna dimensions are selected to meet surface coverage requirements, keeping range and Doppler ambiguities minimized. The vertical resolution of the solution is then checked, and the process is repeated by varying the antenna dimensions and the pulse repetition frequency until the desired vertical resolution is achieved.

A key constraint that applies in this iterative process is that the maximum azimuthal resolution for an uninterrupted surface strip map is half the azimuthal width of the antenna, and that breaking the coherent integration time into N equal sub-intervals allows N overlapped images to be generated at $1/N^{\text{th}}$ the original azimuthal resolution. This constraint is used to achieve in 1 m vertical and 10 m horizontal resolution for the for the InSAR instrument.

It is not always possible to attain a sufficiently accurate pixel-to-pixel height statistic by increasing power to increase the signal-to-interference ratio. In the present case it was necessary to generate an average statistic from overlapped images to narrow the variance in the height statistic sufficiently to achieve the required vertical resolution.

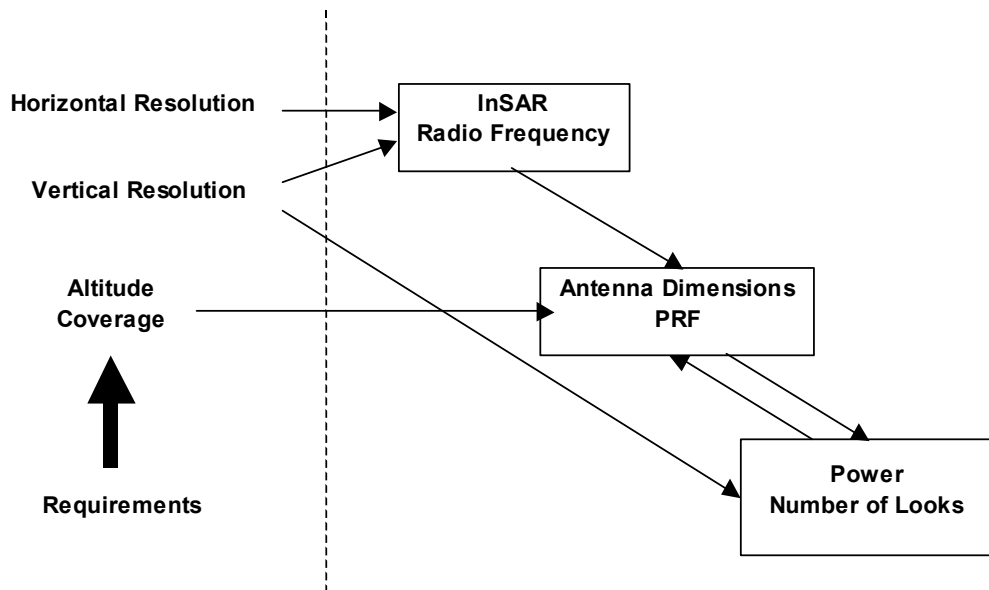


Figure 11.2-1: InSAR trade space flow diagram.

The InSAR is designed to operate at 35 GHz (8 mm). There has been discussion within the community as to the optimum frequency. It is clear that the instrument needs to operate at very high frequency in order to avoid too much penetration of the surface. The frequency of 35 GHz was taken from [Ref 11.2-1]. It is acknowledged that the issue of surface penetration at 35 GHz is open; this design choice was pursued in order to assess the feasibility of a representative instrument. While ongoing frequency trades due to ice sheet thermal emissions and upper regolith scattering structures are anticipated, some baseline needed to be chosen. Frequencies lower than 35 GHz (longer wavelengths) are undesirable because as the wavelength increases the instrument becomes proportionally larger. At wavelengths longer than 35 GHz the size of the instrument would pose an unnecessary mass/volume problem. The selection of 35 GHz is advantageous from a technology development perspective as there are a number of existing and proposed efforts to develop 35 GHz technologies for advanced weather and precipitation radars and these efforts could be leveraged by the JIMO InSAR. Such efforts include the proposed space borne Global Precipitation Mission (GPM).

If a higher frequency is desired the magnitude of the antenna separation (boom length) would decrease. The frequency range with the greatest level of technology development is at 94 GHz. Ground based 94 GHz cloud radars have been in existence since the 1980s. The Airborne Cloud Radar (ACR) also operates at 94 GHz and the CloudSat Radar will operate at 94 GHz.

Icy moon geophysical parameters (radius, rotation rate, etc.), frequency, altitude, ground sample distance, a loss budget, antenna dimensions, and noise equivalent cross section were used as inputs in determining power and maximum

range of operation for the radar. Because Europe is the most stressing case for orbit coverage (due to the relatively short mission time of 30 days), Europa geophysical parameters were used in sizing the instruments. Antenna dimensions compatible with the performance and frequency selection are shown are shown in Table 11.2-1.

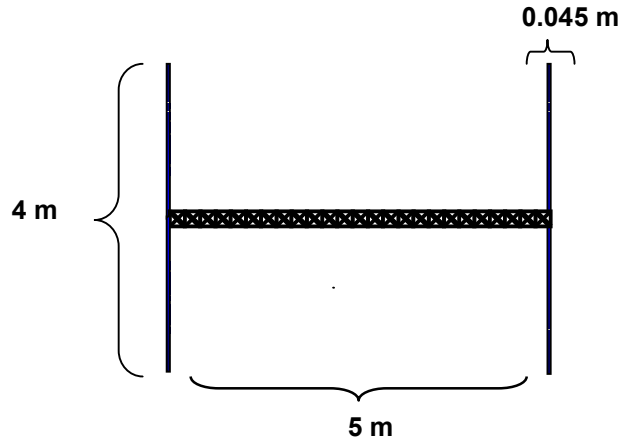
Table 11.2-1: InSAR Antenna Sizing

	100 km	400 km
Antenna Size	2 m x 0.045 m	2 m x 0.150 m

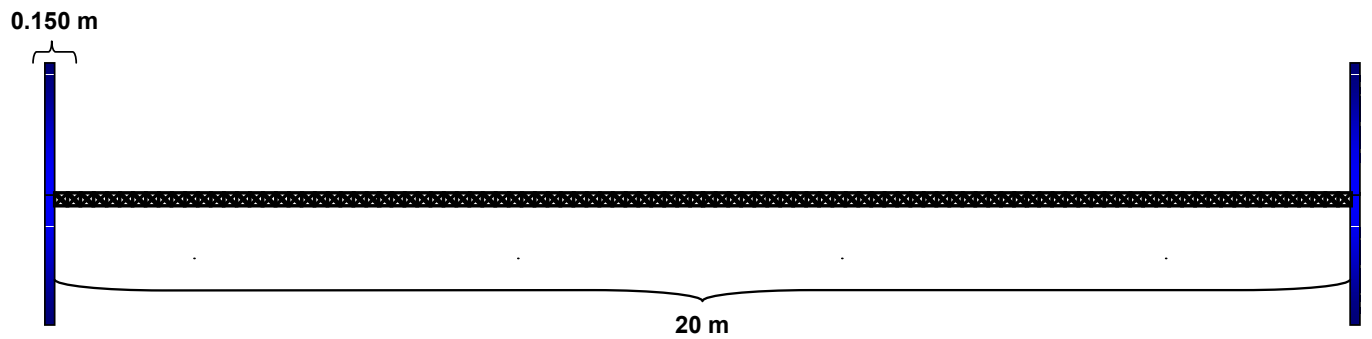
11.3 Baseline Instrument Description

Baseline instrument concepts operating at nominal altitudes of 100 km and 400 km were studied in order to determine the sensitivity to the primary science orbit selection. Additionally, the performance of these cases was assessed at altitudes up to 10,000 km, for operation during a spiral-in and spiral out. In order to produce useful observations (i.e. required SNR and avoidance of range ambiguities) at these higher altitudes, changes to the instruments in both antenna size and power were considered. A summary of how the instrument design changes with altitude is included.

The InSAR is composed of two electronically steered antenna (ESA) pairs separated by a boom whose length is dependent on the nominal operating altitude for the instrument. Each antenna pair contains a receive only (passive) antenna and a radar (active) antenna, for a total of four antennas. The transmit power is evenly spilt between each transmit/receive antenna pair. Each antenna beam will point between 20 and 45 degrees off nadir. The boom length (antenna separation) of 5 m was originally proposed by Masden et al. and confirmed by independent calculation for the 100 km altitude case. For the case of 400 km altitude, the boom length scales linearly with altitude to 20 m. A higher frequency selection for the InSAR would decrease the boom length at the 400 km altitude. Simple schematics (to scale) of the deployed antennas are shown in Figure 11.3-1.



Antenna Configuration at 100 km Altitude



Antenna Configuration at 400 km Altitude

Figure 11.3-1: InSAR antennas (deployed).

In addition to sizing the antenna and power, OrbSAR computed the minimum usable pulse repetition frequency (PRF). A summary of the instrument design parameters is shown in the table below. Note that the power values reflect required power from the bus, not transmitted power.

Table 11.3-1: InSAR Design Parameters

	100 km	400 km
Average Power	1.65 kW	6.63 kW
Peak Power	7.89 kW	32.92 kW
Duty Factor	20%	20%
Frequency	35 GHz	35 GHz
Bandwidth	58.2 MHz	58.2 MHz
Minimum PRF	2.667 kHz	2.456 kHz

The InSAR was designed to map two 30 km swaths, one to the left and one to the right of the ground track. The swath has a Nadir hole, so a complete map is generated with the sum of the orbits. The purpose of mapping two swaths on either side of the ground track is to mitigate the fact that the spacecraft altitude will not be known with sufficient accuracy to provide accurate absolute height. Altitude can be determined by processing the information from both swaths. These swaths will provide global coverage of Europa twice in 30 days. The maximum usable swaths for the present design will exceed the required 30 km swath widths. This results in relaxed pointing requirements, shown in Table 11.3-2.

Table 11.3-2: InSAR Pointing Requirements

	100 km	400 km
Pointing Requirements	3.0°	1.5°
Minimum Grazing Angle	53.2°	54.6°
Maximum Grazing Angle	70.0°	70.0°

A mass and power budget for the InSAR is shown below. The mass of the antenna was calculated using an antenna density of 20 kg/m² (including structures). The boom mass was calculated to support the antenna mass and the canister was sized to hold the boom. Space qualified Ka band transmitters at this power level do not exist and will require development. A transmitter efficiency of 50% was assumed. The mass of the data processing sub-system is sized for seven 1 Gflop capacity processors at 100 km and six 1 Gflop processors at 400 km. These processors do not yet exist in a space qualified design. The mass estimates shown do not include margin.

Table 11.3-3: InSAR Mass and Power Budget

		Mass (kg)		Average Power (kW)	
		100 km	400 km	100 km	400 km
Antenna Subsystem	Antenna 1a	1.80	6.00	0.00	0.00
	Antenna 1b	1.80	6.00	0.00	0.00
	Antenna 2a	1.80	6.00	0.00	0.00
	Antenna 2b	1.80	6.00	0.00	0.00
	Boom 1	2.70	2.70	0.00	0.00
	Boom 2	2.70	2.70	0.00	0.00
	Canister 1	4.00	4.00	0.00	0.00
	Canister 2	4.00	4.00	0.00	0.00
	Cabling	10.00	25.00	0.00	0.00
RF Subsystem	Signal Generator 1	1.00	1.00	0.01	0.01
	Signal Generator 2	1.00	1.00	0.01	0.01
	Transmitter 1	50.00	210.37	0.78	3.29
	Transmitter 2	50.00	210.37	0.78	3.29
	Power Supply	1.00	1.00	0.01	0.01
	Power Distribution Unit	1.00	1.00	0.01	0.01
	Receiver 1	10.00	10.00	0.01	0.01
	Receiver 2	10.00	10.00	0.01	0.01
Digital Subsystem	A to D Converter	2.00	2.00	0.01	0.01
	Spacecraft Interface and Timing	1.00	1.00	0.01	0.01
	Data Processing	42.00	36.00	0.01	0.01
Radiation Shielding	Electronics Shielding	121.90	121.90	0.00	0.00
Total		321.50	668.03	1.65	6.63

11.4 Design Options Description

11.4.1 Repeat Pass Interferometry and Height Change Detection

In addition to the single pass interferometry provided by the InSAR it is also possible to use the instrument as a repeat pass interferometer. Repeat pass interferometry could be used to measure changes in surface features occurring in the time duration between one orbit pass and a subsequent pass. Such changes might include deformation, displacement, and deposition. This technique would require the orbit geometry from the first pass be repeated to a high degree of precision in the subsequent pass. Thus, very precise knowledge of the spacecraft position is required to use this technique. However, a much less taxing approach is possible employing the InSAR. In this approach the detection of surface deformation would actually not be achieved by classic repeat pass interferometry per se, but rather by differencing two digital elevation maps generated by the interferometric SAR at two times. This could be considered an interferometric change detection technique. The result would be displayed as a deformation map. By using the InSAR one would also not risk degradation of the results due to volumetric scatter and the repeat track requirements are less stringent by two orders of magnitude.

11.4.2 Altimetry

The desirability of a radar altimeter on JIMO has also been considered. It is possible to use the InSAR as a radar altimeter. An altimeter and an InSAR both measure surface altitude. As discussed above, the InSAR uses two sets of antennas to obtain height measurements of the surface. An altimeter is a specific mode or instrument that measures the absolute altitude of the radar above the surface. Operating as an altimeter, the InSARs ESAs would need to incorporate a capability to squint directly downward to direct the beam nadir. The instrument would also need to incorporate an additional one meter or higher resolution waveform. It is important to note that the accuracy of the horizontal position of the height measurement is dependent upon the topography of the surface being measured. The radar return giving the height measurements could only be associated with the point directly below the radar (the nadir point) if the surface were extremely flat. Otherwise, there is a horizontal uncertainty in the knowledge of exactly where the height measurement originated. It is also important to note that the InSAR could only be used as an altimeter when it was not being used for traditional interferometric global mapping. Thus, in a 30-day mission at Europa the instrument would not have time to globally map the surface twice as well as twice produce global altimetry, however it is not clear that altimetry is required twice globally.

11.4.3 Science During Spiral In/Out

The possibility of performing science observations during spiral in/out was assessed from two points of view. First, the performance of each instrument (as designed for 100/400 km) was assessed at the spiral in/out altitudes of up to 10,000 km. When the instrument design is held constant two problems arise. First, the signal to noise ratio (SNR) of the return decreases by a factor of $1/h^4$ where h is the altitude. However, this is offset by the increased coherent integration gain achieved due to the increased synthetic aperture length and slower orbital velocity. Second, the number of range ambiguities increases from zero ambiguities up to 80 (depending on altitude and whether the 100 km or 400 km instrument is used). Any range ambiguity is unacceptable. Therefore, the utility of the instrument cannot be maintained if the altitude is increased beyond its design altitude. It is important to note that this means that the 100 km instrument cannot be used at 400 km, however an instrument designed for a higher altitude can be used at a lower altitude, i.e. the 400 km design can be used at 100 km if the beam is defocused to increase the antenna footprint on the surface to maintain the required range coverage.

Approaching the problem from the perspective that an InSAR instrument designed for higher altitude can be used effectively at lower altitudes, the relationship between power and antenna dimensions and operating altitude was explored. This may provide insight into overall instrument growth with altitude. As the operating altitude of the instrument increases, the elevation dimension of

the antenna must increase to eliminate range ambiguities. This unavoidable change increases the gain of the antenna upon both transmission and reception of the signal. This decreases the power requirement to maintain image quality, but the signal to noise ratio for a returned pulse will also decrease in proportion to $1/h^4$. With the required increase in antenna elevation dimension to suppress ambiguities the variation in SNR is proportional to $1/h^2$. However, all else being equal, the length of the synthetic array increases in proportion to altitude. Consequently, so does the coherent gain achieved in azimuth compression. Taking this into account the signal to noise ratio for a pixel after azimuth compression would then vary as $1/h$. However, the orbital velocity also decreases with increasing altitude by the square root of the altitude. This also increases the synthetic array time and proportionally increases the number of pulses and coherent gain during coherent integration. Thus, to maintain the image quality in the final output SAR imagery at very high altitude, power must be increased roughly the order of $h^{1/2}$.

For a high altitude spiral in or spiral out scenario, it must be pointed out that there is also a great drop in the image area coverage rate. This is because the amount of time required to form a synthetic array increases in proportion to $h^{3/2}$ for altitudes large relative to the moon's radius. Because range coverage is fixed to control range ambiguities the area rate would drop in proportion to $1/h^{3/2}$. The lower area rate would result in over sampling in Doppler, so the PRF could be relaxed to increase range without incurring range ambiguities, thereby increasing the area rate.

Figures 11.4-1 and 11.4-2 illustrate the relationship between power, antenna size, and operating altitude. The azimuth dimension of the antenna, and the required swath widths of 30 km, and the minimum and maximum grazing angles are held constant in these figures. The maximum grazing angle of 70 degrees was used instead of the assuming the worst-case (maximum range) corresponding to the minimum 45 degree grazing angle. Using the maximum range worst-case would be unnecessarily pessimistic at relatively moderate altitudes. As the instrument is moved to higher altitudes it can be operated at steeper grazing angles and still maintain the same swath. As shown in Figure 11.4-1, the elevation dimension of the antenna scales linearly with altitude. At 10,000 km, the elevation dimension of the antenna increases from 0.150 m to 3.6 m. This increases the total antenna area from 0.3 m² to 7.2 m². Although significantly larger this is, in general, not an unreasonable size. That said, increasing antenna size to permit science during spiral in/out would naturally increase the mass and volume of the InSAR as well.

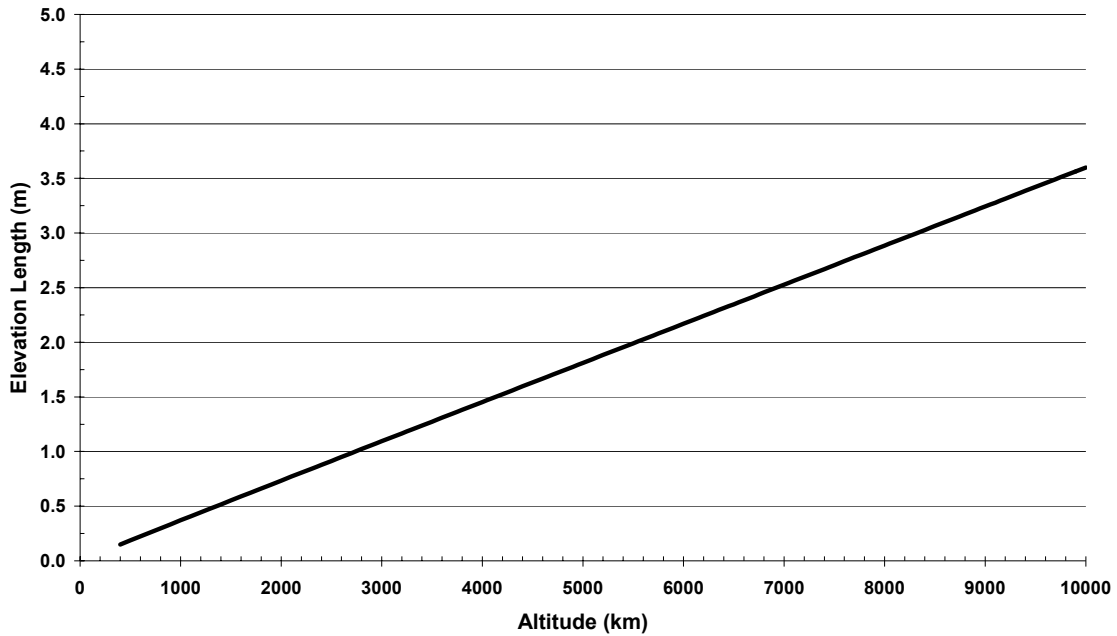


Figure 11.4-1: InSAR antenna elevation vs. altitude.

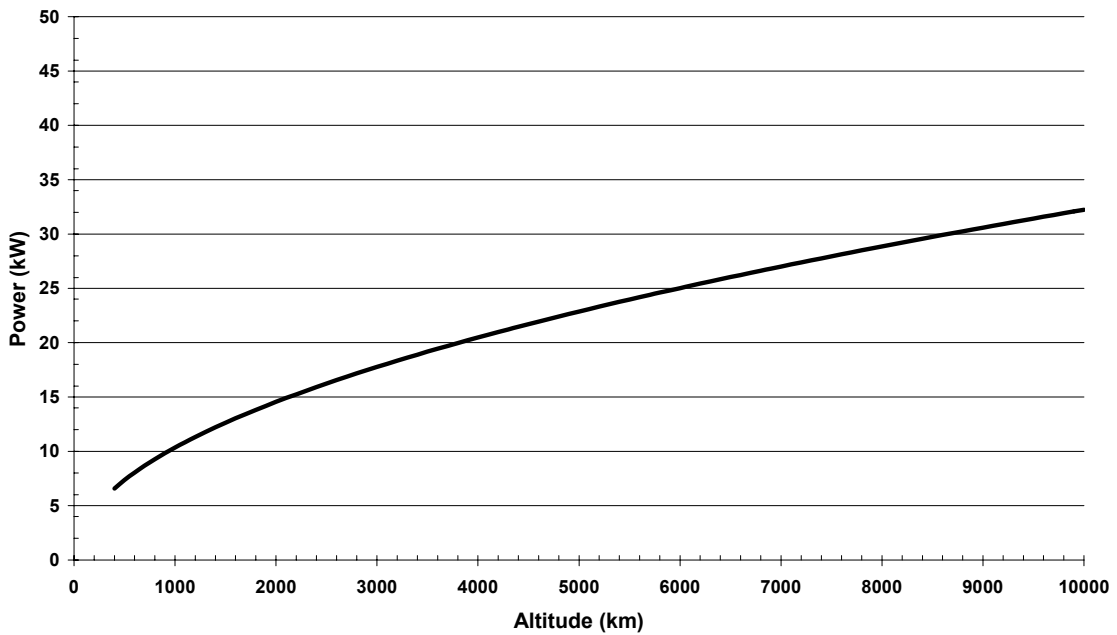


Figure 11.4-2: InSAR power vs. altitude.

Due to the increase in antenna size, increase in the SAR aperture length, and decrease in orbital velocity with altitude the required increase in power to maintain image quality does not increase as h^4 but as $h^{1/2}$ for high altitudes. The approximate required power as a function of altitude is shown in Table 11.4-2.

11.5 Key Technology Developments

Very few space-based single pass radar interferometry experiments have been flown at any frequency. Space-qualified Ka band transmitters of the power levels needed do not exist and will require development. Two 4 kW (peak) transmitters are required for the 100 km design and two 16 kW (peak) transmitters are required for the 400 km design. High-powered transmitters that can provide the required capability are currently between TRL 3 and 4 as they have been demonstrated on the ground but have not been demonstrated in a relevant environment. Further development of low mass/low volume/radiation tolerant radar electronics would clearly be beneficial as well. Sandia National Labs is currently developing a “mini SAR” system with these goals.

There is also a requirement relative to the line of sight vibration associated with the InSAR antennas. Vibration in a SAR instrument causes increased side lobes in the impulse response (i.e. image of) an ideal point scatterer. For an imaged surface the observable effect can be decreased contrast in the image. The figure of merit for addressing this phenomenon is the integrated side lobe ratio (ISLR), which is a ratio of energy in the side lobes of the impulse response to the energy in the main lobe of the impulse response. For a science mission like JIMO a reasonable specification on the ISLR would be perhaps -20dB . For phase noise-induced ISLR due to vibrations small relative to a wavelength the ISLR is approximately the integrated power spectral density of the phase noise. Assuming the phase noise for JIMO will result from vibration at a single frequency the maximum tolerable vibration amplitude would be $\lambda/20$.

Technology development will also be required to support the high data rate produced by the instrument. These developments include 1 GFLOP or greater space qualified processors, on-board processing algorithms and/or development of higher than anticipated data rate communications. Processors that can provide the required capability are currently between TRL 3 and 4 as they have been demonstrated on the ground but have not been demonstrated in a relevant environment. The development of processing techniques will be detailed in the data rate/throughput and processor loading discussion in Section 12.8.

11.6 Schedule Estimate

As stated in Section 11.5, the primary technologies that would need to be developed are the high-powered transmitters required for the instrument as well as increased on-board processing capability. Both of these technologies are between TRL 3 and 4 and are required to progress to TRL 5 before Phase B initiation. A recent study identified that the average time to progress from TRL 3 to TRL 4 is 1.4 years and the average time to progress from TRL 4 to TRL 5 is 1.5 years [3]. Given that these technologies are between TRL 3 and 4, it would be safe to assume that it would take less than three years to mature these technologies to TRL 5.

The schedule for developing the InSAR is based upon analogies to the development schedules of comparative legacy instruments as described below. The primary legacy instrument is the interferometric SAR from the Shuttle Radar Topography Mission (SRTM). SRTM included some new development but also incorporated the SAR radar developed for the Shuttle Imaging Radar-C (SIR-C) mission. Given that a substantial component of the SRTM mission was already developed, the completed development time for SRTM was on the order of 40 months. The development time of SRTM is relatively short compared to the original development time of SIR-C, at 89 months, and planetary SAR radars built for Cassini, at 83 months, and Magellan, at 60 months. A comparatively new system, the Advanced Synthetic Aperture Radar (ASAR) instrument on the European Space Agency's Envisat mission, which was a follow on to two SAR instruments developed for the ERS-1 and ERS-2 mission, took 73 months to develop. The estimated development time, using the averages of the instruments listed above, is 69 months. The average excluding the SRTM instrument, given that the SRTM instrument used existing hardware, is 76 months. Based on the historical difficulties of the development of SAR instruments and the added complexity of a one-pass interferometric SAR system, 76 months should be a reasonably conservative approximation of the development time for the InSAR instrument, once the needed technologies are matured to TRL 5.

11.7 Legacy Instrument Description

The Shuttle Radar Topography Mission (SRTM) is the best example of a heritage instrument to the InSAR. As shown in the table below, the primary differences between SRTM and the JIMO InSAR are mass and frequency band related. The JIMO InSAR is less massive due to the difference in antenna sizes, due to being Ka band vs. X and C band, and due to InSAR's significantly shorter boom length and corresponding reduced structural stiffness requirement. The SRTM instrument was also required to be designed to meet human rated structural and safety requirements for its shuttle flight that do not apply to InSAR. Additionally, minimizing mass was not a key design driver for SRTM due to the substantial payload capability of its shuttle launch. It is important to note that SRTM did not require high data processing rates given that all SRTM data was recorded and stored on-board for processing after its return to Earth.

Table 11.7-1: InSAR Heritage

Instrument	JIMO InSAR (100 km)	SRTM
Mass (kg)	321.5 kg	830 kg
Power (W)	7890 (Peak)	9000 (Peak)
Data Rate (Mbps)	2332 (Unprocessed) Approaches to addressing this data rate are discussed in Section 12.8.	180
Frequency Bands	35 GHz (Ka Band)	5.3 GHz (C Band), 9.6 GHz (X Band)
Resolution (m)	1 m Vertical, 10 m Horizontal	10 m – 20 m
Boom Length (m)	5 m	60 m
Boom Mass (kg)	5.4 kg	290 kg
Antenna Width (m)	0.045 m	X-band: 0.4 m C-band: 0.9 m
Antenna Length (m)	4 m	X-band: 6 m C-band: 8.1 m
Antenna Mass (kg)	131.2 kg	360 kg

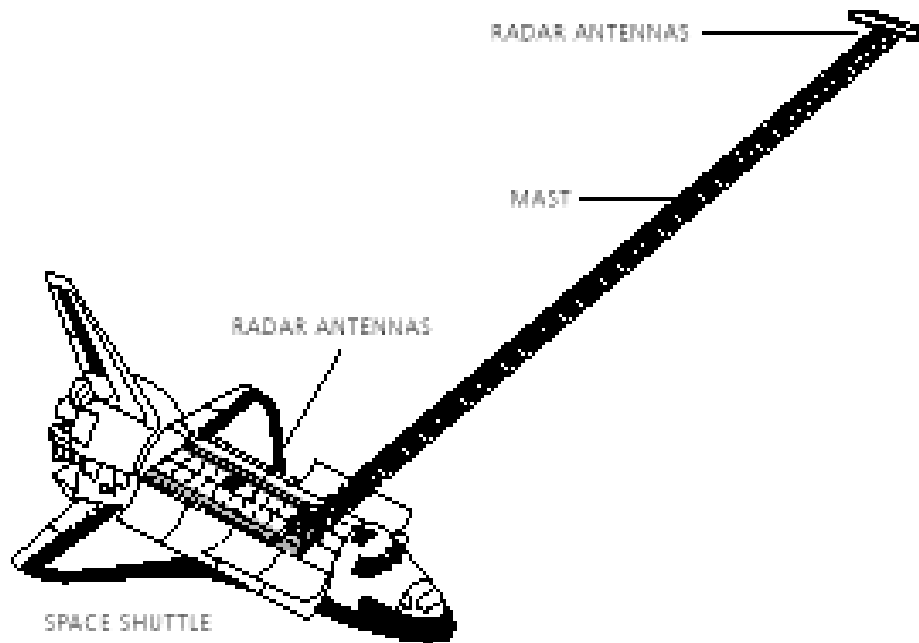


Figure 11.7-1: Shuttle radar topography mission (SRTM) (Reprinted courtesy of NASA).

References

[Ref 11.2-1] "Fine Resolution Topographic Mapping of the Jovian Moons: A Ka-band High Resolution Topographic Mapping Interferometric Synthetic Aperture Radar," S. N. Madsen et al., LPI Forum on Concepts and Approaches for JIMO. June 12-14, 2003.

12.0 Polarimetric SAR

12.1 Science Utility

The Polarimetric SAR (PSAR) was designed to map the moons at a resolution of 10 m horizontally, with penetration into the shallow subsurface in order to uncover the properties of the icy regolith and its relationship to the mapped distributions of surface constituents, physical structures, and thermal features. In particular the cross-polarized return provides a measure of multiple scattering associated with an icy regolith.

12.2 Design Drivers and Options Examined

Mapping near surface regolith requires the use of a polarimetric SAR at a radio frequency where surface penetration is achieved while constraining antenna size. Radio frequencies are selected that provide surface penetration and designs composed of a pulse repetition frequency and a set of antenna dimensions are generated that will allow the SAR to cover the moon's surface within the allotted time without suffering from (unacceptable) range and Doppler ambiguities. It is then observed whether a reasonable antenna size is generated. Small antennas were required at a 10 cm wavelength, whereas larger antennas were called for at a 1 m wavelength in order to limit the illuminated area on the surface sufficiently to avoid unacceptable range and Doppler ambiguities. This process is illustrated in the following figure.

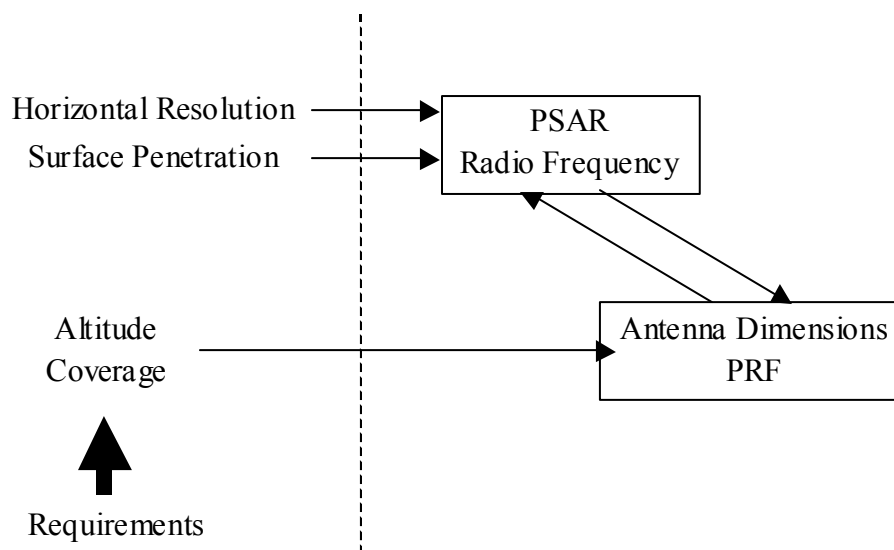


Figure 12.2-1: PSAR trade space flow diagram.

In designing the SARs the study team considered wavelengths over two orders of magnitude (approximately 10 cm – 1 m). Wavelengths of the order of 1 m and

larger were also considered, to penetrate further into the subsurface and return information on different sized scatterers. SAR designs were generated, but it was found that quite large antennas were required to manage ambiguities. There is a frequency trade between deep probing of the regolith and the desire for improved discrimination in the surface echo. For design purposes, we chose 3 GHz (10 cm wavelength). This choice results in the antenna sizes shown in Table 12.2-1.

Table 12.2-1: PSAR Antenna Sizing

	100 km	400 km
Antenna Size	6 m x 0.212 m	5 m x 0.900 m

12.3 Baseline Instrument Description

As in the case of the InSAR, baseline instrument concepts operating at nominal altitudes of 100 km and 400 km were studied in order to determine the sensitivity to the primary science orbit selection. Additionally, the performance of these cases was assessed at altitudes up to 10,000 km, for operation during a spiral-in and spiral out. In order to produce useful observations (i.e. required SNR and avoidance of range ambiguities) at these higher altitudes, changes to the instruments in both antenna size and power were considered. A summary of how the instrument design changes with altitude is included.

The PSAR is a fully polarimetric instrument measuring HH, VV, VH, and HV linear polarizations. The antenna is a cylindrical reflector, which will point between 20 and 45 degrees off nadir. In addition to sizing the antenna and power, OrbSAR computed the minimum usable pulse repetition frequency (PRF). A summary of the instrument design parameters is shown in Table 12.3-1.

Table 12.3-1: PSAR Design Parameters

	100 km	400 km
Average Power	200 W	250 W
Peak Power	1420 W	730 W
Duty Factor	10%	30%
Frequency	3 GHz	3 GHz
Bandwidth	52.8 MHz	52.8 MHz
Minimum PRF	0.987 kHz	0.893 kHz

In order to fully cover Europa twice in 30 days the PSAR must map a minimum swath width of 60 km. The swath width generated by this instrument are well in excess of 60 km, leading the the relaxed pointing requirements shown in Table 12.3-2 below.

Table 12.3-2: PSAR Pointing Requirements

	100 km	400 km
Pointing Requirements	8.0°	3.0°
Minimum Grazing Angle	43.5°	58.0°
Maximum Grazing Angle	70.0°	70.0°

A mass and power budget for the PSAR is shown below. The mass of the antenna was calculated using an antenna density of 10 kg/m² (including structures). A transmitter efficiency of 50% was assumed. Five 1 Gflop processors will be required for data processing at both altitudes. The mass estimates shown do not include margin.

Table 12.3-3: PSAR Mass and Power Sizing

		Mass (kg)		Average Power (kW)	
		100 km	400 km	100 km	400 km
Antenna Subsystem	Antenna	12.72	45.00	0.00	0.00
	Mounting Brackets	5.50	8.25	0.00	0.00
	Cabling	1.00	2.00	0.00	0.00
RF Subsystem	Signal Generator	1.00	1.00	0.01	0.01
	Transmitter	17.00	15.00	0.14	0.21
	Power Supply	1.00	1.00	0.01	0.01
	Power Distribution Unit	1.00	1.00	0.01	0.01
	Receiver (4 Channels)	12.00	12.00	0.01	0.01
Digital Subsystem	A to D Converter	2.00	2.00	0.01	0.01
	Spacecraft Interface and Timing	1.00	1.00	0.01	0.01
	Data Processing	30.00	30.00	0.01	0.01
Radiation Shielding	Electronics Shielding	42.60	42.60	0.00	0.00
Total		126.82	160.85	0.20	0.25

12.4 Design Options Description

12.4.1 Science During Spiral In/Out

The possibility of performing science observations during spiral in/out was assessed from two points of view. First, the performance of each instrument (as

designed for 100/400 km) was assessed at the spiral in/out altitudes of up to 10,000 km.

The problems encountered are identical to those for the InSAR. When the instrument design is held constant two problems arise. First, the signal to noise ratio (SNR) of the return decreases by a factor of $1/h^4$ where h is the altitude. However, this is offset by the increased coherent integration gain achieved due to the increased synthetic aperture length and slower orbital velocity. Second, the number of range ambiguities increases from zero ambiguities up to 100 (depending on altitude and whether the 100 km or 400 km instrument is used). Any range ambiguity is unacceptable. Therefore, the PSAR as designed cannot be used during spiral in/out. Generally, the utility of the instrument cannot be maintained if the altitude is increased beyond the designed altitudes of 100 km and 400 km. It is important to note that this means that the 100 km instrument cannot be used at 400 km, however an instrument designed for a higher altitude can be used at a lower altitude, i.e. the 400 km design can be used at 100 km if the beam is defocused to increase the antenna footprint on the moon surface to ensure the required range coverage is maintained.

Following the same approach as was taken for the InSAR, the relationship between power and antenna dimensions and operating altitude was explored. This may provide insight into overall instrument growth with altitude. As the operating altitude of the instrument increases, the elevation dimension of the antenna must increase to eliminate range ambiguities. This unavoidable change increases the gain of the antenna upon both transmission and reception of the signal. This decreases the power requirement to maintain image quality, but the signal to noise ratio for a returned pulse will also decrease in proportion to $1/h^4$. With the required increase in antenna elevation dimension to suppress ambiguities the variation in SNR is proportional to $1/h^2$. However, all else being equal, the length of the synthetic array increases in proportion to altitude. Consequently, so does the coherent gain achieved in azimuth compression. Taking this into account the signal to noise ratio for a pixel after azimuth compression would then vary as $1/h$. However, the orbital velocity also decreases with increasing altitude by the square root of the altitude. This also increases the synthetic array time and proportionally increases the number of pulses and coherent gain during coherent integration. Thus, to maintain the image quality in the final output SAR imagery at very high altitude, power must be increased roughly the order of $h^{1/2}$.

For a high altitude spiral in or spiral out scenario, it must be pointed out that there is also a great drop in the image area coverage rate. This is because the amount of time required to form a synthetic array increases in proportion to $h^{3/2}$ for altitudes large relative to the moon's radius. Because range coverage is fixed to control range ambiguities the area rate would drop in proportion to $1/h^{3/2}$. The lower area rate would result in over sampling in Doppler, so the PRF could be relaxed to increase range without incurring range ambiguities, thereby increasing the area rate.

Figures 12.4-1 and 12.4-2 illustrate the relationship between power, antenna size, and operating altitude. The azimuth dimension of the antenna, and the required swath widths of 30 km, and the minimum and maximum grazing angles are held constant in these figures. The maximum grazing angle of 70 degrees was used instead of the assuming the worst-case (maximum range) corresponding to the minimum 45 degree grazing angle. Using the maximum range worst-case would be unnecessarily pessimistic at relatively moderate altitudes. As the instrument is moved to higher altitudes it can be operated at steeper grazing angles and still maintain the same swath. As shown in Figure 12.4-1, the elevation dimension of the antenna scales linearly with altitude. At 10,000 km, the elevation dimension of the antenna increases from 0.900 m to 22.5 m. This increases the total antenna area from 4.5 m² to 112.5 m². An antenna of this size would require significant mass and volume.

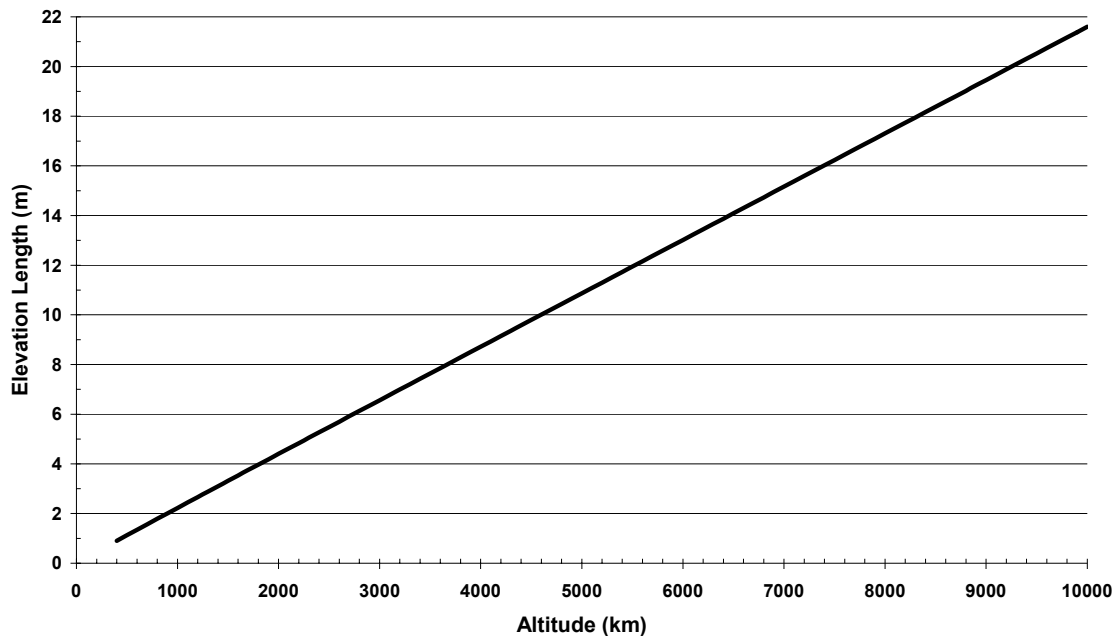


Figure 12.4-1: PSAR antenna elevation vs. altitude.

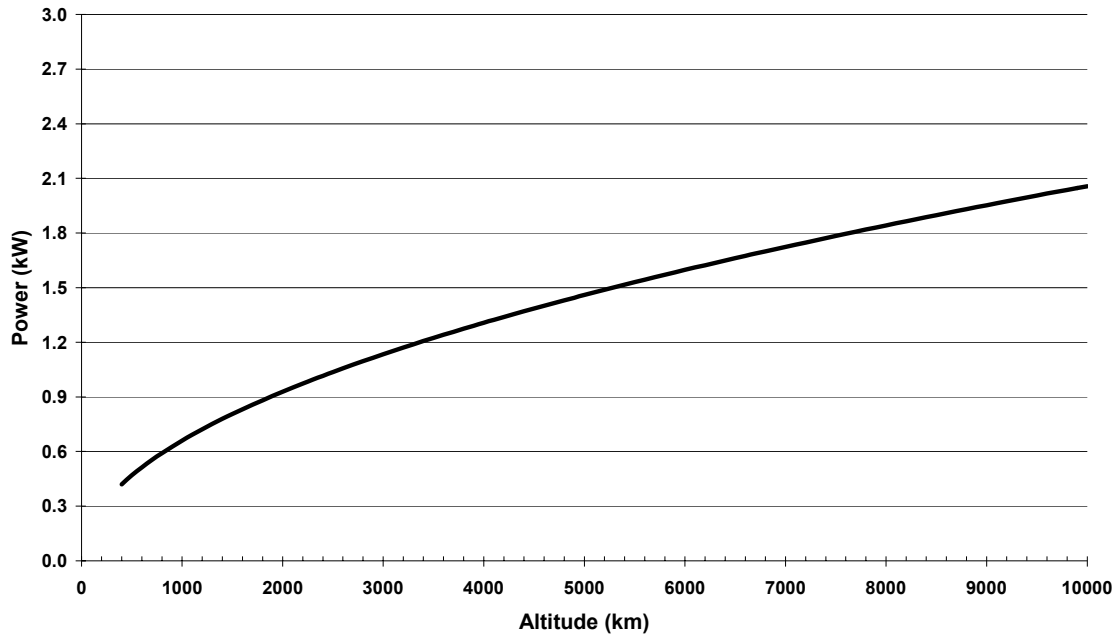


Figure 12.4-2: PSAR power vs. altitude

Due to the increase in antenna size, increase in the SAR aperture length, and decrease in orbital velocity with altitude, the required increase in power to maintain image quality does not increase as h^4 but as $h^{1/2}$ for high altitudes. The approximate required power as a function of altitude is shown in Table 12.4-2.

12.5 Key Technology Developments

Further development of low mass/low volume/radiation tolerant radar electronics would be beneficial. Sandia National Labs is currently developing a “mini SAR” system with these goals. The relatively high data rate for this instrument (discussed in the following section) will require mitigation. Such mitigation could take the form of on board processing and/or development of advanced communications techniques. There is also a potential trade between the requirements which lead to a high data rate (high resolution and rapid global coverage) and the data rate. The development of processing techniques will be detailed in the data rate/throughput and processor loading sections. InSAR required three years to develop power and processors to get to TRL 5.

12.6 Schedule Estimate

The primary technologies that would need to be developed are identical to that of the InSAR instrument, and are the high-powered transmitters required for the instrument as well as increased on-board processing capability. Both of these technologies are between TRL 3 and 4 and are required to progress to TRL 5 before Phase B initiation. A recent study identified that the average time to

progress from TRL 3 to TRL 4 is 1.4 years and the average time to progress from TRL 4 to TRL 5 is 1.5 years [3]. Given that these technologies are between TRL 3 and 4, it would be safe to assume that it would take less than three years to mature these technologies to TRL 5.

The schedule for developing the PSAR is based upon analogies to the development schedules of comparative legacy instruments as described below following the same methodology as described in the schedule estimate for the InSAR. The primary legacy instruments for the PSAR are the SIR-C and Envisat-ASAR polarimetric SAR instruments. As noted previously, SIR-C and ASAR took 89 and 73 months, respectively, to develop. The estimated development time for the PSAR instrument, using the average of the SIR-C and ASAR instruments, is 81 months. Based on the historical difficulties of the development of SAR instruments with multiple polarizations, 81 months should be a reasonable approximation of the development time for the PSAR instrument, once the needed technologies are matured to TRL 5.

12.7 Legacy Instrument Description

The SIR-C mission is the best example of a heritage instrument to the PSAR. As shown in the table below, the two most obvious differences between SIR-C and the JIMO PSAR are in power and mass. The JIMO PSAR requires less power mainly due to its lower altitude. The JIMO PSAR is less massive due to its lower power requirement and smaller antenna requirement. Additionally, the SIR-C instrument was required to meet human rated structural and safety requirements that do not apply to this instrument. The substantial payload capability of its Shuttle launch made it such that minimizing mass was not a key design driver for SIR-C. It is important to note that SIR-C did not require high data rates as all SIR-C data was recorded and stored on-board for processing after return to Earth.

Table 12.7-1: PSAR Heritage

Instrument	JIMO PSAR (100 km)	SIR-C
Mass (kg)	126.82	900
Power (W)	1420 (Peak)	9000 (Peak)
Data Rate (Mbps)	149.95 (Unprocessed)	90
Frequency Bands	3 GHz	1.25 GHz (L Band), 5.3 GHz (C Band), 9.6 GHz (X Band)
Antenna Size (m)	6 m x 0.212 m	L-band: 12 m x 2.9 m C-band: 12 m x 0.8 m X-band: 12 m x 0.4 m
Polarization	HH, VH, HV, VV	HH, VH, HV, VV
Resolution (m)	10 m (Ground Plane)	20 m – 30 m

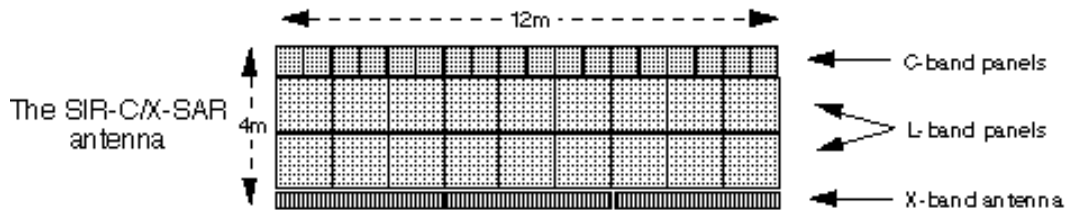


Figure 12.7-1: SIR-C SAR (Reprinted courtesy of NASA).



Figure 12.7-2: ASAR (Reprinted courtesy of NASA).

12.8 SAR Data Rates

The data rates for both SAR instruments were estimated using a tool developed for this purpose. Initially it was assumed there would be no onboard processing and the raw data rates from a Block Floating Point Quantizer (BAQ) were calculated followed by the data rates, which would result after performing onboard processing. A BAQ can be considered a kind of data compression technique for raw SAR data to minimize the bandwidth requirement for transmitting SAR data to Earth. It was first employed on the Magellan SAR that mapped Venus. That BAQ compressed each I and Q measurement with one bit representing sign and one bit representing amplitude. The Magellan SAR performed these functions onboard with hardware. Thus no digital computer was necessary. In the JIMO case however, 2 bits are insufficient, enough bits are needed to be equivalent to (i.e. the same quantization and saturation noise as) a conventional 6 bit I and 6 bit Q A/D converter. Therefore, 4 bits I and 4 bits Q, was assumed for these calculations.

Although PSAR is a 4-channel system the data stream can be reduced to 3 channels. The 12.8-1 is based partially upon this assumption. Specifically, the PSAR is a 4 channel (HH, VV, HV, and VH) fully polarimetric instrument. However due to the principal of reciprocity in electromagnetics, (assuming no electrical components violate reciprocity) the two depolarized channels (HV and VH) are identical except for thermal noise. They can be coherently combined for a gain of 6 dB in signal to noise as well as a decrease in data rate. Thus, the total data rate is 3 times the data rate for a single channel. The above computations took the conservative approach that assumed the range resolution employed in the slant plane could not vary with grazing angle but would always support resampling down to the required resolution in the ground plane in the worst-case geometry. It was assumed that the pixels are down-sampled to the

required ground plane resolution. Assuming on board processing and 3.5 bits per pixel (bpp) the output data rate decreases to the rates shown below.

Additional, more extreme methods for reducing the data rate also exist. If the proposed fully polarimetric SAR were scaled back to a conventional single channel SAR the data rates would drop by a factor of 3. For the InSAR the raw bit rate out of the BAQ per image must be multiplied by a factor of 20 due to the fact that there are 10 conventional image pairs per final interferometric image. As noted for the PSAR above, computations used the conservative assumption that the range resolution employed in the slant plane could not change with grazing angle but would always support resampling down to the required resolution in the ground plane for the worst-case geometry. It was assumed that the pixels are down-sampled to the required ground plane resolution. Upon registering and interfering the 10 image pairs and averaging the results the data rate is decreased by a factor of 20. If the only output product desired were imagery, then as per the arguments employed for the fully polarimetric SAR the data rate could be decreased by an additional factor of somewhat less than half (specifically $3.5/8$). However, altitude (the most important unique product of an InSAR) is also required, and although the compression of altitude data would no doubt be possible, this is an area where there are many unknowns and for which there would probably be little if any ability to justify a lower communications link bandwidth. To illustrate, consider the fact that 8 bpp out of the BAQ corresponds roughly to 8 bpp in the output complex image. Then if 3.5 bpp represents the compressed visible (i.e. power detected) image, this leaves 4.5 bpp for altitude information. Without data compression, since altitude resolution is required to be 1 meter, this would leave the capability to obtain the altitude for a surface, which deviates up to plus or minus 8 meters from mean elevation. Data compression in this case could serve the purpose of widening the dynamic range in altitude and taking advantage of correlation in altitude in adjacent pixels to both increase accuracy and dynamic range, but not to decrease the output bandwidth based upon what is currently known.

It is important to note that data collection is assumed to run continuously and the bandwidth of the communications link is assumed to be sufficient to handle the data. During the time when downlink is not available the data must be stored or it will be lost. The expected communications bandwidth (10 Mbps) does not meet the above requirements. In the past the concept of operations for high-resolution instruments such as these have been to take data over representative areas only and not cover the entire surface. The selection could be made a priority or perhaps on the basis of the return from other onboard sensors, e.g. the SARs on the basis of sounding data or the InSAR on the basis of PSAR data (perhaps descope to a conventional single channel SAR). Another solution would be to increase the time duration of the mission at each moon.

Table 12.8-1: SAR Data Rates

		100 km	400 km
From BAQ	InSAR (Mbps)	2.332 x 10 ³	1.819 x 10 ³
	PSAR (Mbps)	149.946	165.644
Post Down-sampling	InSAR (Mbps)	1.120 x 10 ³	1.031 x 10 ³
	PSAR (Mbps)	83.970	77.301
Post Data Processing	InSAR (Mbps)	55.980	33.382
	PSAR (Mbps)	36.737	33.819

It should be noted that the InSAR data rate is 56 Mbps with on board processing and data compression, and that might increase to the order of 100 Mbps when transmitting multi-look SAR image along with the digital elevation map. This would correspond to about half the data rate of the Shuttle Radar Topography Mission.

12.8.1 Onboard SAR Processor Loading

Estimates of processor loading were made for both SAR instruments in terms of complex floating point operations (additions or multiplications) per second for single-look image formation, and averaging from multi-look imagery. In the case of the InSAR, this did not include the final stages of surface height computation (e.g. phase unwrapping), which is assumed to be performed on the ground from the processed voltage images. Generally there are parameters, which are computed once, or a limited number of times, within the synthetic aperture formation times. This is done improve efficiency in performing the pulse-to-pulse and sample-to-sample processing. The major bulk of the processing is performed by the sample-to-sample processor. The pulse-to-pulse processor, requires relatively little throughput load, but this is more difficult to estimate and is therefore calculated here by scaling the loading estimate for the sample-to-sample processing by 20%. Radix 2 FFTs were assumed throughout for range and azimuth compression and subswath filtering where necessary.

The depth of field for both polar format and “rectangular format” processing was evaluated for both the InSAR and PSAR instruments. It was determined that polar format processing was not necessary for the InSAR and there was also no need to break the swath into subswaths to accommodate the depth of field associated with rectangular format processing. In the case of PSAR however it was determined that the more processor intensive polar format processing was

necessary. Additionally, data had to be filtered into subswaths due to depth of field limitations. This allows efficient FFTs to be employed without unacceptable geometric distortion and impulse response degradation. Efficient “hopping FFTs” were assumed to be employed to segment the data into subswaths as necessary. It was found necessary for the PSAR swaths to be filtered into 8 subswaths at 100 km altitude and 4 subswaths at 400 km altitude.

Individual pixels in raw SAR images are of generally such wide dynamic range that the human eye cannot interpret them. Because of this fact digital images are remapped to decrease the dynamic range of the images so they can be viewed. Remapping by taking the logarithm of pixel power was employed resulting in 3/8 dB per gray shade, which gives excellent results. As an initial estimate for processor throughput estimation it was assumed the computation of one logarithm takes the same amount of time as 4 floating point operations.

The InSAR instrument is designed to operate 100% of the time to continuously generate 10 overlapped images (in order to achieve the required vertical resolution). However, the PSAR only has to operate 25% to 30% of the time (at 400 km and 100 km altitude respectively) in order to continuously map a swath. In estimating processor throughput this “slow time duty factor” was not taken advantage of. Specifically, “immediate” processing with minimal data storage was assumed. The estimated throughput rate for the PSAR instrument was found to be approximately 5 billion operations per second for at both altitudes (5.2 at 100km decreasing somewhat to 4.8 at 400km altitude) and the estimated InSAR instrument throughput requirement was found to be 6.8 billion operations per second at 100 km altitude, decreasing somewhat to 6.3 billion operations per second at the 400 km altitude.

13.0 Subsurface Radar Sounder

13.1 Science Utility and Measurements

The radar sounder measurement consists of vertical profile maps of the subsurface of each moon at two resolutions: 10 m vertical resolution (100 m – 2 km depth) and 100 m vertical resolution (2 km – 30 km depth).

13.2 Design Drivers and Options Examined

A flow diagram of the radar sounder trade space is shown in Table 13.2.1. The key drivers were vertical resolution and near-simultaneous subsurface probing at multiple frequency bands. The broad frequency range then drove the selection of the antennas. A single, efficient antenna was not possible in the desired frequency band, therefore two antennas were selected.

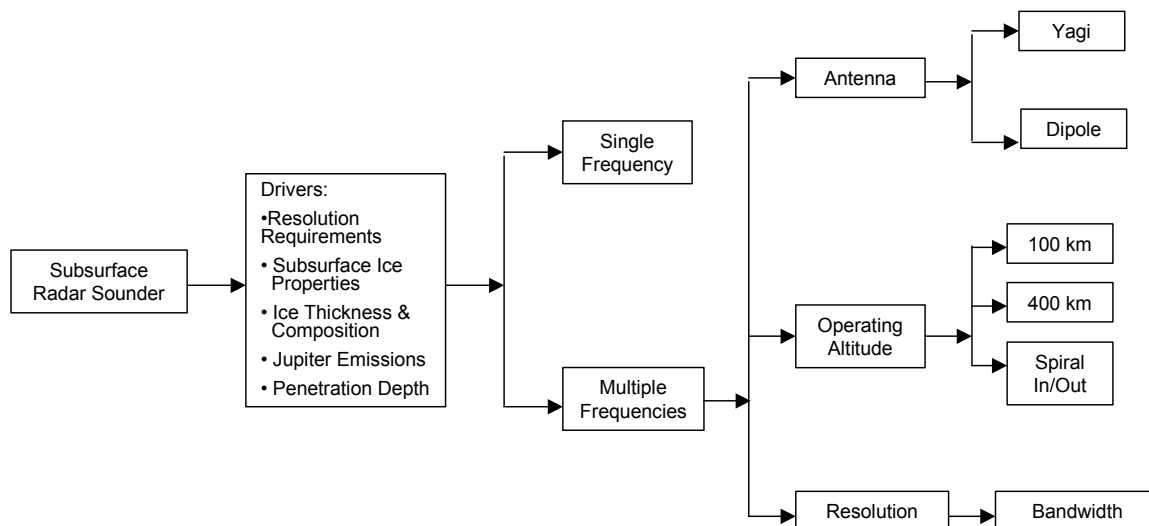


Figure 13.2-1: Subsurface radar sounder trade space.

Jovian noise is present to some extent up to 40 MHz. This is one reason why previous radar sounder designs for the icy moons used a 50 MHz center frequency. Here, 50 MHz was selected for the upper bound of the JIMO radar sounder. Because the JIMO spacecraft provides far greater power and greater mass allocations than previously proposed missions, lower frequencies can also be utilized. The advantage of including lower frequencies is increased penetration and potentially increased knowledge about the subsurface. The lower bound of 5MHz was selected because it is above the maximum plasma frequency of the ionospheres of the icy moons; lower frequencies would not penetrate through the ionosphere to the surface. Five center frequencies were

selected within the 5-50 MHz band to represent a strawman instrument. Center frequencies are listed in Table 13.2-1.

Table 13.2-1: Radar Sounder Frequencies

Band	Center Frequency
A	5 MHz
B	10 MHz
C	30 MHz
D	40 MHz
E	50 MHz

13.3 Baseline Instrument Description

The subsurface radar sounder utilizes two antennas, one for higher frequency (above 10 MHz) operation and a second for lower frequency (10 MHz and below) operation. The low frequency antenna is a dipole optimized in the 5 and 10 MHz frequency range, with a length between 15 and 30m, respectively. The high frequency antenna is a 10 m Yagi antenna with 3 Yagi radiators of 3 m (optimized to 50 MHz). Both antennas will be oriented in the cross-track direction pointing directly nadir. A schematic of the Yagi antenna (to scale) is shown below:

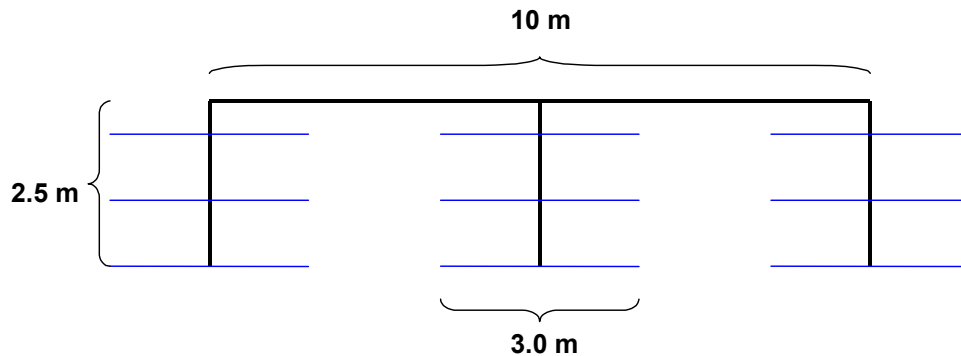


Figure 13.3-1: High frequency radar sounder antenna.

The lower frequencies (5 MHz and 10 MHz) will transmit with a bandwidth of 1.5 MHz, which will provide 100 m resolution. The higher frequencies will transmit with a bandwidth of 15 MHz, which will provide 10 m resolution. Both the low and high frequencies will transmit in separate linear frequency swept pulses with a duration of 300 μ s. Frequency sweep is a type of waveform control that can be used to account uncertainties in the subsurface structure and composition. Similar to the approach employed on the Europa Orbiter strawman radar

sounder, a linear-FM (chirp) waveform is transmitted in each frequency sub-band and a numerically controlled oscillator is used to derive the frequency modulated sine-wave output. The high dynamic range requirement, due to uncertainties in subsurface composition, results in the need for dynamic gain control. The deramp design uses the transmit chirp waveform to downconvert the chirp rather than using a conventional LO signal. This deramp technique may be used to reduce the system data rate by performing analog chirp compression. It may also be possible to use a variable gain amplifier to reduce the dynamic range by weighting the deramped chirp as a function of time or frequency.

The five frequency channels of data will then be able to be processed simultaneously. In order to obtain good horizontal resolution in the along track direction the radar sounder could be operated at nadir, employing Doppler beam sharpening. This concept is being used in the MRO/SHARAD system. In addition, in order to improve the detection and location of subsurface features SAR processing could be employed in the cross-track direction by coherently integrating data from several close orbit passes. The PRF of the instrument set at 150 Hz to avoid aliasing in both range and Doppler. Note that the optimum PRF for the higher altitudes (i.e. the 400 km case) is lower, on the order of 130 Hz. PRF can be optimized at higher altitudes down to about 60Hz in order to avoid aliasing. The 60 Hz is the lower bound on the PRF that is needed to achieve the vertical resolution.

The transmit power was calculated using a scaling from the Europa Orbiter Radar Sounder strawman [ref 13.3-1] which utilized 100 W peak power at up to an average altitude of 300 km. The power was scaled to take into account altitude, frequency, and antenna geometry. A constant signal to noise ratio of 20 dB was used across the entire 5–50 MHz band. A summary of the transmit power at each frequency is shown in Table 13.3-1. As can be seen in the table, the power increases by four orders of magnitude from the 50 MHz high frequency sub-band to the 5 MHz sub-band, with the largest power being in the lowest frequency sub-band. The 5MHz sub-band requires over 3000 kW at 400 km to maintain 20dB SNR. It would still be possible to operate the instrument at 5 MHz at the lower power level, however the SNR of the return would be much lower. Note that for the 400 km case is restricted to the 4 highest frequency sub-bands because of the very high power requirement at the lower sub-band.

Table 13.3-1 Radar Sounder Beam Transmit Power

	Peak Power (kW)					Average Power (kW)				
	50 MHz	40 MHz	30 MHz	10 MHz	5 MHz	50 MHz	40 MHz	30 MHz	10 MHz	5 MHz
100 km	0.001	0.002	0.005	0.134	13.4	2.47E-04	3.86E-04	0.001	0.027	2.68
400 km	0.316	0.494	1.37	34.3	3429	0.063	0.099	0.274	6.86	686

Both antennas are fed by a single transmitter which transmits a maximum peak power of 13 kW at 100 km and 34 kW at 400 km. The transmitter operates with a 20% duty factor for 3 kW of average power at 100 km and 6.86 kW of average

power. A summary of the instrument design parameters is shown in Table 13.3-2. Note that the power values reflect required power from the bus, not transmitted power.

Table 13.3-2: Radar Sounder Design Parameters

	100 km	400 km
Frequency Bands	5, 10, 30, 40, 50 MHz	10, 30, 40, 50 MHz
Average Power	2.68 kW	6.86 kW
Peak Power	13.40 kW	34.29 kW
Duty Factor	20%	20%
Maximum Frequency	50 MHz	50 MHz
Minimum Frequency	5 MHz	10 MHz
Pulse Length	300 μ s	300 μ s
PRF	150 Hz	150 Hz

The mass of the radar sounder was estimated using scaling from existing technology. Space qualified transmitters in the bands and powers levels of the subsurface sounder have not been flown and will require development. A transmitter efficiency of 50% was assumed. The mass estimates shown do not include margin.

Table 13.3-4: Radar Sounder Mass and Power Sizing

		Mass (kg)		Average Power (kW)	
		100 km	400 km	100 km	400 km
Antenna Subsystem	Yagi Antenna	10.00	10.00	0.00	0.00
	Mounting Brackets	12.00	12.00	0.00	0.00
	Dipole Antenna	Included in Radio Plasma Sounder Sizing			
	Mounting Brackets				
	Cabling	2.00	25.00	0.00	0.00
RF Subsystem	Low Frequency Signal Generator	1.00	1.00	0.01	0.01
	High Frequency Signal Generator	1.00	1.00	0.01	0.01
	Transmitter	15.00	125.00	2.68	6.86
	Power Supply	1.00	1.00	0.01	0.01
	Power Distribution Unit	1.00	1.00	0.01	0.01
	High Frequency Receiver	10.00	10.00	0.01	0.01
	Low Frequency Receiver	10.00	10.00	0.01	0.01
Digital Subsystem	A to D Converter	2.00	2.00	0.01	0.01
	Spacecraft Interface and Timing	1.00	1.00	0.01	0.01
	Data Processing	2.00	2.00	0.01	0.01
Radiation Shielding	Electronics Shielding	48.60	48.60	0.00	0.00
Total		116.60	249.60	2.77	6.92

13.4 Design Options Description

13.4.1 Science During Spiral In/Spiral Out

Two point designs, at altitudes of 100 km and 400 km, were studied for the radar sounder. The possibility of performing science during spiral in/out was assessed from two points of view. First, the performance (as designed for the 100/400 km) was assessed at the spiral in/out altitudes of up to 10,000 km. When the instrument design is held constant, two problems arise. First, the signal to noise ratio (SNR) of the return decreases by a factor of $1/h^4$ where h is the altitude. As shown in Table 13.3-1, the power required at the lower frequency sub-bands to maintain SNR becomes very large as altitude is increased, making this approach prohibitive. Second, the pulse transmit/receive timing scheme is rendered ineffective as the returns from prior pulses begin to overlap with pulses yet to be transmitted. The timing scheme was calculated for each altitude based upon the pulse length and the time for the pulse to return with no overlap. As the distance from the moon increases, the return time increases and thus interferes with a pulse yet to be transmitted. This is called eclipsing and is analogous to the range ambiguity problem encountered with the SAR instruments. This problem can be mitigated to a point by restricting operation to the higher frequencies, which will yield higher SNR performance at the same power levels, and reducing the pulse length to combat pulse eclipsing. Like in the cases of the SAR instruments, it is possible to design the instrument for high altitude operation. A logical approach

here would be to restrict use of the instrument to higher frequency probing until the altitude was decreased to the point where the lower frequency sub-bands could be used with acceptable SNR.

13.5 Key Technology Developments

Space qualified transmitters in the bands and powers levels of the subsurface sounder have not been flown and will require development. High-powered transmitters that can provide the required capability are currently between TRL 3 and 4 as they have been demonstrated on the ground but have not been demonstrated in a relevant environment. In addition to the heritage instruments presented later, airborne and ground-based radar sounders have been used on Earth to penetrate the ice sheets of Antarctica and Greenland. Lake Vostok is located approximately 4 km under the Antarctic ice sheet. The lake was initially discovered and has been studied extensively with ice-penetrating radar. This site would provide the best analogue to the icy moons in testing instruments on Earth.

13.6 Schedule Estimate

As stated in Section 13.5, the primary technology that would need to be developed is the high-powered transmitters required for the instrument. Given that this technology is between TRL 3 and 4, it would be safe to assume that it would take less than three years to mature this technology to TRL 5.

The schedule for developing the radar sounder is based upon analogies to the development schedules of comparative legacy instruments. The Mars Advanced Radar for Subsurface and Ionosphere Sounding (MARSIS) built for the Mars Express mission was completed in 39 months while the SHallow RADar Sounder (SHARAD) instrument, being built for the Mars Reconnaissance Orbiter (MRO), is scheduled to be completed in 31 months. The estimated development time for the radar sounder, using the average of the MARSIS and SHARAD instruments, is 35 months. Given that the SHARAD instrument is not completed yet, the actual MARSIS instrument development duration of 39 months should be used as a reasonable approximation of the development time for the radar sounder, once the technology is addressed.

13.7 Legacy Instrument Description

Radar sounders have been used to explore both the lunar and Martian surface and subsurface. The best heritage instruments for comparison to the JIMO radar sounder are MARSIS (onboard Mars Express) and SHARAD (onboard the Mars Reconnaissance Orbiter). A comparison of the JIMO radar sounder with these heritage instruments is provided in the table below.

Table 13.7-1: Radar Sounder Legacy

Instrument	JIMO Radar Sounder	Mars Express/MARSIS	MRO/SHARAD
Mass (kg)	116.6	17	16
Power (W)	630 (Average)	57 (Average)	60 (Average)
Data Rate (kbps)	3995	65	1000
Frequency Bands	3 – 50 MHz	1.3 – 5.5 MHz	15 – 25 MHz
Resolution	10 m/100m	70 m	7 m



Figure 13.7-1: Mars express/MARSIS (Reprinted courtesy of NASA).



Figure 13.7-2: MRO/SHARAD (Reprinted courtesy of NASA).

References

[Ref 13.3-1] Europe Orbiter Mission and Project Description Document, undated.

14.0 Radio Plasma Radar Sounder

14.1 Science Utility

The radio sounder has the objective of using plasma sounding to measure the potential ionospheric characteristics of each icy moon. In addition the radio sounder may supplement in-situ plasma and magnetic field measurements. The radio sounder will provide a profile of ionospheric density along the radar line of sight at an assumed 3 km resolution. The 3km range resolution is based on previous space plasma sounding instruments. It is envisioned that the JIMO spacecraft will orbit each of the three icy moons for a minimum of 30 days providing opportunities for both day and night measurements, and in particular, affording a means of determining potentially increased ionization during sunlit periods. Present data on these ionospheric characteristics are inconclusive and have been derived through occultation measurements as a part of the Galileo Program. The radio sounder will provide the capability to refine the knowledge of the ionospheric characteristics of the Jovian moons.

14.2 Design Drivers and Options Examined

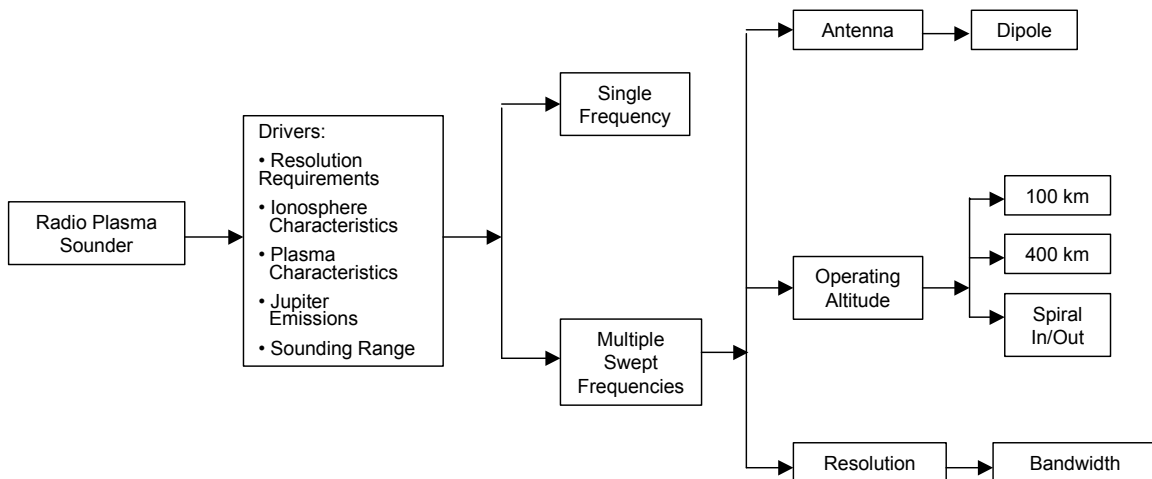


Figure 14.2-1: Radio plasma radar sounder trade space.

A flow diagram of the radio sounder trade space is shown in Figure 14.2-1. The JIMO radio sounder design follows the earlier sounders implemented in efforts to further understand the Earth's ionosphere by using satellite-borne sounders. These designs are generally referred to as "topside sounders" and were flown on the Alouette and ISIS Programs in the 1960s. A significant amount of design description and data results for these satellites may be found in the June 1969 Proceedings of the IEEE and a top-level summary of the sounder characteristics is presented in the heritage section of this report. The JIMO sounder design

differs from these earlier efforts because the ionospheric characteristics of the Jovian moons differ from the Earth's ionosphere.

Present knowledge of the ionospheric characteristics of the Jovian moons is uncertain, and the available data is derived from S-band occultation measurements. The estimated ionospheric values from this data range from no ionosphere to peak electron densities of 5000 to 20,000 cm^{-3} . The latter electron density values correspond to plasma frequencies of 635 and 1270 kHz respectively. By contrast, the electron density of our Earth's ionosphere is on the order of 10^6 corresponding to plasma frequency of about 9 MHz. The more tenuous ionosphere of the Jovian moons is apparent, and consequently in comparison to the earlier Earth sounders, an appropriate frequency range for the JIMO sounder is about 400 kHz to 2 MHz, corresponding to peak electron density values of about 2,000 to 50,000.

14.3 Baseline Instrument Description

The antenna design for the JIMO application is a key issue. Because the ionospheres of the icy moons are believed to be more tenuous than the Earth's ionosphere, coverage at the higher frequencies used in the earlier designs is not required, and thus short dipoles are not required. For the JIMO application, the appropriate frequency coverage is 400 kHz to 2 MHz. In this frequency range, the longer dipole as used in Alouette II and in the ISIS Program is well suited. The 73.2 m dipole has a resonant frequency of about 2 MHz corresponding to the upper frequency of the required bandwidth, the pattern coverage will be that of a dipole over the frequency range, and the antenna mismatch loss is well behaved below the resonant frequency. Such dipole elements can be deployed from the spacecraft. One deployable design used in Alouette II is shown in Figure 14.3-1 below where the material for the dipole is beryllium copper and the diameter of the dipole element is one-half inch. Other concepts can be developed.

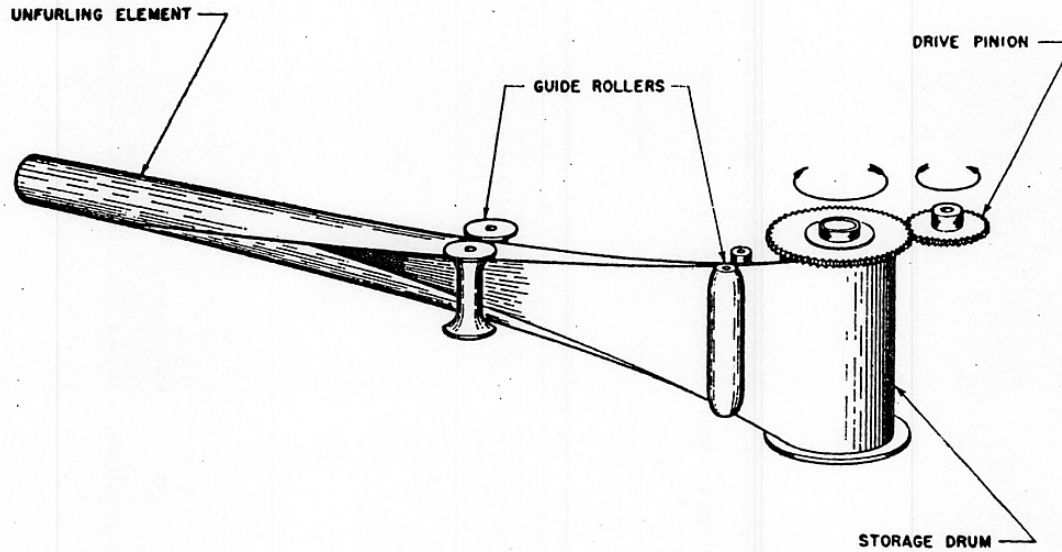


Figure 14.3-1: Deployable dipole antenna (Reprinted courtesy of IEEE).

Accordingly, such a dipole design is selected for the preliminary sounder design. The antenna gain equals the product of the directivity and the mismatch loss, and follows the calculations used in the previous design. At the lower portions of the frequency coverage range, the antenna is electrically small, highly reactive, and has a low radiation resistance. The mismatch loss is quite high as a consequence, as demonstrated in Figure 14.3-2. Some experimentation with matching networks was used in Alouette I. However, because of the low radiation resistance, the matching network loss proved to be sufficient to offset any advantages in overall antenna efficiency.

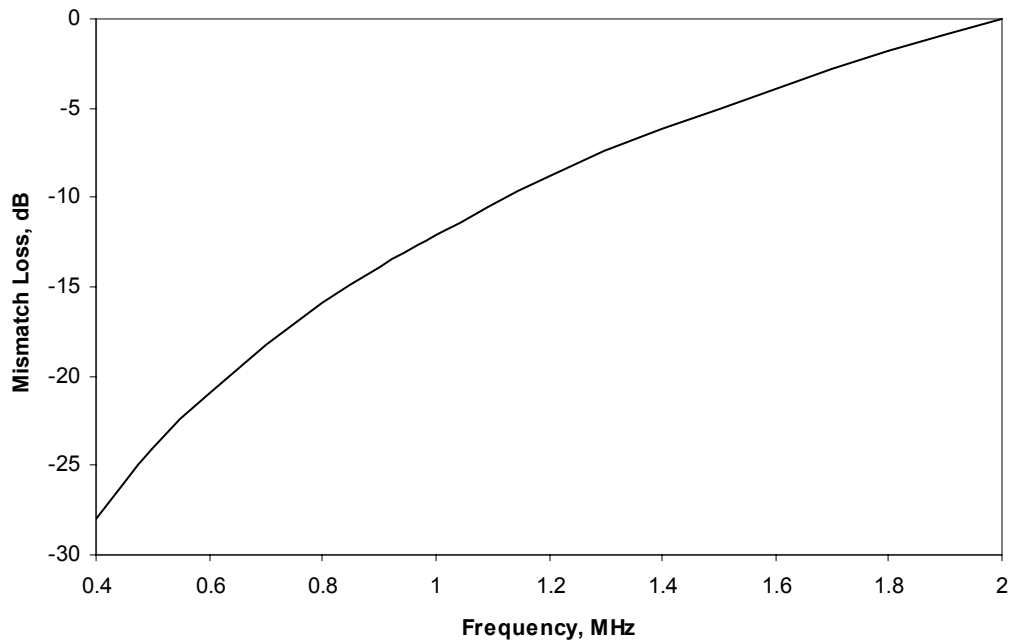


Figure 14.3-2: Antenna mismatch loss values.

The low antenna efficiency at the lower frequency range has different impacts between the transmit and receive operations. The transmit operation is limited by the antenna efficiency because the radiated power is reduced by the antenna efficiency. The receive operation, however, is not impacted by the antenna efficiency because of the high external noise level. In the receive case, the external noise levels dominate the system noise temperature. The antenna efficiency reduces the signal and noise equally, and the system sensitivity is not degraded. This situation is equivalent to the operation at the AM frequency band where acceptable receiver performance is achieved by an antenna having a very small electrical size.

The noise level in this frequency range is dominated by the Galactic component; the assumption is made that other noise levels, particularly those from the spacecraft itself, are at lower levels than the Galactic values. The Galactic noise figure used in this analysis is given by:

$$NF_{\text{atm}} = 52 - 23 \log f(\text{MHz})$$

The resulting noise temperature values are plotted in Figure 14.3-3. It should be noted that these temperature values multiplied by the antenna efficiency values presented above result in noise levels that greatly exceed any noise contributions from the sounder receiver. Thus, the system noise level is established by the external Galactic noise level and, as previously stated, both the signal and Galactic noise levels are equally reduced by the antenna mismatch loss.

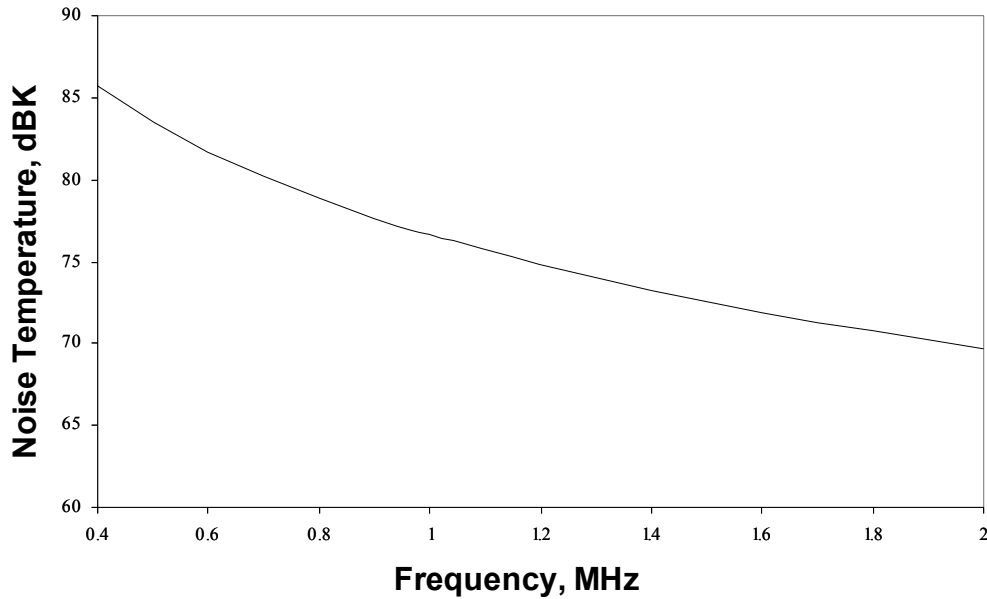


Figure 14.3-3: Noise levels.

The remaining link budget issues involve propagation losses, implementation loss, and transmitter waveform loss. The link loss includes the splitting into the ordinary and extraordinary waves (3 dB), polarization mismatch loss (3 dB), fading (5 dB), and a design implementation loss of 5 dB to cover those factors not incorporated into the link analyses. A total loss of 16 dB is assumed in this preliminary sizing. In contrast to the earlier topside sounders, transmitter and processing technology have vastly improved. The solid-state transmitter used in the original sounders is archaic. Today's technology would consist of a driver using a coherent frequency reference and a sweep generator to sweep the frequency over the bandwidth. Since the system would be coherently referenced to the reference oscillator, coherent integration can be used to reduce the required transmit power. The pulse duration of 100 microseconds will be used again resulting in a bandwidth of 10 kHz.

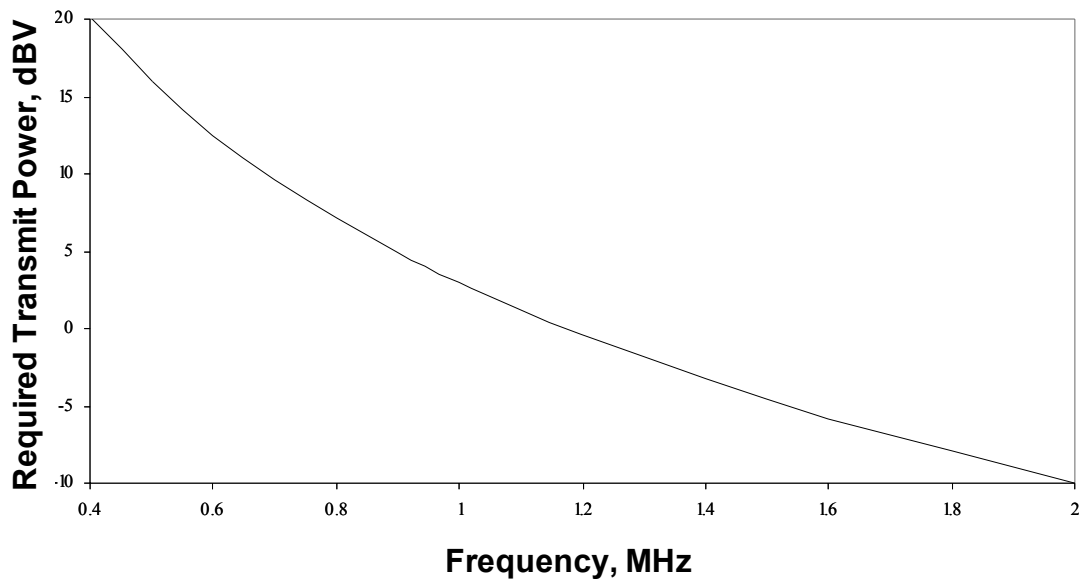


Figure 14.3-4: Transmitter power requirements.

These assumptions are then used to calculate the required transmitter power to obtain a preliminary sizing of the system. The range assumed in these calculations is 400 Km and a 10 dB signal-to-noise ratio is used. The transmitter power requirements, shown below, result from these assumptions, and a 100 W (20 dBW) level is required.

An examination of the link equations reveals a $1/f^{2.15}$ frequency dependence that results in a substantial increase in transmitter power requirements at the lower frequencies. Future investigations should further examine this dependence and investigate means of varying the pulse duration/frequency sweep rate over the bandwidth to achieve a more frequency independent transmitter power requirement.

This preliminary design provides an initial sizing for such a subsystem that can be refined in future efforts. Some further alternatives for extended frequency coverage to lower frequencies can be entertained. However, the required transmitter power would dramatically increase. Lower frequencies further require design attention to isolating the system from frequencies used in power supply switching, etc. Almost independent of the frequency range of this subsystem, design attention is also required to controlling ESD (electrostatic discharge) emissions to avoid interference to this subsystem.

A preliminary system sizing has also been performed to estimate the required weight and power for the sounder. These weights are based on the past designs with updates for the electronics.

Table 14.3-1: Radio Sounder Mass and Power Sizing

		Mass (kg)		Average Power (W)	
		100 km	400 km	100 km	400 km
Antenna Subsystem	Antenna	8.18	8.18	0.00	0.00
	Mounting Brackets	5.00	5.00	0.00	0.00
	Cabling	1.00	1.00	0.00	0.00
RF Subsystem	Signal Generator	1.00	1.00	10.00	10.00
	Transmitter	5.00	5.00	15.00	15.00
	Power Supply	1.00	1.00	10.00	10.00
	Power Distribution Unit	1.00	1.00	10.00	10.00
	Receiver	3.00	3.00	10.00	10.00
Digital Subsystem	A to D Converter	2.00	2.00	10.00	10.00
	Spacecraft Interface and Timing	1.00	1.00	10.00	10.00
	Data Processing	2.00	2.00	10.00	10.00
Total		30.18	30.18	85.00	85.00

14.4 Design Options Description

14.4.1 Observation of Jupiter

There has been discussion of using the radio sounder to observe the ionosphere of Jupiter. In extending the coverage to the Jovian ionosphere, the required range is the problem. Extending the link analysis to the greater range results in power levels that are impractical. Furthermore, the link has a different range dependence. The lower altitude sounder assumes the source is imaged by the ionosphere and thus has an h^2 dependence. At the distance to Jupiter, the image concept does not apply. Essentially, in this range, Jupiter appears as a sphere and the ionosphere merely changes its diameter. Thus the sounder would change frequency when looking for the change in the apparent sphere diameter from the specular return. In this case the dependence is h^4 and even more power would be required. Thus, the range extension for the Jovian ionosphere is not practical.

14.5 Key Technology Developments

There are no new technology developments required for this instrument.

14.6 Schedule Estimate

The schedule for developing the radio sounder is based upon analogies to the development schedules of comparative legacy instruments. The Radio Plasma Imaging (RPI) instrument developed for the Imager for Magnetopause-to-Aurora

Global Exploration (IMAGE) mission, which took 24 months to develop. The development time of a similar instrument, the Radio And Plasma Waves instrument on the WIND mission, took 43 months to deliver. The estimated development time for the radio sounder, using the average of the IMAGE-RPI and WIND-WAVES instruments, is 34 months. Based on the relative simplicity of the instrument, 34 months should be a reasonable approximation of the development time.

14.7 Legacy Instrument Description

A significant amount of design description and data results for “topside” imaging satellites may be found in the June 1969 Proceedings of the IEEE and a top level summary of the sounder characteristics is presented below. The JIMO sounder design differs from these earlier efforts because the ionospheric characteristics of the Jovian moons differ from the Earth’s ionosphere.

Table 14.7-1: Early Radio Sounder Characteristics

	Alouette I	Alouette II	ISIS 1	ISIS B
Frequency Coverage, MHz	0.5 - 12	0.12 – 14.5	0.1 - 20	0.1 - 20
Transmit Power, W	100	300	400	400
Antenna Lengths, m	45.7/22.9	73.2/22.3	73.2/18.8	73.2/18.8

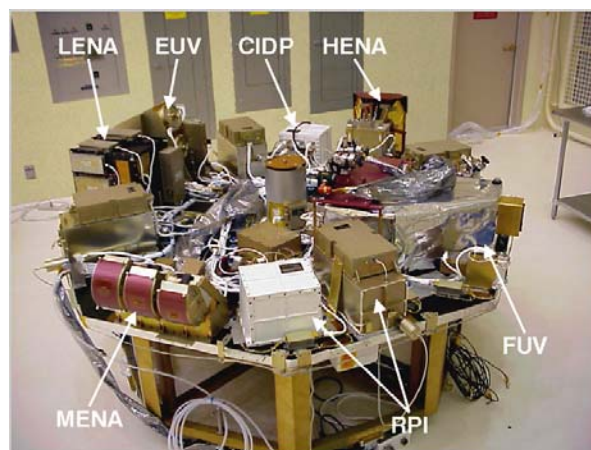


Figure 14.7-1: Radio plasma imager as flown on IMAGE (Reprinted courtesy of NASA).

The IMAGE/RPI mission also presents a good heritage for the radio sounder, however, the portion of the mission performed in the low frequency range from

3 kHz to 20 kHz is not relevant as it is only used for local coverage as opposed to remote coverage. In this frequency range the measurement is of the plasma media surrounding the spacecraft, not of the ionosphere remote to the spacecraft.

14.8 Sounder Data Rates

The maximum radius of the moons is 2,630 km (Ganymede), therefore the unambiguous range was set at 2,730 km at 100 km altitude (and 3,030 km at 400 km altitude), the radius of the moon plus the proposed altitude (a very conservative assumption). The waveform was set achieve the maximum 10 m resolution for the radar sounder and 3 km resolution for the radio sounder. For the radar sounder, the coarser resolution at greater depths will be achieved by integrating the higher resolution range bins at the greater depths (if significant resolution degradation occurs due to propagation through dispersive media, then less integration or no such integration would be applied). The motivation for this procedure is to achieve higher signal to interference at the greater depths where the radar attenuation will be greater. The estimated data rates for the sounders assuming onboard processing are given in the table below.

Table 14.8-2: Sounder Data Rates

	100 km	400 km
Radar Sounder (Mbps)	5.18	5.18
Radio Sounder (Mbps)	0.13	0.48

15.0 Shared Instrument Resources

The baseline instrument architecture assumes the use of shared resources in order to accommodate common instrument needs such as thermal management, pointing and control, power conversion, processing, distribution and shielding, data storage, telecommunication, and instrument articulation via a scan platform. This section addresses each of these topics.

15.1 Scan Platform for Electro Optical Instruments

The proposed JIMO mission calls for the use of a scan platform for the electro-optical instruments. The platform is intended to point the electro-optical instruments during the spiral-in phase of JIMO's trajectory and to fine point the instruments and aid in the rejection of unintended movement from the JIMO spacecraft throughout the science mission. During the spiral-in portion of the trajectory, the orientation of the JIMO spacecraft is determined by the needs of the propulsion system. The scan platform points the instruments in the desired direction during this phase. During nominal science data collection, the scan platform will be nadir pointing while the spacecraft is in a gravity gradient orientation. Often, scan platforms are used to slow down the scan rate of various instruments using back scanning. The thermal mapper and infrared spectrometer are designed such that back scanning is not necessary, thereby eliminating this need for the proposed scan platform.

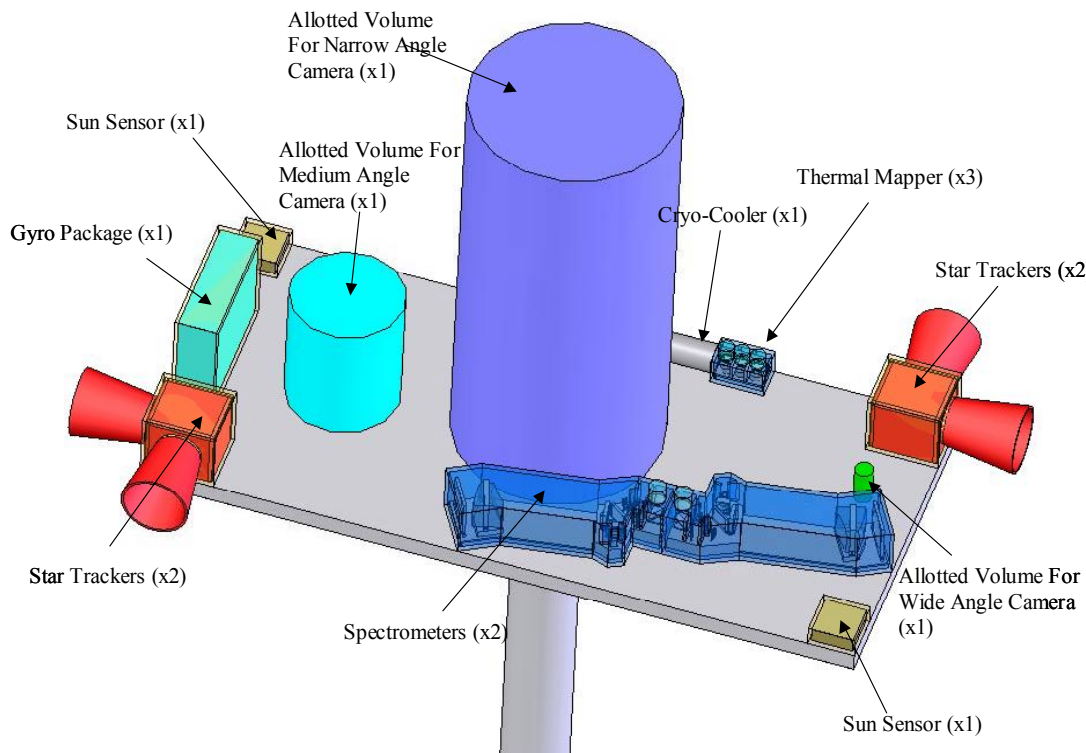


Figure 15.1-1: Isometric view of scan platform with labeled components.

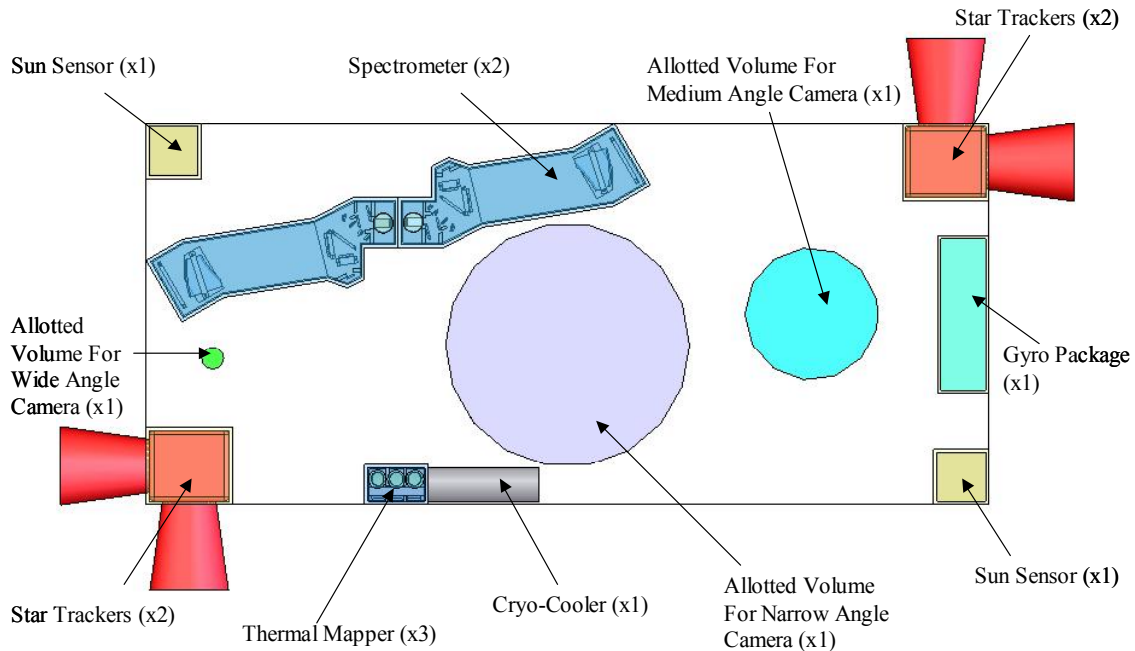


Figure 15.1-2: Top view of scan platform with labeled components.

15.1.1 Instrument Interface to Scan Platform

The scan platform concept described here supports five separate instruments. The wide, medium, and narrow angle cameras (not included as part of this study) along with the infrared spectrometer and thermal mapper are located on the scan platform. Instruments are placed such that there is an unobstructed field of view for each instrument. They are also placed in an attempt to balance the mass distribution on the platform, with the larger mass items closer to the center near the platform gimbal. This reduces the amount of torque necessary for the platform actuators. The following table shows masses of all the instruments included on the platform including radiation shielding in addition to the mass of the scan platform. Mass allocations for the wide, medium, and narrow angle cameras were based on values provided in the Jovian Icy Moons Tour Study and were not considered within the scope of the study presented here.

Table 15.1.1-1: Mass Breakdown of Scan Platform Components

<i>Component</i>	<i>Mass (kg)</i>
Narrow Angle Camera	20
Medium Angle Camera	5
Wide Angle Camera	3
IR Spectrometer	71.1
Thermal Mapper	36.2
Digital Sun Sensors	14.8
Gyros	54.8
Star Camera Assembly	56.6
Integration Hardware/Bracketry	13.1
Wire Harness	13.7
Platform Mass	78.5
Actuator Mass	26.9
Total Mass of EO Platform	393.6

The mass for the spectrometer and thermal imager in the above table includes the mass of the electronics and the radiation shielding for the electronics. The electronics must be mounted on the platform in close proximity to the focal plane arrays to minimize noise. Figure 15.1.1-1 shows the electronics mounted to the backside of the scan platform underneath their respective instrument.

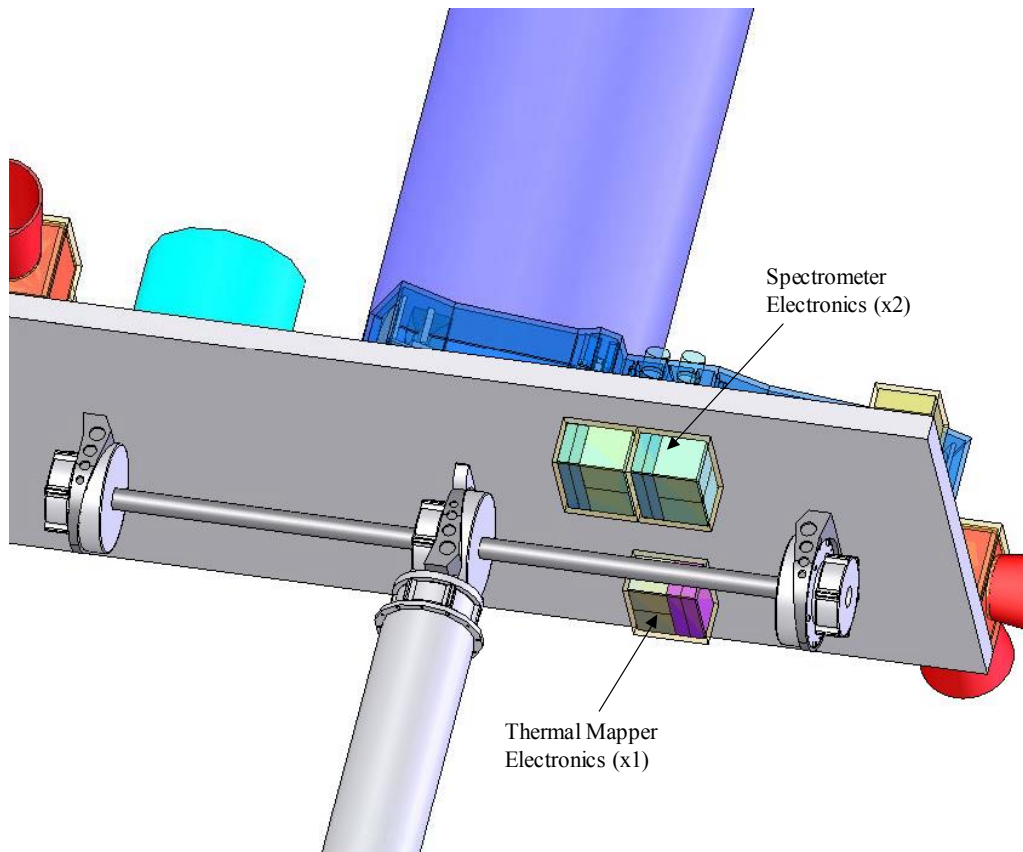


Figure15.1.3-1: Bottom view of scan platform.

In the present configuration, the scan platform supports five instruments. One might consider reducing the number of instruments on the platform to reduce the overall size, mass, and complexity of the platform. In addition, it is possible to place the instruments onto two separate less complex and less massive platforms. This, however, may complicate the JIMO vehicle configuration by placing more stringent pointing and stability control requirements on the spacecraft bus.

15.1.2 Scan Platform

The mass of the platform is based parametrically on the mass of the instruments located on the platform. The approximate dimensions of the platform are determined by creating enough area for all the instruments to fit. Further investigation into the thickness and construction of the platform is highly suggested. Distortion in the platform will lead to instrument alignment errors that must be accounted for. This should be accounted for in an alignment budget supported by thermo-elastic analyses. The mass of the platform and actuator is located in Table 15.1-1.

The mass of the biaxial drive system is based on a design developed by Moog. A custom actuator may need to be developed to handle such a large platform. This is accounted for in the mass by adding an additional 60% to the largest biaxial drive system listed in the Moog catalog. This additional mass also accounts for the precision resolvers integrated into the drive to sense its angular position. Figure 15.1-4 shows what the scan platform biaxial drive might look like.

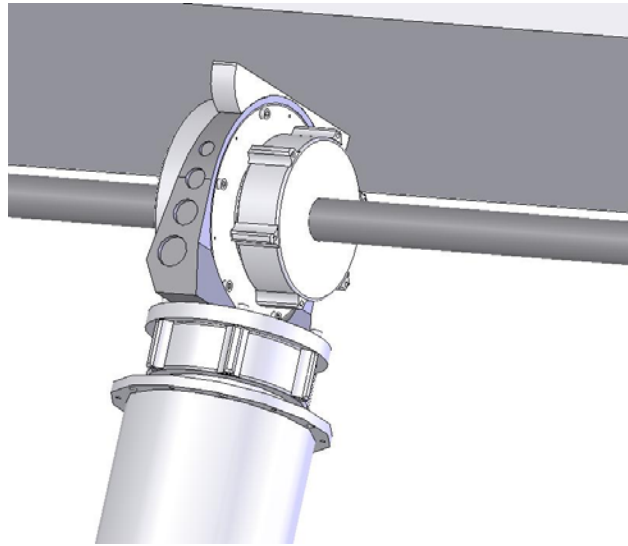


Figure 15.1-4: Scan platform biaxial drive.

15.1.3 Platform Sensing

There are several methods for sensing the scan platform orientation relative to the spacecraft and in inertial space. Four star trackers heads are placed on the scan platform for inertial reference, two of which are for redundancy. The star trackers also aid in correcting the drift of the gyros located on the scan platform. The gyros serve to give relative position of the scan platform to the spacecraft. The mass of the gyro package was based off of the Northrop Grumman SIRU-Dual String consisting of two identical 3-axis IRUs. In addition 2 dual-axis Sun sensors are placed on the scan platform to assist with instrument safe hold to avoid the Sun. Also in place are resolvers integrated into the scan platform gimbals actuators, which give relative position of the scan platform. A list of the various sensors and their masses including radiation shielding is located in Table 15.1-2. This table does not include the mass for the resolvers integrated into the actuators which is already accounted for in the actuator mass.

Table 15.1-2: Scan Platform Attitude Sensor Mass Breakdown

<i>Sensor</i>	<i>Mass (kg)</i>
Digital Sun Sensors	14.8
Gyros	54.8
Star Camera Assembly	56.6
Sensor Mass Total	126.2

A significant amount of redundancy has been built into the attitude sensing of the scan platform. Depending on the amount of risk acceptable to the mission, one might consider reducing the amount of attitude sensors on the scan platform. For instance, some redundancy could be provided by using three star camera heads instead of four, however, in the event of a single failure, performance could be degraded somewhat. Further investigation should be considered weighing the acceptable risk and the amount of redundancy on board the scan platform.

15.2 Pointing and Stability

In the discussion below, roll is the along-track direction, yaw is nadir, and pitch is the cross-track direction opposite to the orbit plane normal. Pointing requirements shown are for each instrument boresight.

The IR spectrometer/visible imager and the thermal mapper are mounted on a scan platform that has its own attitude reference. The scan platform will nominally be aligned such that the instrument boresights point to nadir.

The radar and laser instruments are fixed to the spacecraft bus, and the bus will provide pointing control and an attitude reference for those instruments. The expectation is that the bus attitude sensors will be mounted close to the radar and laser instruments. There could be misalignments between each instrument reference frame and the bus attitude reference. In general, these misalignments can either be estimated or do not impact science objectives. However, bus pointing requirements will be need to be tighter than those shown for the instruments to allow for misalignments. This would normally be addressed in a system level error budget.

Table 15.2-1 summarizes zero-to-peak requirements for instruments designed for a 100-km altitude. The tightest pointing control and knowledge requirements are for the Interferometric Synthetic Aperture Radar (InSAR), while the tightest pointing stability requirements are for the laser altimeter. Since the InSAR and the laser altimeter are fixed to the bus, there are implications for what the bus must provide. The InSAR control and knowledge requirements would not be difficult to meet for a typical Earth orbiting spacecraft, but they may be difficult to meet while operating in the high radiation environment around Jupiter. The laser pointing stability requirements would also not be difficult to meet for a smaller

bus, but they may be a challenge for JIMO because of its very large and flexible structure.

Table 15.2-1: 3-Sigma Pointing Requirements for Instruments Designed for 100 km Altitude

	Pointing Control (mrad)			Pointing Knowledge (mrad)			Pointing Stability (mrad/sec)		
	roll	pitch	yaw	roll	pitch	yaw	roll	pitch	yaw
IR Spectrometer/Visible Imager	13	13	39	6.5	6.5	19.5	1.31	1.31	3.93
Thermal Mapper	13	13	39	6.5	6.5	19.5	1.31	1.31	3.93
Interferometric SAR	52	0.8	0.8	17.5	0.4	0.4	100	7.1	7.1
Polarimetric SAR	140	3.34	3.34	47	1.67	1.67	78	2	2
Radar Sounder	123	123	NA	62	62	NA	NA	NA	NA
Radio Sounder	123	123	NA	62	62	NA	NA	NA	NA
Laser Altimeter	13	13	39	2	2	6	0.183	0.183	0.549
Laser Spectrometer	13	13	39	6.5	6.5	19.5	1.31	1.31	3.93

In addition to the requirements listed above, there is an issue regarding the effects of vibration on InSAR measurement quality. Translational vibration of an InSAR antenna in the direction of its boresight would lead to phase modulation that tends to increase the level of side lobes in SAR imagery. This has the effect of decreasing image contrast. The vibration amplitude should be limited to maintain good image quality. This is a relatively small value for a structure as large and flexible as JIMO, it may require vibration isolation of the InSAR and/or other measures to mitigate the effects of vibration.

Table 15.2-2 summarizes pointing requirements for instruments designed for an altitude of 400 km. The tightest pointing control and knowledge requirements are still for the InSAR, and the tightest pointing stability requirements are still for the laser altimeter. Note that the pointing stability requirements for this case are tighter than for the 100-km altitude case and would pose more of a challenge than in the 100-km case.

Table 15.2-2: 3-Sigma Pointing Requirements for Instruments Designed for 400 km Altitude

	Pointing Control (mrad)			Pointing Knowledge (mrad)			Pointing Stability (mrad/sec)		
	roll	pitch	yaw	roll	pitch	yaw	roll	pitch	yaw
IR Spectrometer/Visible Imager	3.25	3.25	9.75	1.625	1.625	4.875	0.255	0.255	0.765
Interferometric SAR	26	0.8	0.8	5.2	0.4	0.4	28	1.5	1.5
Polarimetric SAR	52	4	4	11	2	2	5	0.65	0.65
Radar Sounder	37	37	NA	18.5	18.5	NA	NA	NA	NA
Radio Sounder	37	37	NA	18.5	18.5	NA	NA	NA	NA
Laser Altimeter	4.4	4.4	13.2	1.13	1.13	3.39	0.036	0.036	0.108
Laser Spectrometer	4.4	4.4	13.2	2.2	2.2	6.6	0.255	0.255	0.765

In addition to the requirements listed above, there is again an issue regarding the effects of vibration on InSAR measurement quality. The translational vibration amplitude should be limited to less than 0.4 mm, the same as in the 100-km altitude case.

15.3 Power Conversion, Processing, Distribution and Shielding

The Jupiter Icy Moons Orbiter (JIMO) will encounter the most intense levels of radiation ever experienced by a man-made spacecraft. Every subsystem on the spacecraft will have to be designed to accommodate levels that could be up to 100 times greater than the worst levels seen in an Earth orbit. This section briefly addresses the issue from the standpoint of several critical technologies, including power conversion electronics and wiring.

15.3.1 Current Technology

High-efficiency power converters are comprised of switching components, control electronics, and passive elements. The control circuitry performs the basic task of maintaining the correct output voltages by determining the appropriate on/off signals to the switching devices. Control circuits also perform ancillary tasks such as generating housekeeping voltages for other control circuits, detecting over voltage or over current conditions, and other functions. Passive components (inductors, transformers, capacitors) are relatively immune to ionizing radiation and displacement damage. Switching components control the flow of electrical energy into and out of the inductors and transformers. Modern switching components are among the most radiation-hardened of solid-state components. The radiation hardness of control circuits depends on the underlying solid-state technologies and device geometries employed. Using bipolar transistor technology or large-geometry CMOS instead of newer, small

geometry technologies gives the best radiation performance for the control circuitry.

The present state of the art for total dose in power electronic devices is approximately 1MRad for power MOSFETs, 300kRad for Schottky and ultra fast rectifiers, 200kRad for low-dropout linear voltage regulators, and 1MRad for small, standalone modular converters. Pulse-width modulator controllers and MOSFET drivers are hard to 200-300kRad.

15.3.2 Silicon Carbide

The preceding values are all based on silicon as the basic material for the devices. Going to high-band gap materials such as silicon carbide (SiC) would result in better radiation displacement damage tolerance, as well as high-temperature operation. SiC devices have been under development for many years. Presently, there are commercial Schottky diodes and high-temperature sensors being made using SiC. It is reasonable to assume that the next few years will bring improvements in yield and more reliable devices for power electronics, including power MOSFETs with total dose hardness in excess of 100MRad, but it is not certain that the technology will mature in time for incorporation into the JIMO design.

The advertised radiation resistance of SiC devices is a consequence of the lower level of integration on current state-of-the-art devices. As SiC devices achieve higher levels of integration, circuit band gaps will become smaller, and the devices will become more susceptible to neutron displacement damage. Highly integrated SiC devices are likely to be no less susceptible to ionizing radiation than current deep-well six-micron CMOS technology. Nevertheless, this area holds promise for the development of high temperature, electronics with some radiation tolerance advantages, particularly at low levels of integration and should be studied further for technology investment for the JIMO application.

If SiC devices cannot be used, it is still possible to design robust power converters using existing technologies by adding shielding. Fortunately, much of the volume and mass of a power converter is comprised of magnetic components and capacitors, which require minimal shielding. However, the power electronic devices and control circuits would require substantial shielding, up to one inch of aluminum in thickness. One approach to minimize the mass increase would be to use a single aluminum "box" to house all of the semiconductor components for a particular converter. This would necessitate increasing the wire lengths of these components, which complicates the circuit design, perhaps forcing the power converters to operate at lower frequencies.

Other options include using control circuitry designed with discrete, large-geometry transistors to achieve hardness levels greater than 1MRad, and using power MOSFETs as synchronous rectifiers in place of the "softer" Schottky

rectifiers. If all of the semiconductor devices can be made hard to 1MRad, the shielding thickness required drops from one inch to roughly one third of an inch.

From a system design perspective, it would probably be preferable to centralize power conversion as much as possible, using a few high-power converters in a shielded compartment rather than many low-power converters distributed throughout the spacecraft. Some local power regulation or filtering may still be necessary, but it will save a great deal of weight to avoid having a complete power converter in every unit or instrument.

15.3.3 Wire Insulation

Wire insulation exists that can withstand 1000 Mrad. It is recommended that all wiring undergo radiation total dose qualification testing. This should include the combined mechanical environments of clamping, flexing, and thermal cycling. The flexing and thermal cycling can be done after the radiation testing.

The radiation hardness of the most commonly used insulation materials is in Table 15.3.3-1 [Ref 15.3-1, -2, -3]. The insulation is listed in order of usage.

Teflon is commonly used as a jacket for shield-twisted pair wire, coaxial cable dielectric, and as an adhesive and outer and inner layer in Kapton-insulated wiring. Boeing and Raytheon have shown that wrapped insulation withstands less radiation than extruded insulation. Boeing and Raytheon also showed that radiation degrades flex life [ref 15.3.3]. Radiation life can be increased by radiation shielding. Boeing and Raytheon also showed that the FEP extruded form of Teflon had a longer radiation life than the tape form, a longer life than PTFE, and has tested it to 180 MRad. PTFE was failing at 15 MRad when in wrapped form and flexed. Also Teflon is about 50 times more radiation resistant in a vacuum because of the lack of oxygen.

Kapton is less flexible, less fuel compatible, hydroscopic, and more susceptible to arc-tracking than Tefzel. Kapton can burn in a vacuum forming a conductive carbon-like material. This means a short can spread from one wire to many wires in a wire bundle. In the worse case, the entire wire harness can burn causing extensive thermal damage to surrounding hardware.

Table 15.3.3-1: Radiation Hardness of the Most Common Wire Insulation Materials

Insulation	Radiation Resistance
Cross-Linked Tefzel	100 MRad
Tefzel	1 MRad
Kapton	1000 MRad
Polyalkene	100 MRad
Teflon	1 MRad

References

[Ref 15.3-1] G. Ginsberg, *Connectors and Interconnections Handbook, Volume 4, Material*, The Electronics Connector Study Group, Fort Washington, PA, 1977.

[Ref 15.3-2] NASA Wire Insulation Guidelines, http://nepp.nasa.gov/npsl/Wire/insulation_guide.htm, 17 October 2003.

[Ref 15.3-3] Raychem, Specification 55 Wire and Cable, Raychem Corporation, Menlo Park, California, 1977.

[Ref 15.3-4] W. Baumert, "Report on Teflon Wire Total Dose Test," Hughes Interdepartmental Correspondence, El Segundo, CA, 5 June 1995.

15.3.4 Shielding for Power Electronics

Common practice for radiation shielding is to convert all shielding materials to equivalent Aluminum thickness by correcting for the density variations. This takes into account the primary effect of radiation attenuation with mass; however, it does not consider the secondary effects of material properties on shielding different types of radiation. Research [Ref 15.3-5] has shown that these secondary effects may be important when designing radiation-shielding housing and may permit improved shielding efficiency by using layered shielding with more than one material.

Energetic electrons and protons are the main components of total radiation dose in the space environment. Computer simulations have shown that some materials are better at stopping electrons than protons and vice versa. Materials such as Tungsten and Tantalum have a relatively high atomic mass (Z). The high atomic mass materials are better at attenuating electrons. As a consequence of decelerating the electrons, energetic photons are emitted in the form of Bremsstrahlung or braking radiation. This occurs whether the material is of high or low atomic mass; however, high atomic mass materials are more efficient at absorbing Bremsstrahlung. With regards to attenuation of protons, materials with

relatively low atomic mass such as Aluminum are more efficient at stopping protons.

Testing [Ref 15.3-6] has shown that the optimal structure for radiation shielding is an Aluminum-Tungsten-Aluminum tri-layer. In this configuration incoming radiation first hits the outer layer of Aluminum, which is effective in stopping much of the high-energy electrons and protons. As a result, the creation of secondary electrons and braking radiation occurs. The middle layer (Tungsten) will absorb the braking radiation efficiently; however, this also generates secondary electrons through the Compton effect. Generation of braking radiation in the Tungsten (high Z) is less of a concern because the first layer of Aluminum effectively absorbed the high-energy electrons. The middle layer of Tungsten is efficient at absorbing the remaining electrons at lower energies. The final layer of Aluminum acts to absorb the secondary electrons and braking radiation produced by the middle layer.

15.3.5 Advanced Shielding for High Radiation Environments

The primary contribution to total ionizing dose (TID) in the JIMO mission will be due to the natural Jovian radiation environment [Ref 15.3-7]. During the science mission and transfer between the Galilean moons, the JIMO spacecraft will be exposed to high-energy electrons and protons in the Jovian radiation belts. This environment will be particularly severe at Europa. Because the JIMO mission design is currently in development, the Jupiter Icy Moons Tour (JIMT) mission design has been used as a reference for establishing shielding requirements. Based on available radiation hardened electronics, we have assumed an allowable TID of 100 krad. Using a curve fit of the data from the JIMT study, shown in Figure 15.3.5-1, this implies an equivalent shielding thickness of 2080 mil Al or a shielding “mass thickness” (product of thickness and density) or 14.8 g/cm^3 which is independent of shielding material choice.

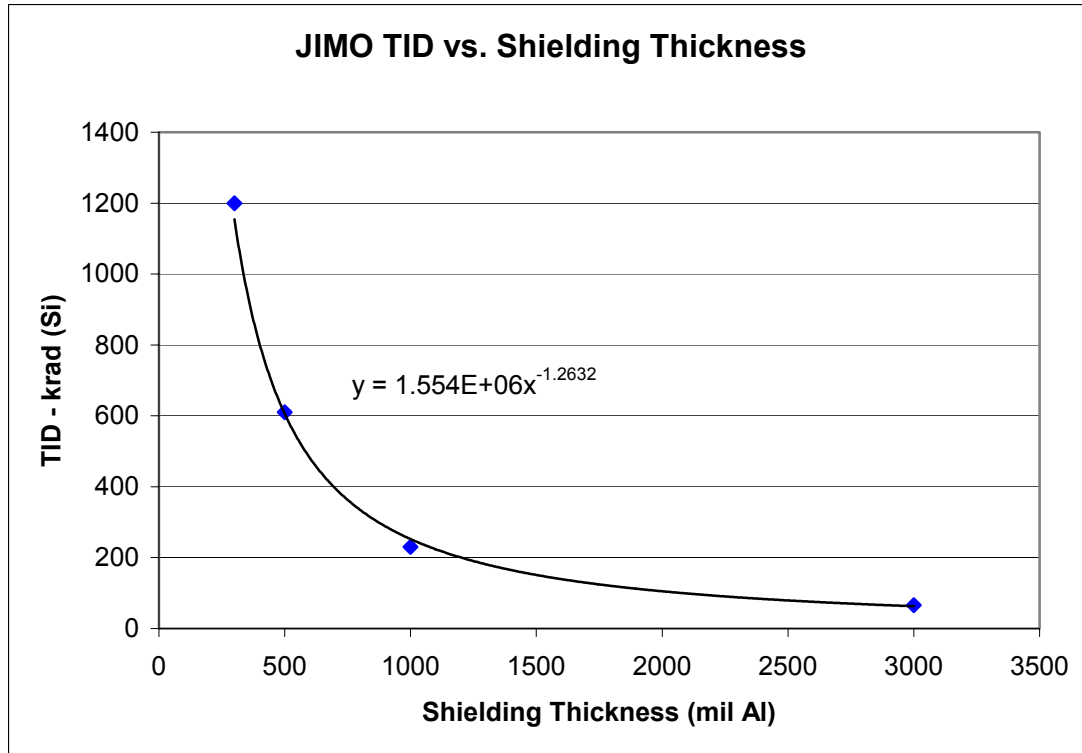


Figure 15.3.5-1: JIMO radiation shielding thickness

According to investigations of tri-layer radiation shielding conducted by Mangeret [Ref 15.3-5], mass thickness efficiency can be improved by 30-50% by using a very dense material such as Tungsten (W) or Tantalum (Ta) in combination with Aluminum. Assuming one can achieve an improved mass thickness efficiency of 0-25%, this implies that we can shield to 100 krad using approximately 5.8-7.7 mm of W or 6.7-8.9 mm of Ta. It is recommended that for preliminary design purposes, no mass thickness efficiency improvement should be assumed, however, as design fidelity improves, an investigation of optimal shield layer selection is recommended.

Tungsten (W) with a thickness of 7.7 mm was the material of choice for shielding the various instruments. Each instrument's electronics was packaged and shielded separately. This does not represent the most efficient method for packaging electronics in terms of shielding mass and thermal control; however, it should give an upper bound to the mass for shielding. Separate packaging allows for separate instrument development. Once the final set of instruments is decided upon it is recommended that a more efficient packaging scheme be investigated which may incorporate multiple instrument units in a shielded enclosure. Shielding was necessary to protect the optics and focal plane array of the spectrometer and thermal imager. A Tungsten box and a Cesium Iodide aperture cover surrounded the optics of both systems. Internal shielding was also placed within the box to protect the optics and focal plane arrays from stray radiation

that enters through the aperture during observation. Shielding for the radar instruments was only necessary for the electronics. The antenna portion of the radar instruments did not need to be shielded. For this reason the shielding mass as a percentage of total sensor mass came out lower for the radar instruments when compared to the optical instruments as shown in Table 15.3.5-1.

Table 15.3.5-1: Radiation Shielding Mass Breakdown

Instrument	Shielding Mass (kg)	% Instrument Mass
Vis & IR Spectrometer		88%
Optics Shielding	50	
Electronics Shielding	14.6	
Thermal Mapper		58%
Optics Shielding	7.6	
Electronics Shielding	12.6	
Laser Altimeter		13%
Electronics Shielding	10	
Laser Reflection Spectrometer		20%
Electronics Shielding	10	
Interferometric SAR		36%
Electronics Shielding	121.9	
Polarimetric SAR		32%
Electronics Shielding	42.6	
Subsurface Radar Sounder		37%
Electronics Shielding	48.6	
Radio Plasma Sounder		60%
Electronics Shielding	48.6	
EO Scan Platform		
Gyro Package Shielding	46.2	84%
Sun Sensor Shielding	14	95%
Star Tracker Shielding	44.6	79%
Totals	471	55%

Table 15.3.5-1 is a mass breakdown of the radiation shielding for each instrument. The column labeled percentage of total sensor mass is the radiation shielding mass/total sensor mass * 100%. Overall, the shielding accounts for more than half of the total mass of the instruments, which suggests that further investigation into optimization of the radiation shielding mass would be valuable.

There are several approaches to optimizing the amount of radiation shielding needed. As previously mentioned a tri-layer combination of material may reduce the amount shielding thickness thereby reducing the mass. In addition, savings can be achieved by increasing the packing density of instruments and electronics, when possible. Increasing the packing density of electronics can lead to more stringent requirements on the thermal system. Mass savings can also be accomplished by the strategic placement and integration of components to take advantage of shielding from other components and structure from the spacecraft bus.

[Ref 15.3-5] Mangeret R., Carriere T., Beaucour J., Jordan T., “Effects of Material and/or Structure on Shielding of Electronic Devices.” IEEE Transactions on Nuclear Science, Vol. 43, No. 6, December 1996.

[Ref 15.3-6] IBID

[Ref 15.3-7] McAlpine W., Insoo J., Garrett H., Narvaez P., “Jupiter Icy Moons Orbiter Radiation, EMI, and Magnetics Environment, 12 June 2003.

15.4 On-Board Data Storage and Processing

The final suite of instruments selected for use on board JIMO will ultimately determine data rates, amount of storage required and number of intervals of data required to be stored. Processed data rates will vary, but ultimately there will be a vast quantity of data stored until the opportunity to transmit to Earth is available. Table 15.4-1 identifies the proposed data rates for the suite of instruments currently under consideration for inclusion on the JIMO mission.

Table 15.4-1: Projected Data Rates for JIMO Suite of Instruments

Instrument	Qty	Raw Data Rate (Mbps)	Processed Data Rate (Mbps)
Vis / IR Imaging Spectrometer	3	62.34	62.34
Thermal Mapper	2	0.436	0.436
Laser Altimeter	1	1	1
Laser Reflection Spectrometer	1	1	1
Interferometric SAR	1	2332	55.98
Polarimetric SAR	1	149.9	36.73
Radar Sounder	1	5.18	5.18
Radio Sounder	1	0.13	0.13

The storage device, either mechanical or entirely electronic, will provide mass storage for all science data collected by suite of instruments. It will be necessary to store all data until it can be down linked to Earth and confirmation that the data was successfully received. Absent confirmation, the data can be retransmitted, if necessary. The Command and Data Handling (C&DH) subsystem should be capable of extracting any required meta data regarding the science data. The C&DH subsystem should also be capable of processing and/or performing data compression as required. In all cases the source data will be preserved in the mass data store.

Storage capabilities and techniques are driven by the availability of technology to support the desired amount of data storage required. Currently there are few vendors in the space based data storage arena as the aerospace industry consolidates. Major contractors have garnered the capability through mergers and acquisitions, but there are still a few small companies that have survived and prospered in this area.

15.4.1 Existing Data Storage Technology

Technologies available for space-certified, on-board data storage range from mechanical and magnetic to solid state. Mechanical and magnetic technology consists primarily of reel-to-reel magnetic tape transports. This technology has a long history of successful space operation. Solid state technology is primarily solid-state digital recorders (SSDR). This is newer technology, however, SSDRs have a decade long space legacy.

Reel to reel and SSDR technologies have comparable storage capacity, ranging from gigabits ($10E9$ bits) to terabits ($10E12$ bits). Increased capacity for either technology is accomplished by adding more physical media. Tape recorders add more tape; either by placing more tape on one drive spool or by adding multiple drives. SSDRs increase capacity by adding more storage semiconductors or use semiconductor integrated circuits that contain more bits on a single chip. These technologies will store one collection interval of data. This is currently thought to be one complete map of the moon's surface. The exact size is subject to final evaluation of the instrument packages, but it should be in the terabit range.

15.4.2 Retrieval Time and Rate

Retrieval time (latency) for tape recorders depends on the length of the tape and the location on the tape of the information requested at the time of retrieval. It can range from microseconds to seconds. The latency of the solid state data recorder depends on the semiconductor technology being used. Retrieval speed ranges from microseconds to nanoseconds. For large amounts of data, such as images, the data transfer rate is one of the dominant factors. The total time to acquire the data is the sum of the latency and the product of the transfer rate and the data file size. Transfer rates generally range in the megabit per second rate,

anywhere from 10 to 100 Mbps. One to 10 megabits is a representative image file size. The total time is in the range of 1 second to 10 milliseconds.

15.4.3 Flight Certification/Availability

Both reel-to-reel recorder and SSSDR technologies have been available for space applications for some time. The Seakr Corporation produces a representative 198-legacy product SSSDR.

15.4.4 Limitations of Tape Recorder Mechanisms

While tape recorders have a long history in space, they have exhibited some limitations. The tape media is subject to stretching and/or breaking. The media is subject to wear and portions of the media can fail to record data or can fail to play back already recorded data.

Solid state data recorders (SSDR) have overcome many tape recorder mechanism limitations.

15.4.5 Radiation and Shielding Issues

Space-based hardware normally requires radiation shielding to some extent. One hundred mills (0.1 inch) of Aluminum enclosure around electronic circuit boards is the typical shielding utilized. The use of heavier metals, e.g., Titanium, provides greater attenuation for the same thickness. Shielding protects the electronics from receiving a total dose of radiation from the natural space environment. It does not provide adequate protection from the radiation responsible for transient single event effects such as single event upset (SEU). Shielding does not impede high-energy particles responsible for single event effects. Special circuit design, special semiconductor fabrication processes, and special architecture of hardware and/or software provide for mitigation of single event effects. The various approaches have trade-offs—primarily, the result is a loss of processing speed and a potential increase in component size.

SSDRs use integrated circuit semiconductors similar to those utilized in computer memory systems. These devices are designed for speed, ease of manufacture (high yield), and highest capacity per chip. A variance in these parameters will result with an increase in robust radiation performance. Speed and capacity favor small feature size, however, small devices are more easily upset by lower levels of radiation energy. Small simple circuits can be produced at the expense of more involved, larger, mitigation circuit features.

These issues are well understood, and similar to those encountered for most spacecraft microelectronic circuits. Mitigation techniques involve the use of more radiation hardened semiconductor material and processes. Silicon-on-Insulator (SOI) chips provide orders of magnitude more radiation hardness than

commercial circuits, and have been in production for decades. However, they are more expensive than commercial integrated circuits, have lower yield, and are not available in as many circuit configurations. Typically, these circuits are purpose built for specific space applications. Manufacturers such as Honeywell, Plymouth MN; BAE, Manassas, VA; and UTMC, Colorado are sources of purpose built radiation hardened microcircuits.

15.4.6 Potential Future Technologies

There are several technologies that may have the potential for space applications in the near future. With a technology cutoff date of 2007, one of the following technologies may be ready for use in a space environment.

Rotating disk storage devices possess greater storage capacity than SSDRs but typically less than tape. One terabyte (1,000 gigabytes) of memory – non redundant – weighs 3.2 Kilogram with current technology, unshielded. They can be more radiation hardened than SSDRs but have mechanical limitations imposed by the rotating bearings intrinsic in their design.

Limitations to conventional rotating disk storage devices include similar life limitations as space gyros and/or reaction wheels. Bearings eventually fail when the lubricant fails. The issues of lubricity, metal-to-metal contact, heat, viscosity, contamination and so forth are at work. To date, no rotating disk drives have flown in space.

Non-contact bearing uses a magnetic field to separate the two metallic interfaces. When the device is rotating there is no wear since the metallic surfaces do not touch. There is, however, measurable erosion to the surfaces during the transient start time. This limits the number of useable cycles the mechanism may experience. Further life test testing and data is required. There are, currently no space-qualified air bearing rotating disk products available, because all current spacecraft rotating bearing requirements are being met with conventional lubricated bearings. These are used in gyros and reaction wheels, and have achieved long life and reliability based on legacy evolved designs. There does not appear to be any funding to develop new technology since existing requirements are being met. However, the federal government is funding low-level innovative research to convert existing commercial disk drives, such as the Hitachi, to non-contact bearings suitable for space applications. The existing head and surface plating technology is preserved and the lubrication system is replaced with a potentially longer-lived non-contact bearing.

15.4.7 Longevity and Redundancy

Solid state data recorders have lifetimes identical to any other space-qualified electronics. With appropriate redundancy and mapping of memory to allow for excess capacity at beginning of life, the units should be reliable for fifteen years. There are the traditional trades between mean mission life, probability of mission success and so forth.

Redundancy capabilities and requirements depend upon the probability of success and mean mission time but approximately 150% is the order of magnitude. This allows for two-thirds to be used at the beginning of life, one third redundant. This is usually called fifty percent margin.

15.5 Telecommunication Resources

The sample JIMO baseline instrumentation suggests that robust, high data rate communications far in excess of 10 Mbps are needed to take full advantage of the instruments' data return capabilities. Current proposed communication architectures options under consideration are targeting 10 Mbps bandwidth for the science data downlink. In this section, a number of options to greatly increase the data rate are presented. As shown in Table 15.5-1, instrument data rates vary from a low of 436 Kbps for the thermal mapper to 2332 Mbps for the InSAR instrument. Even the baseline, 300-channel visible and imaging spectrometer exceeds the 10 Mbps data rate target by a factor of four.

The sample JIMO baseline instrumentation suite includes the following: IR imaging spectrometer, laser altimeter, radio plasma sounder, subsurface radar sounder, interferometric synthetic aperture radar (SAR), and polarimetric SAR. The raw data rates and processed data rates for these instruments are contained in Table 15.5-1 below.

Table 15.5-1 Instrument Data Rates

Instrument	Qty	Raw Data Rate (Mbps)	Processed Data Rate (Mbps)
Vis / IR Imaging Spectrometer	3	62.34	62.34
Thermal Mapper	2	0.436	0.436
Laser Altimeter	1	1	1
Laser Reflection Spectrometer	1	1	1
Interferometric SAR	1	2332	55.98
Polarimetric SAR	1	149.9	36.73
Radar Sounder	1	5.18	5.18
Radio Sounder	1	0.13	0.13

The data return problem is mitigated to some extent by considering the amount of data processing or compression that can be achieved for each instrument, and then sizing the communication system based on this number. It is evidenced that the amount of data to be transmitted is reduced by a factor of 18 by transmitting the processed data, on average, for the baseline instrument suite. Clearly not all of the instruments considered in this study will fly as part of the JIMO payload, however, those that do will be operating at very high duty cycles, leaving very little off time. This means that the communication link needs to be sized, to first order, in order to allow simultaneous operation and data transmission from multiple high data rate instruments.

Available communications time throughout the JIMO mission is lessened by blockage due to solar incursion, Jupiter blockage, and most notably blockage from the Jovian moon being orbited. An analysis was conducted using an in-house software program (Satellite Orbit Analysis Program, SOAP) with the ephemeris data file Jup100.bsp obtained from the Jet Propulsion Laboratory (JPL). Physical properties for the Galilean satellites used in this analysis are shown in Table 15.5-2. This analysis assumes the solar exclusion region to be 10 solar radii from the geometric Sun center. With this exclusion angle, a loss of communication occurs once per year with an outage lasting approximately 5.5 days.

Table 15.5-2: Physical Properties of the Galilean Satellites

Galilean Satellites	Physical Parameters			Orbital Parameters				
	Mean radius (km)	Mass (10^{21} kg)	Gravitational Constant (10^{12} m ³ /s ²)	Semi-major axis (10^3 km)	Inclination (deg)	Eccentricity	Orbital Period (days)	Rotation Period (days)
Callisto	2410.3	107.59	7.180998	1882.7	0.51	0.007	16.689018	16.7
Ganymede	2631.2	148.19	9.886997	1070.4	0.21	0.0015	7.154553	7.2
Europa	1560.8	48.00	3.201000	670.9	0.47	0.0101	3.551181	3.6
Io	1821.6	89.32	5.961000	421.6	0.04	0.004	1.769138	1.8

Outage due to Jupiter blockage occurs once per orbit period of the Jovian moon being orbited. While orbiting Europa, communication outages due to Jupiter occur once every 3.55 Earth days lasting approximately 2.4 hours. Orbits around Ganymede will experience the outage duration of about 2.1 hours every 7.15 Earth days. Jupiter blockage rarely occurs at Callisto due to the greater distance from Jupiter and the orbital geometry of Callisto, Jupiter, and Earth. A summary of the blockage frequency and duration for each Jovian moon can be found in Table 15.5-3.

Table 15.5-3: Communication Outages Due to Jupiter Blockage

<i>Jovian Moon</i>	<i>Blockage Frequency (Earth Days)</i>	<i>Duration Outage (Hours)</i>
Europa	3.55	2.4
Ganymede	7.15	2.1
Callisto	N/A	N/A

Assuming an orbit altitude of about 100 km and a worst-case right ascension of ascending node (minimum angle between spacecraft to Earth vector and the spacecraft orbit plane), the communications blockage is between 39-42% of the orbit period or 124–155 minutes depending on the Jovian moon (further detail shown in Table 15.5-4). This presents the worst-case, however, much less blockage will occur as angle between the spacecraft to Earth vector and the orbit plane approaches 90 degrees. The initial right ascension of ascending node at the Jovian moon for the science orbit should be selected with both the desired phase and the desired communications time in mind. Compromises may be available that would offer few communications outages during times of high data collection that may also meet required lighting constraints.

Table 15.5-4: Communication Outages Due to Jovian Moon Blockage

<i>Jovian Moon</i>	<i>Orbit Altitude (km)</i>	<i>Outage Time (min)</i>	<i>Orbit Period (min)</i>	<i>Percent Orbit Blackout (%)</i>
Europa	100	63.3	154.5	41.0%
Ganymede	100	62.2	150.3	41.4%
Callisto	100	48.2	123.9	38.9%

Since the Earth is visible approximately 60% of the time during the JIMO orbit, the full data rate that the instruments produce has to be transmitted at a rate of 1.0/0.60 or 1.67 times the collection rate. For the Ganymede and Callisto science missions, data can be stored on board the spacecraft for retrieval at a later time, and science observations and telecommunications can be more easily de-conflicted because the spacecraft will be able to remain longer. At Europa, which orbits Jupiter in a high radiation environment, the time available to do science and telecom is constrained by the spacecraft radiation lifetime. During the Europa orbit, it is more likely that science collection and data downlink will need to occur simultaneously. Storing data for later retrieval will risk the loss of that data in the event of an earlier than predicted spacecraft failure. Spacecraft operations at Europa may be further impacted by increased system faults, resets,

and safe-mode entries caused by the very high levels of ionizing radiation. These options argue for increased transmit data rates, in order to mitigate against data loss and increase the system operability margin at Europa.

Three alternatives to increase the possible telecommunication downlink data rate are discussed in succeeding sections. The first method employs a 3-meter or 5-meter antenna on the JIMO spacecraft operating at 35 GHz to transmit data via the 70m DSN antennas. The second method utilizes multiple lasers on board JIMO operating in the THz band with an optical relay orbiting Earth. The third method is to use an RF relay satellite in high orbit around Jupiter or possibly in a Heliocentric, Jupiter trailing or leading orbit.

15.5.1 RF Communication Using 3-meter or 5-meter Dish Antenna

This approach radiates RF at 35 GHz through a 3 or 5 m diameter antenna. Amplification is achieved at Ka band using klystrons in the 250–2500 W to transmit power. Assuming also that the 70m DSN sites are upgraded to Ka-band receive capability, the project antenna gain would be approximately 84 dBi. An analysis was made using multiple klystrons, along with varying the antenna diameter. The achievable data return for Ka-band telemetry for this scenario is shown in Table 15.5-1.

Multiple klystrons are ganged together, either staggered tuned or synchronously tuned, in order to achieve the power output shown in the table. Both methods would provide the same net result in data throughput. The method of tuning becomes a function of programmatic constraints.

A major driver for risk for this system is the high-power transmitter. The highest continuous wave (CW) power, space-qualified tube available at 35 GHz with good DC-to-RF conversion efficiency is the Extended Interaction Klystron (EIK), a fixed-tuned permanent magnet focused amplifier with multiple depressed collectors. Communications and Power Industries (CPI) of Ontario, Canada (formerly Varian Associates of Canada) manufactures the tube. Over 1000 EIKs have been manufactured to date. An electronic power conditioner (EPC) needs to be tailored to each tube. Although CPI does not build EPCs, Boeing Electron Dynamic Devices (BEDD) in Torrance, CA builds space-qualified EPCs, as do two sources in Germany. CPI has delivered two flight models of a conduction-cooled tube at 94 GHz (the first launch of the NASA CloudSat Mission is scheduled for late 2004), and a third unit is under construction. Other conduction-cooled models have been built at 30 GHz (Ka band) for antenna-mounted terrestrial operations.

The nominal power output of a tube for JIMO would be 1000 W with a bandwidth of 250 MHz at a constant temperature, although the tube can operate over the temperature range from -40°C to $+50^{\circ}\text{C}$ without damage. The power bandwidth product is a constant, however, and a temperature change detunes the tube. A

variation of as little as 10°C, however, would require that the bandwidth be increased to 267 MHz; this would lower the power output to 937 W.

Table 15.5.1-1: Achievable Data Return for RF Communication System at Ka-band

Number of Klystrons	Tx Power (W)	Tx Antenna (m)	Total Telemetry Data Rate (Mbps)
1 klystron	250	3	1.00
1 klystron	500	3	2.50
1 klystron	1000	3	5.00
1 klystron	250	5	4.00
1 klystron	500	5	8.00
1 klystron	1000	5	16.00
1 synchronously tuned	2500	5	43.75
2 synchronously tuned	2500 ea	5	87.50
4 synchronously tuned	2500 ea	5	175.00
2 staggered tuned	2500 ea	5	87.50
4 staggered tuned	2500 ea	5	175.00

Prime power input to a 1 kW tube and its EPC is expected to lie between 3.2 and 4.4 kW. The lower power corresponds to a 4-stage depressed collector (typical of Ku-band tubes), but space limitations at 35 GHz and permanent magnet material limitations may limit the design to a 3-stage collector and thus higher input power.

Although EIK lifetimes can be as much as 10 years, a longer life (12 years or more) can be achieved with a larger oxide reservoir behind the porous tungsten surface (matrix cathode) or with a lower cathode temperature and increased beam convergence since failures are due to cathode depletion. A combination of the two approaches may prove optimum. It is necessary to build a few experimental tubes to optimize both the electrical and mechanical design and

then to build several prototype models for EPC development and space qualification testing of the integrated tube and EPC. Vibration testing and thermal testing both in the atmosphere and then in vacuum will be necessary.

Ancillary electronic components of the transmitter that were not costed are the modulator, square root raised cosine baseband filter, preamplifier, upconverter, driver amplifier, predistortion linearizer and low-power RF filter, commandable attenuator, high-power isolator, high-power RF filter, multiplexer combining network, or multiple, overlapping antenna feed horns for space combining the signals.

An additional risk factor for this method is the pointing accuracy required by the antennas. The half-power beamwidth of a 5 m antenna is 0.12 degrees, producing an antenna pointing accuracy requirement of 0.012 degrees. Also, the half-power beamwidth of a 3 m antenna is 0.22 degrees, producing an antenna pointing accuracy requirement of 0.022 degrees. In order to achieve the data rates tabulated in Table 15.5-1, it is assumed that the pointing accuracies stated here are achieved which might require closed loop pointing control.

15.5.2 Method 2: Laser Communication Option for JIMO

The option of a free-space laser communications link from JIMO to an Earth-orbiting relay satellite is a second alternative for ultra high data rate communications from Jupiter. Using an optical receiver on an Earth-orbiting relay satellite avoids the severe atmospheric losses that may be experienced in direct optical transmission to a ground-based receiver. High data transmission rates can be achieved by using Wavelength Division Multiplexing (WDM) with multiple optical carriers each at different wavelengths. A single transmitting telescope on JIMO can support the transmission of an optical beam that optically combines or multiplexes the data-modulated outputs from a multiple number of laser transmitters, each operating at different wavelengths.

Transmitting telescope optical aperture diameters comparable to that proposed for military geosynchronous intersatellite laser communications are considered here. In particular, transmit optical aperture diameters ranging from 30 cm to 90 cm are evaluated. A single receiving telescope on the Earth-orbiting relay satellite is required with an optical aperture size that must be large enough to collect a sufficient amount of propagated light from the arriving optical light beam for carrying out reliable data demodulation and decoding. Receive optical apertures of 2.4 m and 3.6 m comparable to the Hubble space telescope size are considered here.

The large geometric space loss for communicating with deep space optical missions such as JIMO requires power-efficient communication techniques. Pulse Position Modulation (PPM) coupled with a direct optical detection receiver is proposed to provide a highly power-efficient high data transmission rate

system with reasonable implementation complexity. Specifically, a 256-slot PPM modulation scheme with RZ pulse shaping is considered, where each symbol carries 8 bits, requiring a three-fold bandwidth expansion relative to the conventional binary on-off keying modulation normally employed in terrestrial fiber networks. By using the best available EDFA optically pre-amplified direct detection receivers to demodulate the transmitted PPM pulse slot position results in a receiver sensitivity of approximately 3 photons per bit at 10^{-6} BER. A hard decision (255, 128) Reed Solomon provides an additional 8 dB coding gain to enhance power efficiency. A high-power laser source at each wavelength can be implemented using a conventional laser diode followed by an EDFA power amplifier to produce 5 watts of launch power. Link closure at a 1.55 micron wavelength is then achieved for a 2.4 m receive aperture at data rates ranging from 2.5 Mbps for a 30 cm transmit aperture to 25 Mbps for a 90 cm transmit aperture. Increasing the receive aperture to 3.6 m increases the corresponding data transmission rates to 6 Mbps and 55 Mbps, respectively. These data rates will scale directly with the number of wavelengths employed. Summaries of the achievable data returns for a laser communication system are given in Table 15.5.2-1.

Table 15.5.2-1: Achievable Data Returns for Laser Communication System

Laser w/ 5W Tx Power w/ Rx Orbiting Telescope	Tx Aperture (m)	Rx Aperture (m)	Total Telemetry Data Rate (Mbps)
1 Laser w/ Amplifier	0.3	2.4	2.50
1 Laser w/ Amplifier	0.4	2.4	5.00
1 Laser w/ Amplifier	0.6	2.4	10.00
1 Laser w/ Amplifier	0.9	2.4	25.00
2 Lasers w/ Amplifiers	0.6	2.4	20.00
2 Lasers w/ Amplifiers	0.9	2.4	50.00
1 Laser w/ Amplifier	0.3	3.6	6.00
1 Laser w/ Amplifier	0.4	3.6	11.00
1 Laser w/ Amplifier	0.6	3.6	25.00
1 Laser w/ Amplifier	0.9	3.6	55.00
2 Lasers w/ Amplifiers	0.6	3.6	50.00
2 Lasers w/ Amplifiers	0.9	3.6	110.00
4 Lasers w/ Amplifiers	0.6	3.6	100.00
4 Lasers w/ Amplifiers	0.9	3.6	220.00

Radiation damage and performance degradation effects must be evaluated for 3 GHz electronic and photonic components at 100 Mbps data rates per wavelength. The generic component classes include photonic and electronic components. The photonic components include InGaAsP laser diodes, InGaAs avalanche photodiodes (APD), erbium-doped single-mode optical fibers, single-mode optical fibers including polarization preserving fiber, thin film optical filter band silicon waveguide grating based wavelength multiplexers and demultiplexers. The electronic components include GaAs/SiGe/CMOS analog ICs for laser diode drivers and photodiode transimpedance amplifiers (TIA) and

limiting amplifiers, Si/Ge/CMOS mixed signal ICs for clock and data recovery (CDR), and Si/Ge/CMOS digital ICs for serializer/deserializers, data framers, and forward error correction (FEC) coding.

Published radiation damage test results currently available from GSFC/NASA Radiation Effects Research Center indicate negligible performance degradation up to 100 krad exposure for Corning SMF-28 single-mode fiber (commonly deployed in terrestrial optical fiber networks) and polarization preserving fiber up to 100 m length, and 0.25 and 0.18 micron CMOS 500 MHz – 1 GHz microprocessors. Components exhibiting negligible performance degradation up to 30 krad exposure include 1 Gbps GbEthernet optical transmitters and receivers based on 850 nm VCSEL arrays and GaAs pin arrays.

Based on these results, it appears that radiation shielding of the electronic and photonic components to reduce the exposure level to between 30 and 100 krads is recommended. Outstanding issues on radiation damage and related performance degradation that need to be addressed include, radiation effects for erbium-doped fiber critical for high-power laser sources, radiation effects for thin film optical filter and waveguide grating technology critical for WDM multiplexers and demultiplexers.

Published work suggests that radiation effects on electronics components will be greater than that on photonic components. Soft single-event upset (SEU) errors may be mitigated through error correction and compensation in system design. Published results show that hard functional errors appear to occur at TID levels exceeding about 500 krad even for 10 MHz electronic and photonic components.

The primary technology risk factors identified for this laser communication system for JIMO include reliability of high-power EDFA optical amplified laser systems, radiation effects on EDFA optical amplifier and WDM multiplexers and demultiplexers, and high pointing accuracy for acquisition and tracking subsystem.

15.5.3 Method 3: RF Communication Using a Relay Satellite

The proposed third method for relaying instrumentation data from JIMO back to Earth is to use an RF relay satellite in high orbit around Jupiter or possibly in a Heliocentric Jupiter trailing or leading orbit. Since JIMO is may be required to telemeter all its data in real time, a relay satellite can be used to buffer the huge amount of data and telemeter it back to Earth over a long period of time with the option of re-sending data as needed. The data transfer from the relay satellite to Earth could be accomplished through the approaches described in Methods 1 and 2, at potentially lower data rates, if massive buffering was used. For this analysis, a relay satellite approximately a million km away from JIMO was considered. The proposed communication frequency used was 35 GHz, and both 3 m and 5 m antennas were analyzed. In addition, the klystrons detailed in Method 1 above were considered with transmit powers up to 2500 W.

The achievable data rates from JIMO to the relay satellite are provided in Table 15.5-3. The transmit antenna on JIMO is sized to be 3 m and the relay satellite is analyzed with a 3 m and a 5 m antenna.

Table 15.5.3-1: Achievable Data Return from JIMO to Relay Satellite

Tx Power (W)	Tx Antenna (m)	Rx Antenna (m)	Total Telemetry Data Rate (Mbps)
250	3	3	150.00
500	3	3	300.00
1000	3	3	600.00
2500	3	3	1500.00
250	3	5	415.00
500	3	5	830.00
1000	3	5	1660.00
2500	3	5	4000.00

15.6 Instrument Thermal Management

Thermal management resources include heat pipes, radiator area and active cooling systems to maintain instrument thermal balance. The radar and laser instruments do not require active cooling and can be managed thermally using heat pipes and radiators. In the proposed instrument architecture, the thermal management is accomplished by a single parasitic radiator that is sized to accommodate the subset of those that are instrument selected. The required thermal resources are calculated for the individual instruments so that the contribution of the resource needs from each instrument can be clearly seen. The total area does not take into account efficiencies that may be gained by integrating instrument electronics, heat pipe pathways or other approaches that might be expected in the actual system. For the instruments that required active cooling, cryocoolers and cryoradiators need to be integrated into the instrument. These discussions are presented in the respective instrument sections (Section 7 and Section 8) but are repeated here, for completeness.

15.6.1 Visible and IR Imaging Spectrometer Thermal Management

The imaging spectrometer individual unit dissipates roughly 100 mW at the focal plane array (FPA). The temperature requirement at the FPA is 105 K. Because of the relatively high temperature of the device and the relatively low expected cooling requirements, a standard cryoradiator has been selected for the cooling objectives.

The cryoradiator will remove heat directly from the housing of the spectrometer, and will most likely be interfaced to the housing with a single conventional heat pipe. Due to the sensitivity of the cryoradiator to environmental heat loads, a carefully designed solar/planet shield will need to be fitted to the cryoradiator to ensure its cold-temperature operation.

Assuming no environmental loading (perfect shielding), the cryoradiator area was calculated to be 0.080 m². The corresponding radiator mass (including heat pipe and shielding) is between 1 and 2 kg. The parasitic heat loads are expected to be low, on the order of approximately 200 mW, based on a relatively simple radiation calculation using the dimensions of the spectrometer housing. The parasitic loads are expected to be minimal because the environmental temperature will likely be very close to the instrument target temperature of 105 K. Because the spectrometer housing has a fairly large footprint on the optical bench, however, conduction heat transfer from the bench could be significant in the presence of an appreciable bench-to-housing or bench-to-optics temperature gradient. High thermal resistance filler materials may be used to minimize bench-to-instrument heat transfer, and hence keep radiator size and weight to a minimum.

A uniform coating of high emissivity material or paint on the inside of the spectrometer housing enclosure should be used to help distribute interior heat effectively, achieving thermal uniformity for the optical components. A high thermal conductivity housing material will also help to create a thermally uniform environment within the enclosure. The outer surface of the housing will probably be shielded with multi-layer insulation to prevent environmental heat gains/losses by radiation.

An alternative possibility to the cryoradiator solution is to incorporate a pulse tube cryocooler. The main disadvantage is that at temperatures in the range of 100 K, most pulse tube models are optimally designed to remove on the order of several Watts of heat—an order of magnitude greater than the heat removal required for the spectrometer. Since the actual FPA dissipation is small and parasitic heat loads are anticipated to be low as well, the cryocooler will be operating in a regime of very low efficiency.

From heritage data, at a cold tip temperature of 100 K, for 300 mW of total cooling (the sum of the cooling requirement for the instrument plus assumed parasitic losses), the total specific power was extrapolated to be between 35 and 45 W/W and the total specific mass was estimated to be between 12 and 15 kg/W. These estimates yielded a total mass (thermo-mechanical unit plus control electronics) of 3-5 kg and a total input power (to both the thermo-mechanical unit and control electronics) of 11-14 W.

The imaging spectrometer system also includes a digital signal processor (DSP) and analog signal processor (ASP). The DSP dissipates 5.5 W of heat, and the ASP dissipates 800 mW of heat. The operating temperature range of both processors is between 230K and approximately 300 K. A simple spreadsheet thermal analysis was used to determine whether insulation/heaters are required for the processor units. A mean environmental temperature of 100 K was assumed, and the temperature drop from the processor units to the optical bench below was assumed to be 15 K. Somewhat conservative values were assumed for surface emissivities, contact thermal resistances, and insulation thermal conductivity.

It was concluded that the DSP should be able to operate within its desired temperature range without any insulation, achieving a steady-state temperature of near 300 K assuming a steady 5.5 W dissipation. The ASP, however, will need to be insulated heavily (several inches of blanketing required) to ensure that it remains at its minimum specified temperature of 230 K. Positioning the ASP unit close to the DSP should also aid in keeping the ASP warm.

A summary of the derived thermal resources is presented in Table 15.6-1.

Table 15.6-1: Vis/IR Imaging Spectrometer Thermal Resource Requirements

Vis/IR Imaging Spectrometer	Temperature Requirement (K)	Cooling Required (mW)	Power Required (W)	Number of Heat Pipes	Radiator Area (m ²)	Total Mass (kg)
Option 1 Environmentally Shielded Radiator	105	100 per Instrument	N/A	1	0.1	1 to 2
Option 2 Pulse Tube Cryocooler	105	100 per Instrument	11 to 14	N/A	N/A	3 to 5

15.6.2 Thermal Mapper Thermal Management

The heat dissipation from each of the thermal mapper's focal plane arrays (FPAs) is 2.34 mW. The total dissipation from the three FPAs is 7.02 mW. The temperature requirement of the FPA is 60 K. Because of the very low power dissipation and small physical dimensions involved, it was concluded that the most efficient thermal management technique would be to cool the entire housing enclosing the optical components, which are in turn secured to an optical bench.

A single mini pulse tube cryocooler has been selected for the cooling objectives. The cryocooler will remove heat directly from the housing. The size and performance specifications for the cryocooler have been determined based on an evaluation of heritage instruments.

It is assumed that the optical components (mirrors and FPAs) will be fixed to the optical bench, which will be maintained at a (yet unknown) temperature, but most probably on the order of 100 K. The cryocooler will remove the 7 mW generated at the FPAs, in addition to heat loads from the optical bench to the components and housing. The housing temperature must be maintained below 60 K to ensure a 60 K mean temperature on the optical components, due to parasitic heat contributions. Depending on the temperature of the optical bench and the interface design between the optical components and the bench, conduction heat transfer could contribute significantly to the overall heat load to the optical instruments. It is reasonable to conclude that the parasitic heat load will be on the order of a few hundred milliwatts, significantly larger than the aggregate heat dissipation at the FPAs.

The housing itself will be shielded from the environment using multi-layer insulation, with very low IR absorptivity/emissivity to prevent radiation heating from surrounding surfaces. On the inside of the enclosure, a uniform coating of high emissivity material or paint will help distribute the heat effectively, achieving thermal uniformity for the optical components. The use of high conductivity material for the housing will also assist in efficient heat distribution. The cryocooler cold tip will be in physical contact with one side of the housing; it is recommended that the FPAs be positioned near this interface wall.

Regarding pulse tube cryocooler heritage, one specific and reasonable point of reference is the TRW Advanced Mini Pulse Tube cryocooler, Model PTC-001A-065-I. This unit was delivered in 1995, and has no reported flight history. However, it is capable of removing roughly 200 mW of heat while maintaining a cold tip temperature of 60 K (with heat rejection at 300 K). The total power input at this condition is 49 W. The thermo-mechanical unit weight is 2.25 kg, and the electronics weight is approximately 6 kg (8.25 kg total). It is expected that technology developments since this design should drive down both the power input and the weight for state-of-the-art models, which may be at TRL 7 levels by the JIMO technology freeze date of 2007.

A large quantity of heritage data shows that the total specific mass (total mass of thermo-mechanical unit and cooling electronics divided by cooling capacity) becomes increasingly large as the cooling requirement diminishes. For cooling requirements of approximately 400 mW, this ratio can be inferred by existing heritage data to be on the order of 20-30 kg/W. If the cooling requirement in the present case is conservatively assumed to be 400 mW—or 60 times the nominal power dissipation at the three FPAs—a total mass of 8-12 kg is anticipated. If in reality the parasitic heat loads are much smaller, and the cooling requirement is

on the order of only 100 mW (14 times the nominal dissipation), then the total specific mass is expected to be appreciably larger—probably on the order of 40-50 kg/W (limited heritage data exist at such low cooling conditions). In that case, the total expected mass is approximately 4-5 kg.

Similar heritage data is also available for the total specific power (total input power required, to both the thermo-mechanical unit and the cooling electronics, divided by cooling capacity). For cooling on the order of 400 mW, this ratio is approximately 80-110 W/W. For a cooling requirement of 400 mW, a total input power of 32-44 W is expected. As with the total specific mass, the total specific power estimates increase with diminished cooling requirements. For a cooling load of only 100 mW, for example, the total specific power may be extrapolated from existing data to be as high as on the order of 150 W/W, yielding input powers of approximately 100 W.

The results illustrate that designing for smaller cooling capacity (a result of smaller parasitic heat load estimates) imposes greater demands on mass and power. A practical option is to expend less effort into reducing the parasitic gain from the housing and optical components and employ a larger capacity cryocooler with vastly superior efficiency, operating closer to the unit's optimized design point.

A small conventional radiator, operating at approximately 290 K, will remove the waste heat generated by the pulse tube cryocooler. For a mean input power of 38 W, the area of this radiator is calculated to be roughly 0.12 m². The radiator is expected to weigh on the order of 0.70 kg.

The thermal mapper system also includes a digital signal processor (DSP) and analog signal processor (ASP). The DSP dissipates 5.5 W of heat, and the ASP dissipates 35 mW of heat. The operating temperature range of both processors is between 230 K and approximately 300 K. A simple spreadsheet thermal analysis was used to determine whether insulation/heaters are required for the processor units. A mean environmental temperature of 100 K was assumed, and the temperature drop from the processor units to the optical bench below was assumed to be 15 K. Somewhat conservative values were assumed for surface emissivities, contact thermal resistances, and insulation thermal conductivity.

It was concluded that the DSP should be able to operate within its desired temperature range without any insulation, achieving a steady-state temperature of near 300 K assuming a steady 5.5 W dissipation. The ASP, however, will need to both be insulated heavily (several inches of blanketing required) and heated with a surface heater dissipating on the order of 1 W to ensure that it remains at its minimum specified temperature of 230 K. One or more Kapton surface heaters on the ASP surface, under the insulation, should suffice. Positioning the ASP unit close to the DSP should also aid in keeping the ASP warm.

A summary of the derived thermal resources is presented in Table 15.6-2.

Table 15.6-2: Thermal Mapper Thermal Resource Requirements

Thermal Mapper	Temperature Requirement (K)	Cooling Required (mW)	Power Required (W)	Number of Heat Pipes	Radiator Area (m ²)	Total Mass (kg)
Pulse tube cryocooler cooling enclosure housing FPAs	60	2.4 per Instrument	32 to 45	N/A	N/A	8 to 14

15.6.3 Radiator and Heat Pipe Thermal Management

The radiator and heat pipe combination treatment was selected for instruments with relatively high power dissipation. This thermal management combination has been selected for the following instruments:

Subsurface radar sounder

Radio sounder

Interferometric SAR

Polarimetric SAR

Laser altimeter

Laser spectrometer

The radiator area was calculated by performing an energy balance using the heat flux from the Sun, the reflected solar load from the moon, the infrared contribution of the moon itself, and the electronics waste heat. The radiator temperature was selected at 275 K in all cases.. The solar, albedo, and moon IR heat flux calculations are discussed in the Environmental Heat Loads section.

The radiator surface was assumed to be coated with white S13-GLO paint, with an emissivity of 0.88. The absorptivity was conservatively assumed to be 0.60. Typical beginning of life absorptivity for S13-GLO white paint is on the order of only 0.20. However, given the strong charged-particle environment of Jupiter's moons and its acknowledged impact on S13-GLO paint, the possibility of relatively fast surface deterioration is strong.

The heat dissipation for each instrument was assumed to occur at its respective electronics box. This heat was to be transported from the electronics box to a radiator using conventional linear heat pipes, spaced apart from each other at regular intervals of 8 inches. Without any details of the instrument layout or information about potential interference from other objects on the spacecraft, the average heat pipe length was assumed to be 3 m. The overall normalized weight

of the heat pipes was assumed to be 0.11 kg per linear meter [Ref 15.1-1]. This may be slightly conservative, particularly in light of weight-reducing materials that may be ready for launch by 2007.

The working fluid for the heat pipes will be ammonia, with a boiling temperature at atmospheric pressure of roughly 240 K. For boiling to occur at 275 K, the heat pipe must be pressurized slightly (to an absolute pressure of roughly 67 psi [Ref 15.1-2]).

The radiator itself was assumed to weigh between 6 kg/m² and 12 kg/m², with the higher value being the conventionally accepted figure for a heavy deployable radiator and its support structure [Ref 15.1-3]. These estimates are somewhat conservative. For the lower power dissipation instruments, the radiator may be comprised of part of the spacecraft support structure (such as a panel), in which case no additional weight penalty would be incurred. Furthermore, the analysis assumes that every instrument is thermally connected to its own individual radiator; in reality, multiple instruments may be tied to a single radiator. Note that the weights cited in this report use the 6 kg/m² figure; a fully deployable radiator may double these estimates.

A summary of the derived thermal resources is presented in Tables 15.6-3 and 15.6-4 for the 100 km and 400 km nominal science orbit options. Note that the baseline laser spectrometer uses active cooling for the laser, similar to the thermal mapper. However, operating temperatures have not been determined for this device and insufficient detail exists at this time to provide further thermal design detail for the active cooler. For the purposes of comparison, the laser spectrometer using passive thermal control is presented in Tables 15.6-3 and 15.6-4

Table 15.6-3: High Power Instrument Thermal Resource Requirements at 100 km Science Orbit

	Assumed Ave Power Dissipation (W)	Efficiency	Number of Heat Pipes	Radiator Area (m ²)	Radiator Mass (kg)	Total Mass (kg)
Laser Altimeter, 100 km	1350	5%	12	5	27	31
Laser Spectrometer, 100 km	690	2%	6	2.5	14	16
Interferometric SAR, 100 km	340	80%	3	1.2	7	8
Polarimetric SAR, 100 km	40	80%	1	0.2	0.8	1
Subsurface Radar Sounder, 100 km	550	80%	5	2	11	12
Radio Plasma Sounder, 100 km	18	80%	1	0.1	0.4	1
Total at 100 km	2988		28	11	60	69

Table 15.6.3-4: High Power Instrument Thermal Resource Requirements at 400 km Science Orbit

	Assumed Ave Power Dissipation (W)	Efficiency	Number of Heat Pipes	Radiator Area (m ²)	Radiator Mass (kg)	Total Mass (kg)
Laser Altimeter, 400 km	7790	5%	69	29	155	178
Laser Spectrometer, 400 km	931	2%	34	14	80	92
Interferometric SAR, 400 km	1326	80%	17	7	40	46
Polarimetric SAR, 400 km	50	80%	6	1	5	6
Subsurface Radar Sounder, 400 km	1372	80%	29	11	63	69
Radio Plasma Sounder, 400 km	18	80%	1	0.1	0.4	1
Total at 400 km	11487		156	63	344	391

References

[Ref 15.1-1] Spacecraft Thermal Control Handbook, Volume 1: Fundamental Technologies, 2nd Edition, The Aerospace Press, El Segundo, CA, 2002.

[Ref 15.1-2] Reynolds, W.C., "Thermodynamic Properties in SI: Graphs, Tables, and Computational Equations for 40 Substances," Department of Mechanical Engineering, Stanford University, 1979.

[Ref 15.1-3] Donabedian, M., Curran, D.G.T., Glaister, D.S., Davis, T., and Tomlinson, B.J., "An Overview of the Performance and Maturity of Long Life Cryocoolers for Space Applications", 30 April 2000, Aerospace Report No. TOR-98(1057)-3, Revision A.

16.0 Instrument Test

The actual JIMO High Capability Instrument baseline suite considered here, consist of low power passive electro optical devices with active and passive cooling, passively cooled high powered laser devices and passively cooled high powered RF devices. Instrument EMC/EMI compatibility for the operation of any single instrument as well as the operation of multiple instruments simultaneously requires careful planning. This becomes increasingly important because of the intensity of the natural EM environment and the local EM environment induced by high power RF from the radar and telecom subsystem, as well as the electric propulsion subsystem. Success in development and implementation of such a test program will likely the use of existing NASA and other U.S. government test facilities, as well as the use of commercial facilities. This section summarizes relevant issues related to facilities, test planning, design for test, and EMC/EMI issues to address as part of a comprehensive test approach.

16.1 Facilities

Currently, there is not one test facility capable of supporting all the necessary testing activities required for the JIMO program. There are several NASA and/or U.S. government test facilities that can accommodate portions of the testing activities. They include the Benefield Anechoic Facility located at Edwards AFB, Propulsion/TVAC chambers/test facilities located at NASA GRC, the EPL Vacuum Facility #5, NASA Plum Brook Station (SPF, B2), the Aerospace Propulsion/TVAC/EMI chamber, the Magnetics chambers/test facilities located at JPL, and the GSFC Magnetic Test Facility.

16.2 Notional Test Plan

A comprehensive test plan identifies required test cases and unique test requirements for an EMC development test flow, an EMC instrument test flow and an overall systems EMC test flow. The EMC development test flow should address spacecraft charging issues at the component level, and should include piece part testing, piece part passive inter-modulation testing of surface and RF front ends, antenna-to-antenna and structure RF isolation full scale testing, and complete EMI characterization of ion propulsion engine. Shielding tests at this level should include Faraday cages shielding effectiveness testing, wire/connector shielding effectiveness testing and magnetic piece part testing.

EMC instrument test flow should address testing the bonding and shielding effectiveness for every wire harness. Additionally, at the instrument level, MIL-STD-1541A tailored or NASA GSFC GEV tailored ESD testing, DC Magnetic degaussing/measurement and compensation and passive inter-modulation testing all need to be performed and results documented. Also, the susceptibility of thermal and radiometer instruments measured in a TVAC with calibrated cold

targets should be verified. A check of all EMI structural, unit, and EMI connector bonds and grounds during installation should also be accomplished during this test phase.

For success-oriented system EMC test flow, the MIL-STD-1540E should be utilized for testing and verifying critical circuit margins, power quality (ripple with persistence), power transients, conducted emission, magnetic moment measurement/compensation, radiated susceptibility and emissions, passive inter-modulation and RF compatibility (instrument performance in RF environment).

16.3 Design for Test

Testing requirements should be addressed during the design and development phases. Building in a degree of testability helps insure successful testing that meets schedules and minimizes cost. Some examples of a proactive approach to identifying testing requirements include antennas that are deployable in 1 G. Since Faraday cages often require opening after EMC testing, install sense wires that can be excited externally to perform a high bay check for workmanship. This could also be addressed with an EMI cancellation receiver.

Identify instruments required to work at extremely cold temperatures. Since EMI testing is typically done at room temperature with a corresponding loss of sensitivity, add test ports to measure sensor noise to allow some of the sensitivity to be recovered.

Ion plume causes interference to RF instruments below 500 MHz, and possibly to all RF instruments and communication receivers above 500 MHz. It may also cause ESD on solar arrays and external surfaces including instrument optical surfaces. With the projected size and power of the IPS, testing to determine these possible effects requires EMI characterization measurements at the engine level in a combined TVAC/EMI chamber. This includes time domain measurement of electric and magnetic fields, coupon testing of surface materials for ESD and ion to plume isolation testing.

16.4 Potential EMC/EMI Test Issues

The following information points out some potential EMC/EMI issues and/or considerations that should be addressed during the I&T phase.

16.4.1 Systems Issues

The Jovian higher radiation environment implies a higher surface and bulk-charging environment. At these greater fluence levels this impacts the MLI design to use conductively loaded insulating material to prevent severe erosion. It also affects the amount of shielding required for bulk charging. Additionally, the reactor temperature may severely impact the wiring if the temperature on the

wiring is not kept below 100 to 135 C. Existing wiring suffers increased resistance over time as well as reduced flexibility along with silver whisker growth at high temperatures. The data rate based on past experience will also grow from 10 Mb/s to the 100 to 1000 Mb/s range.

16.4.2 Magnetometer Issues

The 10 nT magnetometer requirement requires a Class 1 magnetic cleanliness program similar to Cassini. The effects of the reactor propulsion plume on the magnetic moment needs to be evaluated.

16.4.3 Infrared Instrument Issues

The cryocooler will produce larger bus ripple that will be difficult to isolate from the instrument amplifiers. The cryocooler is also hard to shield because of heat leaks to prevent interference with the RF instruments. The first optics will have to be conductively doped to prevent radiated emissions from interfering with the RF instruments and the RF instruments from interfering with infrared instrument(s). The optical coating on the first optics will have to be conductively loaded to prevent ESD from eroding the coating and to prevent ESD from interfering with the RF instruments. Additionally, at the proposed temperatures it will not be possible to verify dynamic range without doing a combined thermal chamber and EMI radiated susceptibility test with cold calibrated targets.

16.4.4 RF Instrument Issues

Radiated emissions requirements of the RF instruments need be determined to estimate the feasibility of meeting the required RF sensitivity. RF fields on the RF instruments as well as other instruments are required to estimate the feasibility of meeting them, but could represent an order of magnitude increase over typical levels. Additionally, this will be required to size the limiters required in the RF receivers. The electrical propulsion system will interfere with RF instruments especially in the VLF and HF bands. This system will also cause spacecraft charging, potentially resulting in ESD and the possible need for large limiters in the receivers. The Io moon has a severe electrical environment that needs to be evaluated for the amount of interference and potential damage to the RF receivers. In the dense plasma predicted, in order to prevent surface currents from interfering with the receivers by direct current flow through the plasma, a true single point grounding system similar to CNOFS with all the secondary grounds floating may be required. The HF transmitter is in the nearfield for the instruments. This will require a modified radiated susceptibility test as the RS103 underestimates the coupled energy. A modified CS114 test will be required instead to directly inject the RF into the instrument wiring shields. The vehicle resonates at the receiver frequencies, making this effect worse. The reactor plume may charge the vehicle creating very large ESD.

Appendix A. Tables and Figures

Table of Figures

Figure 4.0-1:	Study approach	9
Figure 5.0-1:	Pre decisional JIMO spacecraft concept [Ref 5.1].....	12
Figure 7.0-1:	Visible and IR imaging spectrometer.....	31
Figure 7.2-1:	Visible and infrared imaging spectrometer trade space	32
Figure 7.3-1:	Infrared imaging spectrometer	34
Figure 7.3.2-1:	Imaging spectrometer view of optical configuration in dispersive plane with visible channel.	37
Figure 7.3.2-2	Raytrace (YZ profile) of shared front-end optics with only IR backend, and only one wavelength visible.	37
Figure 7.3.2-3:	Raytrace (XZ profile) of shared front-end optics with only IR backend and only one wavelength.	38
Figure 7.3.4-1:	Baseline spectrometer with structural components.	40
Figure 7.3.7-1:	Spectrometer external dimensions - top view.	45
Figure 7.3.7-2:	Spectrometer external dimensions – side view.	45
Figure 7.4-1:	Sensor trades for sensors tailored to gsds and altitudes.....	49
Figure 7.4-2:	GSD vs. altitude for “spiral in”.	51
Figure 7.4-3:	SNR scale factor vs. altitude for “spiral in”.	51
Figure 7.7-1:	MRO/CRISM instrument.	55
Figure 7.7-2 :	Cassini/VIMS instrument.....	55
Figure 8.0-1:	Thermal mapper.....	57
Figure 8.2-1:	Thermal mapper trade space.	58
Figure 8.3-1:	Thermal mapper instrument design.....	60
Figure 8.3.2-2:	Thermal mapper optical YZ profile.	65
Figure 8.3.2-3:	Thermal mapper optical XZ profile.	66
Figure 8.3.4-1:	Thermal mapper optical bench and stand-offs.....	68
Figure 8.3.4-2:	Possible aperture mechanism configuration.	69
Figure 8.3.3-3:	Cryo cooler volume comparison to thermal mapper.....	71
Figure 8.3.5-1:	Thermal mapper radiation shielding.....	72
Figure 8.7-1:	Mars Odyssey THEMIS instrument.....	82
Figure 8.7-2:	Mars Global Surveyor TES instrument.....	82
Figure 9.2-1:	Laser altimeter trade space.....	84
Figure 9.3-1:	Planet coverage method: orbit track is wider than a single altimeter or spectrometer pixel by scanning.	85
Figure 9.4-1:	Three mirror unobscured anastigmat with a 15-degree field-of-view, FOV limits are indicated by different colored rays.	86
Figure 9.4-2:	On axis telescope system with a 5-degree linear field-of-view.	87
Figure 9.4-3:	Bistatic baseline schematic of laser altimeter.....	88
Figure 9.6-1:5.	Co ⁶⁰ γ -ray test results for Si and InGaAs APDs.	90
Figure 9.7-1:	15cm un-obscured anastigmat off-axis telescope with 15 degree linear FOV.	91

Figure 9.7-2:	Mechanical realization of the 25 cm on-axis telescope with 5 degree FOV. Blackened Mylar would cover the exterior tube skeleton to keep out stray light.....	92
Figure 9.10-1:	MGS/MOLA2.....	96
Figure 9.10-2:	ICESat/GLAS.....	97
Figure 10.2-1:	Laser absorption spectrometer trade space.....	99
Figure 10.3-1:	NASA ESTO diode stacking technology developed for solid-state laser pumping.	100
Figure 10.3-2:	Multicolor stack of ten diode bars; two bars each at wavelengths 2.5, 3.5, 4.5, 5.5, 6.5 and 10 microns.....	103
Figure 10.4-1:	25cm unobscured anastigmat spectrometer receiver telescope with 15 FOV.....	104
Figure 10.4-2:	50 cm telescope on-axis telescope for 5 deg FOV and 400 km data case.	102
Figure 10.4-3:	Spectrometer transmitter detail. Scanner is a rotating multi-facet mirror with N sides.	103
Figure 15.3.5-1:	JIMO radiation shielding thickness.....	169

Table of Tables

Table 3.0-1:	Top Level Instrument Requirements.....	5
Table 3.0-2:	Top Level Payload Accommodation Parameters.....	6
Table 6.0-1:	Baseline Instrument Summary – 100 km Altitude.....	21
Table 6.0-3:	Baseline Thermal Mapper Performance Summary.....	29
Table 6.0-4:	Baseline Laser Altimeter Performance Summary.....	29
Table 6.0-5:	Baseline Laser Reflection Spectrometer Performance Summary.....	29
Table 6.0-6:	Baseline Interferometric SAR Performance Summary.....	29
Table 6.0-7:	Baseline Polarimetric SAR Performance Summary.....	29
Table 6.0-8:	Baseline Radar Sounder Performance Summary.....	29
Table 6.0-9:	Baseline Radio Sounder Performance Summary.....	29
Table 7.3.3-1:	Data Rate Considerations.....	39
Table 7.3.3-2:	Processor Mass, Power and Volume.....	39
Table 7.3.7-1:	Spectrometer System Summary.....	44
Table 7.3.7-2:	Spectrometer Mass and Power Summary and Breakdown.....	46
Table 7.4-1:	Sensor Trades for Sensors Tailored to GSDs and Altitudes....	48
Table 7.4-2:	Design Sensitivity GSD=100 m, Altitude = 100, 400 km.....	50
Table 7.4-3:	Performance Sensitivity of 100 and 400 km Point Designs Operating at Higher Altitudes.....	50
Table 7.7-1:	JIMO Spectrometer Compared with Heritage Instruments.....	54
Table 8.3-1:	HgCdTe Channel Description and Performance.....	63
Table 8.3-2:	Microbolometer Channel Description and Performance.....	63
Table 8.3.3-1:	Data Rates.....	67
Table 8.3.3-2:	Processor Mass, Power and Volume.....	67
Table 8.3.6-1:	Thermal Mapper Instrument System Summary.....	73

Table 8.3.6-2:	Thermal Mapper Mass and Power Breakdown	74
Table 8.4.1-1:	Results of Thermal Mapper Trades at 100km Altitude and 125 Micron Pitch at Various GSD and Time Delay Integration Options.....	75
Table 8.4.1-2:	Thermal Mapper Excursions with Increased TDI for Uniform SNRs at or Above 100	76
Table 8.4.1-3:	Baseline Sensor Performance	77
Table 8.7-1:	JIMO Thermal Mapper Compared to Heritage Instruments	82
Table 9.7-1:	Motor Requirements.....	93
Table 9.7-2:	Summary of Contributing Masses and Powers for the Laser Altimeter.....	94
Table 9.10-1:	Proposed Laser Altimeter vs. Legacy Instruments	96
Table 10.3-1:	Sample Selections for Laser Lines for Five Species of MSSRL.....	101
Table 10.3-2:	Point Design Calculation of MSSRL for the Two Cases (100 km & 400 km).....	101
Table 10.9-1:	Proposed MSLS vs. Legacy Instruments	110
Table 11.2-1:	InSAR Antenna Sizing.....	115
Table 11.3-1:	InSAR Design Parameters	116
Table 11.3-2:	InSAR Pointing Requirements	117
Table 11.3-3:	InSAR Mass and Power Budget.....	118
Table 11.7-1:	InSAR Heritage	124
Table 12.2-1:	PSAR Antenna Sizing	128
Table 12.3-1:	PSAR Design Parameters.....	128
Table 12.3-2:	PSAR Pointing Requirements	129
Table 12.3-3:	PSAR Mass and Power Sizing.....	129
Table 12.7-1:	PSAR Heritage.....	134
Table 12.8-1:	SAR Data Rates.....	137
Table 13.2-1:	Radar Sounder Frequencies	140
Table 13.3-1:	Radar Sounder Beam Transmit Power	141
Table 13.3-2:	Radar Sounder Design Parameters	142
Table 13.3-4:	Radar Sounder Mass and Power Sizing	143
Table 13.7-1:	Radar Sounder Legacy	145
Table 14.3-1:	Radio Sounder Mass and Power Sizing.....	153
Table 14.7-1:	Early Radio Sounder Characteristics	154
Table 14.8-2:	Sounder Data Rates.....	155
Table 15.1.1-1:	Mass Breakdown of Scan Platform Components	159
Table 15.2-1:	3-Sigma Pointing Requirements for Instruments Designed for 100 km Altitude	163
Table 15.2-2:	3-Sigma Pointing Requirements for Instruments Designed for 400 km Altitude	164
Table 15.3.3-1:	Radiation Hardness of the Most Common Wire Insulation Materials	167
Table 15.3.5-1:	Radiation Shielding Mass Breakdown.....	170
Table 15.4-1:	Projected Data Rates for JIMO Suite of Instruments.....	171
Table 15.5-1:	Instrument Data Rates	176

Table 15.5-2:	Physical Properties of the Galilean Satellites	176
Table 15.5-3:	Communication Outages Due to Jupiter Blockage.....	177
Table 15.5-4:	Communication Outages Due to Jovian Moon Blockage	177
Table 15.5.1-1:	Achievable Data Return for RF Communication System at Ka-band	179
Table 15.5.2-1:	Achievable Data Returns for Laser Communication System	182
Table 15.5.3-1:	Achievable Data Return from JIMO to Relay Satellite	184
Table 15.6-1:	Vis/IR Imaging Spectrometer Thermal Resource Requirements.....	186
Table 15.6-2:	Thermal Mapper Thermal Resource Requirements	189
Table 15.6-3:	High Power Instrument Thermal Resource Requirements at 100 km Science Orbit.....	190
Table 15.1.3-4:	High Power Instrument Thermal Resource Requirements at 400 km Science Orbit.....	191

Appendix B. Coverage Analyses

Instrument Coverage

JIMO coverage requirements and the proposed mission design have a substantial impact on the top-level requirements for the science instruments. The science orbit duration at each Jovian moon is the primary design driver for the instrument fields of view (FOV). The longer one can stay at the body of interest, the more relaxed the FOV requirements may be. Due to the severe radiation environment at Europa, the anticipated science orbit duration (about 30-60 days) is relatively short for the purpose of a global mapping mission. A particular priority is the ability to observe potential changes due to tidal effects, which would require revisiting locations of interest. For the purposes of preliminary design estimates of the high capability instruments, most fields of view were chosen to permit 80-90% two-fold coverage within about 30 days and at least 97% two-fold coverage within 60 days.

Orbit altitude and inclination have a lesser effect on the required FOV when compared to science orbit duration. The orbit inclination has a more substantial influence on the accessible latitude bands. A polar orbit will guarantee that the higher latitude bands are covered. As one decreases the orbit inclination, less access will be provided to the higher latitudes. A scan platform may compensate for this to a moderate degree for the electro-optical instruments; however, there is a limit to the angle at which the EO instruments can look off nadir (about 30 degrees, depending on required signal to noise ratio). The radar instruments require a particular incidence angle and generally cannot be pointed far off their nominal orientations. Orbit inclination may also affect the way a region is covered, for instance if crossing orbits are desired when revisiting a particular location (such as for some radar concepts), an inclination lower than 90 degrees becomes necessary. Orbit altitude will influence instrument coverage in terms of ground track velocity. The ground track velocity will drive the required instrument scan rates, having the greatest effect on the design of the imaging spectrometer and the thermal mapper. Due to the physical properties of the Jovian moons, the highest ground track velocity for a fixed orbit altitude occurs at Ganymede. This served as a driving requirement for sensor integration time.

Orbit altitude will influence instrument coverage in terms of ground track velocity. The ground track velocity will drive the required instrument scan rates, having the greatest effect on the design of the imaging spectrometer and the thermal mapper. Due to the physical properties of the Jovian moons, shown in Table B-1, the highest ground track velocity for a fixed orbit altitude occurs at Ganymede. This served as a driving requirement for sensor integration time. Figure B-1 shows the ground scan rates for Europa, Ganymede, and Callisto at different orbital altitudes. These ground scan rates were calculated assuming the spacecraft is nadir pointing. Note that Ganymede is the most stressing case. Ground scan speed is an important parameter for consideration in the instrument

design. For one, the ground scan speed will help determine the data rates of the scanning instruments. The higher the ground speed, the larger the data rates from these instruments will be. In addition, various instruments (such as the imaging spectrometer) may be limited in the maximum scan rate at which they can observe in order to achieve acceptable signal to noise ratios (SNRs). If the scan rates necessary for the instruments cannot meet that of the spacecraft, back-scanning becomes necessary. This may complicate the instrument design (by requiring an additional scanning mirror), or may require the use of an individual scan platform mounted to the bus for the instrument of interest.

Table B -1: Physical Properties of the Galilean Satellites

Galilean Satellites	Physical Parameters			Orbital Parameters				
	Mean radius (km)	Mass (10^{21} kg)	Gravitational Constant (10^{12} m ³ /s ²)	Semi-major axis (10^3 km)	Inclination (deg)	Eccentricity	Orbital Period (days)	Rotation Period (days)
Callisto	2410.3	107.59	7.180998	1882.7	0.51	0.007	16.689018	16.7
Ganymede	2631.2	148.19	9.886997	1070.4	0.21	0.0015	7.154553	7.2
Europa	1560.8	48.00	3.201000	670.9	0.47	0.0101	3.551181	3.6
Io	1821.6	89.32	5.961000	421.6	0.04	0.004	1.769138	1.8

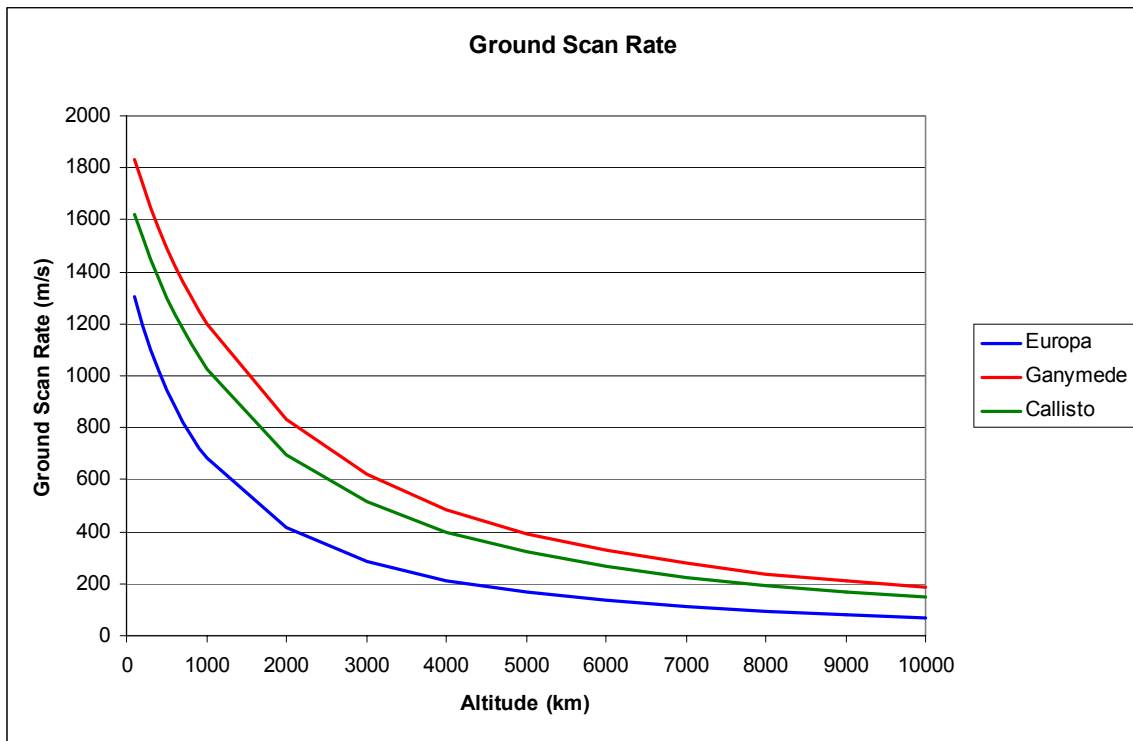


Figure B-1: Ground scan rate vs. orbit altitude at Europa, Ganymede, and Callisto.

In order to provide a rough initial estimate of the required fields of view, an analytical estimate of the required swath width was initially made. This analysis assumed the worst-case coverage occurs at the equator of Europa while in a polar orbit. The science instrument was assumed to be on continuously (100%

duty cycle) with no lighting constraints and nadir pointing. Results in Figure B-1 show the minimum required mapping time vs. instrument swath width. In order to provide two-fold coverage under these conditions, a minimum instrument swath width of about 30 km is required. At an altitude of 100 km, this corresponds roughly to a 15 deg FOV. All the high capability instruments should be capable of operating at any time during the orbit with the exception of the imaging spectrometer, which can only observe a ground point that is illuminated by the Sun. As a result, the nominal FOV required for this instrument was estimated to be 30 deg. It is important to note, however, that instrument operation may be affected by the need for orbit maintenance and the operation of the JIMO electric propulsion system. As shall be shown, in some cases, the high capability instrument duty cycles may be further reduced without loss of desired coverage by operating less frequently near the poles since the coverage there is several-fold.

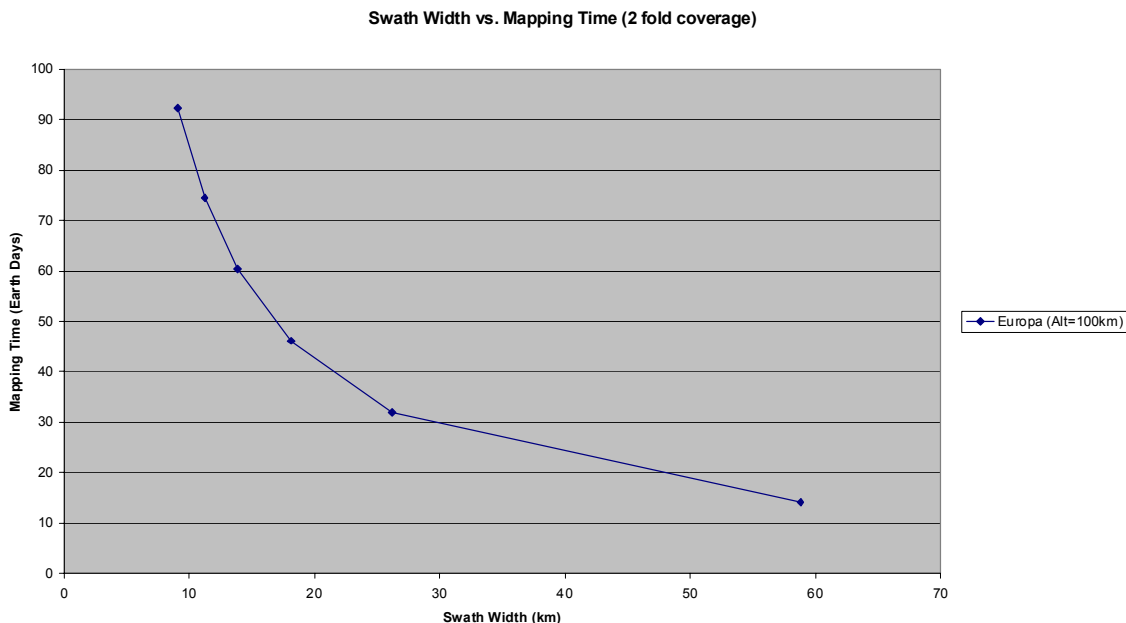


Figure B-2: Required minimum swath width vs. mapping time at Europa (two-fold coverage).

Results in Figure B-2 show how altitude and inclination affect the required FOV for the instruments to achieve a minimum of two-fold coverage at 100% duty cycle. As one decreases the orbit inclination from 90 degrees to 45 degrees, the FOV requirements become more relaxed; however, this change in inclination decreases the latitude coverage of the planet. Orbit altitude also affects the FOV. Increasing the orbit altitude reduces the required FOV. When changing the altitude, one must consider the effect upon the instrument design. As one increases the altitude, this typically increases the complexity, mass, and power required for the instruments. For example, preliminary numbers indicate that

increasing the orbit altitude from 100 km to 400 km will increase the power required for the laser altimeter by a factor of 20.

Results in Figure B-4 show how altitude and inclination affect the required field of view (FOV) for the instruments if the science duration at Europa is allowed to increase to 60 days, assuming a minimum of two-fold coverage. If, for instance, a FOV of 15 degrees is chosen and an altitude of 100 km or greater is chosen, the instrument duty cycle can be reduced below 100% by turning off at the polar regions. The system tradeoff between science orbit duration, instrument FOV, and instrument duty cycle presents a key program decision, which will significantly impact the design of the JIMO space vehicle. In particular, the science orbit duration will likely drive the amount of shielding desired for JIMO electronics and the instrument duty cycles will set requirements for the JIMO communications and data storage as well as overall system reliability. Instrument FOV will have a great impact on the size and complexity of each of the JIMO high capability instruments.

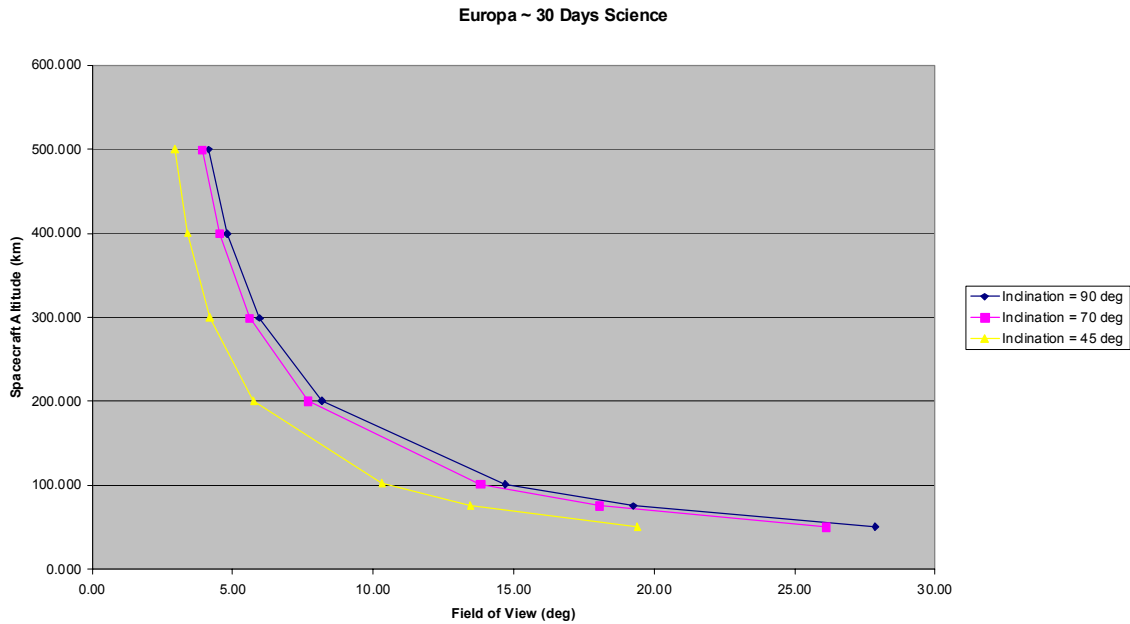


Figure B-3: Minimum instrument field of view for 30-day science mission (two-fold coverage).

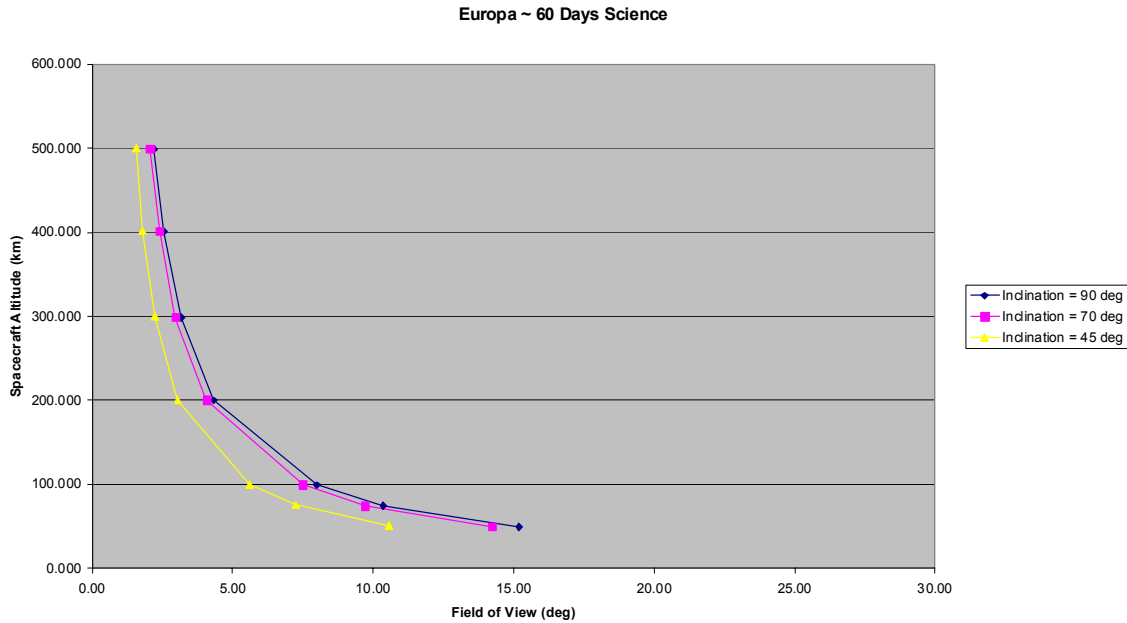


Figure B-4: Minimum instrument field of view for 60-day science mission (two-fold coverage).

In order to examine in more detail, issues of coverage, instrument duty cycling, and lighting constraints, analysis using Aerospace simulations, REVISIT and DCYCLE were utilized. The REVISIT simulation computes global coverage access times over a given time interval for a specified instrument footprint. This result essentially provides all the possible observation opportunities over the globe. The program DCYCLE is a post-processor to the REVISIT program which uses the access times computed by REVISIT to assign instrument viewing times based on the desired fold of coverage, the maximum available instrument duty cycle and lighting constraints, if present. This result provides the expected coverage performance, given the duty cycle plan. In both simulations, the body of interest is discretized as a latitude/longitude grid and access times are determined between the satellite in orbit and each ground point on the latitude/longitude grid. In the program DCYCLE, each orbit is broken into discrete time steps, which are given an observation score based on the number of ground points viewed. In turn, each ground point viewed is weighted inversely to the number of future observation opportunities over the science mission duration. If a ground point has already been observed to the desired fold of coverage, it receives a score of zero. If the ground point does not satisfy an imposed lighting constraint, it also receives a score of zero. Each time step is sorted in the order of the highest score for the orbit. Based on the maximum duty cycle specified, only the top scoring time steps are used for observation. This sets the duty cycle schedule for the instrument at each orbit. Once the duty cycle schedule is determined, the actual coverage is determined based on the ground points visible while the instrument is on. Output of the program yields two

contour plots including ground point accessibility results from REVISIT (100% duty cycle) and observed coverage (specified duty cycle) from DCYCLE.

For analysis of the JIMO mission, REVISIT and DCYCLE were applied for coverage scenarios at Europa, which are anticipated to be the worst-case for the JIMO mission. Of primary interest was the coverage for 15-, 30-, and 60-day science missions while in a circular polar orbit at 100 km altitude. The objective was to establish the available coverage for given sensor footprints at different maximum duty cycle levels, applying lighting constraints where necessary. Table B-2 provides coverage results from REVISIT/DCYCLE under selected duty cycle levels. The duty cycle levels were chosen based on the desire to provide 97% one-fold coverage within 30 days and 97% two-fold coverage within 60 days.

**Table B-2: Instrument Duty Cycling Coverage Summary
(Altitude = 100 km, Inclination = 90 deg)**

Instrument(s)	Footprint	Selected Duty Cycle (%)	Lighting Constraint?	Percent 1-fold/2-fold Coverage		
				15 day	30 day	60 day
Thermal Mapper, Laser Altimeter	15 deg FOV, Nadir Pointing	80%	No	75/28	97/75	100/97
IR Imaging Spectrometer	30 deg FOV Nadir Pointing	80%	Yes	91/51	98/85	100/98
Subsurface Radar Sounder, Radio Plasma Sounder	33.4 deg FOV, Nadir Pointing	50%	No	88/49	98/90	100/100
Interferometric SAR	2 x 30 km Swath	50%	No	86/60	98/87	99/99
Polarimetric SAR	1 x 60 km Swath	50%	No	90/56	98/89	99/98

The FOV of the thermal mapper and laser altimeter is 15 deg oriented in the nadir direction. Cumulative global coverage for these instruments was computed over a 60-day period using REVISIT/DCYCLE in order to establish a reasonable limit on duty cycling, which could still achieve the mission objective of two-fold global coverage. Figures B-5 and B-6 show the cumulative one-fold and two-fold global coverage respectively for duty cycle values ranging from 10-100%. At 100% duty cycle, the best that can be achieved is complete one-fold coverage in 30 days and complete two-fold coverage within about 40 days. In order to account for the need for spacecraft station-keeping as well as the competing interest of other instruments, an 80% duty cycle will still yield 97% one-fold coverage in 30 days and 97% two-fold coverage in 60 days. If the two-fold coverage requirement can be reduced to 90%, then the duty cycle can be reduced to 60%. Figures B-7 and B-8 show the global access and global coverage for 80% duty cycle respectively. One of the main effects of the DCYCLE algorithm in this case is to reduce the coverage at the poles as shown in the difference in higher latitudes for both plots. An important limitation of the DCYCLE algorithm that must be noted is that DCYCLE applies the same duty cycle limit throughout the mission. For the JIMO mission, it may be possible to improve coverage if the maximum duty cycle is varied over the course of the mission. For example, in this orbit, the most stressing regions occur at or near the equator. When the system needs to observe the polar regions, time can be taken away from the equatorial regions. In these instances, it might be more efficient to run the instrument at a higher duty cycle for a limited time in order to

achieve better coverage with the same amount of total instrument operating time. In particular, this may help eliminate some of the small red (uncovered) regions in Figure B-7.

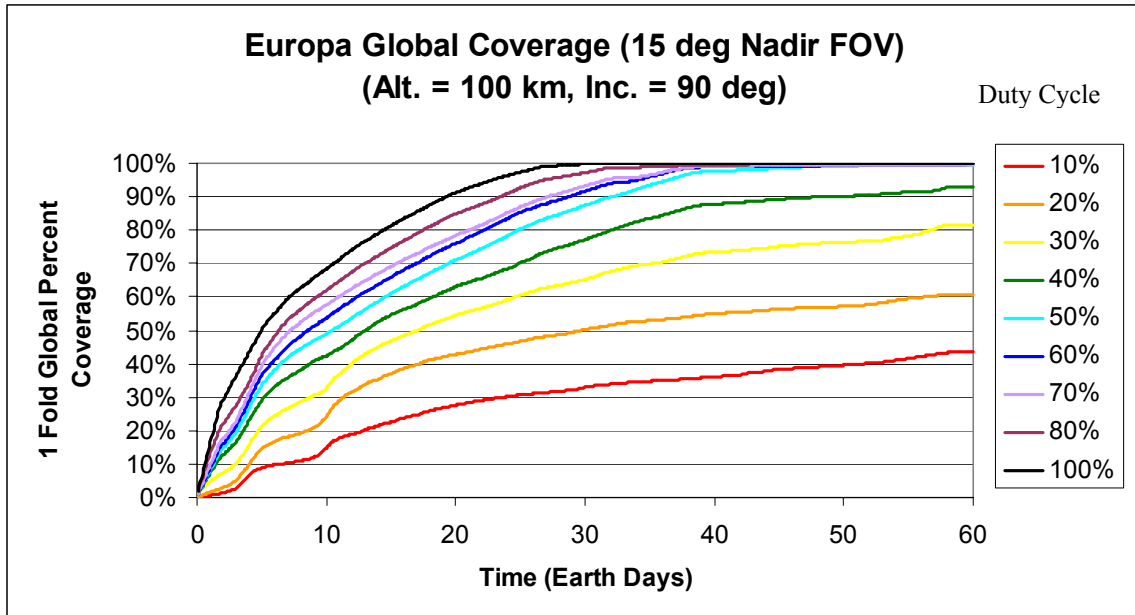


Figure B-5: One-fold cumulative global coverage at different duty cycle levels – thermal mapper and laser altimeter.

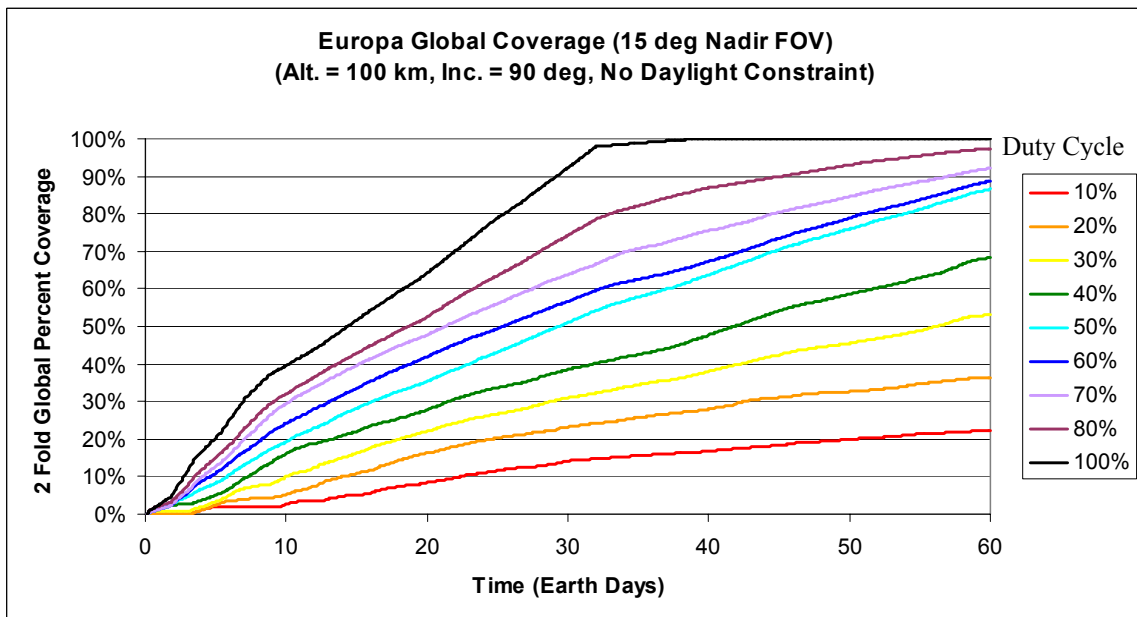


Figure B-6: Two-fold global coverage at different duty cycle levels – thermal mapper and laser altimeter.

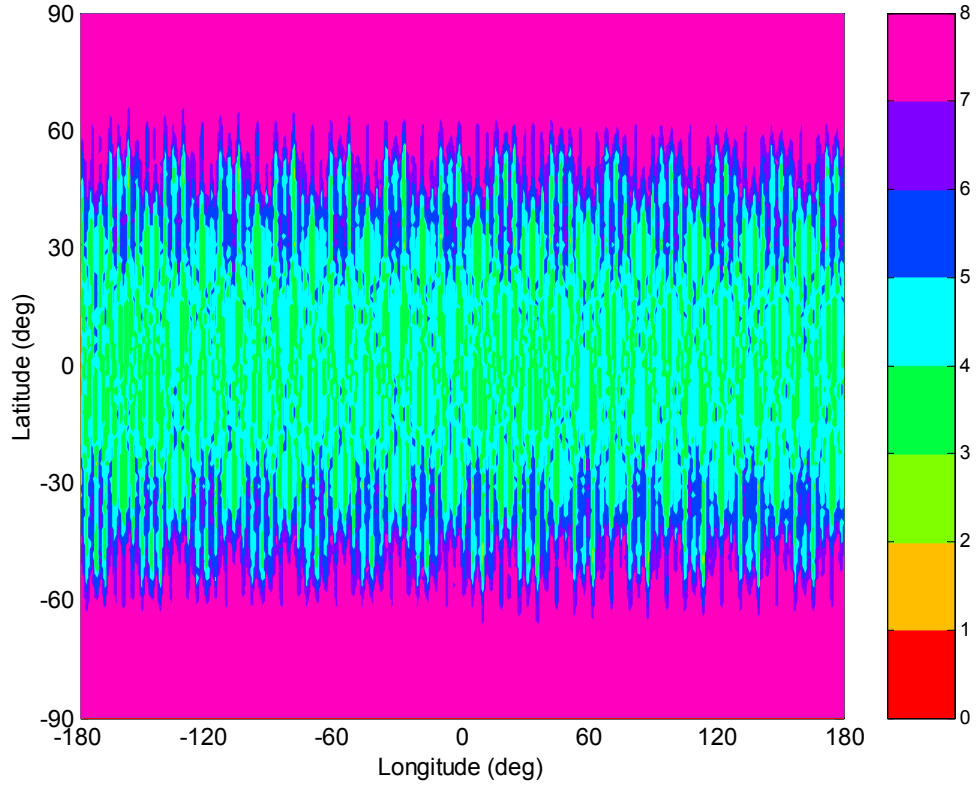


Figure B-7: Europa 60-day global access opportunities for thermal mapper and laser altimeter with 80% duty cycle at 100 km altitude and 90 deg inclination.

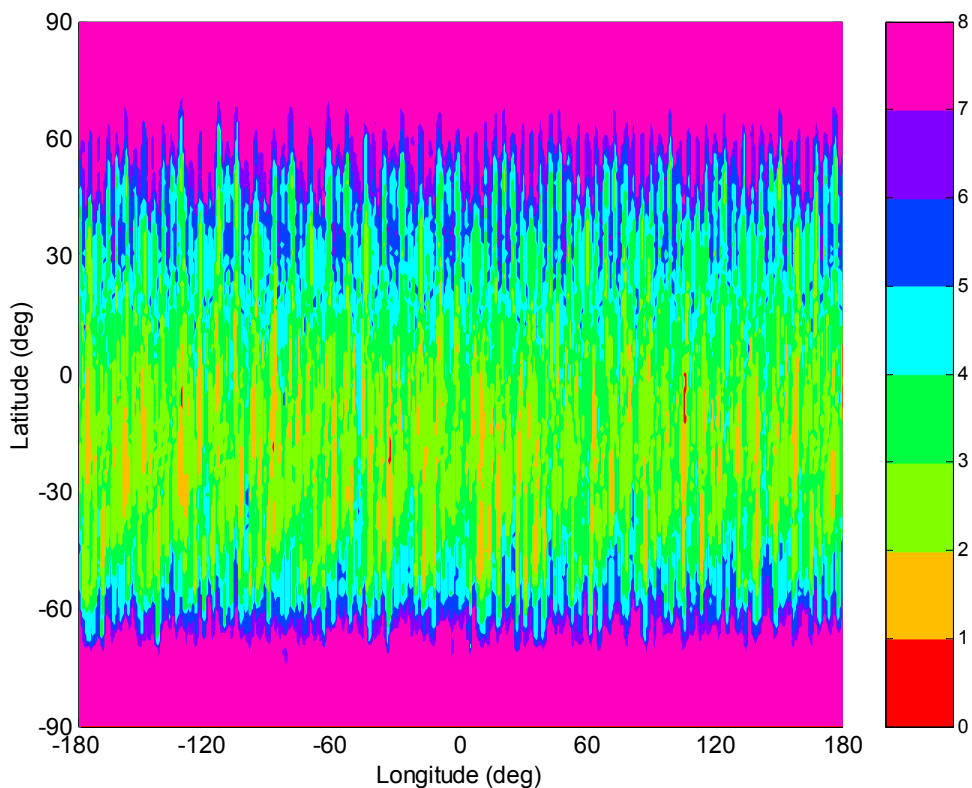


Figure B-8: Europa global folds of coverage for thermal mapper and laser altimeter with 80% duty cycle at 100 km altitude and 90 deg inclination.

Coverage with the IR imaging spectrometer presents a particular challenge because of its need to observe terrain that is in sunlight. An important instrument requirement that must be derived is the minimum solar elevation angle. The value of this quantity will affect the signal to noise performance of the instrument and a minimum threshold will likely be necessary. For the purpose of this analysis, the only additional coverage constraint imposed was that the ground point was illuminated which encompasses solar elevation angles from 0 – 90 deg. As a result, illuminated ground points will be observable from the mission orbit more than 50% of an orbit period but less than 100%. Due to the relatively coarse discretization of the orbit in the DCYCLE analysis (12.3 minutes per duty cycle time increment), additional performance was realized at duty cycle values above 60%. This is a result of instances where the separation between illuminated viewing and un-illuminated viewing occurred in the middle of a time increment. This effect could actually be realized depending upon the amount of time necessary to turn the instrument on and off, but likely will not be as coarse as 12 minutes, so the anticipated coverage may improve. However, it is also

anticipated that instrument performance may be degraded at low solar elevation angles which will further decrease the available coverage.

A nadir oriented FOV of 30 deg was assumed for the IR imaging spectrometer in order to account for the lighting constraint while still achieving the desired level of coverage. Figures B-9 and B-10 show the cumulative one-fold and two-fold global coverage over a 60-day mission at Europa. Based on this analysis, it appears that with a FOV of 30 deg, the desired level of coverage can be achieved; however, this assumes no stringent solar elevation angle limit. Given that duty cycle limits may be further constrained by solar elevation angle limits, these coverage performance results may be expected to decrease somewhat as requirements are further refined. Figures B-11 and B-12 show the global access opportunities and global coverage at 80% duty cycle respectively for the IR imaging spectrometer. As with the previous case, some improvement in coverage performance may be realized by reducing the duty cycle time increment, however, this is not anticipated to change the results significantly. Additional coverage performance may be realized by increasing the instrument FOV, though there may be performance limits beyond 30 degrees depending upon sensor and lighting characteristics.

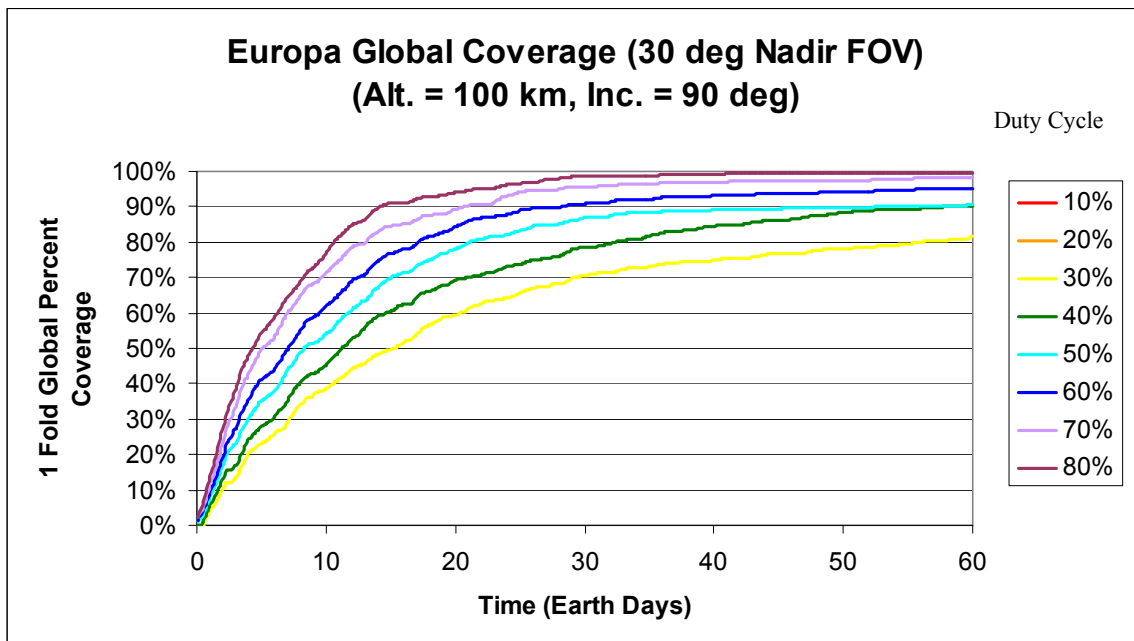


Figure B-9: One-fold global coverage at different duty cycle levels – IR imaging spectrometer.

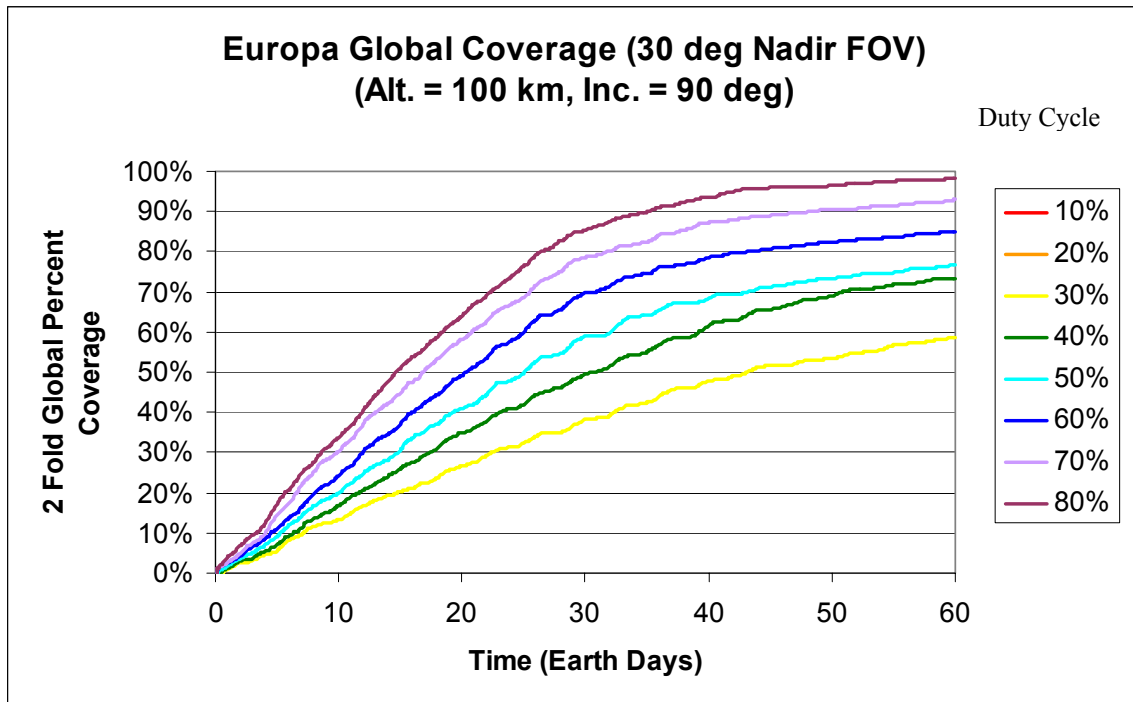


Figure B-10: Two-fold global coverage at different duty cycle levels – IR imaging spectrometer.

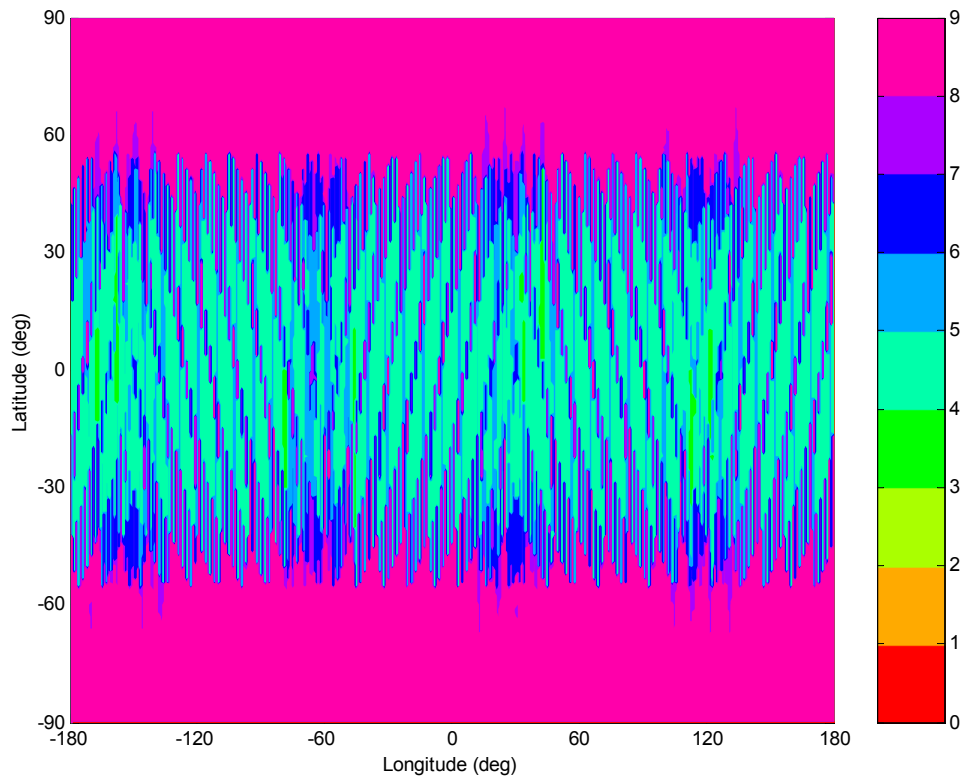


Figure B-11: Europa 60-day global access opportunities for IR imaging spectrometer with 80% duty cycle at 100 km altitude and 90 deg inclination.

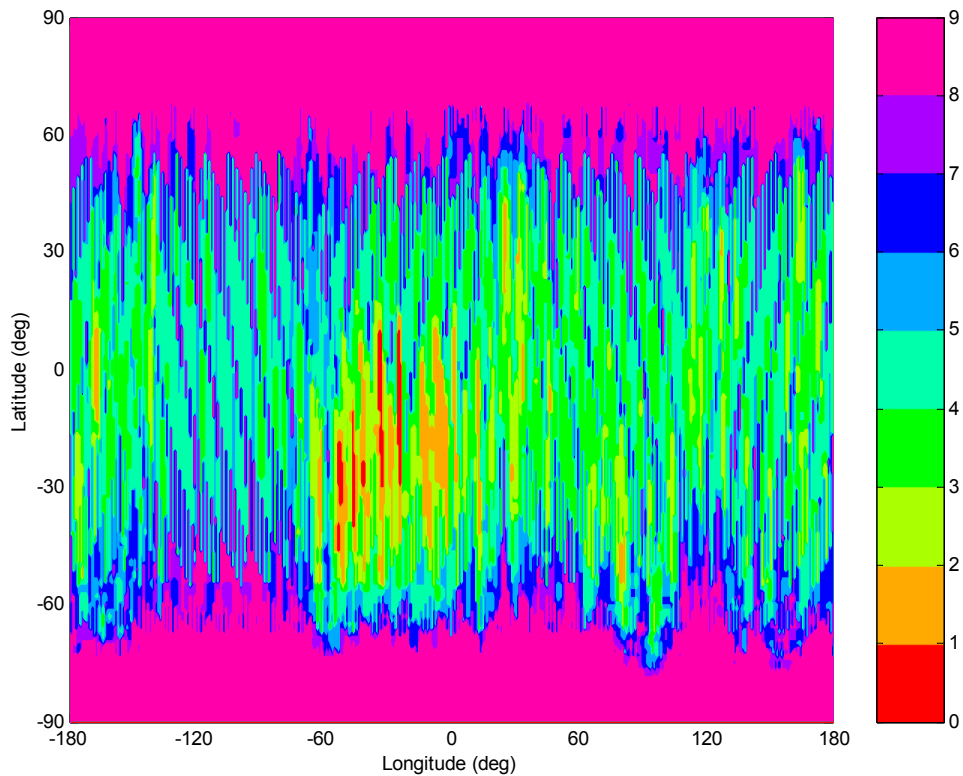


Figure B-12: Europa global folds of coverage for IR imaging spectrometer with 80% duty cycle at 100 km altitude and 90 deg inclination.

The radar subsurface sounder and the radio plasma sounder both have a relatively wide FOV at 33.4 deg, oriented in the nadir direction with no lighting constraints. Global coverage can generally be achieved with lower duty cycle values than for the imaging instruments. Cumulative one-fold and two-fold global coverage for the radar sounding instruments is provided in Figures B-13 and B-14 respectively. At a 60% duty cycle, 100% one-fold coverage can be achieved within 15 days and 100% two-fold coverage can be achieved within 30 days. If the mission duration is extended to 60 days, the two-fold global coverage requirements can be satisfied at a lower duty cycle of about 45%. It is interesting to note that the rate of accumulated coverage varies dramatically for this sensor footprint. In particular, the accumulated coverage rate starts out high, then flattens and then increases in rate. This may be attributed to the spacing of adjacent ground tracks. A low rate of accumulated coverage (at a particular fold of coverage) indicates that regions are being overlapped. It is possible that this may be alleviated somewhat by relatively small changes in the orbit altitude which may slightly alter the spacing of adjacent ground tracks to improve the rate of coverage of new regions, increasing the slope of the accumulated coverage. An important system engineering trade is to find the best compromise altitude that works for the entire instrument suite. Figure B-15 shows the global folds of coverage for the sounder instruments at a 50% duty cycle over a 60-day mission

for a 100 km circular polar orbit. A minimum of three-fold coverage is achieved, making it possible to reduce the instrument operation time somewhat.

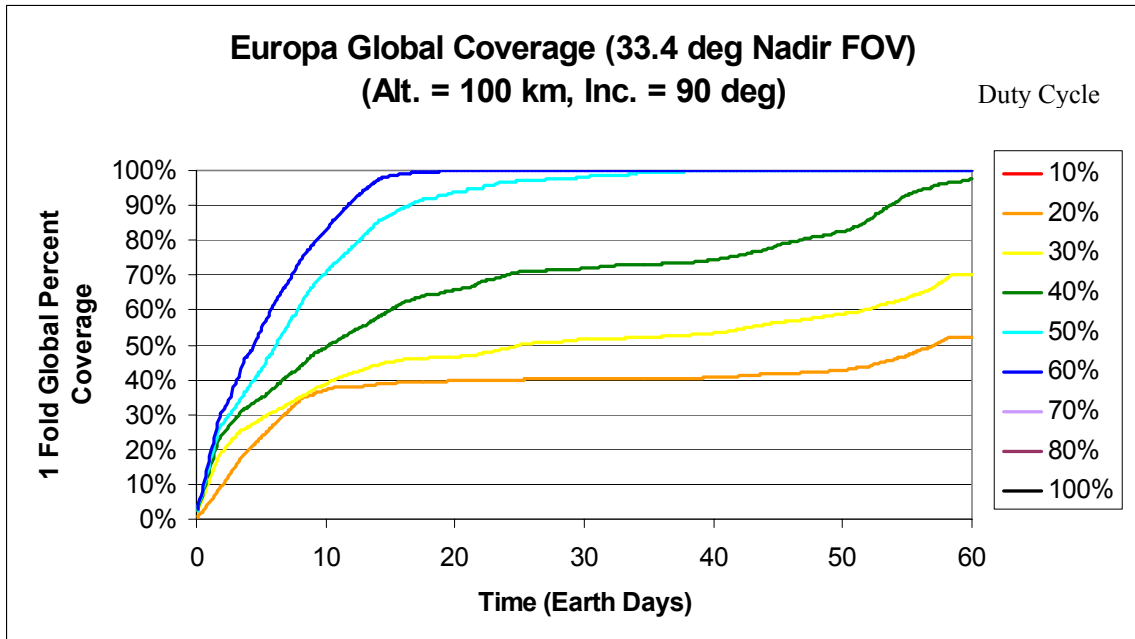


Figure B-13: One-fold global coverage at different duty cycle levels – subsurface radar sounder and radio plasma sounder.

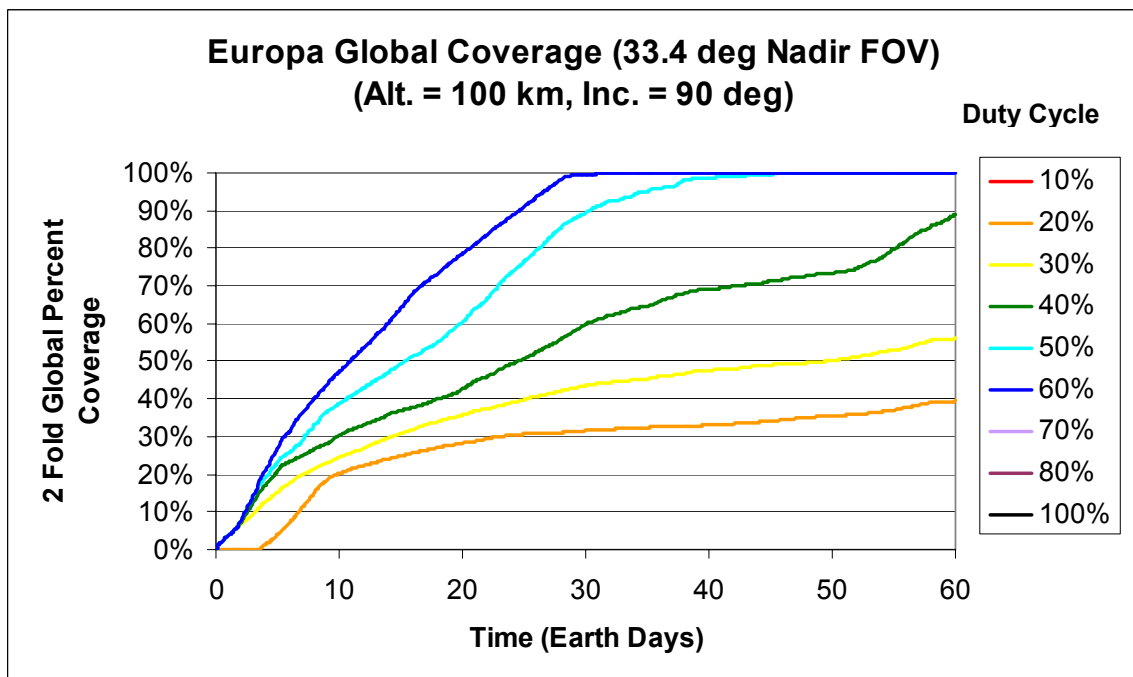


Figure B-14: Two-fold global coverage at different duty cycle levels – subsurface radar sounder and radio plasma sounder.

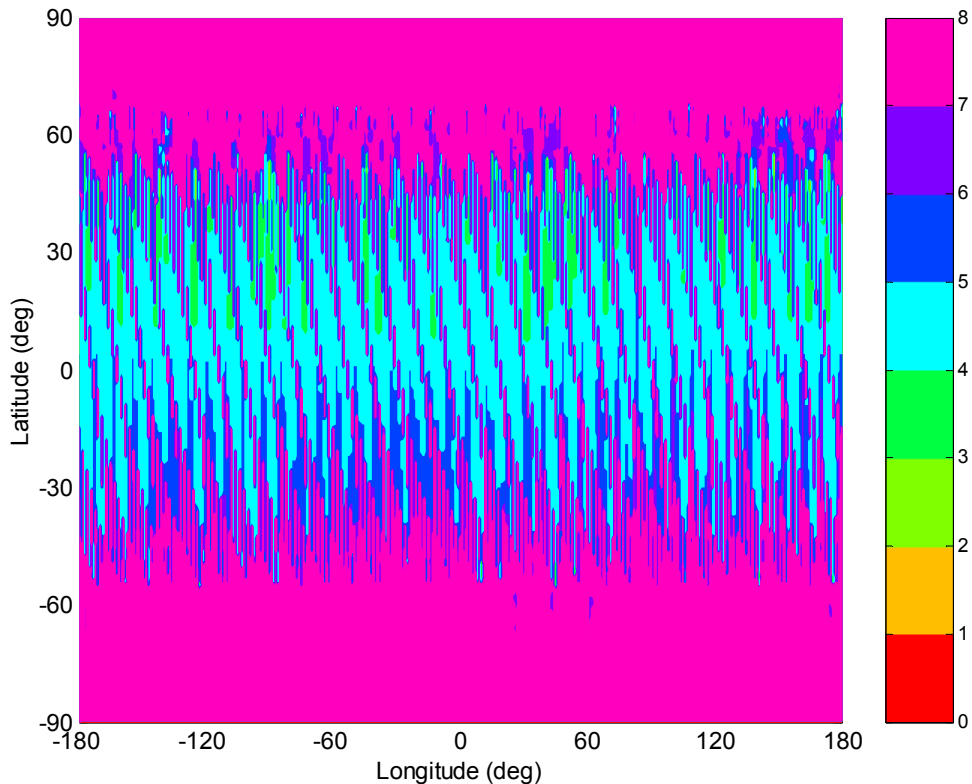


Figure B-15: Europa global folds of coverage for subsurface radar sounder and radio plasma sounder with 50% duty cycle at 100 km altitude and 90 deg inclination.

The interferometric SAR coverage is defined by two 30 km wide swaths that are oriented off nadir. At a 100 km circular orbit, the ground incidence angle for these swaths ranges from 56.4 – 70 deg at the ends of the swath width. The proposed design for the interferometric SAR actually has a slightly wider swath, but this has been budgeted toward coverage overlap, which helps to relax vehicle pointing requirements. This was necessary because the SAR antennas body fixed to the JIMO spacecraft bus and do not have separate fine pointing control. The cumulative one-fold and two-fold coverage over a 60-day science mission at Europa is shown in Figures B-16 and B-17 respectively. From these plots, it is apparent that little benefit is gained by increasing the maximum duty cycle from 50% to 60%. At a 50% duty cycle, 98% one-fold coverage is achieved in 30 days and 98% two-fold coverage is achieved in 60 days. If the two-fold coverage requirement is further relaxed to 95%, the duty cycle can be reduced to 40%. Because this instrument is side looking, a small portion of the poles (within about 1% of the global surface area) will always be left uncovered. Possible mitigation strategies for this problem could include choosing an inclination slightly off of 90 deg or actively pointing the spacecraft over the poles. Figures B-18 and B-19 show global access and coverage for a 50% duty cycle, respectively, over a 60-day mission at Europa. As shown, global access is relatively high due to the wide swath width, which provides at least three viewing opportunities. Applying a

duty cycle of 50% still enables coverage objectives to be achieved within a 60-day mission.

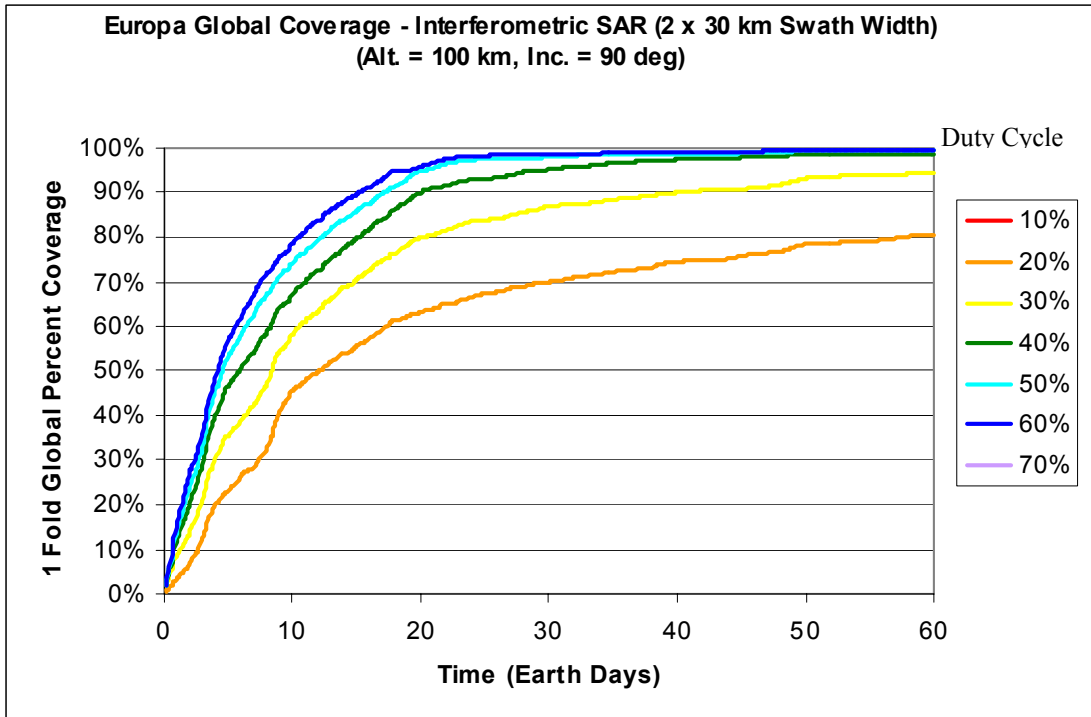


Figure B-16: One-fold global coverage at different duty cycle levels – interferometric SAR.

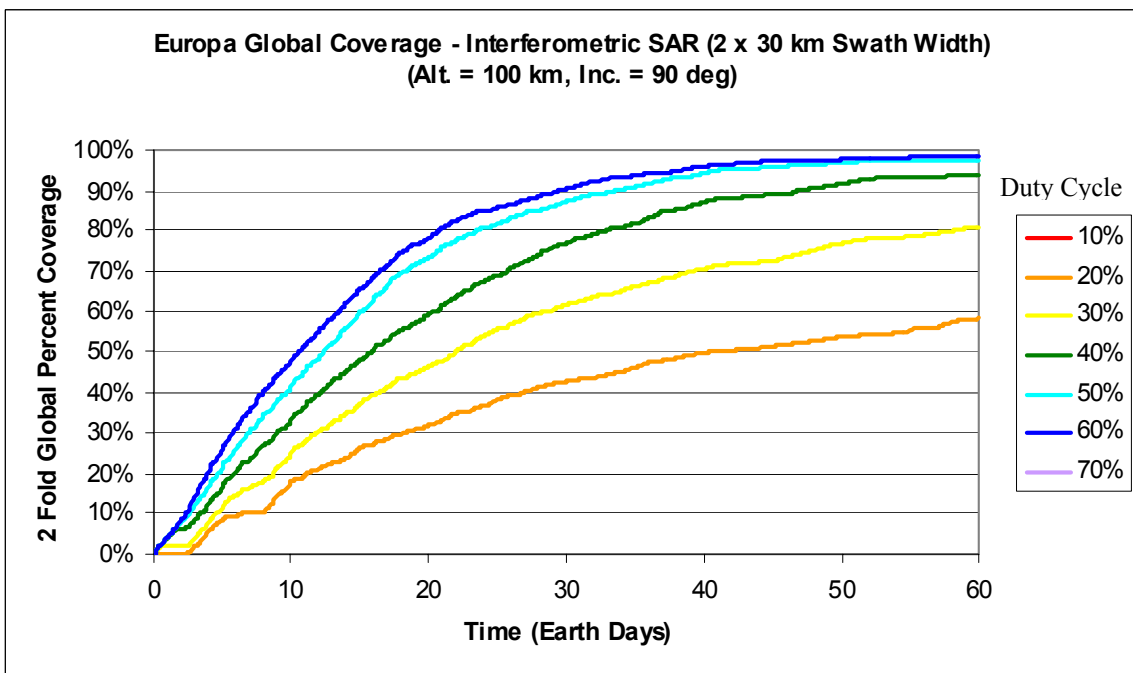


Figure B-17: Two-fold global coverage at different duty cycle levels – interferometric SAR.

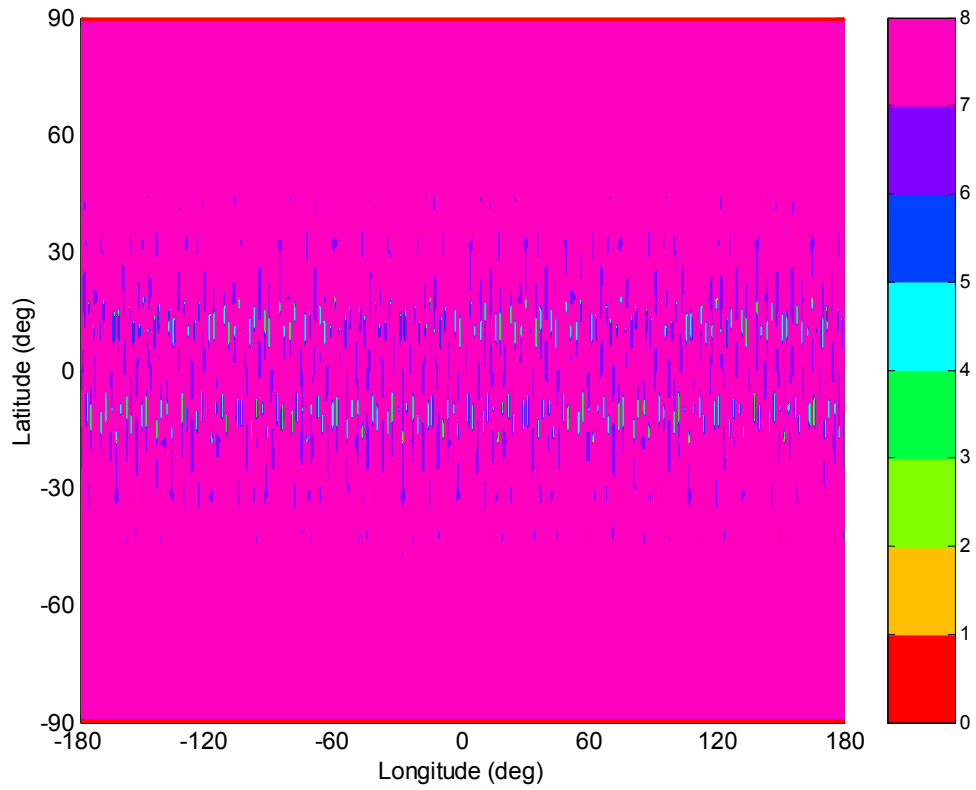


Figure B-18: Europa 60-day global access opportunities for interferometric SAR at 100 km altitude and 90 deg inclination.

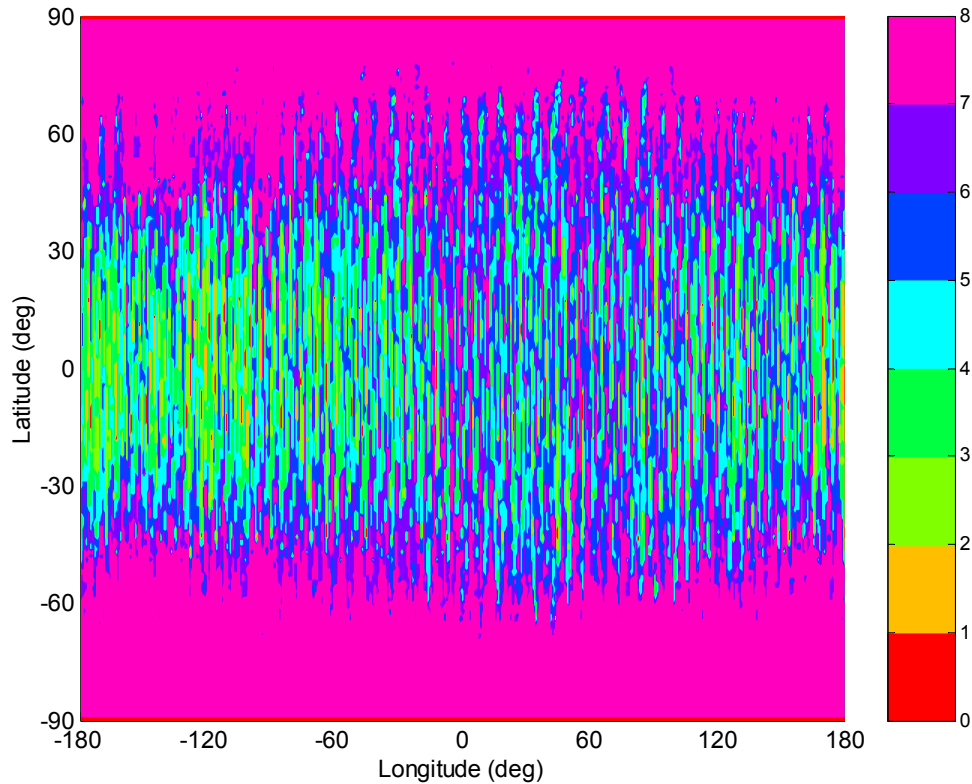


Figure B-19: europa global folds of coverage for interferometric SAR with 50% duty cycle at 100 km altitude and 90 deg inclination.

The polarimetric SAR has a side looking antenna with a single swath, which is about 60 km wide. The ground incidence angle ranges from 46.1 – 75 degrees at each end of the swath. As with the interferometric SAR, the actual instrument swath width is somewhat larger, but this difference has been budgeted toward coverage overlap to help relax pointing requirements. Figures B-20 and B-21 show the cumulative global coverage over a 60-day mission at Europa in a 100 km circular polar orbit for different duty cycle levels. It is apparent from these plots that little benefit is realized by increasing the duty cycle from 50% to 60%. At a maximum duty cycle of 50%, 98% one-fold coverage can be achieved within 30 days and 98% two-fold coverage can be achieved within 60 days. As with the interferometric SAR, a small region at the poles (within 1% of the global surface area) will remain uncovered in a perfect polar orbit. As was discussed earlier, this may be mitigated by choosing an orbit slightly off a polar inclination or by active pointing of the spacecraft at the poles. It is anticipated that a certain amount of deviation from 90 deg inclination can be expected due to orbit insertion and orbit perturbations, however this was not accounted for in this analysis.

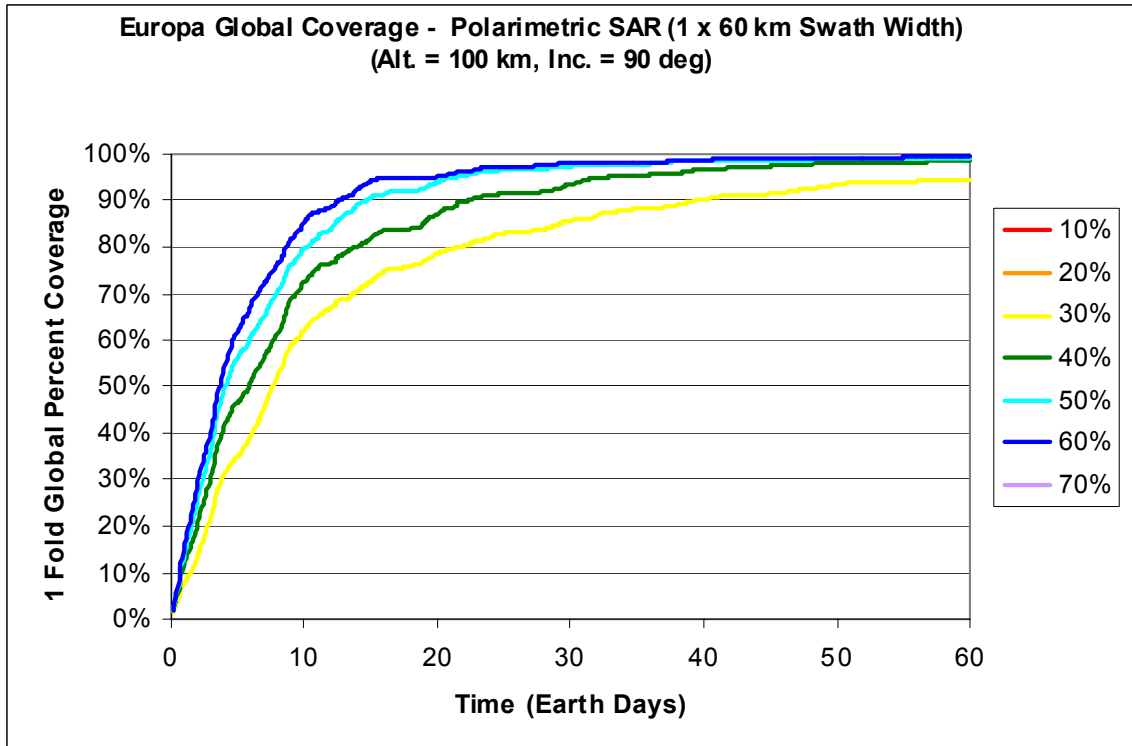


Figure B-20: One-fold global coverage at different duty cycle levels – polarimetric SAR.

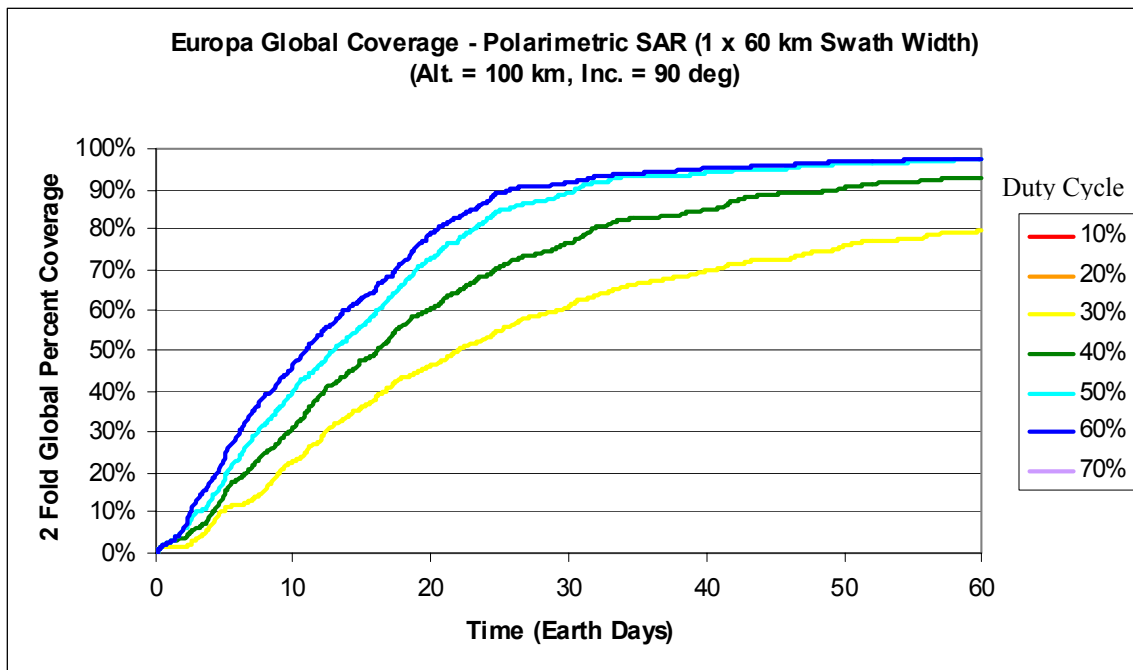


Figure B-21: Two-fold global coverage at different duty cycle levels – polarimetric SAR.

Summary

The proposed fields of view appear to satisfy the objective of achieving two-fold coverage over a 60-day Europa science mission with the exception of the imaging spectrometer. This analysis was performed for a nominal 100 km circular orbit at 90 deg inclination. When the altitude is increased, coverage performance improves, but this comes at the cost of either degraded resolution or a larger and more complex instrument. Decreasing the inclination will improve the coverage rate of accessible areas, but reduces the total accessible area. In particular, coverage at the poles will be sacrificed. From a coverage standpoint, the imaging spectrometer may prove to be the most stressing case based on the requirement to view ground points, which are illuminated by the Sun. In order to more accurately assess the coverage limits for this instrument, it is recommended that a solar elevation angle limit be specified based on a radiometric analysis and the science coverage needs for this data should be justified to determine whether or not global coverage is necessary or if selected coverage is sufficient.

Appendix C. Communication Linkage

Available communications time throughout the JIMO mission is lessened by blockage due to solar incursion, Jupiter blockage, and most notably blockage from the Jovian moon being orbited. An analysis is conducted using an in-house software program (Satellite Orbit Analysis Program, SOAP) with the ephemeris data file Jup100.bsp obtained from the Jet Propulsion Laboratory (JPL). This analysis assumes the solar exclusion region to be 10 solar radii from the geometric Sun center. With this exclusion angle a loss of communication occurs once per year with an outage lasting approximately 5.5 days.

Outage due to Jupiter blockage occurs once per orbit period of the Jovian moon being orbited. While orbiting Europa, communication outages due to Jupiter occur once every 3.55 Earth days lasting approximately 2.4 hours. Orbits around Ganymede will experience the outage duration about 2.1 hours every 7.15 Earth days. Jupiter blockage rarely occurs at Callisto due to the greater distance from Jupiter and the orbital geometry of Callisto, Jupiter, and Earth. A summary of the blockage frequency and duration for each Jovian moon can be found in Table C-1.

Table C-1: Communication Outage Due to Jupiter Blockage

<i>Jovian Moon</i>	<i>Blockage Frequency (Earth Days)</i>	<i>Duration Outage (Hours)</i>
Europa	3.55	2.4
Ganymede	7.15	2.1
Callisto	N/A	N/A

Assuming an orbit altitude of about 100 km and a worst-case right ascension of ascending node (minimum angle between spacecraft to Earth vector and the spacecraft orbit plane), the communications blockage is between 39-42% of the orbit period or 124–155 minutes depending on the Jovian moon (further detail shown in Table C-2). This presents the worst-case, however, much less blockage will occur as angle between the spacecraft to Earth vector and the orbit plane approaches 90 degrees. The initial right ascension of ascending node at the Jovian moon for the science orbit should be selected with both the desired phase and the desired communications time in mind. Compromises may be available that would offer few communications outages during times of high data collection that may also meet required lighting constraints.

Table C-2: Communication Outage Due to Jovian Moon Blockage

<i>Jovian Moon</i>	<i>Orbit Altitude (km)</i>	<i>Outage Time (min)</i>	<i>Orbit Period (min)</i>	<i>Percent Orbit Blackout (%)</i>
Europa	100	63.3	154.5	41.0%
Ganymede	100	62.2	150.3	41.4%
Callisto	100	48.2	123.9	38.9%

Appendix D. Relevant Radiation Environments

The overall JIMO environment presents numerous challenges to be addressed in order to insure a successful mission. Environmental challenges come from numerous external and internal sources. Radiation sources are encountered during the Earth spiral out, during the Jovian moon tour, and internally from the on-board reactor. EMC and magnetic environmental influences result from the on-board power distribution systems and the ion propulsion system. The SARs will produce large radiated E-fields. Additionally, the on-board instruments require a radiator and heat pipe treatment due to their high power dissipation.

Radiation - External

The JIMO radiation environment cannot be exactly defined due to mission-dependent factors. These include reactor power level, shielding, and distance, the duration of the Earth spiral out trajectory and the duration of Jovian moon spiral in trajectory and science orbit. Previous results from the JIMT SLO radiation study can be used to provide an assessment of the radiation environments that the science instruments will be exposed to during the JIMO mission for the reactor, the Earth-trapped radiation exposure during spiral out and the Jovian trapped radiation exposure during spiral in, trajectory between moons, and the science collection at the moons, as well as the spiral out to a safe orbit at Europa.

Radiation – Internal (Reactor)

The reactor produces highly a penetrating radiation of neutrons and Gamma radiation in the MeV range. The reactor-induced radiation is dependent on power level and operation time. A combination of shielding and distance (25 m) was used to limit the reactor radiation exposure over mission life to the spacecraft electronics to 25 krads and $1E11$ 1 MeV equivalent neutrons/cm². The neutron flux ~ 500 1 MeV n (cm²-s)⁻¹. This is similar to Cassini RTG flux levels for instruments (100-400) 1 MeV n (cm²-s)⁻¹. Since reactor gamma and neutron radiation cannot be easily attenuated by local shielding, the total dose and displacement damage floor for the mission needs to be established because this limits radiation soft device selection.

Radiation – Earth Spiral Out

During the Earth spiral out, the spacecraft will be exposed to electrons and protons trapped by the Earth's magnetic field. This includes electrons with energies up to 7 MeV (moderately penetrating), and protons with energies up to ~ 400 MeV (highly penetrating). The radiation exposure is dependent on two factors; the starting altitude and the spiral time. Exposure during Earth spiral out to electrons and protons results in total ionizing dose (TID) and displacement

damage dose (DDD). This radiation can be significant for thinly shielded materials. The secondary photon, primary electron, and primary proton fluxes are insignificant compared to the Jovian environments.

Radiation – Jovian Moon Tour

During the Jovian Moon Tour, the spacecraft will be exposed to electrons and protons trapped by the Jovian magnetic field. Expectations are electrons with energies up to 100 MeV (highly penetrating), and protons with energies up to ~300 MeV (highly penetrating). The JIMT SLO trajectory to Ganymede and Europa also results in significant exposure to the Jovian radiation belts. The Jovian environment will be responsible for the bulk of the total ionizing dose and displacement damage dose for the JIMT SLO mission. The high energy of Jovian electrons are difficult to shield compared to Earth spiral out phase, and results in significant exposures for shielding > 1 inch aluminum. There are high flux rates for secondary photons, primary electrons and protons at detector locations; however, the Galileo science instruments have successfully operated in environments that are more severe than Europa (Io observations). Table D-1 and D-2 show representative total ionizing dose, and displacement damage dose, respectively, for the JIMO mission, for various thicknesses of aluminum shielding.

**Table D -1: JIMT SLO TID Summary; RDF=1; Dose in Kilorads (Si)
(Reprinted courtesy of NASA)**

Spherical Shell Thickness	Jovian	Reactor	Earth Spiral	Total
10 mil Al	25000	25	12000	37000 krad
30 mil Al	12000	25	1700	14000 krad
50 mil Al	7400	25	720	8100 krad
100 mil Al	4100	25	140	4300 krad
300 mil Al	1200	25	14	1200 krad
500 mil Al	580	25	8	610 krad
1000 mil Al	200	25	5	230 krad
3000 mil Al	38	25	3	66 krad

**Table D-2: JIMT SLO DDD Summary; RDF=1;
Equivalent 1 MeV Neutrons/cm² (Reprinted courtesy of NASA)**

Spherical Shell Thickness	Jovian	Reactor	Earth Spiral	Total
10 mil Al	6.0E13	1.0E11	5.3E11	6.1E13
30 mil Al	1.7E13	1.0E11	3.3E11	1.7E13
50 mil Al	1.0E13	1.0E11	2.1E11	1.0E13
100 mil Al	5.7E12	1.0E11	1.5E11	6.0E12
300 mil Al	1.9E12	1.0E11	1.3E11	2.1E12
500 mil Al	9.7E11	1.0E11	8.5E10	1.2E12
1000 mil Al	3.4E11	1.0E11	5.2E10	4.9E11
3000 mil Al	3.2E10	1.0E11	3.0E10	1.6E11

Radiation – Io

Io science observation will dramatically increase JIMO TID and DDD environments due to higher electron and proton populations between 9.5 R_J and 6.0 R_J. Adding Io science observations to the JIMO mission multiplies moon tour TID and DDD by factors of 3 to 7 assuming the same transfer, spiral down, and science durations as during the Ganymede to Europa JIMT mission phases. The transfer between Europa and Io is 55 days. The spiral down into Io science orbit is 57 days, and the Io observation 30 days. Secondary photon, primary electron and primary proton fluxes are an order of magnitude larger than experienced at Europa for detectors, however, the Galileo science instruments successfully operated during several Io passes.

EMC – RF Environments

The Ice Penetrating Radar (IPR) is mentioned because its RF fields may be relatively high. This project uses a Yagi antenna array as its baseline. The frequency that may be used for this project may be between 15 and 50 MHz. Because of the directivity of the Yagi antenna, the RF fields impinging on other spacecraft hardware may be only modest levels compared to prior missions with dipole or monopole antennas. Based on estimated power levels, the nearest spacecraft parts may have a design requirement to tolerate 350 V/m fields (1000 Watt, G = dB, 1 meter distance, and 2x margin for design).

The use of a 1 kW Ka-band (~13 GHz) antenna will have a greater than usual spill-over of RF fields on the spacecraft than the usual 20 Watt (or more recently, 100 Watt) spacecraft transmitters. The RF Field specification will be about 150 V/m for the 1 kW ka-band transmitter (spill-over gain, 0 dB; 2 meter distance to spacecraft; safety margin of 2X). This compares to 100 Watt (60 V/m at 3m) and 20 Watt (50 V/m at 1 m) history.

The use of UHF has been a problem on prior missions, and we expect no difference for JIMO. At these frequencies (~400 MHz), it is relatively easy to couple RF noise from a source into the air, where it can be received by the UHF omni-directional antenna on the spacecraft. In recent programs, instruments were tested to 100 V/m at UHF to ensure compatibility with UHF transmitter. Most were able to operate, some were sensitive to as low as 5 V/m at 400 MHz.

Magnetic Environment

AC magnetic fields will be produced by JIMO sources, possibly causing disturbance to plasma or particle and fields instruments. The 400 VAC at 1 to 1.5 kHz is a possible source of low frequency magnetic and electric fields. E-field levels of about 40 dB $\mu\text{V}/\text{m}$ at 1 meter from this source could be achieved at low frequencies. Low frequency H-field levels of about 60 dB pT when measured at 1 meter from source could also be achieved. The low frequency spectrum will include 1.5 kHz and harmonics up to several tens of kHz, thus polluting the spectrum for instruments up to 20 kHz for H-fields and 100 kHz to 5 MHz for E-field only. If parallel wires are used to transport the current on the 20-meter boom, the magnetic field would be about 100 nT at the magnetometer sensor. Although this is AC vs the DC sensitivity of the magnetometer, it still might cause some disturbance if the magnetometer is sensitive at 1 kHz. Solar panels may be a contributor 1.5 kHz noise for wave instruments.

Stray magnetic fields from JIMO are expected to be quite high. Four groups of sources will be the most significant contributors of magnetic fields. These are the 2 kW solar arrays that will produce current-generated magnetic fields. The 20 Thrusters are expected to be significant contributors to magnetic fields due to permanent magnets. The actuators, RF components, and power bus are also contributors to stray fields. The instrument scan platform is the closest system to magnetometer instruments.

Considerable detail effort must be expended to create a low magnetic field at the magnetometer sensor to permit proper measurement of interplanetary fields. Magnetic fields will also impact instruments measuring energized particles.

A 10-meter boom will provide field reduction relief due to inverse cube fall off spacecraft fields. No relief is available for instruments measuring energized particles if these are mounted near thrusters. Due to the number of magnetic sources on JIMO and the experience with magnetic cleanliness on Voyager, Galileo, and Cassini, the expected magnetic cleanliness levels are:

- 10 nT at the end of the 10-meter boom could be achievable
- A dynamic field level of about 1 nT could be achieved

- Lower levels could be achieved with considerable efforts in reducing the fields from the 20 highly magnetic thrusters and solar arrays

Electrostatic Discharge Protection for JIMO Optical Instruments

Due to the extreme environment of the JIMO mission, there is concern regarding the effects of electrostatic discharge (ESD) on the optical instruments that could lead to pitting of the optical surfaces or could result in electromagnetic interference (EMI) that could damage RF sensitive hardware such as the radar instruments. Possible measures for mitigating ESD risks include doping the transmissive (non-conductive) instrument optics with conductive materials, applying thin-film coatings of conductive materials to the optical surfaces, or using beryllium-copper ground rings to provide a discharge path. Doping the optics with conductive materials would fall within the current state of practice for government space programs, however the use of transparent thin-film coatings may require some technology development work. These measures could potentially increase instrument mass by up to 5% depending on instrument size.

Environmental Heat Loads

The environmental heat loads around the three moons of Jupiter (Europa, Callisto, and Ganymede) were calculated by running a SOAP (Satellite Orbital Analysis Program) simulation of a cube, 1 m per side, for several orbits. The variable parameters were the beta (β) angle, or inclination of the orbit plane relative to the solar vector, and the altitude. Beta angles of 0° and 90° were investigated. A beta angle of 0° yields the longest eclipse period, whereas a beta angle of 90° leads to Sun exposure at all orbital positions (no eclipse). Nominal altitudes of 100 km and 400 km were examined. The total heat loads (solar, reflected solar, and moon IR) were time-averaged over the orbit period. The results are compiled in Tables D-3 through D-5. The individual loads are also shown in bar-graph format in Figures D-1 through D-3 for the three moons.

As indicated in the computed data, the maximum moon IR flux is roughly 27 W/m^2 (Callisto, 100 km), and the maximum solar plus albedo load is approximately 73 W/m^2 (Callisto, $\beta = 90^\circ$, 400 km). When averaged over all six-cube faces, however, the maximum loads are only about 12 W/m^2 (Callisto, $\beta = 90^\circ$, 400 km) for the solar plus albedo contribution and 11 W/m^2 (Callisto, $\beta = 0^\circ$ and 90° , 100 km) for the moon IR contribution.

Based on these peak and average load results, the average combined solar/albedo and moon IR heat flux values were conservatively selected at 30 W/m^2 and 20 W/m^2 , given that the orientation of the radiators and shielding details are as yet unknown. These values were used to size all radiators. In general, the environmental loads are sufficiently low that they only impact the most sensitive on-board instruments.

Table D-3: Total Environmental Contributions [W/m²]

$\beta = 0 ; h = 100 \text{ km}$						
	Q101 (nadir)	Q102 (zenith)	Q103	Q104	Q105	Q106
CALLISTO	31.8	19.9	22.9	23.8	13.1	10.9
EUROPA	14.3	16.2	14.2	15	6.26	4.4
GANYMEDE	30.2	19.3	22.2	23	12.7	10.5
$\beta = 0 ; h = 400 \text{ km}$						
CALLISTO	27.7	19.9	20.7	21.6	8.83	6.26
EUROPA	13	16.2	14.5	15.2	4.31	2.09
GANYMEDE	30.3	22.6	22.8	23.8	10.1	7.24
$\beta = 90 ; h = 100 \text{ km}$						
	Q101 (nadir)	Q102 (zenith)	Q103	Q104	Q105	Q106
CALLISTO	27.6	0	9.72	9.71	71.6	9.64
EUROPA	5.15	0	1.69	1.69	52.5	1.44
GANYMEDE	22	0	7.88	7.88	68.2	7.73
$\beta = 90 ; h = 400 \text{ km}$						
CALLISTO	26.4	0	6.72	6.72	80.0	6.59
EUROPA	5.85	0	1.28	1.28	66.5	0.91
GANYMEDE	21.5	0	5.66	5.66	76.4	5.38

Table D-4: Average Solar and Albedo Contributions [W/m²]

$\beta = 0 ; h = 100 \text{ km}$						
	Q101 (nadir)	Q102 (zenith)	Q103	Q104	Q105	Q106
CALLISTO	31.8	19.9	22.9	23.8	13.1	10.9
EUROPA	14.3	16.2	14.2	15	6.26	4.4
GANYMEDE	30.2	19.3	22.2	23	12.7	10.5
$\beta = 0 ; h = 400 \text{ km}$						
CALLISTO	27.7	19.9	20.7	21.6	8.83	6.26
EUROPA	13	16.2	14.5	15.2	4.31	2.09
GANYMEDE	30.3	22.6	22.8	23.8	10.1	7.24
$\beta = 90 ; h = 100 \text{ km}$						
	Q101 (nadir)	Q102 (zenith)	Q103	Q104	Q105	Q106
CALLISTO	27.6	0	9.72	9.71	71.6	9.64
EUROPA	5.15	0	1.69	1.69	52.5	1.44
GANYMEDE	22	0	7.88	7.88	68.2	7.73
$\beta = 90 ; h = 400 \text{ km}$						
CALLISTO	26.4	0	6.72	6.72	80.0	6.59
EUROPA	5.85	0	1.28	1.28	66.5	0.91
GANYMEDE	21.5	0	5.66	5.66	76.4	5.38

Table D-5: Average Moon IR Contributions [W/m²]

$\beta = 0 ; h = 100 \text{ km}$						
	Q101 (nadir)	Q102 (zenith)	Q103	Q104	Q105	Q106
CALLISTO	4.34	19.9	13.3	14.2	3.46	1.21
EUROPA	9.84	16.2	12.8	13.5	4.8	2.94
GANYMEDE	8.54	19.3	14.5	15.3	4.93	2.73
$\beta = 0 ; h = 400 \text{ km}$						
CALLISTO	5.81	19.9	15.1	16	3.25	0.684
EUROPA	9.77	16.2	13.7	14.5	3.6	1.38
GANYMEDE	9.74	22.6	17.4	18.4	4.69	1.86
$\beta = 90 ; h = 100 \text{ km}$						
	Q101 (nadir)	Q102 (zenith)	Q103	Q104	Q105	Q106
CALLISTO	0.174	0	0.07	0.07	62	0
EUROPA	0.679	0	0.25	0.25	51.1	0
GANYMEDE	0.356	0	0.15	0.15	60.5	0
$\beta = 90 ; h = 400 \text{ km}$						
CALLISTO	0.501	0	0.13	0.13	73.4	0
EUROPA	1.73	0	0.38	0.38	65.6	0
GANYMEDE	1.04	0	0.28	0.28	71	0

Callisto

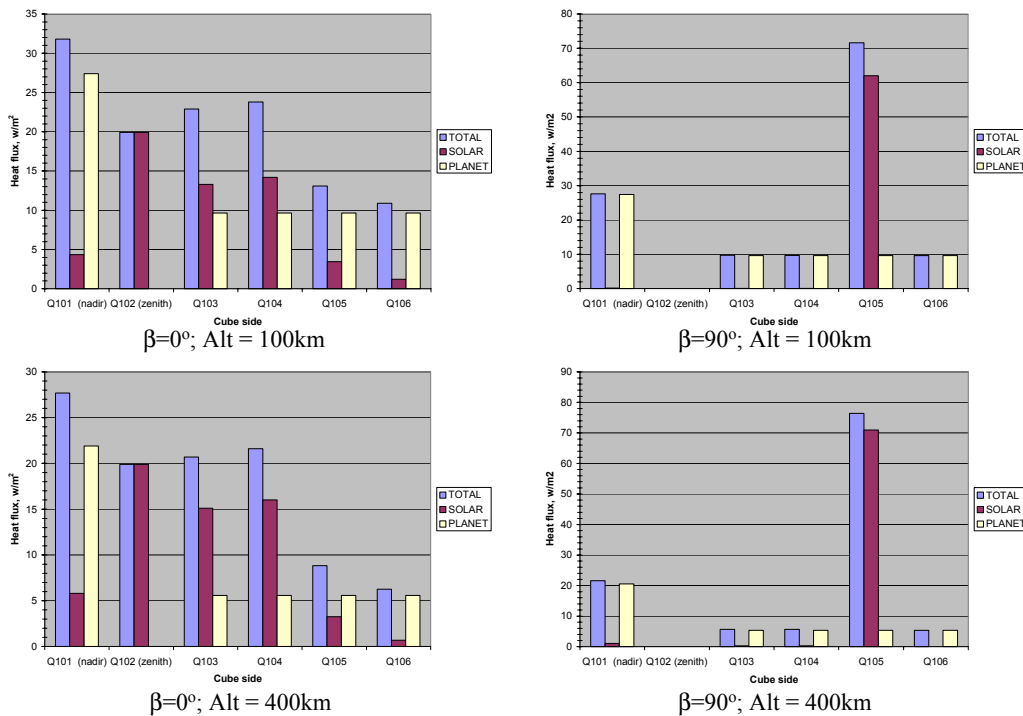


Figure D-1: Environmental loads on Callisto.

Europa

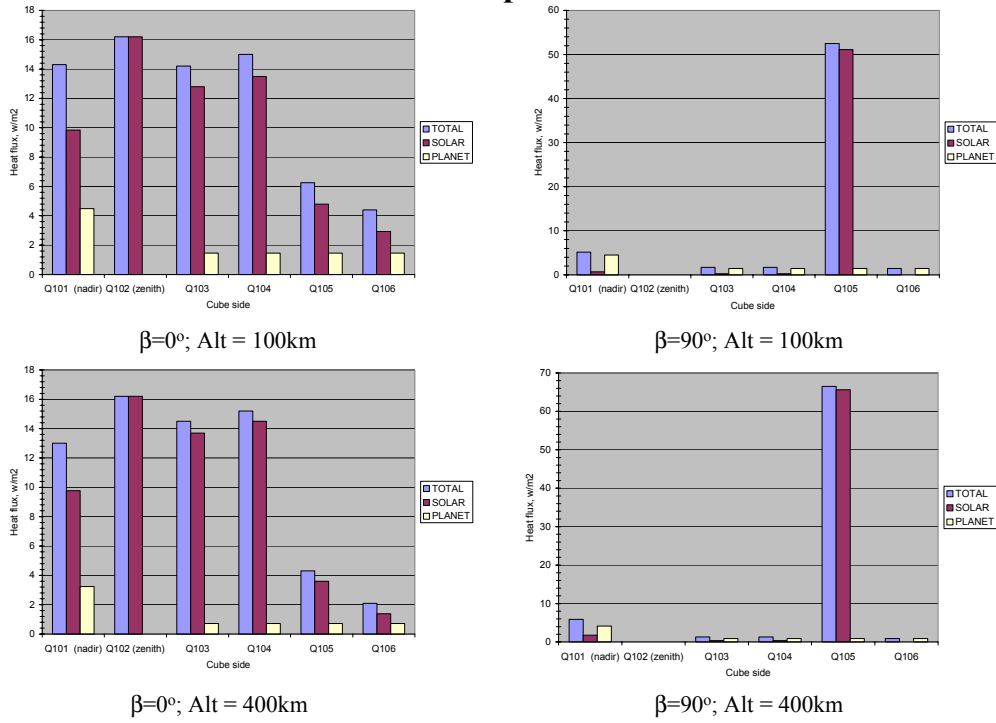


Figure D-2: Environmental loads on Europa.

Ganymede

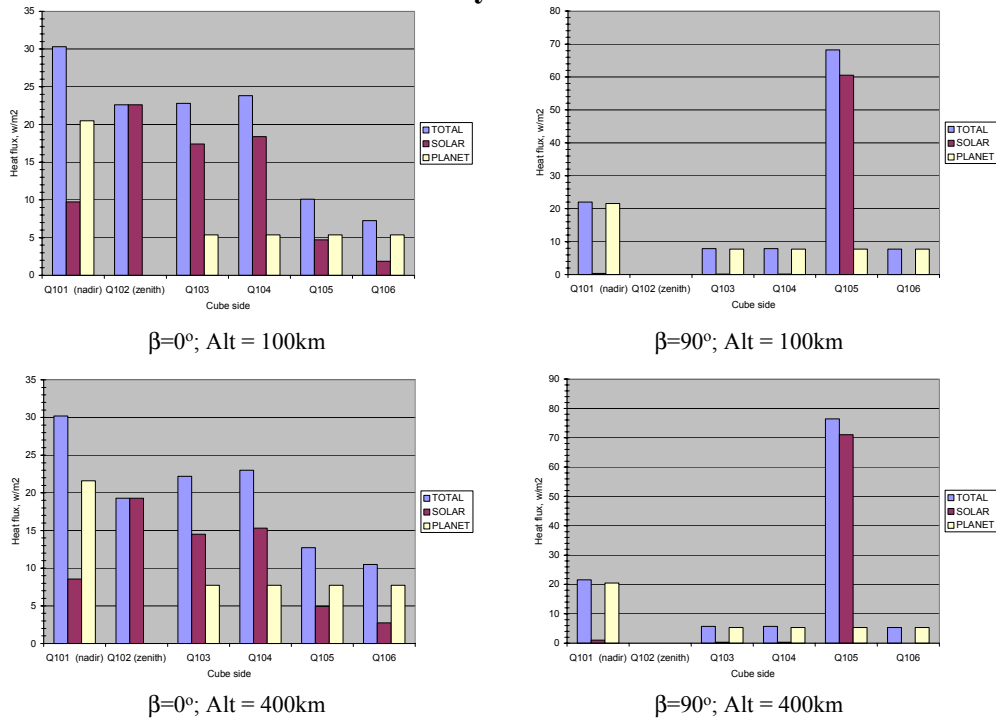


Figure D-3: Environmental loads on Ganymede.

Appendix E. Ion Plume Effects

The Jupiter Icy Moons Orbiter may employ advanced electrostatic gridded Ion propulsion engines for primary propulsion. One area of concern generated by the use of this type of propulsion system is the potential impact the ion plume may have on the operation of the spacecraft instruments, particularly the electro-optical sensors. A number of factors regarding this issue must be taken into consideration.

Ion Plume Environment

Current ion propulsion engines commonly use Xenon as the propellant. There is documented research regarding the effects of the Xenon ion plume on the materials used in spacecraft and instrument surface construction. This research includes the deposition rate of Xenon ions as well as the deposition rate of ions resulting from the deterioration of the grids on surfaces in close proximity to the thrusters. A study performed by The Aerospace Corporation¹ on a Xenon ion propulsion engine, based upon a British ion thruster, designated T5 Mk3 utilizing a 10 cm thruster, has measured the deposition rate on a variety of materials in three categories, solar absorbers, white paints and solar reflectors. The T5 configuration used three molybdenum grids, however, carbon grids are being considered for the JIMO engine due to the extended cruise period and the overall length of the mission. Carbon grids have a slower deterioration rate, therefore extending the life of the engines, but carbon deposition on optical surfaces may be more severe than that with molybdenum. There are currently no known studies to determine the deposition rate of carbon ions on spacecraft surfaces as a result of carbon grid deterioration. This erosion and subsequent deposition of carbon ions may present a significant problem on spacecraft instrument operations, particularly on the EO instruments. Any impact in large part may or may not be mitigated by the final spacecraft configuration and a function of the proximity of the thrusters and instruments.

Ion Plume Geometry

The use of ion propulsion engines has introduced the issue of the deposition of ions as a result of grid erosion, the Xenon ions themselves, and the ionized ambient particles (through charge exchange with the Xenon ions) that are moving more slowly and may have a greater chance of deposition on spacecraft and instrument surfaces. In the Aerospace Corporation study, it was determined that the deposition rate was most prevalent in the 20°–35° area off the grid plane. Deposition rate was maximized at 45° off the grid plane (Figure 16.2-1). These deposition rates were determined from materials located from 10°–65° off the

¹ Ahmed, L. N., and Crofton, M. W., "Surface Modification Measurements in the T5 (UK-10) Ion Thruster Plume," AIAA Paper 95-2827, July 1995.

grid plane, within 54 cm of the thruster. The deposition rates also varied as a result of changes to the accelerator and decelerator grid voltages, propellant mass utilization and the background pressure of the test facility. Under consideration is use of a larger ion propulsion system with 60–65 cm thrusters. If a larger ion propulsion system and thrusters are utilized, then the deposition rate and angular dissipation of the ions may be in all likelihood an order of magnitude greater. Placement of the instrument platform is critical to insure the least amount of modification to spacecraft and instrument surfaces. If instruments are physically located at least 90° aft of the ion plume axis, this should mitigate a high deposition rate. Instrument placement testing in the ion propulsion system induced environment, using witness plates to measure local deposition rate as a function of location is recommended.

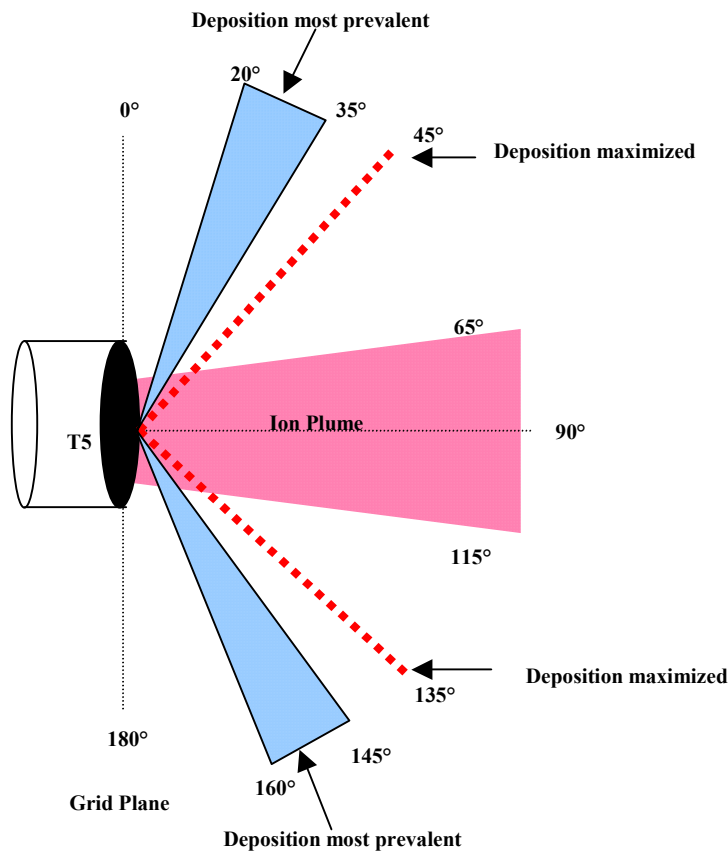


Figure E -1: Ion deposition.

Susceptible Surfaces

In the Aerospace Corporation study, there were a total of 10 spacecraft materials, divided into three categories exposed to the engine plume.

Solar absorbers:

MH21S/LO®, black paint on a 25-mm aluminum disk

Edmund Scientific SuperCell® Solar Cell, 2.5 x 6.2 cm

Dupont Kapton® film, 0.05-mm on 25-mm aluminum disk

White Paints:

YB-71/PS-7®, white paint on 25-mm aluminum disk

Z93®, white paint on 25-mm aluminum disk

Z93P®, white paint on 25-mm aluminum disk

S13GP/LO-1®, white paint on 25-mm aluminum disk

Solar reflectors (second surface mirrors):

Indium-tin-oxide- (ITO) coated CMX, 20 x 20 x 0.15 mm

Pilkington, silver Teflon, FEP/Ag/Inconel, 0.13 mm on 25-mm aluminum disk fused silica optical solar reflectors, 40 x 20 x 0.02 mm

These materials are representative of those found on most spacecraft. Materials not represented in this study are those used in the construction of EO instruments, specifically, materials used in the construction of lenses, mirrors, gratings and prisms, etc.

Deposition Rates

Per the Aerospace Corporation study, "Slight degradation of spacecraft exterior surfaces can be expected as a result of the ion thruster. The problem facing other electrostatic ion thruster with extraction grids are similar..." The materials tested were placed in close proximity to the ion plume, so there is a reasonable expectation that if the instrument suite on JIMO were located a sufficient distance aft of the grid plane, the deposition rate resulting from the ion plume may be insignificant; however, if other than molybdenum is used for the grid material, the deposition rate may differ. The use of another grid material may warrant further study of the specific deposition rate.

Mitigation Approaches

There are numerous approaches to mitigating the potential effects of the ion propulsion system on the EO instruments. The design of the EO instruments should incorporate removable, replaceable covers to shield optics from the ion propulsion system environment when not in use, then commanded to lift or open during instrument operation. Transparent coatings such as calcium fluoride may allow the IR spectrum to operate with a cover on, further extending its life. The use of sputter shields on thrusters is to protect the instruments during engine operation. Limited instrument operation during the spiral in/spiral out phases, when the ion propulsion system will be operating, requires a spacecraft configuration that locates the instrument suite away from the thrusters and plume. These approaches may allow instrument operation during the thrusting portions of the mission, such as spiral in/out and Jovian cruise.

Conclusion

Due to the numerous unknown variables, further investigation of the possible effects from the ISP on the instruments seems warranted as this and other JIMO studies proceed to insure all factors are taken into consideration in the final spacecraft design and development of operations concepts.

Appendix F. On-Board Storage Technology Examples

Galileo Millennium Mission Status

NASA's Galileo spacecraft has begun transmitting high-priority scientific information that was collected and stored on its **tape recorder** during the orbiter's early-November dash by Jupiter, which brought it closer to the planet than ever before. Reference http://www.kc4cop.bizland.com/space_news_7.htm

The Galileo mission consists of two spacecraft: an orbiter and an atmospheric probe. Launched during the STS 34 flight of the Atlantis orbiter, the two spacecraft were kicked out of Earth orbit by an inertial upper stage (IUS) rocket, sending them careening through the inner solar system. The trajectory that the spacecraft followed was called a VEEGA (Venus-Earth-Earth Gravity Assist), traveling first in toward the Sun for a gravity assist from Venus before encountering the Earth two times (spaced two years apart). These encounters with Venus and the Earth allowed Galileo to gain enough velocity to get it out to Jupiter. Reference <http://galileo.jpl.nasa.gov>

SPOT

SPOT satellites orbit the Earth at an altitude near 825 km and an inclination of 98.7 deg to produce a 26-day repeating ground track pattern with Sun-synchronous conditions. SPOT 3 joined SPOT 1 (February, 1986) and SPOT 2 (January, 1990) after its launch on 26 September 1993. All three spacecraft are in essentially co-planar orbits.

Images can be transmitted in real-time directly to a world-wide network of ground stations or may be stored on board the spacecraft for later down linking via two Odetics tape recorders, which were improved for SPOT 3. SPOT 3 also carried the US Polar Ozone and Aerosol Measurement (POAM) experiment. Reference <http://www.fas.org/spp/guide/france/earth/>

The Near Earth Asteroid Rendezvous (NEAR) spacecraft is the first Applied Physics Laboratory spacecraft to use solid-state data recorders (SSDRs) for mass storage. It is also the first APL spacecraft to use plastic encapsulated microcircuits (PEMs) in significant numbers. Prior to NEAR, APL had launched 18 magnetic tape recorders on nine spacecraft. These tape recorders ranged in storage capacity from 5 megabits (Mb) to 54 gigabits (Gb). Earlier still, the Transit series of APL spacecraft used arrays of magnetic cores with as much as 32 kilobytes of capacity. By comparison, the two NEAR recorders together can store 1.6 Gb of user data in 132 PEMs. Each PEM is a 16-Mb dynamic random access memory (DRAM) integrated circuit.

When radiation-tolerant semiconductor memories reached a density of 256 kilobits per integrated circuit, they began to seriously challenge the use of magnetic tape in space. With the availability of 16-Mb devices, such as those used in the NEAR SSDRs, the 35-year reign of tape recorders has nearly ended. Three tape recorders for Japan and one for Canada are probably the last ones being manufactured to operate aboard unmanned spacecraft. SSDRs have many advantages over tape recorders. They are smaller, lighter, and less expensive; they also use less power and impart no momentum or vibration disturbances to the spacecraft. The inherent redundancy and reconfigurability of their memory arrays and an overall lower parts count improve reliability. They also tolerate a much wider range of operating temperature than magnetic tape. Perhaps their biggest advantage is operational flexibility, since they are randomly addressable and can easily accommodate discontinuous data at widely varying rates. These advantages outweigh the volatility of current SSDRs—if power is lost, all data are lost. This shortcoming is an acceptable trade-off for NEAR. The NEAR spacecraft uses the SSDRs to store science and engineering data temporarily during those periods when effective communication with the Earth is not possible or is constrained by bandwidth. In the former case, the stored data are played back at scheduled times when communication is possible. In either case, an SSDR can play back the data at a fraction of the record rate to accommodate the communications link.

Hubble Space Telescope Servicing Mission 3A

To communicate with its operators on the ground, the Hubble Space Telescope uses a group of NASA satellites called the Tracking and Data Relay Satellite System (TDRSS). By way of TDRSS, Hubble sends the data from its science instruments and spacecraft systems to the Space Telescope Operations Control Center at NASA's Goddard Space Flight Center in Greenbelt, Md. When the TDRSS link is not available, Hubble stores its science and engineering data in onboard recorders for playback at a later time. Hubble records all of its science data to prevent any possible loss of unique information. Prior to the Second Servicing Mission, Hubble used three 1970s-style, reel-to-reel tape recorders. In February 1997, astronauts replaced one of these mechanical recorders with a digital solid state recorder. During Servicing Mission 3A astronauts will remove a second mechanical tape recorder and install a second solid state recorder.

More Storage, No Moving Parts

Unlike the reel-to-reel recorder it replaces, the solid state recorder has no reels, no tape, and no moving parts to wear out and limit lifetime. Data is digitally stored in computer-like memory chips until Hubble's operators command its playback. Although the solid state recorder is about the same size and shape as the reel-to-reel recorder, it can hold approximately ten times as much data. It stores 12 gigabits of data, while the tape recorder it replaces can hold only 1.2 gigabits.

This ten times greater storage has proven essential in allowing Hubble's new, high-tech scientific instruments to be fully productive.

Flexibility and Multi-tasking

State-of-the-art electronics provide the solid state recorder with more capability and flexibility than a reel-to-reel recorder. This digital recorder is designed to perform the tasks of two separate mechanical recorders. Unlike a mechanical recorder, the solid state recorder can record and play back data simultaneously. Another advantage is its ability to record two data streams at the same time, allowing both the science and engineering data streams to be captured on a single recorder. Unlike the reel-to-reel recorders, data can be played back without having to rewind the tape, and information can be instantly accessed.

Reference

http://www.gsfc.nasa.gov/gsfc/service/gallery/fact_sheets/spacesci/hst3-01/hst_ssr.htm

Solid State Recorder

One innovation developed for Cassini is a solid state data recorder that has no moving parts. The recorder has great potential for use in a variety of fields, from aerospace to the entertainment industry, and is expected eventually to find wide applicability in consumer electronics. NASA's Advanced X-ray Astrophysics Facility (AXAF), another major space science mission that will provide new insights into the mysteries of the universe, will use a solid state recorder from the production line established for the Cassini mission.

Appendix G. Legacy Approaches to 100–1000 Micron Remote Sensing

This section briefly discusses a few options for augmenting the strawman thermal mapper with an instrument capable of imaging at wavelengths from 100–1000 microns. Both passive optical and passive radio frequency (RF) instruments could potentially be used for imaging in this interval. There are instruments being developed/flown for astronomy, solar system exploration, and Earth science that might provide heritage for JIMO. Since there is more than one technology and more than one application, the interval is described in several ways corresponding to different applications:

- Far infrared imaging: wavelength range of 100 to 1000 microns
- Fourier transform spectroscopy: wavenumber of 100/cm to 10/cm
- Sub-millimeter RF radiometry: frequency range of 3 THz to 300 GHz

First considerations for imaging in this interval include that the target radiances are relatively weak and have relatively flat profiles, and reflected sunlight is negligible. The lowest average temperature of the 3 icy moons is about 100 K (at Europa). The highest albedo is about 0.64 (also at Europa). The figure below depicts the emitted radiation from an ideal black body at 100 K and reflected sunlight at 5.2 AU from the Sun for an albedo of 0.64.

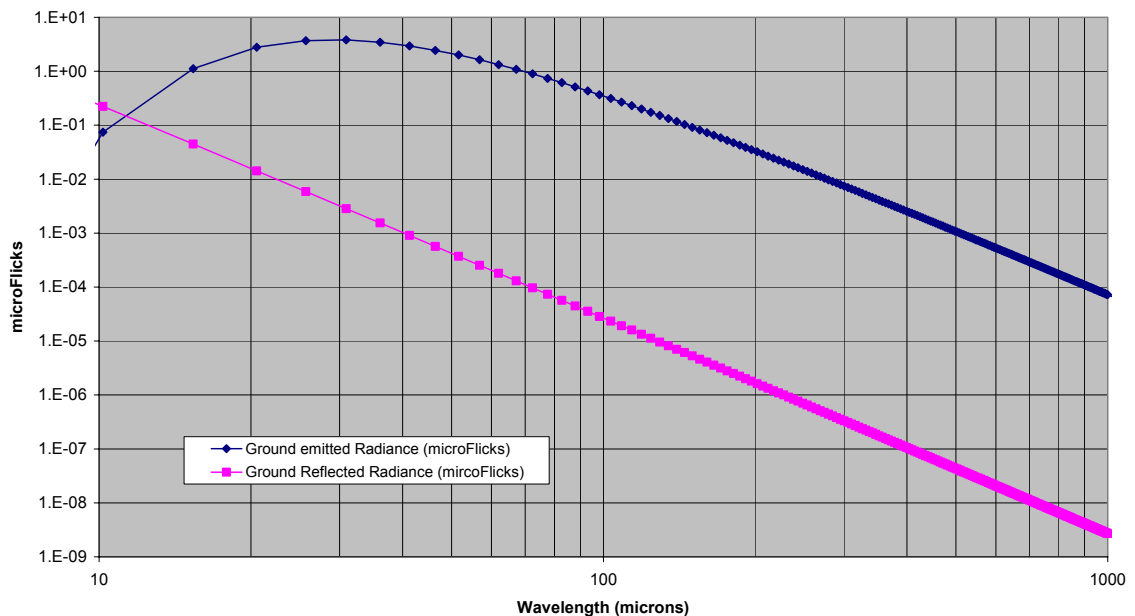


Figure G-1: Emitted radiation from an ideal black body.

Since this is a log-log plot, the nearly straight lines past 100 microns for emitted and reflected radiance correspond to nearly straight lines on a linear-linear plot. The peak emitted radiance is about 4 μ Flicks at 29 microns. Emitted radiance drops to less than 1×10^{-4} μ Flicks at 1000 microns (40,000 times less than at 29

microns). From 100 to 1000 microns, reflected radiance is about 4 orders of magnitude less than emitted radiance at a given wavelength.

There is a question regarding what the science objectives would be in looking at the 100–1000 micron interval. The technology most appropriate for this interval would depend on the specific science objectives. Candidate technologies are considered below.

Optical Imaging

One option would be to use an optical imager with a spectral resolution of 2 similar to the strawman thermal mapper. Assuming no overlap, 5 bands would be needed to cover wavelengths from 100–1000 microns. One choice for these is shown in the Table G-1 below.

Table G-1: Candidate 100–1000 Micron Bands

Center Wavelength (microns)	Channel Bandwidth (microns)	Spectral Resolution	Channel Radiance (ph/cm ² -s-sr)
103.68	±25.92	2	9.40 X 10 ¹⁵
172.8	±43.2	2	4.00 X 10 ¹⁵
288	±72	2	1.80 X 10 ¹⁵
480	±120	2	7.30 X 10 ¹⁴
800	±200	2	2.80 X 10 ¹⁴

Note that the range of wavelengths covered by these 5 bands extends from 77.76–1000 microns. This is just one choice that does not restrict coverage to 100–1000 microns but does provide a reasonable basis for examining SNR achievable in this interval.

Since the bands are fairly broad, particularly at the high end of the interval, the channel radiance values shown in the table above are fairly reasonable on the whole. Compare these to the channel radiances for thermal mapper bands covering 8–100 microns as shown in the Table G-2 below.

The channel radiances for bands centered at 103.68, 172.8, 288, and 480 microns are in the same ballpark as channel radiances for bands centered at 15.6 through 93 microns. The strawman thermal mapper includes an uncooled micro-bolometer array as the detector for wavelengths from 11.7–116 microns. A micro-bolometer array may be suitable out as far as 600 microns. (See further discussion below.)

Table G-2: Thermal Mapper Channel Bands

Center Wavelength (microns)	Channel Bandwidth (microns)	Spectral Resolution	Channel Radiance (ph/cm ² /s/sr)
8	+/- 2	2	2.70 X 10 ¹²
10	+/- 2.5	2	3.18 X 10 ¹³
12.5	+/- 3.125	2	2.11 X 10 ¹⁴
15.6	+/- 3.9	2	8.79 X 10 ¹⁴
19.5	+/- 4.9	2	2.56 X 10 ¹⁵
24.4	+/- 6.1	2	5.53 X 10 ¹⁵
30.5	+/- 7.6	2	9.05 X 10 ¹⁵
38.1	+/- 9.5	2	1.22 X 10 ¹⁶
47.6	+/- 11.9	2	1.40 X 10 ¹⁶
59.5	+/- 15	2	1.42 X 10 ¹⁶
74.4	+/- 18.6	2	1.27 X 10 ¹⁶
93	+/- 23	2	1.05 X 10 ¹⁶

For the lowest three thermal mapper bands (centered at 8, 10, and 12.4 microns), the strawman includes HgCdTe detectors cooled to 60 K. These have relatively high sensitivity and can be used to achieve a relatively high SNR. Using HgCdTe detectors would not be a viable option for the band centered at 800 microns since HgCdTe is not responsive at longer wavelengths, so another approach would be required to achieve a reasonable SNR.

Two types of optical detectors used for the far infrared are bolometers and thermopiles. Cassini is carrying an instrument that uses thermopiles and Herschel (formerly FIRST) will carry an instrument that uses bolometers. The sections below list some of the parameters for these two instruments and consider the relevance of each instrument to JIMO. These are just two examples and not intended to represent the full range of instruments that use bolometers and/or thermopiles. They are provided to give some insight into current applications of these technologies.

Composite Infrared Spectrometer (Cassini)

The Composite Infrared Spectrometer (CIRS) consists of a 0.5-meter F/6 Cassegrain beryllium telescope, a reference interferometer to provide scan mechanism control and timing for data sampling, and two science Fourier transform spectrometers (FTS). One FTS covers mid-infrared and the other covers far-infrared. The Far-infrared interferometer (FIR) is a polarizing Michelson interferometer measuring from 17–1000 microns using two thermopile detectors. Each thermopile detector includes a concentrator and has a 4.3-mrad diameter circular FOV. The operating temperature of the telescope and the FIR focal plane is 170 K. [1, 2, 3]

The CIRS approach involves collecting a relatively large amount of light with a relatively slow telescope and focusing the light on concentrators attached to each

thermopile to boost the SNR. The instrument has a pixel FOV of 0.25 degrees. The exposure time can range from 2–50 seconds. [2]

The CIRS instrument (including both spectrometers) has a mass of 39.24 kg and requires 26.4 Watts of power. [1]

While the CIRS instrument supports the Cassini science goals, it is not designed to meet the JIMO requirements for global mapping or image resolution. Note the following:

- The FOV required for JIMO global mapping is about 15 degrees, which is 60 times larger than the 0.25-degree CIRS pixel FOV.
- To achieve 300-meter resolution from 100-km altitude would require an angular pixel size of 0.17 degrees. CIRS has a single circular pixel with a diameter of 0.25 degrees.
- For a push-broom approach from an altitude of 100-km, the shortest JIMO exposure time would be 0.167 seconds at Ganymede. This is 12 times shorter than the shortest CIRS exposure time.

Conversely, CIRS could provide a single 436-meter pixel from 100-km altitude. And with back-scanning as opposed to a push-broom approach, the JIMO exposure time could perhaps be increased to a few seconds. If the JIMO requirement for global mapping at Europa within 15 days were greatly relaxed or dropped, the CIRS FIR instrument could perhaps be used to investigate a very few selected targets or regions, though the utility of such measurements is unclear.

All of the references below are available on the web. A URL is provided with each reference. A few additional references are included below. In particular, References 4 and 5 provide more detail on the design of the thermopiles.

Note that there is a substantial amount of current research and development effort focused on linear and 2-D thermopile arrays for imaging. A linear array could potentially be used to achieve a wide FOV in the cross-track direction to support a push-broom approach for global mapping. Performance characteristics of a candidate linear thermopile array would need to be considered to determine whether an adequate SNR could be achieved while push-brooming. Back-scanning could be an option, but this would limit coverage unless an extraordinary approach were used (e.g., multiple instruments on separate scan platforms with synchronized back-scanning).

References

1. NSSDC Master Catalog: Experiment, Composite Infrared Spectrometer (CIRS): <http://nssdc.gsfc.nasa.gov/database/MasterCatalog?sc=1997-061A&ex=5>
2. Stephen J. Edberg, "Looking Through: Mapping Air/ Cassini's Composite Infrared Spectrometer," October 29, 1999, http://sgra.jpl.nasa.gov/us-space-vlbi/outreach/S_Edberg.pdf
3. Patricia Losch, James J. Lyons III, and John Hagopian, "Cryogenic optical performance of the Cassini Composite InfraRed Spectrometer (CIRS) flight telescope," <http://cirs.gsfc.nasa.gov/html/instrument/papers/tele98.pdf>
4. Rainer Fettig, et al, "Thermal infrared detectors with improved mechanical stability for the Composite Infrared Spectrometer (CIRS) far infrared focal plane," <http://cirs.gsfc.nasa.gov/html/instrument/papers/thermoel.pdf>
5. John G. Hagopian and Julie Crooke, "Acoustic amplification in the far infrared focal plane assembly of the Composite Infrared Spectrometer (CIRS) for the Cassini mission to Saturn," <http://cirs.gsfc.nasa.gov/html/instrument/papers/acoust.pdf>

Spectral and Photometric Imaging Receiver (Herschel/FIRST)

The Spectral and Photometric Imaging Receiver (SPIRE) will be one of three instruments on ESA's Herschel Space Observatory (formerly known as the Far Infrared Space Telescope or FIRST). [1] SPIRE includes a 3-band imaging photometer that will simultaneously observe at 250, 350, and 500 microns with a spectral resolution around 3. SPIRE also includes an imaging Fourier transform spectrometer (FTS) that will observe the range of wavelengths from 200 to 670 microns. The instrument is sensitivity limited by thermal emission from the telescope, which is cooled to 80 K. Detector arrays will be cooled to 0.3 K using superfluid Helium (^3He). [2, 3] The main objectives are to investigate very distant galaxies and to study the earliest stages of star formation. [4] The instrument is a novel non-polarizing FTS based on the Mach-Zehnder interferometer. [5]

SPIRE will have five arrays of feedhorn-coupled bolometers. These will have a "spider web" design. Each consists of a web-like mesh of silicon nitride, which absorbs light and conducts the energy to the tiny thermistor that sits at the center of the web. The thermistor is made of neutron transmutation doped (NTD) germanium, a substance manufactured in a nuclear reactor. It takes about 100 photons in the far-infrared/submillimeter range to heat it up enough to generate an electrical signal. The bolometer's web-like structure reduces the bolometer's heat capacity and gives SPIRE a relatively high mapping speed. [4]

The photometer will have a 4 by 8 arcmin (0.067 by 0.133 degree) FOV and the imaging FTS will have a FOV greater than 2 arcmin (0.033 degrees). [2, 3] These relatively small FOVs are the consequence of an optical train designed for astronomy.

The Herschel primary mirror will have a 3.5-meter diameter. The vehicle launch mass will be about 3300 kg and vehicle power will be around 1 kW. The vehicle is designed for a lifetime greater than 3 years. [6] The optics are required for the operation of SPIRE as well as for other instruments, and there is no simple way to break out the mass and power requirements for SPIRE alone.

Herschel and SPIRE are clearly designed for astronomical investigations of distant objects that emit very little light. Observation times could be many minutes as opposed to a fraction of a second for JIMO. There is no intention of suggesting that SPIRE should be flown on JIMO, which has drastically different science goals. However, SPIRE does use one type of micro-bolometer in supercooled detector arrays that are sensitive out to 670 microns. It is conceivable that this type of micro-bolometer array could be of use without cooling it to 0.3 K. Its performance at higher temperatures would need to be investigated to determine how useful it would be for JIMO while looking at targets around 100 K over relatively short exposures.

All of the references below are available on the web. A URL is provided with each reference.

References

1. Herschel, <http://www.ipac.caltech.edu/Herschel/Instruments/spire.shtml>
2. Matt Griffin, Bruce Swinyard, and Laurent Vigroux, "The SPIRE Instrument," <http://astro.esa.int/FIRST/Publ/Toledo/Talks/griffin.pdf>
3. M. J. Griffin, B. M. Swinyard, and L. Vigroux, "The SPIRE Instrument for Herschel," <http://astro.esa.int/SA-general/Projects/Herschel/Publ/2001/griffinm.pdf>
4. Herschel Space Observatory: SPIRE Instrument, <http://herchel.jpl.nasa.gov/contributions/spire.html>
5. Peter A. R. Ade, Peter A. Hamilton, and David A. Naylor, "An absolute dual beam emission spectrometer," <http://research.uleth.ca/spire/papers/beamsplitter.pdf>
6. Szczerba Ryszard, "The Herschel Space Observatory: project, instruments, and a scientific overview," <http://www.pta.edu.pl/zjazd/materialy/szczerba.pdf>

Passive Radio Frequency Radiometry

Another alternative would be to use passive radio frequency (RF) radiometry in the sub-millimeter range. A wavelength of 100 microns corresponds to a frequency of 3 THz, and 1000 microns corresponds to 300 GHz. One instrument used to study atmospheric gases at Earth is discussed below. The technology demonstrated in this instrument includes passive radiometers at 640 GHz and 2.5 THz, which could provide some heritage for JIMO.

Microwave Limb Sounder (EOS Aura)

The microwave limb sounder (MLS) instrument to be flown on the EOS Aura spacecraft will have a capability for sub-millimeter radiometry. EOS MLS is a greatly enhanced version of the Upper Atmosphere Research Satellite (UARS) MLS experiment. Microwave limb sounding obtains remote measurements of atmospheric parameters by observing thermal emissions (radiances) as the instrument "FOV beamwidth" is scanned through the atmospheric limb from above. "FOV beamwidth" is defined as the angle between the half-power points of the antenna response. [1]

The EOS MLS instrument has radiometers in five spectral regions, chosen to produce a set of standard geophysical data products. These include radiometers at 118 GHz, 190 GHz, 240 GHz, 640 GHz, and 2.5 THz. Advanced planar-technology mixers are used in all the radiometers, with a monolithic millimeter-wavelength integrated circuit (MMIC) amplifier preceding the mixer in the 118 GHz radiometer. Sub-harmonically pumped mixers are used at 118, 190, 240 and 640 GHz, and a fundamental mixer at 2.5 THz. Local oscillators are solid state except at 2.5 THz, which uses a CO₂-pumped methanol (CH₃OH) gas laser. All radiometers operate at ambient temperature. [1]

Atmospheric signals for the 118, 190, 240 and 640 GHz radiometers are collected by a three-reflector antenna system which vertically scans the limb. The antenna design is very similar to that of UARS MLS, with a primary reflector dimension of 1.6 meter projected in the vertical direction at the limb tangent point. A switching mirror following the GHz antenna system provides radiometric calibration by switching to views of calibration targets or to space. An optical multiplexer, consisting of an arrangement of dichroic plates and polarization grids, spatially separates the signal from the switching mirror into different paths feeding different radiometers. [1]

The atmospheric and calibration signals for the 2.5 THz radiometer are obtained via a dedicated telescope and scanning mirror whose operation is synchronized with that of the GHz antenna and the GHz switching mirror. The 2.5 THz primary mirror dimension in the "limb vertical" direction is ~25 cm, and the field-of-view width at the tangent point is ~2.5 km. [1]

The radiometers have intermediate frequency (IF) outputs in several bands. These IF outputs are fed to spectrometers via a switch network. Digitized data from the spectrometers are passed to the command and data handling system for transmission to the ground. The instrument individual measurement integration time is 1/6 second. [1]

**Table G-3: EOS MLS Field-of-View Beamwidths
(Full Width between Half-power Points)**

Radiometer	FOV Beamwidth in the Vertical Plane at the Limb Tangent Point (degrees)	FOV Beamwidth in the Horizontal Plane at the Limb Tangent Point (degrees)
118 GHz	0.124	0.248
190 GHz	0.0859	0.172
240 GHz	0.0668	0.134
640 GHz	0.0286	0.0573
2.5 THz	0.0477	0.0477

The table above is based on data from Reference 1, assuming that the limb tangent point is at a distance of 3000 km from the spacecraft. The picture below from Reference 1 depicts the scan pattern.

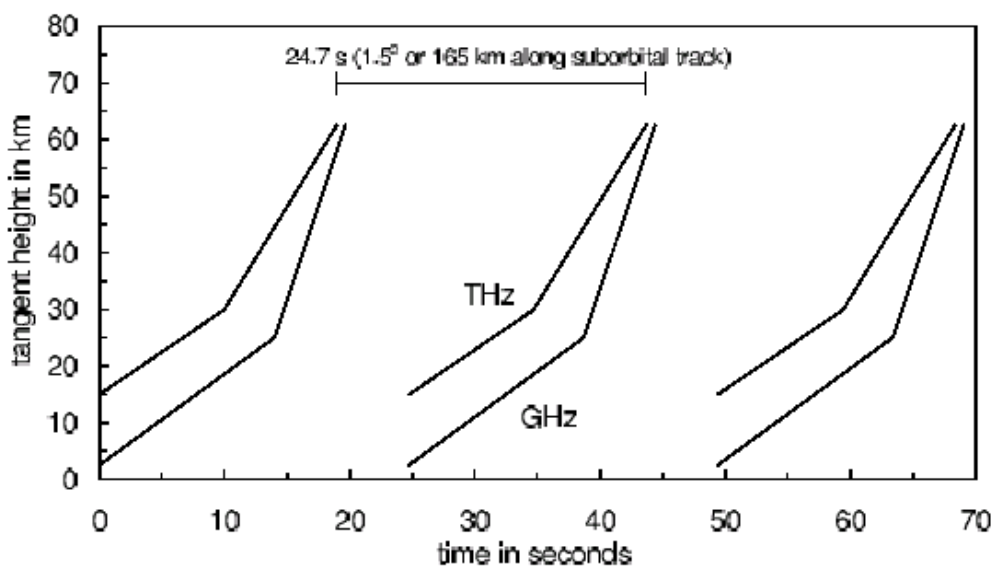


Figure G-2: Scan pattern (Reprinted courtesy of NASA).

Some characteristics of the EOS MLS from Reference 2 are as follows:

- Total mass of 440 kg
- Power of 530 Watts fully on
- Data rate of 100 kb/sec
- 5-year on-orbit design lifetime

The 640 GHz and 2.5 THz radiometers might be of use for JIMO investigation in the sub-millimeter range if there were science goals that warrant it. The EOS MLS will be used to study atmospheric gases at Earth. The expected types and

signal intensities of atmospheric gases surrounding Jupiter's icy moons would need to be considered to determine the utility of the EOS MLS for a comparable investigation.

While MLS is implemented as a limb sounder, an alternative implementation for similar hardware could include cross-track scanning or use of a conical scan. In fact, having both limb and downlooking scanning modes might offer considerable versatility. To achieve practical scanning rates, an MLS type instrument might require a larger footprint than imagers operating at shorter wavelengths. On the other hand, a larger footprint might be appropriate for an instrument investigating new phenomenology.

The EOS MLS scans in the vertical direction over a range of about 60 km. This corresponds to an angular change of about 1.15 degrees in the vertical direction, assuming that the spacecraft is 3000 km from the limb tangent point. Recall that the beamwidth in the vertical direction is less than 0.05 degrees for the 2.5 THz radiometer and even smaller for the 640 GHz radiometer. If the EOS MLS were flown on JIMO and nadir pointed from 100 km altitude with cross-track scanning, its total swath width would be at most 1.2 degrees or about 2.1 km. This is relatively small compared with the 26.3 km swath width needed to meet the global mapping requirements given as guidelines for this strawman design task.

Including time for calibration, EOS MLS takes 24.7 seconds to complete one scan cycle. JIMO's maximum ground speed would be about 1.8 km/sec (at Ganymede), so JIMO would progress through 44.5 km along-track during 24.7 seconds. Since the along-track distance during a cycle is large relative to the cross-track swath width, there would be relatively large gaps in the coverage pattern.

There are also questions regarding potential difficulties operating in and surviving the high radiation environment. Robustness of the EOS MLS components to radiation would need to be addressed.

References

1. Joe W. Waters, "An Overview of the EOS MLS Experiment," Version 1.1, 15 October 1999, Available online at http://mls.jpl.nasa.gov/joe/mls_home_page/ATBD-MLS-01.pdf
2. Joe Waters, "The EOS Microwave Limb Sounder (MLS) Experiment," 27 October 2003, http://mls.jpl.nasa.gov/joe/eos_mls_summary_presentation.pdf

Summary

The science goals for imaging in the wavelength range of 100–1000 microns would need to be well defined to determine which type of technology is most appropriate. There are a few candidate technologies that could be of some use for the JIMO mission. For each, the most difficult requirement to meet would be global mapping of the icy moons within limited time frames. (The most difficult challenge would be global mapping of Europa within 15 days.) The difficulty stems from the relatively low target radiances in this wavelength range and the relatively high ground speed for the baseline 100 km altitude orbits. Given that new phenomenology is being investigated, however, a larger footprint might be acceptable.

Optical imaging could potentially be done using thermopiles or micro-bolometers as detectors. Two instruments were considered as examples that provide some insight into current applications of these types of detectors. One was the CIRS instrument on Cassini and the other was the SPIRE instrument on Herschel.

Another alternative using more mature technology would be to use passive RF radiometry in the sub-millimeter range. The EOS MLS instrument was considered as an example of this technology that provides some insight into current applications for Earth science. The EOS MLS instrument has radiometers in five spectral regions. These include radiometers at 118 GHz, 190 GHz, 240 GHz, 640 GHz, and 2.5 THz. The 640 GHz and 2.5 THz radiometers might be of use for JIMO investigations in the sub-millimeter range.

A system like EOS MLS for JIMO could be used with a conical scan or it could be pointed to nadir and scanned cross-track. This raises questions that need to be addressed regarding what the expected thermal emissions would be and what science measurements would be appropriate. Questions regarding the appropriate footprint and desired coverage would have to be addressed.

There are also questions that would need to be addressed regarding potential difficulties operating in and surviving the high radiation environment.

Overall, imaging in the wavelength range from 100–1000 microns has practical difficulties, but there are technologies that appear promising. A science goal and approach that allows realistic requirements to be evaluated and trades to be made is a necessary first step.

Appendix H. Technology Readiness Levels Descriptions

Background

The following excerpt is from The NASA Technology Plan, Appendix B: Technology Readiness Levels as updated 24 July 2001. The text is almost identical to that found in the Space Science Enterprise Management Handbook dated 4 September 2002. The text in both documents is based on a white paper authored by John C. Mankins, Advanced Concepts Office, Office of Space Access and Technology, NASA, dated 6 April 1995.

Introduction

Technology Readiness Levels (TRLs) are a systematic metric/measurement system that supports assessments of the maturity of a particular technology and the consistent comparison of maturity between different types of technology. The TRL approach has been used on and off in NASA space technology planning for many years and was recently incorporated in the NASA Management Instruction (NMI 7100) addressing integrated technology planning at NASA. The figure below provides a summary view of the technology maturation process model for NASA space activities for which the TRLs were originally conceived; other process models may be used. However, to be most useful the general model must include: (a) “basic” research in new technologies and concepts (targeting identified goals, but not necessary specific systems), (b) focused technology development addressing specific technologies for one or more potential identified applications, (c) technology development and demonstration for each specific application before the beginning of full system development of that application, (d) system development (through first unit fabrication), and (e) system “launch” and operations.

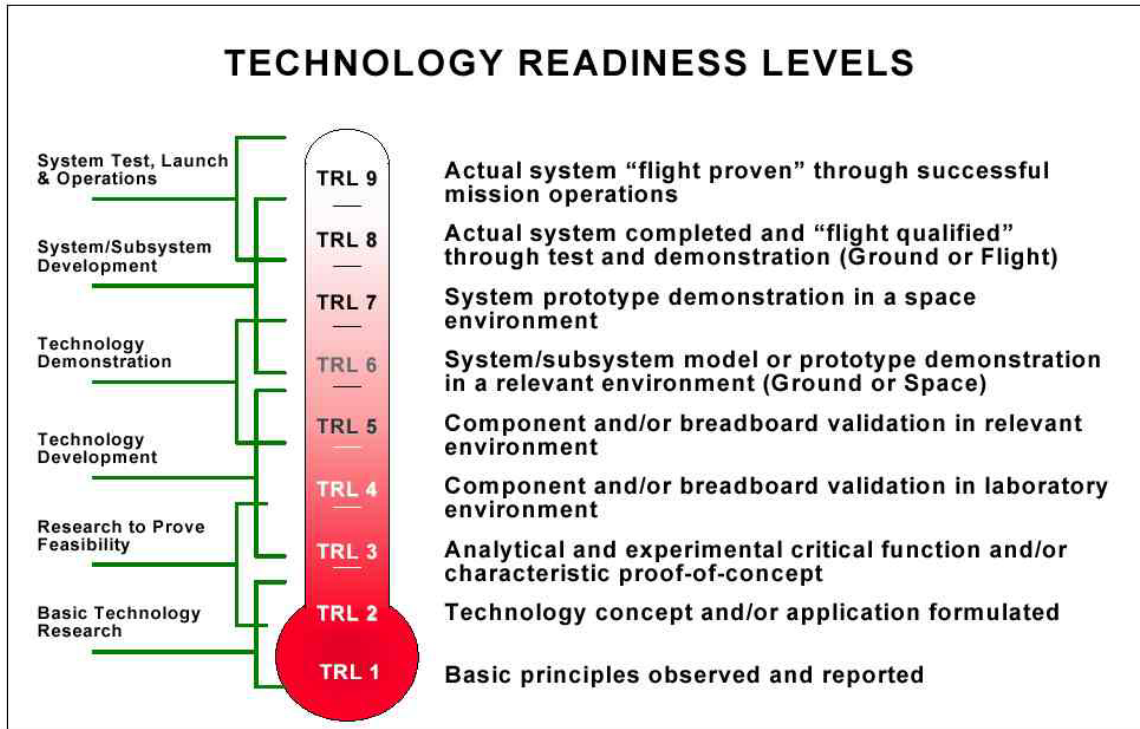


Figure H-1: Technology readiness levels.

Discussion of Each Level

The following paragraphs provide a descriptive discussion of each technology readiness level, including an example of the type of activities that would characterize each TRL.

TRL 1

Basic principles observed and reported

This is the lowest "level" of technology maturation. At this level, scientific research begins to be translated into applied research and development. Examples might include studies of basic properties of materials (e.g., tensile strength as a function of temperature for a new fiber).

Cost to Achieve: Very Low "Unique" Cost (investment cost is borne by scientific research programs)

TRL 2

Technology concept and/or application formulated

Once basic physical principles are observed, then at the next level of maturation, practical applications of those characteristics can be "invented" or identified. For example, following the observation of high critical temperature (Htc)

superconductivity, potential applications of the new material for thin film devices (e.g., SIS mixers) and in instrument systems (e.g., telescope sensors) can be defined. At this level, the application is still speculative; there is not experimental proof or detailed analysis to support the conjecture.

Cost to Achieve: Very Low “Unique” Cost (investment cost is borne by scientific research programs)

TRL 3

Analytical and experimental critical function and/or characteristic proof-of-concept

At this step in the maturation process, active research and development (R&D) is initiated. This must include both analytical studies to set the technology into an appropriate context and laboratory-based studies to physically validate that the analytical predictions are correct. These studies and experiments should constitute “proof-of-concept” validation of the applications/concepts formulated at TRL 2. For example, a concept for high energy density matter (HEDM) propulsion might depend on slush or super-cooled hydrogen as a propellant; TRL 3 might be attained when the concept-enabling phase/temperature/pressure for the fluid was achieved in a laboratory.

Cost to Achieve: Low “Unique” Cost (technology specific)

TRL 4

Component and/or breadboard validation in laboratory environment

Following successful “proof-of-concept” work, basic technological elements must be integrated to establish that the “pieces” will work together to achieve concept-enabling levels of performance for a component and/or breadboard. This validation must be devised to support the concept that was formulated earlier, and should also be consistent with the requirements of potential system applications. The validation is relatively “low-fidelity” compared to the eventual system; it could be composed of ad hoc discrete components in a laboratory. For example, a TRL 4 demonstration of a new “fuzzy logic” approach to avionics might consist of testing the algorithms in a partially computer-based, partially bench-top component (e.g., fiber optic gyros) demonstration in a control lab using simulated vehicle inputs.

Cost to Achieve: Low-to-moderate “Unique” Cost (investment will be technology specific, but probably several factors greater than investment required for TRL 3)

TRL 5

Component and/or breadboard validation in relevant environment

At this step, the fidelity of the component and/or breadboard being tested has to increase significantly. The basic technological elements must be integrated with

reasonably realistic supporting elements so that the total applications (component-level, sub-system level, or system-level) can be tested in a “simulated” or somewhat realistic environment. One to several new technologies might be involved in the demonstration. For example, a new type of solar photovoltaic material promising higher efficiencies would at this level be used in an actual fabricated solar array “blanket” that would be integrated with power supplies, supporting structure, etc., and tested in a thermal vacuum chamber with solar simulation capability.

Cost to Achieve: Moderate “Unique” Cost (investment cost will be technology dependent, but likely to be several factors greater than cost to achieve TRL 4)

TRL 6

System/subsystem model or prototype demonstration in a relevant environment (ground or space)

A major step in the level of fidelity of the technology demonstration follows the completion of TRL 5. At TRL 6, a representative model or prototype system or system—which would go well beyond ad hoc, “patch-cord” or discrete component level breadboarding—would be tested in a relevant environment. At this level, if the only “relevant environment” is the environment of space, then the model/prototype must be demonstrated in space. Of course, the demonstration should be successful to represent a true TRL 6. Not all technologies will undergo a TRL 6 demonstration; at this point the maturation step is driven more by assuring management confidence than by R&D requirements. The demonstration might represent an actual system application, or it might only be similar to the planned application, but using the same technologies. At this level, several to many new technologies might be integrated into the demonstration. For example, an innovative approach to high temperature/low mass radiators, involving liquid droplets and composite materials, would be demonstrated to TRL 6 by actually flying a working, sub-scale (but scaleable) model of the system on a Space Shuttle or International Space Station “pallet”. In this example, the reason space is the “relevant” environment is that microgravity plus vacuum plus thermal environment effects will dictate the success/failure of the system—and the only way to validate the technology is in space.

Cost to Achieve: Technology and demonstration specific; a fraction of TRL 7 if on ground; nearly the same if space is required

TRL 7

System prototype demonstration in a space environment

TRL 7 is a significant step beyond TRL 6, requiring an actual system prototype demonstration in a space environment. It has not always been implemented in the past. In this case, the prototype should be near or at the scale of the planned operational system and the demonstration must take place in space. The driving

purposes for achieving this level of maturity are to assure system engineering and development management confidence (more than for purposes of technology R&D). Therefore, the demonstration must be of a prototype of that application. Not all technologies in all systems will go to this level. TRL 7 would normally only be performed in cases where the technology and/or subsystem application is mission critical and relatively high risk. Example: The Mars Pathfinder Rover is a TRL 7 technology demonstration for future Mars micro-rovers based on that system design. Example: X-vehicles are TRL 7, as are the demonstration projects planned in the New Millennium spacecraft program.

Cost to Achieve: Technology and demonstration specific, but a significant fraction of the cost of TRL 8

TRL 8

Actual system completed and “flight qualified” through test and demonstration (ground or space)

By definition, all technologies being applied in actual systems go through TRL 8. In almost all cases, this level is the end of true “system development” for most technology elements. Example: this would include DDT&E through Theoretical First Unit (TFU) for a new reusable launch vehicle. This might include integration of new technology into an existing system. Example: loading and testing successfully a new control algorithm into the onboard computer on Hubble Space Telescope while in orbit.

Cost to Achieve: Mission specific; typically highest unique cost for a new technology

TRL 9

Actual system “flight proven” through successful mission operations

By definition, all technologies being applied in actual systems go through TRL 9. In almost all cases, the end of last “bug fixing” aspects of true “system development.” For example, small fixes/changes to address problems found following launch (through “30 days” or some related date). This might include integration of new technology into an existing system (such as operating a new artificial intelligence tool into operational mission control at JSC). This TRL does not include planned product improvement of ongoing or reusable systems. For example, a new engine for an existing RLV would not start at TRL 9: such “technology” upgrades would start over at the appropriate level in the TRL system.

Cost to Achieve: Mission Specific; less than cost of TRL 9 (e.g., cost of launch plus 30 days of mission operations)